Nanoparticle Preparation Process Using Novel Microjet Reactor Technology for Enhancing Dissolution Rates of Poorly Water Soluble Drugs

Dissertation

zur Erlangung des Grades

"Doktor der Naturwissenschaften"

im Promotionsfach Pharmazie

am Fachbereich Chemie, Pharmazie und Geowissenschaften

der Johannes Gutenberg-Universität

in Mainz

Akif Emre Türeli

geb. in 20.09.1980

Mainz, den 2015

1. Berichterstatter:

2. Berichterstatter:

Datum der mündlichen Prüfung: 29.04.2015

D77 Dissertation Universität Mainz

Contents

ACKNOWLEDGEMENTS

To Dr. Bernd Penth

Inventor of the MicroJet Reactor and my dear friend

I feel privileged to bring your invention forward

LIST OF FIGURES

LIST OF TABLES

LIST OF ABBREVIATIONS AND SYMBOLS

δ solvent	Hildebrand solubility parameter for solvent [$(MPa)^{1/2}$]
δ water	Hildebrand solubility parameter for water in [$(MPa)^{1/2}$]
P	Density [g/cm^3]
ACN	Acetonitrile
API	Active pharmaceutical ingredient
AUC	Area under the curve
AVG	Average
BCS	Biopharmaceutical classification system
C	Concentration
°C	Degree Celsius
CAS No.	Chemical Abstract Service number
CIJ	Confined impinging jets
CyA	Cyclosporin A
DLS	Dynamic Light Scattering
DMSO	Dimethyl sulphoxide
DoE	Designs of experiments
Eq.	Equation
EtOH	Ethanol
Fig.	Figure
GIT	Gastro intestinal tract
HLB	Hydrophillic-lipophilic balance
HPMCP	Hydroxypropyl methyl cellulose phthalate
i.v.	Intravenous
J	Joule
K	Kelvin
MJR	Microjet reactor
mg	Milligram
min	Minute(s)
mL	Milliliter
MPa	Mega Pascal
MW	Molecular weight
n/a	Not applicable

NCE	New chemical entity
Nm	Nanometer
NTU	Nephelometric turbidity unit
o/w	Oil-in-water (emulsion)
PDI	Polydispersity index
PLGA	Poly (lactic-co-glycolic) acid
R	Gas constant [8.314472 J/mol.K]
SD	Standard Deviation
SEM	Scanning Electron Microscopy
T	Temperature [°C]
Tab.	Table
TEM	Transmission Electron Microscopy
Χ water –solvent:	Water solvent interaction parameter
V	Volume
$V_{solvent}$	Molar volume of the solvent [cm^3/mol]
w/o	Water-in-oil (emulsion)

1. Introduction

It is estimated that 40% of active substances identified through combinatorial screening programs are difficult to formulate as a result of their significant lack of solubility in water [1, 2]. The classical approach to deal with this issue is to generate various salts of a poorly water-soluble molecule, using solubility enhancers or physical milling of the substance so as to improve solubility while retaining the biological activity. Alternatively screening is continued with pro-drugs or analogs of the substance [2]. The major issues regarding the poor water soluble compounds can be summarized as follows [2]:

- Poor bioavailability
- Inability to optimize lead compound selection based on efficacy and safety
- Fed/fasted variation in bioavailability
- Lack of dose-response proportionality
- Suboptimal dosing
- Use of harsh excipients, i.e., excessive use of co-solvents and other excipients
- Uncontrollable precipitation after dosing
- Noncompliance by the patient

Bioavailability of low water soluble drugs can be increased, once solubility and the rate of dissolution are enhanced in the gastrointestinal tract (GIT). According to the Ostwald-Freundlich equation saturation solubility is expected to be increased by decrease in particle size [3].

Eq. 1-1

$$\frac{S(d)}{S_0} = \exp\frac{\gamma \cdot V_m}{RTd}$$

where;

S(d)	Solubility of the crystals with inscribed diameter [mol/kg H_2O]
S_0	Solubility of the bulk material [mol/kg H_2O]
γ	Surface free energy [mJ/m^2]
V_m	Molar volume [m^3/mol]
R	Gas constant [8314.5 mJ/mol K]
T	Temperature[K]
d	Diameter [m]

When all other parameters are kept constant, solubility of the active pharmaceutical agent increases with decreased particle size. However, a significant solubility difference would be obtained when the exponential term is much smaller than 1. This would be only observed in case of nano sizes. Another reason for the increase in saturation solubility is exposure of the lipophilic surfaces from the inner part of the crystal to the aqueous medium. This alters the surface tension (γ) and consequently increases the saturation solubility [3].

The dissolution rate of an active pharmaceutical agent can be calculated with the Noyes-Whitney equation given in Eq. 1-2:

Eq. 1-2
$$\frac{dm}{dt} = \frac{D \times S}{h} \times (Cs - C)$$

where;

m	Amount of drug dissolved [mg]
t	Time [s]
D	Diffusion coefficient [cm^2/s]
S	Surface area [cm^2]
Cs	Local equilibrium concentration of the API in the diffusion layer on the particle surface [mg/mL]
C	Concentration of the API in the bulk solution [mg/mL]
h	Diffusion layer thickness [cm]

In the reference of this equation, in order to increase the dissolution rate, Cs can be increased by trapping the API in the metastable crystalline or amorphous states with higher free energies than the lowest energy equilibrium crystalline state. Other parameter that can be adjusted for this purpose is the S which may be increased by reducing the particle size, increasing porosity or wetting of the API. [4]

When it is the case that drug selection process is affected by the inefficient solubility and low dissolution rate of the molecule, formulation of this molecule as a nanotechnological product can be an alternative and a solution. Decreasing particle size below 1µm size would enhance both saturation solubility and dissolution rate. For this reason, under the lights of the Ostwald-Freundlich and Noyes-Whitney equations, it can be concluded that nanoparticles can successfully contribute to increase the dissolution rate of the drug substances. Increased sur-

face to volume ratio provides additionally increased activity, which is directly related to the efficacy of the drug [5].

Nanoparticles are defined as objects with all three external dimensions ranging from 1 to 100 nm [6]. As a result of the increased surface area to volume ratio, some of physicochemical and biological properties of molecules are altered dramatically in comparison to their larger counterpart.

Pharmaceutical nanoparticles are submicron sized colloidal vehicles that carry drugs to the target or release drugs in a controlled way in the body. Following preparation, nanoparticles are usually dispersed in liquids. Such a system can be administered for example by injection, by the oral route, or used in ointments and ocular products. Alternatively, nanoparticles can be dried to form powder which allows pulmonary delivery or further processing to tablets or capsules.

In case of drug delivery, nanoparticles can be employed to realize targeted drug delivery, long blood circulation times and increased patience compliance (i.e. introducing oral and pulmonary administration instead of intravenous (i.v.) administration). Nanoparticles have been tested widely in case of parenteral applications especially with cytotoxic drugs. Targeting efficiency of drug molecules can be increased in 2 ways. One of them is passive drug targeting where nanoparticles are constructed in a particle range of 100-150 nm so that these particles can penetrate the leaky blood vessels around the tumor cells but stay in circulation around healthy tissues due to the fact that intercellular gaps at the walls of blood vessels are below 100 nm. Furthermore targeting molecules, such as antibodies or proteins on the cell surface of cancer cells, can be introduced on the nanoparticle surface for drug targeting to tumor cells. Due to these applications side effects of the drugs can be decreased by site-targeted nanodrug delivery systems by releasing the drug at the site of action, as well by reducing the dose within the therapeutical window as a result of the increased efficacy. Another possibility is to increase the patient compliance using nanoparticles for oral applications. In this case drugs with low bioavailability due to low solubility in physiological pH can be applied as nanoparticles with a higher dissolution profile compared to the API itself. Higher dissolution profile of the drug will lead to increased bioavailability which results in ability to formulate such drugs as oral preparations instead of parenteral preparations [7].

There are several ways that are used for the preparation of pharmaceutical nanoparticles [8-21]. No matter what approach is chosen to produce drug nanoparticles, in comparison to the larger counterparts, the surface area is increased. This increase in the surface area and surface interactions can positively increase the dissolution rate and provide a platform to control the pharmacokinetic properties of the drug [2]. However, unless properly dampened, this tremendous increase in surface energy can cause the nanometer sized drug particles to spontaneously aggregate into a more thermodynamically stable state.[22]. Larger particles are energetically more favorable than smaller particles. For this reason, when nanoparticles are formed the system tries to compensate for the increase in the surface area by either dissolving the incipient crystalline nuclei and causes precipitation or by agglomeration of small particles [23]. Stability of the nanoparticles in liquid form requires extra care not only for solution stability but also in terms of drug leakage which is the leakage of drug molecules into the aqueous phase during storage of nanoparticles in liquid form [24].

One of the critical steps in the generation of physically stable nanoparticles is the use of various excipients that act to dampen or sensitize the surface energy of the nanoparticles by steric and/or ionic stabilization. An acceptable stabilizer should first be a reagent that is generally recognized as safe for the intended route of administration. Secondly the stabilizer must have the physicochemical properties that allow it to properly wet the surface of poorly water soluble compound. Finally, it should possess properties so as to impart steric and/or ionic stabilization to the surface of nanoparticles. It should be emphasized that surface stabilization does not necessarily involve chemical grafting of the surface stabilizer to the molecule. Stabilization is typically driven by the mere adsorption of the stabilizer to the surface of the poorly water-soluble compound [2].

Another consideration for obtaining a physically stable nanoparticle formulation is the ability to control the phenomenon referred to as Ostwald ripening. Ostwald ripening results from uncontrolled precipitation or crystallization of the active leading to particle size growth following stabilization [25]. Ostwald ripening can be eliminated and/or reduced by controlling a number of formulation parameters such as particle size, size distribution, solid content, choice of stabilizer and a fluid phase with minimal potential to solubilize the poorly water soluble compound [2].

Although the surface area is increased with the preparation of particles smaller than 1 µm, particle size should be more precisely adjusted when drug delivery to a specific target is required, since particle size and size distribution are two major characteristics defining the fate of the nanoparticles *in-vivo.* Before reaching the target site, nanoparticles undergo a biodistribution step possibly after crossing the epithelial barriers and travelling through the vascular bed [26]. Once the nanoparticles are in the vascular system, they are rapidly taken up by mononuclear phagocytic systems either in liver or spleen when the particle size lies between 150-300 nm. Nanoparticles with a smaller size around 30-150 nm are located in bone marrow, the heart, the kidney, and the stomach [26-30]. Nanoparticles smaller than 150 nm can pass the endothelial barrier; but it has been also shown that nanoparticles are able to cross the vascular endothelial barrier through openings present in the endothelium. The size of these openings can get bigger in cancer cells due to discontinuous endothelium with openings of 200 to 780 nm [26]. These data indicate the importance of production of desired particle sizes depending on the site of action.

Many different types of nanoparticles have been used for drug delivery purposes. Polymeric nanoparticles, liposomes, solid lipid nanoparticles, nano-fibers and -spheres, fullerenes, gold nanoparticles and superparamagnetic nanoparticles can be listed as some of the most popular types.

1.1 Nanoparticle preparation techniques

Nanoparticles can be prepared in many ways. All techniques can be listed under two main categories: Top-down and Bottom-up.

1.1.1 Top-down processes

Top-down nanoparticle processes converts large materials into nano sized form by grinding, milling or etching. Even they are more reliable, requirement of complex devices, higher energy usage and removal of produced waste are the main drawbacks of the top-down processes [31].

Mechanical milling

Mechanical milling has been used for the preparation of nanoparticles in top-down manner since many years. In general, with this technique large particles are transformed into small size particles by energy transfer to the particles and mechanical grinding. The fundamental

principle of size reduction in mechanical milling devices is the energy imparted to the sample during impacts between the milling media. Different types of milling equipment are currently available in the market. Nanoparticles prepared by mechanical milling technique show highly polydisperse particle size distributions and imperfection of surface structure. Longer milling times required for preparation of fine particles (10-100 nm) resulting in impurities, which are difficult to be separated from the product, can be noted as other limiting aspect of the technique [32].

High pressure homogenization

High pressure homogenization is another mechanical nanoparticle preparation method which is based on the cavitation forces created in high pressure homogenizers. Substance dispersed in water by high shear mixing is passed through very small homogenization gap of around 25 µm at 1500 bar and homogenization is repeated many times. Velocity of the suspension and the dynamic fluid pressure is increased, whereas the static pressure on the fluid decreases below the boiling point of water at room temperature as a result of the narrowness of the gap [33]. Once water begins to boil at room temperature, formed gas bubbles cause cavitation leading to formation of nanoparticles by breaking microparticles. Particle size can be controlled by adjusting the applied pressure and number of homogenization cycles. Batch to batch differences and possible changes that might be introduced to crystalline structure after applying high pressure can be listed as disadvantages of this technique.

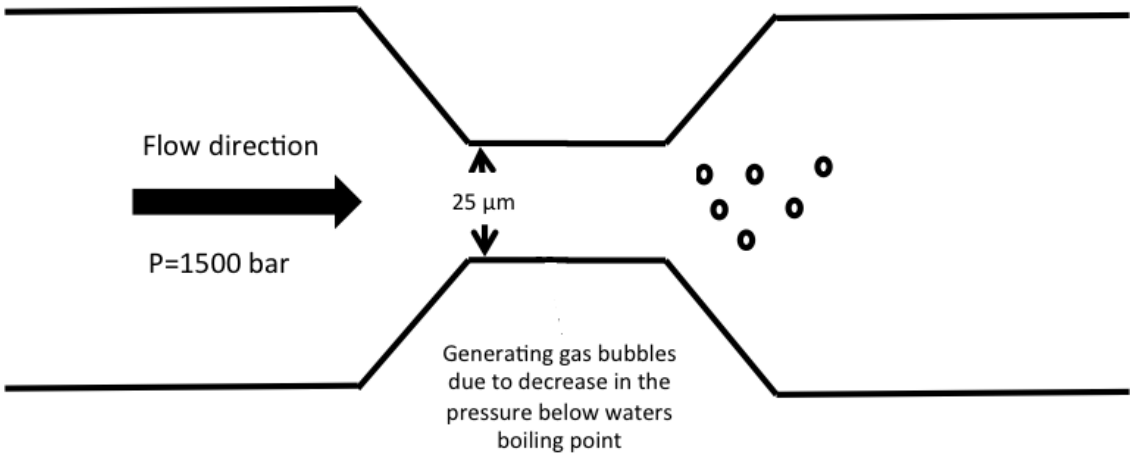

Fig. 1-1:Schematic presentation of high pressure homogenisation.

1.1.2 Bottom-up processes

Bottom-up nanoparticle preparation is achieved by allowing the precursor particles to grow in size. Many different preparation techniques have been developed since years successfully.

Salting out

The salting out method is based on the separation of a water miscible solvent from aqueous solutions by the salting out effect. An o/w emulsion is formed by dissolving the polymer and the drug in a water miscible organic solvent and adding this organic solution into an aqueous medium containing the salting out agent and a colloidal stabilizer. Because of presence of high amounts of salts or electrolytes, solvent diffusion does not take place. Nanoparticles are obtained after addition of excess water in order to induce the diffusion of the organic solvent into water and the formation of nanoparticles. Even drug loading capacity is high and scale up process is relatively easy, the main disadvantage of this method is that it can be only applied to lipophilic drugs [34, 35].

Solvent evaporation

This method is generally based on the formation of the o/w or w/o emulsions. Drug substance is dissolved in a partially miscible solvent and then emulsified in the aqueous solution containing the surfactant. Particle size reduction is done by high energy mixers or homogenizers. After the production of nanoparticles the solvent is evaporated under vacuum at higher temperature or by exposure to open air [3, 20, 36-46].

Supercritical fluid technology

Supercritical fluid technology is nowadays extensively used for the preparation of the nanoparticles. Solvents containing the drug molecule and the polymer or stabilizers are sprayed through a nozzle into a gas, which is in the supercritical state. Generally water or carbon dioxide is used for this type of application where the temperature and pressure is above the critical point where there is no distinct liquid or gas phase exists. Substances in their supercritical state behave like a liquid with the ability to dissolve materials. Thus, when substances in the presence of stabilizing agents and/or polymers are sprayed in this supercritical fluids an over saturation happens due to the poor solubility of these substances in supercritical fluids resulting in the precipitation as nanoparticles. These nanoparticles are fine and uniform and can be easily recovered by the releasing of the gas from the chamber [47-51].

Nanoprecipitation

Nanoprecipitation, also known as solvent displacement method, is one of the easiest methods for preparation of nanoparticles. It was first established and patented by Fessi and co-workers [52, 53]. The substance and the polymer is dissolved in water miscible organic phase (solvent system) and slowly poured into the water phase (non-solvent system) with a controlled flow rate and under mixing conditions. As the organic solvent diffuses into the aqueous medium, nanoparticle formation takes place spontaneously as a result of precipitation. If necessary, surfactant(s) in the aqueous phase can be employed to prevent the agglomeration. After formation of nanoparticles, organic solvent is evaporated under vacuum [19, 54].

The nanoprecipitation method does not require toxic solvents and most of the time use of surfactants is not necessary. Energy input, sonification or very high temperatures are not required by the process. Nanoprecipitation results in the production of nanoparticles in the range of 100-300 nm with relatively narrow particle size distributions [55]. It is mainly suitable for hydrophobic substances with low water solubility [55].The major disadvantage of this method is that it is only applicable to substances with low water solubility and surfactants that are used for this process should be removed from the medium after the nanoparticle formation [19, 56-59].

When nanosuspensions are produced, first the crystal nuclei are formed and then growth takes place. Production of stable nanosuspensions require fast crystal nuclei formation rates but slow growth rate in order to ensure small particle size. Both nuclei formation rate and growth rate are affected by temperature. Another limiting factor can be noted as mixing rate. If mixing times faster than nuclei growth times can be achieved, narrow particle sizes can be realized [60].

Nanoprecipitation method is based on the interfacial deposition due to the displacement of a solvent within non-solvent [52] and predicted to be mainly governed by **Marangoni effect**, which defines the solute movement at an interface caused by longitudinal variations of interfacial tension [53]. Motions of the surface of a liquid are coupled with those of the subsurface fluid or fluids, so that movements of the liquid normally produce stresses in the surface and vice versa. The movement of the surface and of the entrained fluid(s) caused by surface tension gradients is called the Marangoni effect [61]. Concentration gradient and temperature gradient are two causes of surface tension gradient. Under those conditions, nanoprecipita-

tion is driven by solute transfer out of the phase of higher viscosity, which is influenced by high concentration gradients at the interface and by interfacial tension. It is expected that final particle size is influenced by factors influencing interfacial tension. These factors include the polymer concentration, the presence and concentration of surfactant, and the nature of any substance that is co-precipitated into the particles [62].

In 1959, Sterling and Scriven [63] have shown that the fluctuations around the interface are mainly caused by interfacial turbulence and are usually enhanced by

- solute transfer out of the phase with relatively higher viscosity
- low viscosities of both phases
- steep concentration gradients around the interface
- large solute diffusivity differences between two phases

In addition to interfacial turbulence, the mechanism of nanoparticle formation with nanoprecipitation method can be related to water-solvent, water-solute and solvent-solute interactions. When both phases are in contact, it is assumed that solvent diffuses from the organic phase into the water and carries with it some solutes which are still in solution. Then, as the solvent diffuses further into the water, the associated solute aggregates forming nanoparticles. For this reason, it can be concluded that selected solvents would alter nanoparticles as a result of differences in water-solvent interaction [35].

The solubility parameters of the solvents can be employed to explain this situation and provide a numerical basis. In 1936, Joel H. Hildebrand proposed a definition for a “solubility parameter” for description of the miscibility behavior of solvents as a numerical value. The Hildebrand solubility parameter for a pure liquid substance is given in following equation:

Eq. 1-3 $$\delta = \left[\frac{\left(\Delta H_{\upsilon} - RT\right)}{V_m}\right]^{1/2}$$

where:

δ solvent:	Hildebrand solubility parameter [$(MPa)^{1/2}$]
ΔH_v:	Heat of vaporization [J/mol]
V_m:	Molar volume of the solvent [m^3/mol]
R:	Gas constant [8.314472 J/mol·K]
T:	Temperature [K]

In effect, they express the affinity between like molecules. Solubility and miscibility are ensured when the Hildebrand solubility parameters of the solvents are similar. However, even Hildebrand solubility parameter provides an insight for the solvent selection, parameter itself is not enough to explain the solvent-water affinity in nanoprecipitation method. For this reason, a further approximation is needed, such as water-solvent interaction parameter. Water-solvent interaction parameter is provided in the following equation:

Eq. 1-4 χ **water -solvent =** $(V_{solvent} / RT) \times (\delta solvent - \delta water)^2$

where:

χ water –solvent:	Water solvent interaction parameter
Vsolvent:	Molar volume of the solvent [m^3/mol]
R:	Gas constant [8.314472 J/mol·K]
T:	Temperature [K]
δ solvent:	Hildebrand solubility parameter for solvent [$(MPa)^{1/2}$]
δ water:	Hildebrand solubility parameter for water [$(MPa)^{1/2}$]

Generally, it is expected that solvents having high affinity for water (low χsolvent-water values) tend to promote solvent diffusion and solute partition into the aqueous phase, thus lead to formation of smaller nanoparticles.

1.2 Nanoparticle characterization techniques

Characterization of nanoparticles provides a better understanding of the system which is the first requirement for optimization of such systems. Different techniques can be employed to predict the behavior of the nanoparticles under physiological conditions, distribution in the body or fate of nanoparticles in the body.

Scanning electron microscopy (SEM) and **Transmission electron microscopy (TEM)** are usually employed for determination of particle size and morphological properties, such as crystal structure and shape. Even both of the techniques provide descriptive information about the individual nanoparticles; they don't provide quantitative information about the total population. **Atomic force microscopy (AFM)** can provide 3D visualization of the nanoparticles and may provide information about size, morphology, surface properties and roughness [64].

Dynamic light scattering (DLS) technique is ideally suitable for determination of particle sizes and size distributions in nanometer range. Nanosuspensions show random movements of the nanoparticles induced by collisions with the solvent molecules that are moving due to their thermal energy and undergo Brownian motion. When nanosuspensions are subjected to laser beam, the intensity of the fluctuated light depends on the particle size. Smaller particles move more rapidly when they collide with solvent molecules. These intensity fluctuations can be used to determine the Brownian motion in a medium of known viscosity and accordingly particle size by employing Stokes-Einstein relationship provided below [65].

Eq. 1-5 $$D = \frac{k_B T}{6\pi\eta R}$$

where;

D:	Diffusion constant
k_B:	Boltzmann`s constant
T:	Absolute temperature
η:	Viscosity
R:	Radius of the spherical particle

Nanoparticles dispersed in aqueous systems can acquire a surface charge. The liquid layer surrounding the particle exists as inner region (Stern layer) where ions are strongly bound and an outer (diffuse) region where they are less firmly associated. Within the outer region there is a boundary in which ions and particles form a stable entity. When a particle moves, ions within the boundary also move. Those ions beyond the boundary stay with the bulk dispersant. The potential at this boundary is called the zeta potential. Zeta potential measurements can be employed to determine the surface charges. When an electric field is applied to the nanosuspension, particles migrate towards the electrode of opposite charge with a velocity proportional to the magnitude of the zeta potential. This migration in a dispersant of known viscosity is determined with the frequency shift of the laser mean and converted to zeta potential by applying the Smoluchowski equation [65].

Eq. 1-6 $$\zeta = \frac{4\pi\eta}{\varepsilon} \times U$$

where;

ζ:	Zeta potential
η:	Viscosity
ε:	Dielectric constant
U:	Electrophoretic mobility

If the particles in suspension have a large (-) or (+) zeta potential, they repel each other and flocculation is not expected. However, if the zeta potential values are low, there will be no force preventing them to come together and flocculate. The magnitude of the zeta potential gives an indication of the potential stability of the colloidal system. Particles with zeta potentials more positive than +30 mV and more negative than -30 mV are considered as stable, whereas a zeta potential value between +30 and -30 mV indicates unstable systems [65].

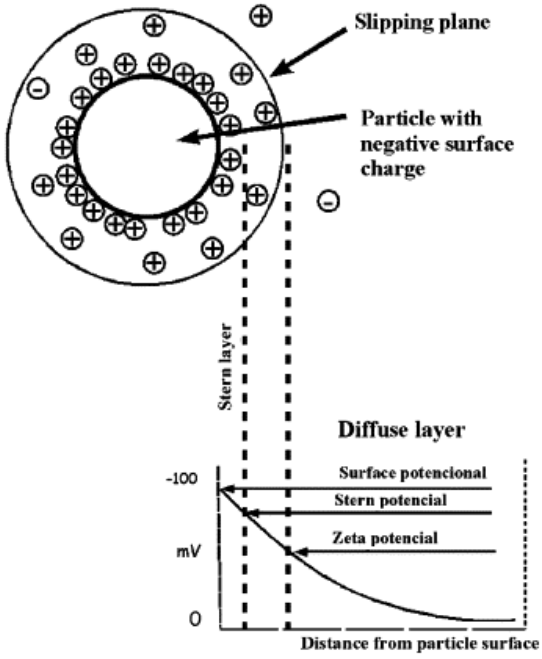

Fig. 1-2: Zeta potential of particulate systems [65]

Factors affecting the zeta potential are pH and conductivity. Depending on the zeta potential value, addition of like ions would lead the particles to acquire more of that charge, whereas addition of counter ions would lead to a drop in zeta potential value. For example, to a colloidal system possessing negative zeta potential value, addition of acid will lead to a drop in the zeta potential value. If the necessary amount of acid is added to neutralize the system, zeta

potential value will reach zero (isoelectric point), where the colloidal system is least stable. Further addition of acid would lead to build up a positive zeta potential. Ionic strength of the medium affects the double layer thickness, since it depends on the concentration of ions in the solution. The higher the ionic strength, the more compressed the double layer becomes.

1.3 Microchannel reactor technologies

Traditional nanoprecipitation method uses so-called bench-top methods where nanoparticle preparations are performed in beakers while realizing mixing with magnetic stirrers. When this approach is used, mixing rate cannot be controlled efficiently. Additionally, nucleation and growth processes which are affected by concentration and temperature gradients are not reproducible as a result of lack of control on those processes. Since particle size and size distribution are directly determined by those parameters, it can be concluded that bench-top nanoprecipitation methods suffer from lack of controllable factors which in turn are the key factor of production of nanoparticles with desired physicochemical properties.

In order to overcome that bottleneck, microreactors have been used by many researchers because of a variety of advantages they provide over bench-top methods. Mixing realized in reduced scale provides shorter mixing times which ensure narrow particle size distribution as a result of controlled nucleation and growth process. Additionally, as a result of the reduced scale provided by microreactors amount of solvents are minimized and consequently amounts of toxic or expensive solvents used are minimized. Increased available reaction surface to volume ratio of microreactors provides enhanced heat and mass transfer in comparison to bench-top methods. Efficient mixing in the micro scale and enhanced mass/energy transfer promotes preparation of monodisperse nanosupensions [66]. The use of microfluidic devices for nanoparticle synthesis is also advantageous in other aspects, including enhanced processing accuracy and efficiency; flexibility for multi-step platform design [67].

Continuous flow microreactors and segmented flow microreactors can be categorized as two main categories of microreactors. In addition to advantages described above, continuous flow microreactors enable changing chemical composition of the mixture continuously. Segmented flow microreactors, on the other hand, eliminates axial dispersion (back mixing) as a result of self-recirculation of flow [68].

Low Reynolds number in continuous microchannels indicates laminar flow properties. Absence of turbulence causes molecular diffusion to predominate the mixing, thus bigger nano-

particles are obtained as a result of long mixing times. Laminar flow also leads to a wide range of residence times, causing higher PDI values [66]. For this reason, tuning the mixing is an important goal in microreactors, when employed for nanoparticle preparation. Rapid and efficient mixing can be achieved by introducing impinging jets. Confined impinging jet (CIJ) consist of two opposing high velocity fluid jets that collide in confined area of microreactors [69]. Producing a region of high turbulent energy dissipation and ensuring that jet streams pass through the high intensity region without bypassing are the two main requirements of achieving rapid mixing. By this way proper scale of being mixed and the desired molar flow ratios are preserved during the rapid mixing process. A high energy dissipation occurs for impinging jets because the kinetic energy of each jet stream is converted into a turbulent-like motion through a collision and redirection of the flow in a very small volume [66]. As an outcome of the high feed velocities and small reactor volume, CIJ reactor residence time is very small [70]. Since short residence times result in lower PDI values, this property of CIJ reactor makes it a good candidate for manufacturing nanoparticles with defined particle size and narrow particle size distribution.

Microjet reactor (MJR) provides a confined micro scale collision chamber for impinging jets, which promotes nanoparticle formation by contributing to interfacial turbulence formation. Mixing rate and efficiency of the mixing in confined impinging jets can be controlled with flow characteristics such as flow rate, Reynolds number and mixer geometry [71].

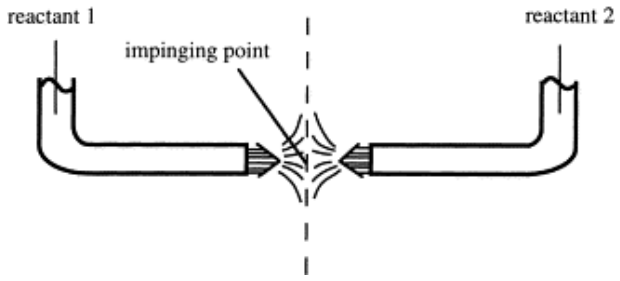

Fig. 1-3: Schematic presentation of impinging jet mixing [72]

In order to control the nucleation and growth during nanoparticle preparation, it is important to achieve mixing time shorter than the formation time which is a combination of nucleation formation time and growth time [60]. These conditions are also easily achieved by confined impinging jets, since the kinetic energy of the jets are converted into a turbulent like motion through the collision in micro liter scale [69]. This high energy dissipation promotes nanoparticle formation as previously described in Section 1.1.2.

MJR technology can serve for nanoparticle preparation under controlled conditions by taking advantages of micro scale mixing. It has been shown that rapid micromixing is required for narrow particle size distributions of the produced particles [69]. Johnson et. al. have shown that characteristic mixing time for turbulent CIJs depends on the velocity of impinging jets, viscosity of the solutions, and geometric shape of the reactor. In confined impinging jets, the chamber size also affects the process performance of the mixer [69].

The time required for micromixing can be calculated using the formula given in Eq. 1-7 [73].

Eq. 1-7

$$t_m = k_m' \sqrt{\frac{n}{e}}$$

where;

t_m:	Micromixing time (s)
k_m:	Mixing constant
ν :	Kinematic viscosity (m^2/s)
ε:	Turbulent energy dissipiation (W/kg)

In a stirred tank, which is normally used for the conventional way of nanoprecipitation, micromixing time τ_m is found to be 5-50 ms. In an aqueous solution, the value of the nucleation induction time is usually on the order of 1 ms or less, therefore mixing time of 5-50 ms lies above the nucleation induction time which will result in difficulties in controlling the particle size and distribution as well as the scale up process [73]. In the MJR the mixing time is under 0.1 ms which is lower in comparison to the nucleation induction time that creates the required environment for the production of nanoparticles with narrow size distributions as well as the ability to scale up the process.

1.4 Nanoparticles for oral applications

When a new chemical is being developed, the first target of a formulation scientist would be to exploit the oral route. Often a quick test to evaluate the oral bioavailability of the new chemical entity (NCE) is to fill the drug into hard gelatine capsules along with lactose as this constitutes the simplest formulation that could be developed for oral administration. Summary of the polymer based drug delivery systems regarding to the GIT mucosa can be found in Tab. 1-1 [22].

GIT provides a variety of barriers, including proteolytic enzymes in gut lumen and on the brush border membrane, mucus layer, gut flora and epithelial cell lining, to the delivery of drugs. Factors which govern the uptake of particles from the gut include particle size, physico-chemical nature of particles, surface charge and attachment of uptake enhancers such as lectins or poloxamer. After oral administration of nanoparticles, they could (i) be directly eliminated in the faeces, (ii) be adhering to the cells (bioadhesion) and /or, (iii) undergo oral absorption as a whole. Oral absorption of the nanoparticles results in passage across the gastrointestinal barriers and delivery of the payload into the blood, lymph and other tissues. Before this translocation can occur, the nanoparticles have to adhere to the surface of the intestine. Translocation of particles across the gastrointestinal wall can occur due to intracellular uptake by the absorptive cells of the intestine or paracellular uptake (i.e. between the cells of the intestinal wall), or phagocytic uptake by intestinal macrophages, or uptake by the M cells of the Peyer's patches [22].

Tab. 1-1: Drugs and polymers previously formulated as for oral drug delivery [22].

Site of action	Incorporated compound	Polymer employed	Size (nm)	Ref
Oral cavity	FITC	Poly(propylcyanoacrylate)	100-900	[19]
	N/A	Lectin-Gliadin	500-600	[74]
Stomach	Carbazole	Gliadin	400-500	[75]
	Amoxicillin	Gliadin	250-400	
	pCMV-lacZ	PLGA	>200	
Small intestine	Streptomycin	Chitosan	50-500	
	Theophylline in depot tablets	PLGA	200-260	[76]
	Tetanus toxoid	Poly(ethyleneglycol-Poly(lactic acid)	150-170	[77]
	Indomethacin	PLGA	100-200	[78]
	Carbon-14	Poly(methyl methacrylate) (PMMA)	100-160	[79]
	5-Fluoroudine	Poly(methylvinylether-co-maleic anhiydride)	200-250	[80]
	RBITC	PLGA	200-300	[80]
	Vancomycin	PEO-PPO	100-200	[78]
	Iodine-125	Sulfobutylated-poly(vinyl alcohol)-PLGA	50-3000	[81]
	Valproic acid	PLGA	100-200	[78]
	pCMV-lacZ	PEO-PPO	150-190	[82]
	N/A	Sulfobutylated-poly(vinyl alcohol)-PLGA	100-130	[83]
	Phenobarbital	PLGA	100-200	[78]
	Amifostine	PLGA	200-300	[84]
	H.pylori lysate	PLGA	300-400	[85]
	DNA	Chitosan	50-75	
	pCR3Arah2	Chitosan	100-1000	
	mEpo gene	Chitosan	70-150	[86]
	Rifampicin	Lectin-PLGA	300-400	[87]
	Pyrazinamide	Lectin-PLGA	300-400	[87]
	Ketoprofen	PLGA	100-200	[78]
	Isoniazid	Lectin-PLGA	300-400	[87]
	Calcitonin	Poly(N-isopropylacrylamide)	148-895	[88-90]
		Poly(Nvinylacetamide)	148-895	[88-90]
		Poly(t-butyl methacrylate)	148-895	[88-90]
		PLGA	200-400	[91]
Site of action	**Incorporated compound**	**Polymer employed**	**Size (nm)**	**Ref**
	Heparin	PCL (Polycaprolactone)	270-300	[92]
		PLGA	250-270	[92]
		Eudragit RS and SL	250-280	[92]
	CyA	Poly(methacyrilic acid methacrylate)	30-110	[93]
		Chitosan	50-60	[74]
		Gelatin	150	[94]
		PLGA	140	[94]
		PCL	100-200	[78]
		Eudragit RS and RL	100-130	[95]
			170-310	[96]
	Fluorescein	Polysteren	50-3000	
		Polysteren+poloxamer 188 and 407	60	
Large intestine	Fluorescent dye	Polysteren	100-1000	[97]
	Rolipram	PLGA	300-500	[98]

Jani et al [81] have shown that particle size plays a major role in the uptake of particles. They measured uptake by using radiolabeled polystyrene nanoparticles ranging from 50 nm to 3.0 µm. They have been able to show that lower size particles (50 nm particles showed a 12% uptake by the cells of the small intestine) are taken up at a higher rate by the small intestine when compared to the larger particles (1 µm particles showed only 1% uptake by the cells of the small intestine). The lower size particles (<500nm) were detected in blood after intestinal uptake whereas larger size particles (>500nm) were not detected in blood. Also, these nanoparticles were detected in other tissues such as liver and spleen. A low surface charge on the surface of nanoparticles is desired for good absorption. While Pluronic F127® or poloxamer (188 and 407) coating onto the surface of 50 nm polystyrene nanoparticles inhibited uptake in the small intestine, a similar coating on the 500 nm polystyrene nanoparticles showed an increased intestinal uptake. There has been yet another report to study the effect of surface modification on the uptake of polymeric nanoparticles using 14C-labeled poly (methylmethacrylate) (PMMA), having a mean size of 130 nm and coated with polysorbate (Tween® 80 or poloxamine 908) [81]. These nanoparticles were administered orally to rats and they were checked for their organ distribution. High radioactivity levels were observed in the stomach contents, below 5% radioactivity was detected in the stomach wall for the coated particles. Highest amount of radioactivity (about 40%) was found in the small intestine, confirming that these coated particles were absorbed in the small intestine. Developments in the field of polymer science have made the delivery of proteins and peptide drugs via the oral route possible, by protecting these molecules against pH/enzyme-induced degradation and also by prolonging the time of delivery to the mucosal sites [88-90].

Cyclosporine A (CyA) is another peptide which has been studied for transport to the gastrointestinal tract using polymeric nanoparticles via the oral route. CyA is a potent immunosuppressive agent and is widely used for the inhibition of graft rejections in the transplant of organs such as heart, liver, skin, lungs, kidney, etc. It is also prescribed in autoimmune diseases such as rheumatoid arthiritis and Bechet's disease [94, 99]. Although various formulations of CyA such as Neoral®(solution), Sandimmune® (microemulsion) and SangCyA® (amorphous nanoparticles) are being marketed, they are faced with the problem of variable bioavailability, and the patient has to be monitored for the blood levels of CyA during the regimen [74]. One of the earlier efforts to improve the bioavailability of CyA was done by preparation of pH sensitive nanoparticles using poly (methacrylic acid and methacrylate) copolymer (Eudragit®) [93]. The results were compared with Neoral® (a universal standard for CyA oral bioavailability)

formulation in rats. Nanoparticles exhibited drug entrapment of >90% for different formulations prepared from different types of Eudragit® systems. CyA nanoparticles prepared from Eudragit® SI 00, an anionic polymer, demonstrated the highest relative bioavailability of 132% with respect to Neoral®. Other polymeric nanoparticles also exhibited more than 110% relative bioavailability, except for nanoparticles prepared from Eudragit® E100 (CyA-E100) which is a cationic polymer. In vitro release studies of CyA from different nanoparticle preparation illustrated that all nanoparticle preparation showed pH-specific release of CyA at pH 7.4, except for CyA-El00 nanoparticles which released the whole payload at pH 2.0. This proves that major CyA from CyA-El00 was released in the stomach upon oral administration accounting for its low relative bioavailability with respect to other nanoparticle preparations.

In another study, Wang et al [74] examined hydroxypropyl methylcellulose phthalate (HPMCP) polymer nanoparticles loaded with CyA for oral delivery. HPMCP is a common enteric coating excipient used in the pharmaceutical industry for the enteric coating of the tablets. It dissolves specifically at a pH of 7.4 and releases the contents in the lower intestine. The investigators used two different CyA nanoparticle preparations made from different molecular weight of the same polymer. Again, a high encapsulation efficiency of over > 95% was observed with the nanoparticle preparation, due to hydrophobicity of the drug. CyA nanoparticles made of high molecular weight HPMCP exhibited a relative bioavailability of greater than 115%, and the ones made from lower molecular weight exhibiting only 82% relative bioavailability against Neoral®. The results from the above studies indicate that pH-sensitive nanoparticles loaded with CyA can be designed as new carriers for CyA, which exhibit a better pharmacokinetic profile compared with the currently marketed CyA formulations. Nanoparticles made from cationic polymers have been explored as surface coatings to improve the oral bioavailability of CyA.[94]. Male beagle dogs were orally administered with CyA nanoparticles coated with chitosan as the poly cationic surface modifier. From the results obtained, it was observed that chitosan coated drug nanoparticles showed the highest relative bioavailability of 173% with respect to Neoral® oral solution. The results were attributed to two properties of the system: (i) cationic polymer facilitated the electrostatic interaction with the negatively charged mucosa, and (ii) chitosan coated CyA nanoparticles facilitated the opening of the tight junctions of the epithelial cells, thus augmenting the paracellular transport pathway. A series of investigations have been directed towards preparation and evaluation of bioavailability and toxicity profile of CyA-loaded polycaprolactone nanoparticles. The nanoparticles, having a diameter of ~100nm were prepared by solvent-evaporation procedure and evaluated for bio-

distribution, immunosuppressive activity and nephrotoxicity. Sandimmune® was used as the standard for this investigation in rats following oral administration. A significantly higher tissue (especially kidney) concentration of CyA was achieved with nanoparticle formulations, compared with the solution indicating probability of a higher nephrotoxicity. However, further toxicological evaluation with kidney function tests indicated no difference in the profiles of the two formulations. In vitro lymphocyte proliferative activity (an indication of immunosuppressive potential) also showed better activity for nanoparticle formulations of comparable doses. The conclusion of the investigation was that the nanoparticle formulations can be effective at lower dose levels, compared with the solution form and thus may help to reduce drug-associated tissue damage. Cho et al . developed several different oral CyA nanoparticle formulations consisting of one alkanol solvent and a polyoxyalkylene surfactant, and tested them in rats for their bioavailability in comparison to Sandimmune® oral solution. Selected formulations based on these pre-clinical investigations were further tested for their pharmacokinetic profile in humans. 48 healthy males were chosen and a randomized, double-blinded, three-way crossover study was conducted with Sandimmune® oral solution as standard formulation. From the results obtained, it was observed that CyA nanoparticles exhibited a C_{max} which was twice as high as those achieved by Sandimmune® oral solution and the T_{max} was much shorter for CyA nanoparticles compared with the standard one. Also, the area under curve (AUC) observed for nanoparticle formulations was significantly higher than the standard formulation.

Spray-dried PLGA nanoparticles have been investigated for the oral delivery of amifostine [84]. Amifostine is an organic thiophosphate prodrug and is dephosphorylated by alkaline phosphatase in the tissue to the active free thiol metabolite. The major drawback of the drug is that it cannot be administered orally in an active form and when administered systemically, it is rapidly cleared from the body. PLGA nanoparticles containing amifostine were administered to mice orally and tissue distribution was monitored for the administered dose. Within 30 min postoral administration, the drug was detected in almost all the tissues including blood, brain, spleen, kidney, muscle and liver [84].

Popescu et al. have proposed the use of biodegradable nanoparticles, prepared from naturally occurring polymers such as chitosan, dextran sulfate, dermatan sulfate, chondroitin sulfate, keratin sulfate etc. for oral delivery of highly cationic active compounds which are highly hydrophilic and could be substrates for P-glycoprotein (Pgp). Such active compounds include the

likes of aminoglycosides, polypeptides, proteins, terefenamate, proglumetacin, tiaramide, apazone, etc. Currently, there are no technologies for delivery of hydrophilic, cationic drugs by oral administration. As an example, streptomycin, which was loaded to chitosan nanoparticles and tested for *in vivo* efficacy using *M. tuberculosis* infected mice. Streptomycin was successfully loaded with an encapsulation efficiency of 50% or higher, with a minimal drug loading of 30% w/w of polymer. After oral administration of these chitosan nanoparticles in mice an one log reduction in colony-forming units of the bacilli was achieved, compared with the control group. These results show that the nanoparticles-based technology can be a breakthrough for the oral administration of aminoglycoside antibiotics, which are otherwise inactive via oral route.

1.5 Formulation of nanoparticles for oral drug delivery

Nanoparticles are generally created in aqueous environments. If the nanoparticle suspension is proven to be stable in liquid form it can be administered directly as suspensions, if not lyophilisation is the most preferred technique. Lyophilisation of the nanoparticles usually obtains cryoprotectants such as mannitol to reduce the adverse effects of lyophilisation in the physicochemical properties of nanoparticles. In such cases the nanoparticles can be obtained as free flowing powders and directly formulated as hard gelatine capsules with a standard diluent like lactose [22].

It is also possible to formulate this free flowing powder as tablets but the point that should be considered in this process is the adverse effects of applied pressure during compression of the tablets on the physicochemical properties of nanoparticles [22].
Another commonly used formulation is the soft gelatine capsules. In this case nanoparticles are dispersed in oil and loaded into the gelatine capsules [22].

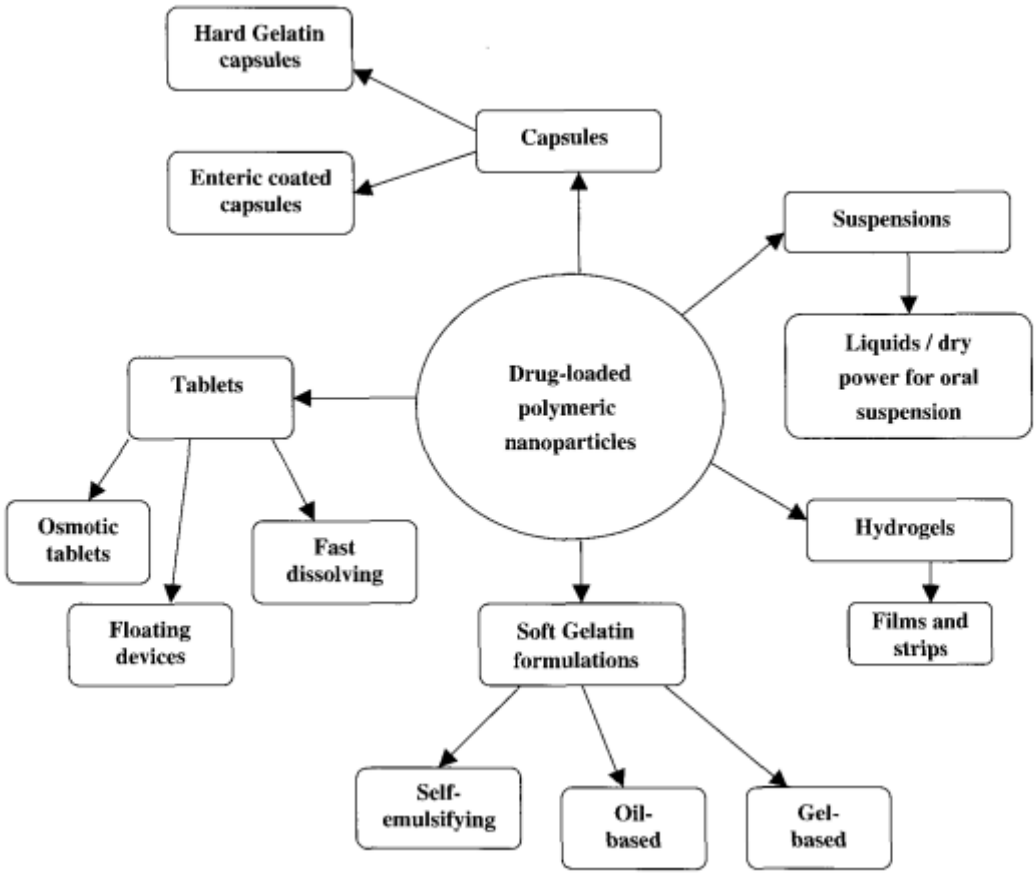

Fig. 1-4: Formulation of nanoparticles [22].

1.6 Design of experiments

Design of Experiments (DoE) enables simultaneous determination of the individual and interactive effects of many factors that could affect the output results in any process. In a traditional experiment, one or more process variables (factors) are changed sequentially in order to observe the effect of the changes made on one or more response variables. Minimizing the number of experiments is always an aim when time consumption and cost are taken into consideration. With DoE, the number of experiments is kept as low as possible in a way by which the most informative combination of the factors is chosen. DoE is an efficient procedure for planning experiments so that the data obtained can be analysed to yield valid and objective conclusions [100].

Two types of variables are employed in DoE: factors and responses, namely input and output. Factors can be categorized into controllable and uncontrollable factors. Controllable factors are observed by the experimenter and can be manipulated, whereas uncontrollable factors are difficult to be regulated since they are usually external factors or noise effecting the sys-

tem or process. Response of a system can change as a result of both of those factors alone or in combination and those effects can be measured based on response(s). A response is the general condition of a studied system during the change of the factors. It is possible to measure multiple responses that react differently on the factor manipulations. Factors can be either quantitative or qualitative. Quantitative factors have a scale whereas qualitative factors have only distinct properties or values in some cases [101, 102]. Experimental designs allow evaluation of both types of factors within one design. However, using both factors in the same design results in multiplication of the number of runs generated by the number of combinations of the qualitative factor levels.

DoE experiments provide estimation of reality with the help of mathematical equations. System in reality is represented in the designs as factors and responses. DoE begins with setting the objectives and selecting the possible factors that might have an effect for the chosen process. Prior to experiments, an experimental design is assigned as detailed experimental plan. Chosen design plays an important role on the investigation.

An experimental design can serve effectively for choosing between alternatives, selecting the key factors affecting a response, optimizing responses when factors are proportions of a mixture or response surface modelling. The choice of an experimental design depends on the objectives set and the number of factors to be investigated. In order to select or screen out the few important main effects from the many less important ones, *screening designs* are used to determine the key factors that are "significant". If the factors are proportions of a mixture and the "best" proportions of the factors are investigated to maximize or minimize a response, then a *mixture design* is used [103]. *Response surface design* serves to

- hit a target
- reduce variability
- maximize or minimize a response
- make a process robust
- seek multiple goals
- regression modelling

Once the objective is assigned statistical design to be used should be chosen. Three main types of statistical designs can be named for different features and application areas: full factorial designs, fractional factorial designs and composite designs. Full or fractional factorial

designs are usually used for screening designs, whereas composite designs are suitable for response surface designs.

If the number of factors to be evaluated for response surface designs is between 2 and 4, Box-Behnken design or central composite design is preferred. General geometric representation of Box-Behnken and central composite designs for three factors are provided in Fig. 1-5**.** Both methods contain a set of center points (shown with black balls). In addition to center points, central composite design contains a set of axial points which are identical to the center points except for one factor, which will take on values both below and above the median of the two factorial levels, and typically both outside their range (shown with red stars).

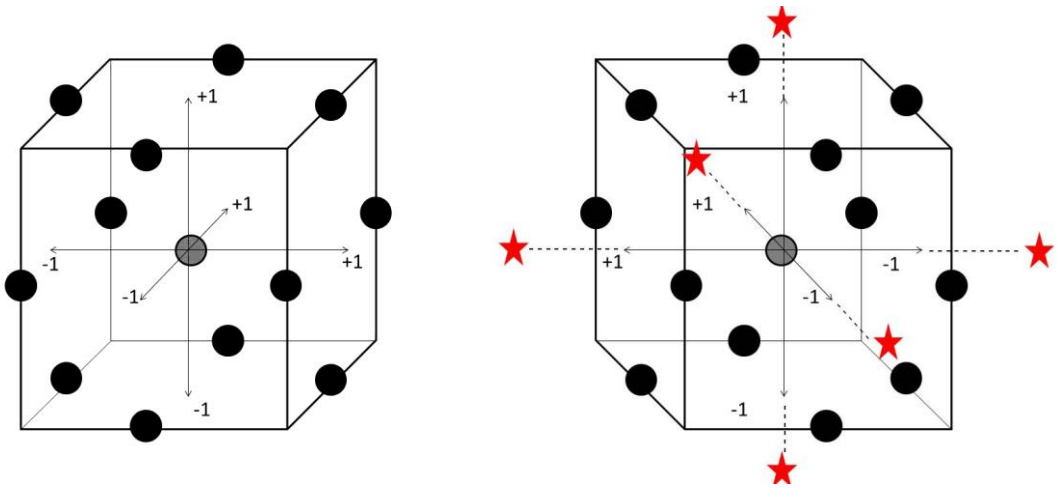

Fig. 1-5: Box-Behnken Design and Central Composite Design for three factors

Experimental region gives these three designs a uniform geometrical form and makes them easy to handle. In cases where the experimental region has an irregular shape, then designs described above cannot be applied. Under these kind of conditions, D-optimal designs are used [100]. D-optimal design matrices are usually not orthogonal and effect estimates are correlated. . D-optimal designs are straight optimizations based on a chosen optimality criterion and the model that will be fit [103]. In other words, D-optimal will create a custom design based on the type of polynomial that you want to fit.

Experimental designs may be carried out in blocks, which serve to remove or minimize the expected variation caused by some change during the course of the experiment, such as different days of experiments or different batch of material. Blocking schemes vary depending

on the design and the number of factors. One block indicates no blocking. Blocking is a restriction on the randomization of the experiment which is used to reduce the error. Unidentified time-based effects could influence the results of the experiment when randomization is restricted. However, when applied correct, blocking and randomization provide reliability to the design against trends.

Once the design is selected and executed, data is examined for outliers. A fit model is created from the data. The model is evaluated using stepwise regression methods and/or parameter p-value significance information. Once the method is established, the model is tested and validated using the residual graphs. Depending on the outcomes of the fit graph, new designs might be necessary to achieve the set objective.

1.7 Aims of thesis

1.7.1 MJR components and theory

MJR uses impinging jets, consisting of two high velocity (100 m•sec^{-1}) linear fluid streams. As a result of rapid collision, the kinetic energies of the jets are directly converted to the construction of solvent/non-solvent interface, forming turbulent like motion in the collision chamber. This results in the diffusion of the solvent into non-solvent together with the polymer and drug molecules. Finally polymer molecules suddenly precipitate and trap the drug inside. The nanosuspension is then pumped out of the reactor with gas flow, which is applied perpendicular to the streamlines.

It has been showed that rapid micromixing is required for narrow particle size distributions of the produced particles [4, 69]. The time required for micromixing can be calculated using the formula given in Eq. 1-7 [73]:

In a stirred tank, which is normally used for the conventional way of nanoprecipitation, micromixing time τ_m is found to be 5-50 msec. In an aqueous solution, the value of the nucleation induction time is usually on the order of 1 msec or less therefore mixing time of 5-50 msec lies above the nucleation induction time which will result difficulties in control of the particle size and distribution as well as the scale up process [73]. In the MJR setup the mixing time is under 0.1 ms which is lower in comparison to the nucleation induction time that creates the required environment for the production of nanoparticles with narrow size distributions as well as the ability to scale up the process.

Up to date microjet reactor has been used successfully for applications such as production of $BaSO_4$ and ZnO_2 nanoparticles [104].

1.7.2 Selection of the substances

Selection of the model drugs

Nanoparticle preparation experiments were conducted with three drug molecules: Danazol, Gliclazid and Fenofibrate.

Danazol is a synthetic steroid with antigonadotropic and anti-estrogenic activities that acts as an anterior pituitary suppressant by inhibiting the pituitary output of gonadotropins. It possesses some androgenic properties. Danazol has been used in the treatment of endometriosis and some benign breast disorders, as well angioedema. It is a hydrophobic drug with a high permeability and slight water solubility which makes it a good candidate for nanoparticle production in order to increase the bioavailability through increase in the solubility. Physicochemical properties of Danazol are provided in Tab. 1-2.

Tab. 1-2: Physicochemical properties of Danazol [105, 106]

Molecular structure	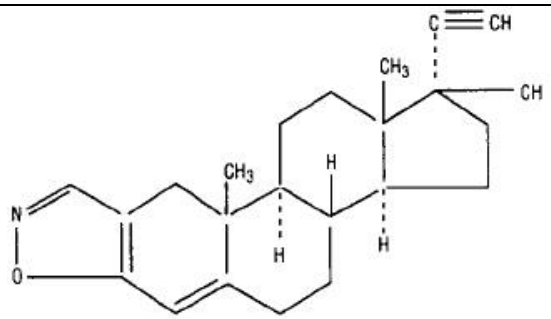
Formula	$C_{22}H_{27}NO_2$
Molecular mass	337.5 g/mol
Solubility in water	0.4 µg/ml
Solubility in EtOH	> 1 mg/mL
Solubility in THF	> 7 mg/mL
Log P (water/octanol)	4.5
BCS classification	Class II

Gliclazide is an antidiabetic agent and is classified as a sulfonylurea. Although it has a higher solubility compared to Danazol, it is classified as Class II according to the BCS classification

with a low solubility and high permeability. Thus bioavailability of Gliclazide can also be enhanced through nanoparticle form of the API.

Tab. 1-3: Physicochemical properties of Gliclazide [107-109]

Molecular structure	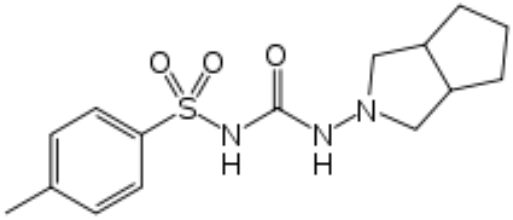
Formula	$C_{15}H_{21}N_3O_3S$
Molecular mass	323.4 g/mol
Solubility in water	200 µg/ml
Solubility in EtOH	1-10 mg/mL
Log P (water/octanol)	2.51
BCS classification	Class II

Danazol and Gliclazide have water solubilities of 0.4 µg/mL and 200 µg/mL and log P values of 4.5 and 2.51, respectively. These values show that Gliclazide is relatively hydrophilic compared to Danazol which gives the opportunity to study the differences between the requirements of hydrophilic and lipophilic molecules in terms of nanoparticle preparation with MJR.

Fenofibrate is an antilipemic agent which reduces both cholesterol and triglycerides in the blood. It is classified as Class II according to the BCS classification with a low solubility and high permeability.

Tab. 1-4: Physicochemical properties of Fenofibrate [110, 111]

Molecular structure	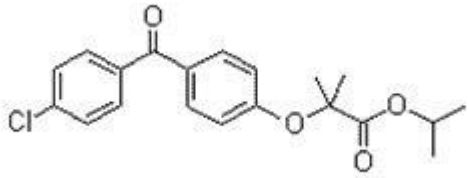
Formula	$C_{20}H_{21}ClO_4$
Molecular mass	360.8 g/mol
Solubility in water	250 µg/ml
Solubility in EtOH	46 mg/mL
Log P (water/octanol)	5.3
BCS classification	Class II

Selection of the pharmaceutical excipients

Selection criteria for the excipients that will be used as stabilizers are determined as follows

- The excipient should be soluble either in the organic phase (ethanol, THF) or in the water phase. This will enable the creation of loaded nanoparticles since the MJR system is based on the solvent/non-solvent precipitation methods. When the exipient is soluble in one of the phases it will be possible to create nanoparticles from the excipients integrated on the surface of the substance
- The excipient should be stable in temperatures between 25-80 ° C
- The excipients should not swell or agglomerate in contact with one of the solvents that will result in blockage of the MJR.
- Available for oral drug delivery

Chitosan is a cationic polymer used in drug formulations. Partial deacetylation of chitin results in the production of chitosan which is a polysaccharide comprising copolymers of glucoseamine and N-acetylglucoseamine [112]. Mechanism of action of chitosan was suggested to be a combination of bio-adhesion and a transient widening of the tight junctions between epithelial cells [41]. Chitosan is not soluble in any organic solvents.

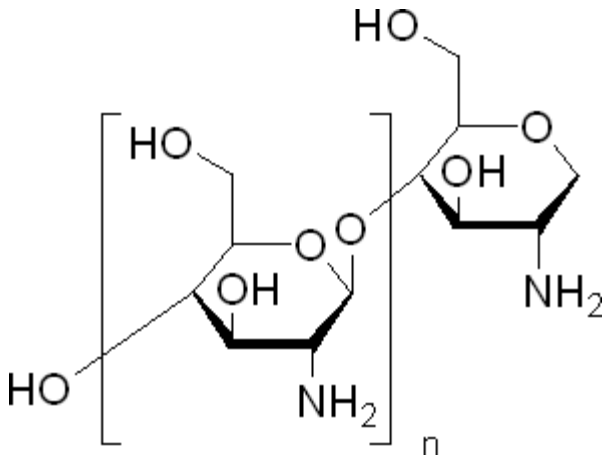

Fig. 1-6: Molecular structure of chitosan

Chitosan is used in cosmetics and is under investigation for use in a number of pharmaceutical formulations. The suitability and performance of chitosan as a component of pharmaceutical formulations for oral drug delivery applications has been investigated in numerous studies. These include controlled drug delivery applications, use as a component mucoadhesive dosage forms, rapid release dosage forms, improved peptide delivery, colonic drug delivery systems and use for gene delivery [112].

Eudragit derivatives are polymers of methacrylic acid and ethyl acrylate in different ratios. These are primarily used in oral capsule and tablet formulations as film coating agents. Depending on the type of polymer used, films of different solubility characteristics can be produced. Eudragit L and S referred to as methacrylic acid copolymers in the USPNF20 monograph are anionic copolymerization products of methacrylic acid and methyl methacrylate with the ratio of free carboxyl groups to the ester approximately 1:1 in Eudragit L and approximately 1:2 in Eudragit S. These 2 polymers are used primarily for enteric coating and are soluble in intestinal fluids pH > 7. [112]. Eudragit S100 is soluble in Acetone, THF, MeOH and EtOH.

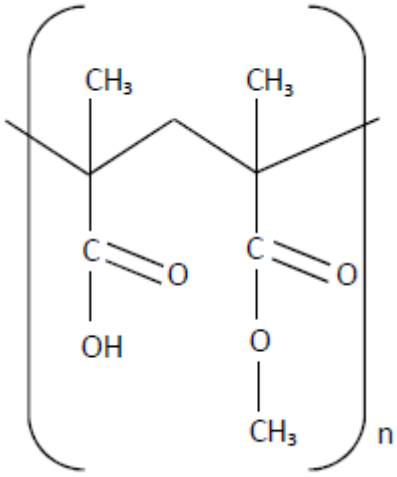

Fig. 1-7: Molecular structure of Eudragit S100 where n=number of repeating units

HPMCP is widely used in oral pharmaceutical formulations as an enteric coating material for tablets or granules. HPMCP is insoluble in gastric fluid but will swell and dissolve rapidly in the upper intestine. The drug release from the HPMCP formulations is based on pH. There are two different types of HPMCP HP-50 and HP-55. This differentiation is based on the viscosity and the molecular weight of HPMCP. Both types are soluble in 1:1 mixture of acetone and ethanol and THF [71]. HPMCP HP50 is soluble in Acetone, Acetone:EtOH 1:1 (w/w) and EtOH:Water 95:5 (w:w) [71].

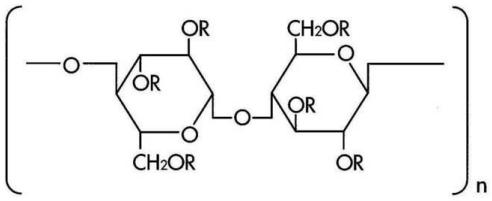

R = -H
-CH_3
-$CH_2CH(CH_3)OH$
-COC_6H_4COOH

Fig. 1-8: Molecular structure of HPMCP HP50 [71].

Eudragit S100 and HPMCP HP50 are conventionally used as enteric coating agents since they are not soluble in pH lower than pH 5.5.

1.7.3 Research objectives and dissertation outline

The aim of the project was the establishment of a continuous production system using microjet reactor technology, which is based on nanoprecipitation method for the production of nanoparticles. In the establishment of the microjet reactor system different parameters such as flow rate, temperature, pressure and solvent were evaluated in order to efficiently control the particle properties such as particle size, PDI and drug loading efficiency. Furthermore a novel oral drug delivery system was developed which consists pH controlled positively charged nanoparticles which show resistance to gastric conditions releasing the drug first in intestines and has an affinity to intestinal mucus due to negative charge of the mucus. This novel drug delivery system was optimized using two different designs of experiments to ensure the desired nanoparticle characteristics. Orthagonal rotatable design was used for the optimization of microjet reactor parameters and D-optimal design was used for the optimization of formulation ingredients and their ratio. The in-vitro characterization of this nanoparticle system was done in comparison to conventional nanoparticles.

2. Material and Methods

2.1. Materials

Danazol, Gliclazide, Fenofibrate, chitosan low molecular weight, Pluronic F127, polyvinyl alcohol, polyvinyl pyrrolidone, hydroxypropyl cellulose and hydroxypropyl methyl cellulose were purchased from Sigma Aldrich, Germany. HPMCP HP50 was a gift from Harke Pharma and Eudragit S100 was a gift from Evonik Industries. Other chemicals that were used in this study were analytical grade or higher.

2.2. Methods

2.2.1. Microjet reactor setups

Basically the working principle of microjet reactor is the controlled solvent nonsolvent precipitation. A substance dissolved in solvent is pumped through openings in microjet reactor and meets with nonsolvent, which is also pumped through the opening placed against the solvent channel. The flow rates of solvent and nonsolvent can reach up to 100 m/s which results in a very quick mixing of solvent and nonsolvent. The mixing rate of two streams is 0.1 milliseconds. Thus the mixing time is smaller than the kern building time resulting in production of nanoparticles. Although microjet reactor is a kind of micro-channel reactor there is a difference in the reaction chamber. In case of microjet reactor two streams meet up in a gas filled room and this gas also helps to carry nanoparticles out of the reactor. Thus no clogging observed in microjet reactor.

HPLC pumps (Jasco P-980) were used for the construction of microjet reactor setups due their precision and low pulsation. Furthermore HPLC pumps bring the advantage of ability to work with small volumes due to the absence of dead volume. Nitrogen gas was used as the inert gas which is controlled by a pressure valve and the temperature of gas is controlled by a water bath.

Feasibility studies were conducted for the establishment of microjet reactor for production of drug nanoparticles. For this purpose two different microjet reactor setups were used throughout this study. The main differences between these setups were the temperature control of solvent, non-solvent, microjet reactor and the nitrogen gas and the dimensions of the capillaries. In the first setup the diameter of capillaries was 2.10 mm and no control of

temperature was added for the microjet reactor. In the second design microjet reactor was placed in a water bath and the diameter of capillaries was 0.17 mm. In the Fig 2-1 the setup of microjet reactor is shown.

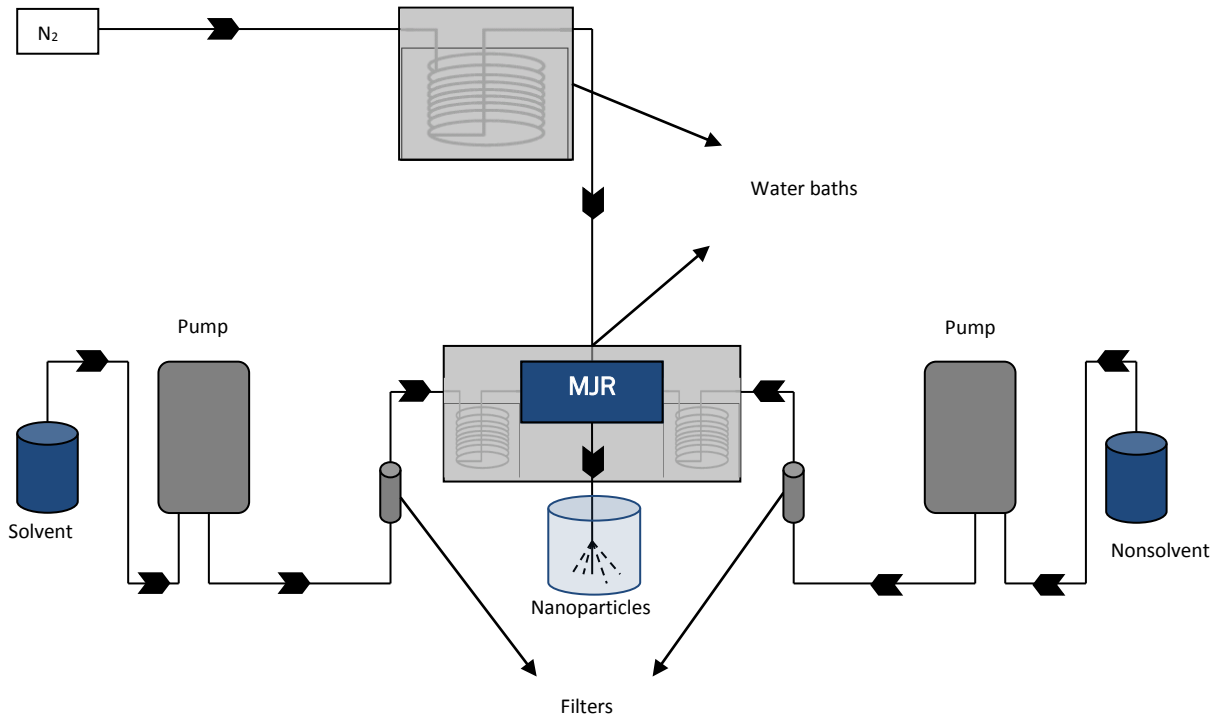

Fig. 2-1 Setup of microjet reactor used for the feasibility study of producing pharmaceutical nanoparticles.

2.2.2. Characterization of nanoparticles

Particle size and ZETA potential determination

Particle size and ZETA potential was determined using dynamic light scattering method. Unless otherwise stated, nanoparticle suspensions were diluted 1:100 with distilled water and particle size and ZETA potential measurements were carried out at 25 °C in distilled water as 3 replicates for all prepared batches. All determinations were done with Nano Zs90 Malvern Instruments, UK

Furthermore scanning electron microscopy (SEM) and transmission electron microscopy (TEM) were used for the determination of the particle size. Scanning electron microscopy

images were taken with a Zeiss EVO HD15 SEM. Diluted nanoparticle dispersions were dried at room conditions on aluminum stubs with carbon discs; the samples were then coated with gold using Quorum Q150R ES sputtering system. In the case of TEM nanoparticle suspension was applied on grids and Poly-Lysin variant B was used as colouring agent. Measurements were conducted with JEOL JEM 2011.

Fourier transform infrared (FTIR) spectrometer

FTIR spectrometer was used to characterize the structure of Fenofibrate containing HPMCP HP50/chitosan nanoparticles in which the interaction of –COOH and $–NH_2$ groups were studied. Thus samples of HPMCP, chitosan and HPMCP HP50/chitosan nanoparticles were measured on a Nicolet 360 FT-IR spectrometer. Samples of pure polymers or nanoparticles were prepared in KBr disks by mixing 2 mg sample in 200 mg KBr. The scanning range was 450–4000 cm^{-1} and the resolution was 1 cm^{-1}.

Differential scanning calorimetry (DSC)

Thermal properties of nanoparticles were studied using differential scanning calorimetry. In this case DSC spectra of Danazol, Fenofibrate and Gliclazide were compared with the polymer nanoparticles of these substances in order to determine if these substances were molecularly dissolved in the polymer. Analyses were realised with a Mettler Toledo DSC-30. Approximately 10 mg of substance or nanoparticle was accurately weighted into a 40 µL hermetic aluminium pan and sealed. A temperature range of 25 °C- 350 °C with a heating rate of 10 °C/min was used for the analyses.

HPLC analytics

Three different HPLC methods were developed and validated for assay determination of Danazol, Gliclazide and Fenofibrate. Perkin Elmer 200 series HPLC with 200 series pump, 200 series autosampler, 200 series Column oven, 200 series UV detector were used in these studies. These methods are given in Tab. 2-1, Tab. 2-2 and Tab. 2-3.

Tab. 2-1 HPLC method for determination of Gliclazide

<table>
<tr><td>Mobile Phase</td><td>A: Methanol

B: Water</td></tr>
<tr><td>Flow</td><td>Gradient 1 mL•min^{-1}
<table>
<tr><td>Time</td><td>Methanol %</td><td>Water %</td></tr>
<tr><td>0.0</td><td>60</td><td>40</td></tr>
<tr><td>4.5</td><td>100</td><td>0</td></tr>
<tr><td>4.6</td><td>60</td><td>40</td></tr>
<tr><td>10.0</td><td>60</td><td>40</td></tr>
</table></td></tr>
<tr><td>Injection Volume</td><td>50 µL</td></tr>
<tr><td>Column</td><td>Lichrospher 100 RP-18 5µm

4 x 125 mm Merck KGaA</td></tr>
<tr><td>Column temperature</td><td>35 °C</td></tr>
<tr><td>Sample tray temperature</td><td>25 °C</td></tr>
<tr><td>UV detection wavelength</td><td>227 nm</td></tr>
<tr><td>Run time</td><td>10 min.</td></tr>
</table>

Tab. 2-2 HPLC method for determination of Danazol

Mobile Phase	A: ACN:MeOH:H_2O (40:30:30 v/v/v %) B: H_2O
Flow	1,5 mL•min^{-1} 70% A 30% B isocratic
Injection Volume	50 µL
Column	Xterra MS C18 5 µm 3 x 50 mm Waters
Column temperature	35 °C
Sample tray temperature	25 °C
UV detection wavelength	287 nm
Run time	5 min

Tab. 2-3 HPLC method for determination of Fenofibrate

Mobile Phase	A: Acetonitrile B: Water pH 2.5 (Phosphoric acid)
Flow	Isocratic A:B 80:20 1mL/min
Injection Volume	100 µL
Column	Symmetry C18, 5 µm, 4.6 x 7.5, Waters
Column temperature	35 °C
Sample tray temperature	25 °C
UV detection wavelength	280 nm
Run time	5 min.

All methods were validation for selectivity, linearity, repeatability, accuracy, precision, and stability. Results are presented in Appendix.

Drug loading efficiency

Drug loading efficiency into nanoparticles was determined in two ways. First nanoparticle suspension was filtered through 1 µm nylon filters and then centrifuged at 16000 g for 45

minutes and redispersed in distilled water before determination of drug loading efficiency. Redispersed nanoparticles were centrifuged again at 16000g for 45 minutes and precipitated nanoparticles were dissolved in the HPLC buffer of each substance for the determination of drug loading ratio. Also the supernatant gathered from the centrifugation step was assayed for drug content. So that recovery was also investigated to find out if there is any microcrystal formation which will be eliminated with filtration through 1 µm nylon filters. The drug loading ratios were calculated from supernatant and dissolved nanoparticles according to Eq. 2-1 and Eq. 2-2 respectively. In Eq. 2-1 drug loading efficiency was calculated from amount of drug dissolved in supernatant. For this purpose concentration found in the supernatant was multiplied with volume of the solution, which was centrifuged and divided, by the theoretical amount of API in this solution revealing percentage of not encapsulated drug. In Eq. 2-2 the drug loading efficiency was calculated same way but this time using the amount of API in centrifuged nanoparticles and its ratio to the theoretical amount of API in solution.

$$\text{Drug loading \%} = 100 - \left(\frac{C_{\text{supernatant}} \times V_{\text{total volume centrfugated}}}{C_{\text{organic phase}} \times V_{\text{organic phase in the solution}}} \times 100 \right)$$

Eq. 2-1

$$\text{Drug loading \%} = \frac{C_{\text{nanoparticles}} \times V_{\text{total volume centrifugated}}}{C_{\text{organic phase}} \times V_{\text{organic phase in the solution}}} \times 100$$

Eq. 2-2

Mucoadhesiveness

In-vitro mucoadhesiveness test were conducted for nanoparticles containing chitosan. 250 mg Mucin was weighted into 250 mL volumetric flask and filled up to volume with water. The solution was vigorously mixed until mucin is fully dispersed. 2ml of nanoparticle dispersion was mixed with 50 ml of mucin dispersion. Incubation was done at RT with magnetic stirrer at

100 rpm. Samples were taken for 3 hours at every 30 minutes and measured for turbidity and ZETA potential[113, 114].

Freeze drying of nanosuspensions

Nanosuspensions were freeze dried prior to drug release tests and stability studies. Firstly organic phase was evaporated under vacuum and aqueous nanosuspensions were supplemented with 3 % lactose as cryoprotectant. Afterwards these suspensions were kept at –80°C for 24 hours and freeze dried for 48 hours until complete dryness.

Drug release studies with drug nanoparticles

Drug release profiles of nanoparticles were studied using different buffers and different methodology. Furthermore in all cases drug release profiles were compared with the drug release profile of the API.

Drug release methodologies for Gliclazide/Eudragit S100 nanoparticles are listed in Tab. 2-4, and Tab. 2-5.

Tab. 2-4 Drug release from Gliclazide/Eudragit S100 nanoparticles using simulated intestinal fluid (SIF)

Apparatus	Paddle USP II
Rotation speed [rpm]	50
Temperature [°C]	37
Medium	SIF pH 6.8 supplemented with 0.5% Tween 20
Volume [mL]	900
Sampling time [min]	2.5, 5, 7.5, 10, 20, 30, 45, 60, 90, 120
Dose [mg]	10

Tab. 2-5 Drug release from Gliclazide/Eudragit S100 nanoparticles using two stage dissolution

Apparatus	Paddle USP II
Rotation speed [rpm]	50
Temperature [°C]	37
Medium	First stage: 0.1 N HCl Second stage: 0.2 M trinatrium phosphate buffer pH 6.8 supplemented with 0.5 % Tween 20
Volume [mL]	First stage: 750 mL Second stage: 250 mL
Sampling time [min]	5, 10, 20, 30, 45, 60, 90, 120, 122.5, 125, 127.5, 130, 140, 150, 165, 180, 210, 240
Dose [mg]	10

Although 0.5 % Tween 20 was enough for the drug release and evaluation of the differences in drug release profiles of Gliclazide and Gliclazide/Eudragit S100 nanoparticles, for Danazol and Fenofibrate 1 % Tween 20 was used to supplement drug release medium since the solubilities of these two substances are lower than that of Gliclazide. Drug release methodologies used for Danazol and Fenofibrate nanoparticles are listed in Tab. 2-6 and Tab. 2-7

Tab. 2-6 Drug release from Danazol/HPMCP HP50 and Fenofibrate nanoparticles using simulated gastric fluid (SGF)

Apparatus	Paddle USP II
Rotation speed [rpm]	50
Temperature [°C]	37
Medium	SGF pH 1.2
Volume [mL]	900
Sampling time [min]	2.5, 5, 7.5, 10, 20, 30, 45, 60, 90, 120
Dose [mg]	10

Tab. 2-7 Drug release from Danazol/HPMCP HP50 and Fenofibrate nanoparticles using two stage dissolution

Apparatus	Paddle USP II
Rotation speed [rpm]	50
Temperature [°C]	37
Medium	First stage: 0.1 N HCl Second stage: 0.2 M trinatrium phosphate buffer pH 6.8 supplemented with 1 % Tween 20
Volume [mL]	First stage: 750 mL Second stage: 250 mL
Sampling time [min]	5, 10, 20, 30, 45, 60, 90, 120, 122.5, 125, 127.5, 130, 140, 150, 165, 180, 210, 240
Dose [mg]	10

In two stage drug release studies first 750 mL 0.1 N HCl was used as medium and samples were taken up to 2 hours. At the end of 2 hours 250 mL 0.2 M trinatrium phosphate buffer pH 6.8 supplemented with 4 % Tween 20 was added to the vessels increasing the pH to 6.8 with a end Tween 20 concentration of 1%.

Furthermore drug release from Fenofibrate nanoparticles and the API was studied using fasted state simulating intestinal fluid (FaSSIF) and fed state simulating intestinal fluid (FeSSIF).

Drug release buffers were prepared from SIF powder (Phares Drug delivery AG). Phosphate buffer for FaSSIF was prepared by dissolving 2.10 g NaOH, 19.77 g of NaH_2PO_4 and 30.93 NaCl in 4.9 liter water followed by adjustment of the pH to 6.5 either with NaOH or HCl and finally filled up to volume of 5 liter. Acetate buffer for FeSSIF was prepared by dissolving 20.20 g NaOH, 43.25 g glacial acetic acid and 59.37 g NaCl in approximately 4.9 liter water followed by adjustment of the pH to 5.0 either with NaOH or HCl and finally filled up to volume of 5 liter. 11.2 g of SIF powder was dissolved in 5 liter of phosphate and let to equilibrate at room temperature for 2 hours for the preparation of FaSSIF and 56 g of SIF powder was dissolved in 5 liter of acetic acid for the preparation of FeSSIF.

USP apparatus II was used for the drug release experiments with a rotation speed of 50 rpm. 10 mg Danazol, Gliclazide or Fenofibrate powder or nanoparticle powder corresponding to 10 mg Danazol, Gliclazide or Fenofibrate were introduced in vessels containing either 500 mL FeSSIF or 500 mL FaSSIF and samples were taken for 120 minutes at time points 2.5, 5, 7.5, 10, 20, 30, 45, 60, 90 and 120 min.

Different sample separation techniques were employed depending of the properties of nanoparticles and drug release media. When API powder was used samples were filtrated through 0.45 µm nylon syringe filters (Puradisc, Whatman) and assayed for substance content. When nanoparticle drug release was investigated in SIF, FaSSIF or FeSSIF medium, samples were filtered through 1 µm nylon disc filters (Puradisc, Whatman), acidified with HCl solution and centrifuged (Universal 320R, Hettich) at 12000 g for 30 minutes. Afterwards supernatants were assayed for substance content. In two stage dissolution, stage I samples were filtrated through 1 µm nylon disc filters (Puradisc, Whatman) and centrifuged (Universal 320R, Hettich) at 12000 g for 30 minutes. In this case since released substance will not be dissolved completely due to the absence of surfactants, precipitated nanoparticles were dissolved in HPLC buffer for each substance and assayed for substance content.

Validation of sample preparation technique was realised with the incubation of drug particles in acidified drug release media for 1 hour and afterwards analysing the supernatant after centrifugation (Universal 320R, Hettich) at 12000 g for 30 minutes. The validation criteria was absence of dissolved drug in the supernatant.

2.2.3. Establishment of microjet reactor setup for the preparation of pharmaceutical nanoparticles

Firstly the parameters related to the microjet reactor setup that will possibly affect the production of nanoparticles are determined. These parameters were:

- Flow rate
- Temperature control
- Diameter of the capillaries
- Gas pressure and temperature

Thus in the setup of microjet reactor HPLC pumps were used for the efficient flow control as well as the ability to work with small volumes. Gas pressure is controlled by a pressure valve and the temperature of gas is controlled by a water bath. Two different microjet reactor designs were realised where the differences were the diameter of the capillaries and the temperature control on the microjet reactor itself. In the first setup the diameter of capillaries was 2.10 mm and no control of temperature was added for the microjet reactor. In the second design microjet reactor was placed in a water bath and the diameter of capillaries was 0.17 mm. In Fig. 2-1 the setup of microjet reactor is shown.

Preparation of nanoparticles

Polymeric Gliclazide and Danazol nanoparticles were used to test the feasibility of microjet reactor for the production of pharmaceutical drug nanoparticles. In the content of this feasibility study, factors affecting the nanoparticle characteristics were also studied. Basically polymer and the drug molecules were dissolved in an organic phase and water was used as the non-solvent. Eudragit S100 was used in the preparation of Gliclazide nanoparticles and HPMCP HP50 was used in the preparation of Danazol nanoparticles. Microjet reactor first setup was only evaluated with Gliclazide/Eudragit S100 nanoparticles whereas the second setup of the microjet reactor was evaluated with both Gliclazide/Eudragit S100 nanoparticles and Danazol/HPMCP HP50 nanoparticles. Total solid content of the solutions were adjusted to 2, 3, 5 or 8 $mg \bullet mL^{-1}$. Polymer:drug ratios were ranged from 1 to 1000. Both solvent and non-solvent were pumped through HPLC pumps with different flow rates ranging from 0.5 to 10 $mg \bullet mL^{-1}$ and solvent/non- solvent ratios ranging from 0.2 to 20. Microjet reactors with diame-

ters of 100, 200 or 300 µm were used and produced nanoparticles were carried to the collection chamber with pressurized nitrogen (0.1 or 1 bar) previously heated to 40, 60, 80 or 100 °C.

Collected nanoparticles were filtrated through 1 µm nylon disc filters to avoid the drug crystals and organic phase was evaporated under vacuum.

2.2.4. Preparation of pH selective positively loaded nanoparticles for oral applications

After the feasibility study a nanoparticle system which releases the drug molecules at pH values above 5.0 and having mucoadhesiveness properties were developed. For this system HPMCP HP50 and chitosan were used as polymers and Fenofibrate was used as model drug molecule. Firstly the nanoparticle system was developed without the drug molecule and in the second part Fenofibrate was loaded in these nanoparticles.

Determination of HPMCP HP50/chitosan ratio for the preparation of positively loaded particles

HPMCP HP50 and chitosan were used as polymers for the preparation of pH selective positively charged nanoparticles. Different concentrations of chitosan and HPMCP HP50 were investigated to determine the optimum conditions for positively charged nanoparticles with a particle size range of 100 – 200 nm. The only modified parameter was the concentrations of the polymers where all the parameters of the microjet were kept constant. Changes in the particle size and the ZETA potential were observed for the determination of the optimum ratio. The parameters of the microjet reactor used in this setup are summarized.

Tab. 2-8 Parameters of microJet reactor setup used for the preparation of pH sensitive and positively charged Chitosan/HPMCP50 nanoparticles

Microjet reactor diameter (µm)	200
Solvent	Acetone:EtOH 50:50 (w/w)
Antisolvent	Water pH 3.5 adjusted with HCl
Flow rate solvent (mL/min)	10
Flow rate antisolvent (mL/min)	10
Gas flow (bar)	0.1
Temperature (ºC)	80

HPMCP HP50 were investigated in 4 different concentrations (3, 5, 8, 10 mg/mL) dissolved in Acetone:Ethanol 50:50 (w/w) and chitosan was investigated in 10 different concentrations;

(0.01, 0.02, 0.05, 0.1, 0.2, 0.5, 1.0, 1.5, 2.0, 3.0 mg/mL) dissolved in distilled water pH 3.5 adjusted with HCl. Organic phase was then evaporated under vacuum at 30 °C before the particle size and ZETA analyses. Structure of the nanoparticles was also evaluated using FTIR using KBr discs to prove that the reaction between the amine group and the carboxylic acid group takes place. For this study nanoparticles that had been produced using 1,5 mg/mL chitosan and 8 mg/mL HPMCP HP50 were used. IR determinations were carried out with nanoparticles which were dried under vacuum until complete dryness.

One way analysis of variance (ANOVA) was used to determine difference at significance level of α=0.05 among groups after which post-hoc tests with the Bonferroni correction were used for comparison between individual groups.

Selection of stearic stabilization agent

Chitosan and HPMCP HP50 concentrations were constant throughout the whole experiment. Chitosan was used in 1 mg/mL concentration and HPMCP HP50 was used in 5 mg/mL concentration. Surfactant molecules were added in different ratios to the chitosan solution. The surfactant molecules used in this part of the study were; PVA(polyvinyl alcohol), Poloxamer F127, PVP(polyvinyl pyrrolidone), HPC (hydroxypropyl cellulose) and HPMC (hydroxypropyl methyl cellulose). All the surfactants other than HPC were prepared in 2 different concentrations 0.5% and 1.0%. HPC were prepared only in 0,5% due to its low solubility in water.

The following MicroJet reactor setup in Tab. 2-9 was used for selection of the stearic stabilization agent.

Tab. 2-9 MicroJet reactor setup for the preparation of chitosan/HPMCP HP50 nanoparticles either with or without surfactant molecule

Microjet reactor diameter (µm)	200
Solvent	Acetone:EtOH 50:50 (w/w)
Antisolvent	Water pH 3.5 adjusted with HCl
Flow rate solvent (mL/min)	10
Flow rate antisolvent (mL/min)	10
Gas flow (bar)	0.1
Temperature (ºC)	80

Nanoparticles were concentrated under vacuum until all the organic phase was evaporated and measured for ZETA potential and particle size using DLS method. The efficiency of the surfactants in coating nanoparticles was evaluated based on increase in the particle size and decrease in the ZETA potential. Since when the nanoparticles are covered with the surfactant molecule the size will increase due to the extra layer and ZETA potential will decrease since the surfactant molecule will affect the interaction of nanoparticles with the ions present in the medium. The formulations were compared with the formulation prepared without any surfactant. Further characterization of nanoparticles was carried out using scanning electron microscopy and transmission electron microscopy.

One way analysis of variance (ANOVA) was used to determine significance (α=0.05) among groups after which post-hoc tests with the Bonferroni correction were used for comparison between individual groups. A value of $p < 0.05$ was considered to be significant.

2.2.5. Drug loading into pH selective positively loaded nanoparticles for oral applications

After establishment of the nanoparticle system in the previous study, drug loading investigations were conducted with the model drug Fenofibrate. Different design of experiment studies were conducted for the determination of optimum conditions for the nanoparticle preparation followed by in-vitro analyses of the nanoparticle formulations.

Design of experiments for the optimization of microjet reactor production parameters

In this part of the study an experimental design was established that would enable the optimization of all the parameters as well as the evaluation of effect of the parameters on the particle size and drug loading efficiency. For this reason a rotatable orthogonal design was used and results are analyzed with analyses of variance (ANOVA).

The parameters are selected according to the results of the feasibility study that is conducted for the set-up of the microjet reactor. According to the results of the feasibility study microjet reactor related most critical parameters can be summarized as:

- Flow rate of the pumps (Factor A)
- Solvent (Factor B)
- Gas pressure (Factor C)
- Temperature (Factor D)

These parameters are unrelated to the formulation parameters that would also affect the in-vivo behavior of the nanoparticles and will only be used for the preparation of the nanoparticles with required particle size and highest drug loading efficiency, independent from the polymers used.

According to the experimental design all the factors tested should be presented in numerical values for the further correlation and analyses. Thus the type of solvent that is used is also numerically expressed.

The relationship between the mean sizes of NP produced with different solvents and the solvent-water affinity is highly dependent on the solvent water interaction parameter which is calculated with the following equation.

$$\chi_{water-solvent} = \frac{V_{solvent}}{RT}(\delta_{solvent} - \delta_{water})$$

Vsolvent: Molar volume of the solvent

R: Gas constant: 8.314472

T: Temperature in K

δ solvent: Hildebrand solubility parameter for solvent

δ water: Hildebrand solubility parameter for water

Eq. 2-3

Using the eq. 2-3, solvents that take place in the experimental set up were given in numerical values. Thus chitosan, HPMCP HP50 and Pluronic F127 concentrations were kept constant throughout the experiments. These concentrations were 2, 5 and 5 mg/mL respectively. HPMCP HP50 was dissolved in 20 % Ethanol (pH 6.00 to ensure the solubility of HPMCP HP50) 70 % Ethanol, 80% Ethanol, Acetone:Methanol (50:50 w/w), Acetone:Ethanol (50:50 w/w) together with the drug substance Fenofibrate. Solvents had the χsolvent-water values of 0.23, 3.89, 7.56, 11.22, and 14.89 respectively. Chitosan was dissolved in distilled water pH 3.5 (adjusted with HCl) together with Pluronic F127.

After the preparation of nanoparticles according to the experimental plan the organic phase was evaporated under vacuum and nanoparticles were further purified with centrifugation at 1000 g for 15 minutes for the separation of drug and polymer crystals. Nanoparticle suspensions were diluted 10 fold with water for particle size and ZETA analyses and centrifuged na-

noparticles dissolved with mobile phase (Acetonitrile:H_2O, 80:20) for drug loading analyses with HPLC.

The parameters of the microjet reactor were tested using a response surface method approach. This approach is designed to allow estimation of interaction and even the quadratic effects and therefore give an idea of the local shape of the response surface of investigation. In a rotatable design, the variance of the predicted values of y is a function of the distance of a point from the center of the design and is not a function of the direction the point lies from the center. The star points are at some distance from the center based on the properties desired for the design and the number of factors in the design. The star points establish new extremes for the low and high settings for all factors.

The results of the orthogonal setup were statistically evaluated with ANOVA analyses to determine the significance of factors solvent, gas pressure, flow rate and temperature. Furthermore surface diagrams were produced for establishment of a model in prediction of particle size, PDI and drug loading in regard to different parameters.

The factors and test sequences are given Tab. 2-10 for the experimental design.

Tab. 2-10 Factors together with the low and high actual values that are used in the orthogonal design

Factor	Name	Units	Low Actual	High Actual	Low Coded	High Coded	Mean	Std. Dev.
A	Flow rate	mL/min	4.00	8.00	-1.00	1.00	6.00	1.79
B	Solvent		3.89	11.22	-1.00	1.00	7.56	3.28
C	Gas pressure	bar	0.50	1.50	-1.00	1.00	1.00	0.45
D	Temperature	ºC	40.00	75.00	-1.00	1.00	57.50	15.65

The extreme real values for each variable were carefully tested by means of phase diagrams with regard to the feasibility of nanoparticle preparation. The intervals between levels were chosen to maintain the rotatable orthogonality of the design. A is calculated as 2 for the axial points.

At the end of the evaluation of design parameters, optimum production parameters were calculated to be used in the next step of optimization of formulation parameters using design of experiments.

Design of experiments for the optimization of formulation parameters

The objective of this part of the study was to establish an experimental design that would enable the optimization of amounts of ingredients of Fenofibrate HPMCP HP50/chitosan formulation in respect to particle size, PDI, ZETA potential, drug loading efficiency, mucoadhesiveness, and drug release at pH 1.2. For this reason a D-optimal design was used where total amount was kept constant and the ratio of ingredients were changed and results are analyzed with analyses of variance (ANOVA).

The parameters are selected according to the results of the feasibility study that is conducted for the set-up of the microjet reactor. According to the results the total amount of the ingredients were set to 12 mg/mL. Furthermore the ratios of the following ingredients were changed in the design:

- HPMCP HP50
- Chitosan
- Pluronic F127
- Fenofibrate

The production parameters of the microjet reactor were kept constant in the D-Mixture design. These parameters were:

Tab. 2-11 Parameters of microjet reactor for the D- optimal design

Solvent	Ethanol:Water 80:20 [w/w]
Non-solvent	Water
Flow rate	8 mL/min
Temperature	64 °C
Gas pressure	0.1 bar

Total amount of API and ingredients were adjusted to 12 mg/mL depending on the previous experimentation with the preparation of Fenofibrate nanoparticles. Furthermore amounts of Fenofibrate, chitosan, HPMCP HP50 and Pluronic F127 were varied in the design matrix.

Tab. 2-12 Factors used for the D-optimal design together with low and high actual values

Component	Name	Units	Low Actual	High Actual	Low Coded	High Coded	Mean	Std. Dev.
A	HPMCP HP50	mg/mL	3.0	10.0	0	0.959	5.739	2.263
B	Chitosan	mg/mL	0.2	1.5	0	0.178	0.801	0.548
C	Pluronic F127	mg/mL	1.0	5.0	0	0.548	2.886	1.558
D	Fenofibrate	mg/mL	0.5	5.0	0	0.616	2.574	1.707

Experimental design was constructed using Design Expert™ 7.0 program and following runs were calculated for the establishment of the design space.

Tab. 2-13 Experimental D-optimal design for the optimization of nanoparticle formulation

		Component 1	Component 2	Component 3	Component 4
Std	Run	A:HPMCP HP50 [mg/mL]	B:Chitosan [mg/mL]	C:Pluronic F127 [mg/mL]	D:Fenofibrate [mg/mL]
6	5	5.756	0.478	1.000	4.767
13	3	7.842	0.919	1.000	2.239
8	9	9.191	1.308	1.001	0.500
19	11	9.191	1.308	1.001	0.500
4	8	10.00	0.203	1.014	0.784
15	10	7.109	0.200	1.020	3.671
5	16	3.418	1.500	2.085	4.998
16	20	3.418	1.500	2.085	4.998
7	19	6.050	1.500	2.201	2.249
11	4	8.590	0.200	2.380	0.830
12	6	5.068	0.200	3.019	3.713
10	15	7.237	0.678	3.585	0.500
20	1	3.192	0.209	3.599	5.000
9	12	3.192	0.209	3.599	5.000
14	7	5.807	0.200	4.180	1.812
18	13	3.001	1.067	4.975	2.957
1	14	3.001	1.067	4.975	2.957
17	17	4.824	1.500	4.998	0.678
3	18	4.824	1.500	4.998	0.678
2	2	4.074	0.271	5.000	2.654

After the preparation of nanoparticles according to the experimental plan the organic phase was evaporated under vacuum and nanoparticles were further purified with centrifugation at 1000 g for 15 minutes for the separation of drug and polymer crystals. Nanoparticle suspensions were diluted 10 fold with water for particle size and ZETA analyses and precipitated nanoparticles were dissolved in mobile phase (Acetonitrile:H_2O, 80:20) for drug loading efficiency analyses with HPLC. Furthermore mucoadhesiveness of nanoparticles were investigated in-vitro with mucin. 0.1 % mucin dispersion was prepared in water by vigorous mixing until the mucin is fully dispersed. 300 µL of sample was mixed with 5 mL of mucin dispersion and incubated for 2 hours under mixing at 100 rpm. Binding of nanoparticles to mucin was determined with turbidity measurements. 3 mL of nanosuspension was mixed with 20 mL 0.1 N HCl for the

determination of drug release under acidic conditions. The samples were mixed at 100 rpm with a magnetic stirrer at 37 °C for two hours. At the end of incubation 5 mL of sample was taken and filtered through 1 µm glass disc filter to avoid the drug crystals. After the filtration samples were centrifuged at 12000 g for 45 min and precipitated nanoparticles were dissolved in 5 mL of 80% ACN in water for the determination of drug content in nanoparticles.
At the end of the D-optimal design formulation parameters were optimized to be used for the further steps.

2.2.6. Comparative evaluation of Fenofibrate nanoparticles

Optimization of Fenofibrate polymer nanoparticles containing HPMCP HP50 and chitosan was done with two different design of experiments. In this section detailed in-vitro analyses of this formulation was done and compared with different Fenofibrate nanoparticle formulations prepared using microjet reactor technology.

Preparation of nanoparticles

Drug nanoparticles of Fenofibrate were prepared in three different formulations. The first one was nanoparticles of Fenofibrate with a surfactant Pluronic F127 for the stabilization, the second formulation contained additionally HPMCP HP50 to the first formulation, and the third formulation contained chitosan together with Fenofibrate, HPMCP HP50 and Pluronic F127. Contents of the formulations are given in Tab. 2-14:

Tab. 2-14 Solutions used for the preparation of different Fenofibrate formulations.

Formulation	Organic phase			Water phase
	Fenofibrate [mg/mL]	Pluronic F127 [mg/mL]	HPMCP HP50 [mg/mL]	Chitosan [mg/mL]
Fenofibrate nano (FN)	1.0	5.0	-	-
Fenofibrate/HPMCP50 nano (FHN)	1.0	5.0	7.84	-
Fenofibrate/HPMCP HP50/chitosan nano (FHCN)	1.0	5.0	7.84	1.368

Although in design of experiments for the optimization of formulation of FHCN, it was found out that 1 mg/mL of Pluronic F127 is enough for the stabilization and efficient drug loading of nanoparticles, Pluronic F127 amount was raised to 5.0 mg/mL for these experiments in order to ensure the stability of Fenofibrate nanoparticles, since the stabilization was only dependent

on the concentration of surfactant, without any electrostatic stabilization as in the case of FHN and FHCN.

The parameters of the microjet reactor is summarized in Tab. 2-15

Tab. 2-15 Parameters of the microjet reactor setup used for the preparation of FN, FHN, FHCN

Solvent	EtOH:Water 80:20
Non-solvent	Water
Nitrogen pressure	0.1 bar
Flow rate	8 mL/min
Temperature	64 °C

Nanoparticle suspensions were concentrated under vacuum at a temperature of 30 °C until the EtOH is completely removed from the suspension. The suspensions were filtered through 1 µm filter after evaporation to eliminate any drug crystals formed.

Characterization of nanoparticles

Particle size and ZETA potential of nanoparticles were determined using DLS method. Furthermore amount of Fenofibrate in nanoparticles were determined using HPLC method for Fenofibrate.

Drug release studies were conducted using SGF, FeSSIF and FaSSIF as medium together with two stage dissolution studies, which are explained in detail in chapter 2.2.2. Furthermore Caco-2 studies were conducted in order to evaluate the in-vitro permeation of nanoparticle formulations.

Caco-2 permeation experiments

Maintenance culture

Caco-2 cells were maintained at 37 °C, 10 % CO_2 and 90 % relative humidity in 75 cm^2 culture flasks with supplemented Dulbecco's Modified Eagle's Medium. The cells were passaged once a week using Trypsin/EDTA solution. About 0.3 x 10^6 cells were seeded per flask. The culture medium was changed three times a week.

Culture on TranswellTM filter inserts for transport studies

For the transport experiments, Caco-2 cells were seeded with a density of 60,000 cells per square centimeter on Transwell™ filter inserts, which were placed into 12-well flat bottom cluster plates. The inserts (apical compartments) were supplied with 0.5 mL and the outer

wells (basal compartments) with 1.5 mL of DMEM culture medium. The cells were cultured at 37 °C, 10 % CO_2 and 90 % relative humidity in DMEM culture medium for 21 days until they formed confluent monolayers. The culture medium was replaced every 2 – 3 days. Confluency and tightness of the cell monolayer was routinely checked by measuring the transepithelial electrical resistance (TEER) using an EVOM™ voltohmmeter

Permeation experiments

Caco-2 monolayers were rinsed with HBSS (pH 7.4) to remove cell culture medium. Fresh HBSS (pH 7.4) supplemented with 4.5% BSA was filled into the acceptor compartments and the transport solution were applied to the donor compartments. Transport solutions contained either FASSIFmod or FESSIFmod with a Fenofibrate concentration of 14 µg/mL

After this pre-incubation, the transport experiment was started by taking samples from the donor and acceptor compartments. The concentration of test compound found in the donor was taken as initial donor concentration (cD0). At 0, 30, 60, 90 and 120 minutes samples of 200 µL were taken from the acceptor compartment and immediately replaced by identical volume of fresh pre-warmed buffer. At the end of the study additional samples were taken from the donor compartment. Between the sampling points, the monolayers were incubated at 37 °C in a CO_2 incubator. All experiments were performed in triplicate. The transepithelial electrical resistance was controlled at the first and the last sampling time to control the integrity of the caco-2 cell layers.

Samples, calibration standards and control samples with a known amount of Fenofibrate, which were also prepared using BSA containing transport solution, were mixed with 200 µL acetonitrile for the precipitation of BSA and centrifuged at 12000 g for 15 min before the HPLC analyses.

The P_{app} was calculated according to below equation

$$P_{app} = \frac{\Delta Q}{\Delta t} \cdot \frac{1}{m_0} \cdot \frac{1}{A} \cdot V_D \text{ [cm·s}^{-1}\text{]} \qquad \textbf{Eq. 2-4}$$

$\Delta Q/\Delta t$ permeability rate (steady state transport rate) obtained from the profile of the transported amount of substrate versus time. Calculated by the linear regression of time and concentration

A area of the exposed cell monolayer [cm^2]

m_0 initial mass of test compound in the donor compartment

V_D buffer volume of donor compartment [cm^3]

Transepithelial electrical resistance (TEER)

The TEER was calculated according to below equation.

$$TEER = R_{c(A)} = \left(R_{c+f} - R_f\right) \cdot A \text{ [Ω·cm²]} \qquad \textbf{Eq. 2-5}$$

$R_{c(A)}$ Electrical resistance of the monolayer with the area A [$\Omega \cdot cm^2$]

R_{c+f} Electrical resistance of the monolayer including the filter [Ω]

R_f Electrical resistance of the filter without cells [Ω]

A Area of monolayer [cm^2]

The electrical resistance of a cell free filter with an area of 1.13 cm² is 100 Ω.

3. Results

In the first part of this study two different setups of microjet reactor were evaluated for the feasibility of the setups for drug nanoparticle preparation. Furthermore effect of different parameters such as flow rate, temperature, pressure, organic solvent used and concentrations of substances were tested for the determination of significant factors affecting the particle size, ZETA potential and drug loading efficiency.

3.1. Results of the experiments with the first microjet reactor set-up

The experiments were started with the first setup of the microjet reactor for preparation of Gliclazide/Eudragit S100 nanoparticles. Because of the insufficient results preparation of nanoparticles was carried on with the second setup of the microjet reactor. This time both Gliclazide/Eudragit S100 and Danazol/HPMCP HP50 nanoparticles were prepared and effects of different parameters on particle size, PDI, ZETA potential and drug loading efficiency were studied.

3.1.1. Effect of flow rate and microjet reactor diameter on the first microjet reactor set-up

In this setup different flow ratios were used with the adjustment of solvent and non-solvent flow rates. Solvent flow rates were adjusted to 0.5, 2, 5, 10 mL/min and non-solvent flow rates were adjusted to 2, 5, 10 mL/min. Furthermore 3 different microjet reactors were used with 100µm, 200µm, 300µm diameters. The results are presented in Tab. 3-1 in terms of drug entrapment efficiency and particle size as well as the PDI.

Tab. 3-1 Parameters of the experimental setup for the evaluation of effect of flow rate and microjet reactor diameter.

Drug	Gliclazide
Polymer	Eudragit S100
Microjet reactor [µm]	**100, 200, 300**
Aqueous phase	Water
Organic phase	Acetone
Temperature [ºC]	80
Gas flow (bar)	0,1
Total solid content [mg•mL^{-1}]	2,0
Polymer:drug ratio	10
Flow rate solvent [mL•min^{-1}]	**0.5, 2, 5, 10**
Flow rate non-solvent [mL•min^{-1}]	**10, 5, 2**

As seen in Tab. 3-2 drug loading efficiency was not affected by the change in the microjet reactor diameter or the solvent/non-solvent ratio. Although it is slightly increased by different solvent/non-solvent flow rate ratios the maximum drug loading ratio that can be gathered was 12% which is not sufficient enough.

Tab. 3-2 Effect of flow rate and microjet reactor geometry on drug entrapment efficiency in Gliclazide/Eudragit S100 nanoparticles

		Drug entrapment efficiency [%]											
Aqueous Phase Flow Rate [mL/min]		**2.0**	**2.0**	**2.0**	**2.0**	**5.0**	**5.0**	**5.0**	**5.0**	**10.0**	**10.0**	**10.0**	**10.0**
Organic Phase Flow Rate [mL/min]		**0.5**	**2.0**	**5.0**	**10.0**	**0.5**	**2.0**	**5.0**	**10.0**	**0.5**	**2.0**	**5.0**	**10.0**
Microjet Reactor Diammeter (µm)	**100 µm**	5.73	7.02	3.42	1.40	2.17	6.47	5.32	2.37	2.35	2.24	6.81	7.77
		6.89	9.54	2.89	0.79	4.56	7.45	4.32	3.86	2.86	5.69	7.25	9.52
		9.56	6.21	3.54	0.87	6.85	8.65	6.35	3.15	3.54	6.45	7.65	8.56
	AVG	**7.39**	**7.59**	**3.28**	**1.02**	**4.53**	**7.52**	**5.33**	**3.13**	**2.92**	**4.79**	**7.24**	**8.62**
	SD	**1.96**	**1.74**	**0.35**	**0.33**	**2.34**	**1.09**	**1.02**	**0.75**	**0.60**	**2.24**	**0.42**	**0.88**
	RSD%	**26.57**	**22.89**	**10.56**	**32.67**	**51.76**	**14.50**	**19.05**	**23.92**	**20.52**	**46.75**	**5.82**	**10.18**
	200 µm	1.49	9.36	4.74	1.20	6.35	8.50	10.46	4.26	3.25	6.76	8.01	10.00
		4.56	7.54	5.96	1.32	5.45	8.75	9.54	3.84	3.45	5.64	7.23	8.95
		5.89	6.54	6.87	0.91	5.23	9.54	8.21	3.54	3.96	5.96	7.65	9.32
	AVG	**3.98**	**7.81**	**5.86**	**1.14**	**5.68**	**8.93**	**9.40**	**3.88**	**3.55**	**6.12**	**7.63**	**9.42**
	SD	**2.25**	**1.43**	**1.07**	**0.21**	**0.59**	**0.54**	**1.13**	**0.36**	**0.36**	**0.58**	**0.39**	**0.54**
	RSD%	**56.62**	**18.30**	**18.23**	**18.44**	**10.43**	**6.06**	**12.02**	**9.32**	**10.27**	**9.47**	**5.14**	**5.68**
	300 µm	5.41	9.00	4.56	0.98	6.23	7.23	9.23	4.21	2.95	5.92	7.01	8.51
		6.41	11.50	5.47	1.59	6.68	8.56	9.27	4.70	3.71	6.02	7.73	9.11
		8.79	10.25	6.54	1.23	5.21	8.23	7.56	3.90	3.65	6.52	7.89	8.23
	AVG	**6.87**	**10.25**	**5.52**	**1.27**	**6.04**	**8.01**	**8.69**	**4.27**	**3.44**	**6.15**	**7.54**	**8.62**
	SD	**1.74**	**1.25**	**0.99**	**0.31**	**0.75**	**0.69**	**0.97**	**0.40**	**0.42**	**0.32**	**0.47**	**0.45**
	RSD%	**25.26**	**12.20**	**17.94**	**24.29**	**12.47**	**8.65**	**11.22**	**9.41**	**12.30**	**5.24**	**6.22**	**5.20**

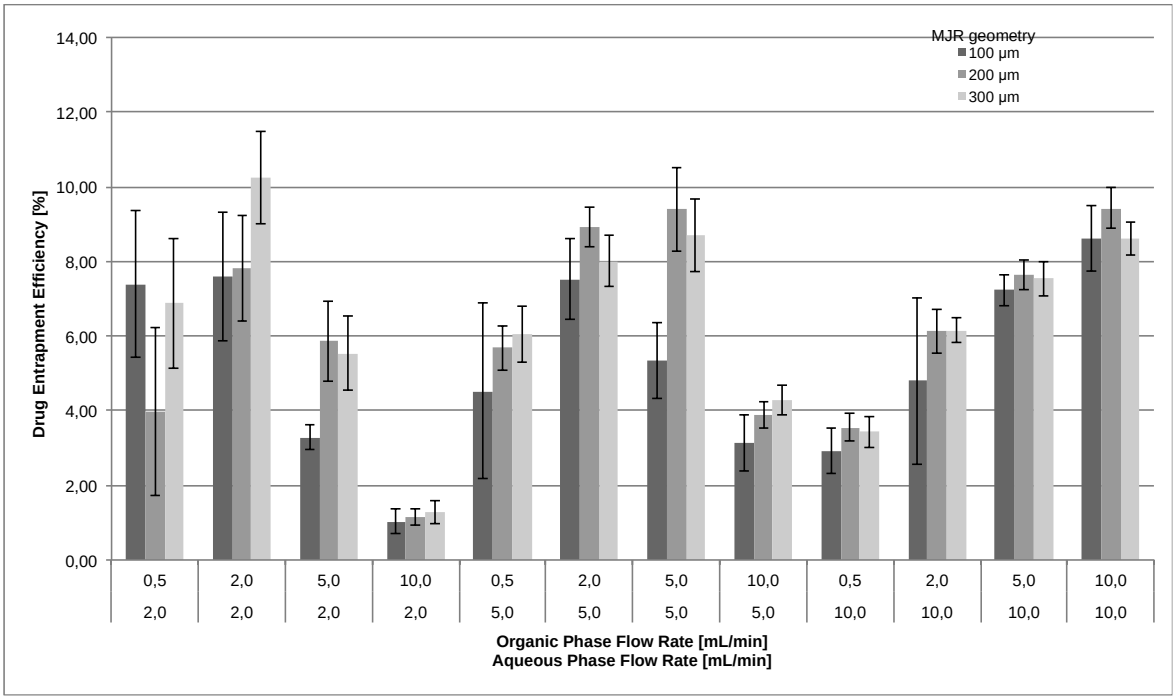

Fig. 3-1 Drug entrapment efficiency in Gliclazide/Eudragit S100 nanoparticles.

Results of the particle size analyses are presented in Tab. 3-3 and Fig. 3-1. Particle size range was found to be between 40 nm and 250 nm with a PDI value of < 0.5. There was no major trend in the change of the particle size depending on the microjet reactor diameter or solvent/non-solvent flow rate ratio.

Tab. 3-3 Effect of flow rate and microjet reactor on particle characteristics in Gliclazide/Eudragit S100 nanoparticles

Aqueous Phase Flow Rate [mL/min]	**2.0**	**2.0**	**2.0**	**2.0**	**5.0**	**5.0**	**5.0**	**5.0**	**10.0**	**10.0**	**10.0**	**10.0**	**10.0**	**10.0**	**10.0**
Organic Phase Flow Rate [mL/min]	**0.5**	**2.0**	**5.0**	**10.0**	**0.5**	**2.0**	**5.0**	**10.0**	**0.1**	**0.2**	**0.3**	**0.5**	**2.0**	**5.0**	**10.0**
Particle size [nm]	156.40	147.50	224.40	51.12	111.40	155.80	151.10	191.80	96.69	126.90	170.60	179.50	130.20	115.60	174.40
	163.41	157.56	233.71	53.59	118.52	166.55	160.11	200.60	105.24	142.51	182.13	189.41	138.85	124.19	185.04
	143.31	166.91	210.81	50.03	129.71	176.39	132.93	186.92	100.87	105.63	187.50	176.34	120.57	138.49	168.68
AVG	**154.37**	**157.32**	**222.97**	**51.58**	**119.88**	**166.25**	**148.05**	**193.11**	**100.93**	**125.01**	**180.08**	**181.75**	**129.87**	**126.09**	**176.04**
SD	**10.20**	**9.71**	**11.52**	**1.82**	**9.23**	**10.30**	**13.84**	**6.93**	**4.27**	**18.51**	**8.64**	**6.82**	**9.14**	**11.56**	**8.30**
RSD%	**6.61**	**6.17**	**5.17**	**3.53**	**7.70**	**6.19**	**9.35**	**3.59**	**4.23**	**14.81**	**4.80**	**3.75**	**7.04**	**9.17**	**4.72**
PDI	0.141	0.419	0.286	0.405	0.113	0.196	0.255	0.206	0.124	0.136	0.119	0.166	0.160	0.338	0.229
	0.245	0.321	0.210	0.256	0.103	0.210	0.230	0.105	0.156	0.103	0.105	0.149	0.189	0.256	0.194
	0.189	0.252	0.298	0.305	0.159	0.180	0.221	0.256	0.189	0.210	0.090	0.157	0.174	0.302	0.145
AVG	**0.192**	**0.331**	**0.265**	**0.322**	**0.125**	**0.195**	**0.235**	**0.189**	**0.156**	**0.150**	**0.105**	**0.157**	**0.174**	**0.299**	**0.189**
SD	**0.052**	**0.084**	**0.048**	**0.076**	**0.030**	**0.015**	**0.018**	**0.077**	**0.033**	**0.055**	**0.015**	**0.009**	**0.015**	**0.041**	**0.042**
RSD%	**27.157**	**25.379**	**18.031**	**23.584**	**23.893**	**7.685**	**7.486**	**40.699**	**20.790**	**36.610**	**13.856**	**5.438**	**8.319**	**13.762**	**22.286**
ZETA [(-)mV]	45.30	45.60	35.10	41.80	47.80	44.50	48.90	44.60	41.30	52.90	49.40	40.10	44.00	41.60	50.00
	40.60	34.50	29.90	35.60	40.50	34.50	37.50	35.60	44.50	44.60	42.10	49.80	40.20	38.40	40.50
	38.40	39.80	32.20	33.50	42.50	30.50	42.50	49.50	49.60	42.50	56.90	45.50	49.80	45.90	41.50
AVG	**41.43**	**39.97**	**32.40**	**36.97**	**43.60**	**36.50**	**42.97**	**43.23**	**45.13**	**46.67**	**49.47**	**45.13**	**44.67**	**41.97**	**44.00**
SD	**3.52**	**5.55**	**2.61**	**4.32**	**3.77**	**7.21**	**5.71**	**7.05**	**4.19**	**5.50**	**7.40**	**4.86**	**4.83**	**3.76**	**5.22**
RSD%	**8.51**	**13.89**	**8.04**	**11.67**	**8.65**	**19.76**	**13.30**	**16.31**	**9.27**	**11.78**	**14.96**	**10.77**	**10.82**	**8.97**	**11.86**

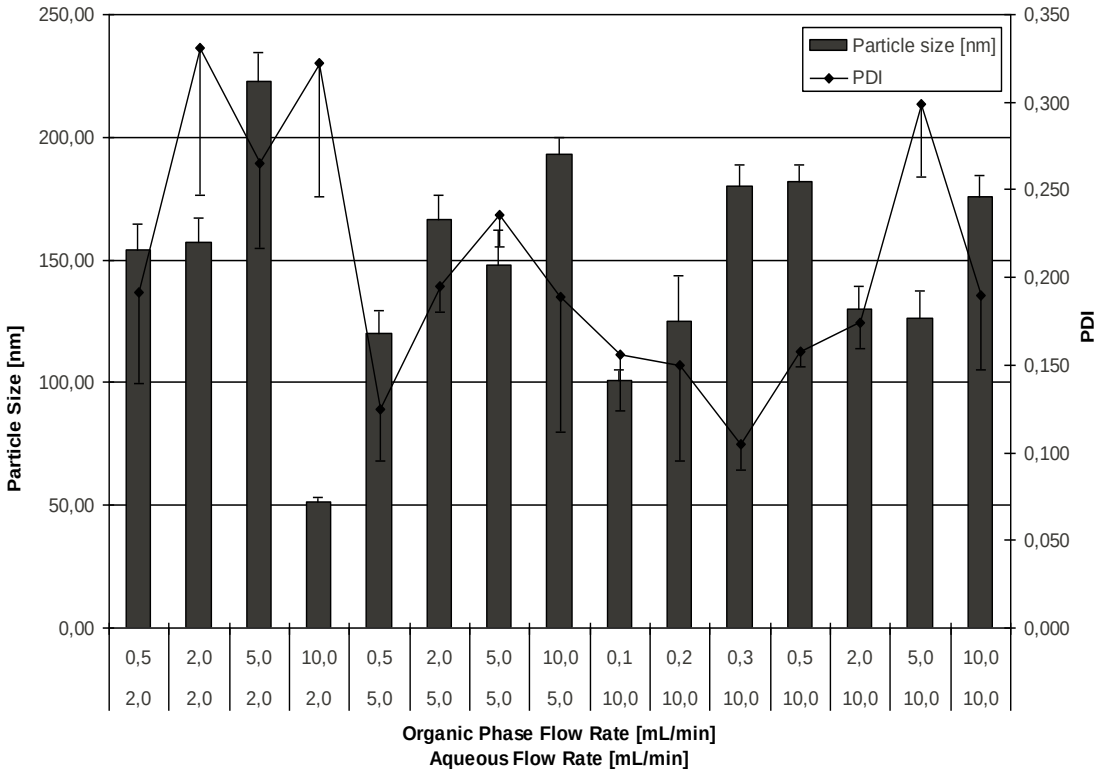

Fig. 3-2 **Effect of flow rate and microjet reactor geometry on particle characteristics in Gliclazide/Eudragit S100 nanoparticles.**

3.1.2. Effect of polymer:drug ratio on the first microjet reactor setup

In order to increase the drug loading efficiency in nanoparticles, polymer:drug ratio was increased upto1:100 w/w and tested with 4 different solvent/non-solvent ratios.

Tab. 3-4 Parameters of the experimental setup for the evaluation of effect of polymer:drug ratios.

Drug	Gliclazide
Polymer	Eudragit S100
Microjet reactor [µm]	300
Aqueous phase	Water
Organic phase	Acetone
Temperature [ºC]	80
Gas flow (bar)	0,1
Total solid content [mg•mL^{-1}]	2
Polymer:drug ratio	**0,5, 1, 2, 5, 10, 20, 100**
Flow rate solvent [mL•min^{-1}]	10
Flow rate non-solvent [mL•min^{-1}]	10

Tab. 3-5 Effect of polymer:drug ratio on drug entrapment efficiency in Gliclazide/Eudragit S100 nanoparticles

	Polymer:Gliclazide Ratio						
	100.0	**50.0**	**10.0**	**5.0**	**2.0**	**1.0**	**0.4**
Drug Loading Efficiency [%]	20.90	15.08	12.72	9.56	7.59	9.81	2.23
	17.54	13.40	9.54	8.26	8.54	6.54	1.56
	21.60	10.20	8.95	13.50	10.50	5.84	3.54
AVG	**20.01**	**12.89**	**10.40**	**10.44**	**8.88**	**7.40**	**2.44**
SD	**2.17**	**2.48**	**2.03**	**2.73**	**1.48**	**2.12**	**1.01**
RSD%	**10.84**	**19.23**	**19.50**	**26.14**	**16.72**	**28.65**	**41.27**

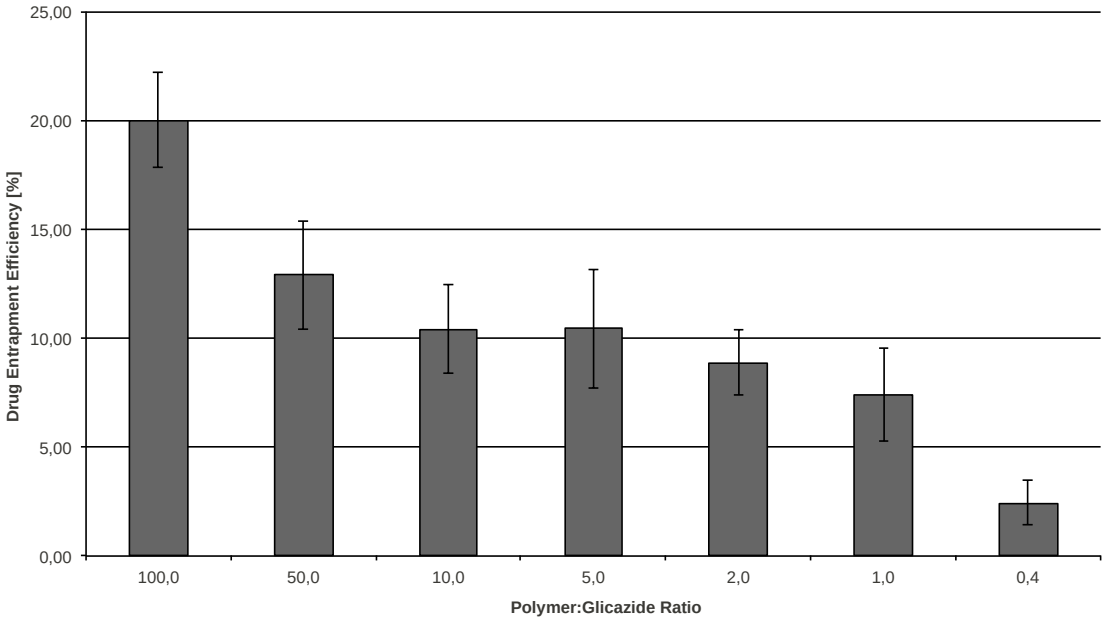

Fig. 3-3 **Effect of polymer:drug ratio on drug entrapment efficiency in Gliclazide/Eudragit S100 nanoparticles.**

Drug loading was increased with the increased polymer:drug ratio as expected; however with 100:1 polymer:drug ratio it was only 20 % which can be also considered as insufficient drug loading efficiency.

Tab. 3-6 Effect of polymer:drug Ratio on particle characteristics in Gliclazide/Eudragit S100 nanoparticles

	Glicazide:Eudragit S100 Ratio						
	1/100	**1/50**	**1/10**	**1/5**	**1/2**	**1**	**2,5/1**
Particle size [nm]	125.2	129.8	183.1	187.7	134.0	132.5	164.6
	100.5	139.6	160.2	199.5	112.9	122.6	188.6
	112.9	154.6	158.9	185.9	145.6	118.6	199.4
AVG	**112.9**	**141.3**	**167.4**	**191.0**	**130.8**	**124.6**	**184.2**
SD	**12.4**	**12.5**	**13.6**	**7.4**	**16.6**	**7.2**	**17.8**
RSD%	**10.9**	**8.8**	**8.1**	**3.9**	**12.7**	**5.7**	**9.7**
PDI	0.149	0.102	0.349	0.322	0.154	0.164	0.251
	0.201	0.122	0.256	0.355	0.244	0.178	0.266
	0.189	0.154	0.298	0.421	0.196	0.145	0.198
AVG	**0.180**	**0.126**	**0.301**	**0.366**	**0.198**	**0.162**	**0.238**
SD	**0.027**	**0.026**	**0.047**	**0.050**	**0.045**	**0.017**	**0.036**
RSD%	**15.154**	**20.817**	**15.473**	**13.773**	**22.744**	**10.203**	**14.990**
ZETA [(-)mV] AVG	**59.9**	**53.3**	**51.1**	**47.9**	**47.4**	**45.5**	**45.6**
SD	**12.1**	**8.7**	**9.5**	**15.0**	**8.6**	**9.8**	**8.1**
RSD%	**20.3**	**16.3**	**18.7**	**31.4**	**18.2**	**21.6**	**17.7**

Nanoparticles in a range of 120 – 185 nm were produced with different polymer:drug ratios. There was no correlation with the change of the particle size and the change of polymer:drug ratio.

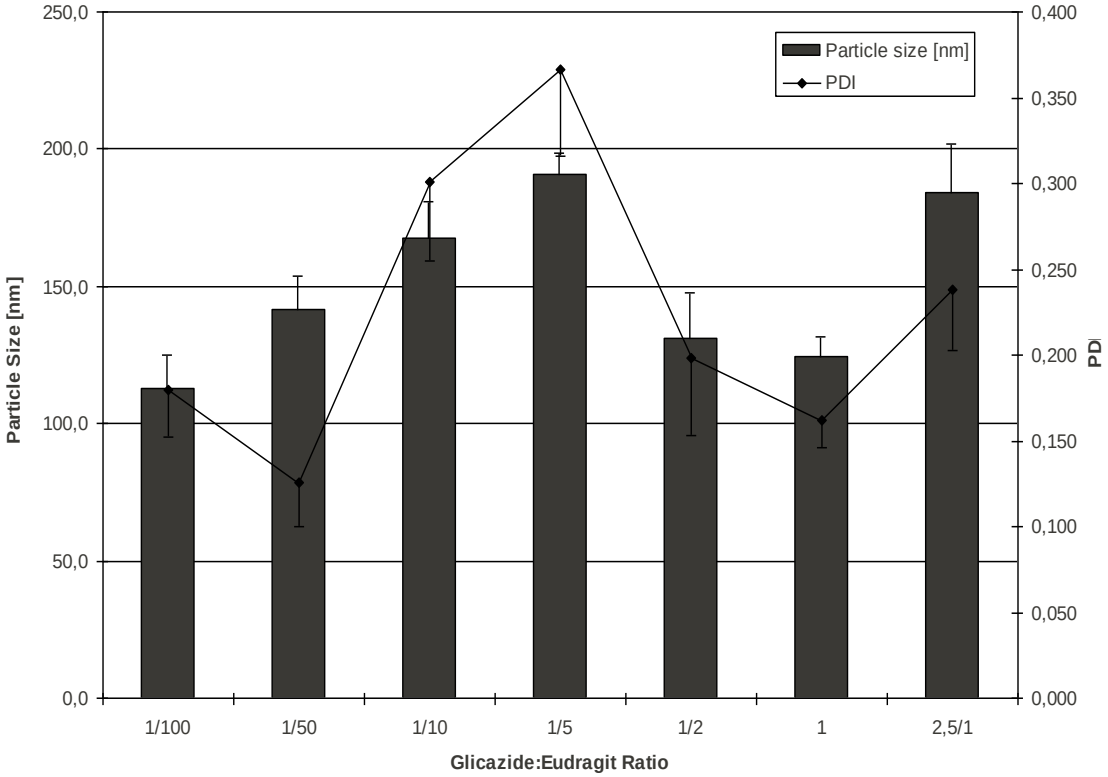

Fig. 3-4 Effect of polymer:drug ratio on particle characteristics in Gliclazide/Eudragit S100 nanoparticles.

3.1.3. Effect of polymer:drug ratio and solvent on the first microjet reactor setup

In order to increase the drug loading into nanoparticles polymer:drug ratio was increased up to 1:1000 (w/W) and each ratio was evaluated by using each of Acetone, THF, MeOH.

Tab. 3-7 Parameters of the experimental setup for the evaluation of effect of polymer:drug ratios and different solvents.

Drug	Gliclazide
Polymer	Eudragit S100
Microjet reactor [µm]	300
Aqueous phase	Water
Organic phase	**Acetone, THF, MeOH**
Temperature [ºC]	80
Gas flow (bar)	0,1
Total solid content [mg•mL^{-1}]	2
Polymer:drug ratio	**20, 100, 200, 400, 800, 1000**
Flow rate solvent [mL•min^{-1}]	10
Flow rate non-solvent [mL•min^{-1}]	10

Highest drug loading efficiencies were observed with Acetone as solvent. However when the polymer:drug ratio was increased more than 200 there was no further increase in the drug loading efficiency as seen in Tab. 3-8.

Tab. 3-8 Effect of polymer:drug ratio and solvent on drug entrapment efficiency in Gliclazide/Eudragit S100 nanoparticles

Drug Entrapment Efficiency [%]		polymer:drug Ratio					
	Solvent	**20**	**100**	**200**	**400**	**800**	**1000**
	THF	12.12	12.32	11.29	11.28	13.38	14.90
		10.98	13.87	12.98	10.56	12.41	15.21
		9.65	14.56	11.56	13.54	12.47	12.54
	AVG	**10.92**	**13.58**	**11.94**	**11.79**	**12.75**	**14.22**
	SD	**1.24**	**1.15**	**0.91**	**1.55**	**0.54**	**1.46**
	RSD%	**11.32**	**8.43**	**7.60**	**13.18**	**4.27**	**10.28**
	MeOH	17.51	19.74	21.74	20.21	19.67	19.89
		16.25	21.05	19.54	18.95	18.24	20.56
		15.98	20.98	23.54	21.91	18.99	22.54
	AVG	**16.58**	**20.59**	**21.61**	**20.36**	**18.97**	**21.00**
	SD	**0.81**	**0.74**	**2.00**	**1.49**	**0.71**	**1.38**
	RSD%	**4.91**	**3.58**	**9.27**	**7.30**	**3.76**	**6.55**
	Acetone	14.18	21.34	29.87	29.75	29.80	27.00
		18.65	22.56	30.25	27.45	27.19	25.65
		19.54	23.45	26.27	30.21	28.65	30.99
	AVG	**17.46**	**22.45**	**28.80**	**29.14**	**28.55**	**27.88**
	SD	**2.87**	**1.06**	**2.20**	**1.48**	**1.31**	**2.78**
	RSD%	**16.46**	**4.73**	**7.63**	**5.08**	**4.58**	**9.96**

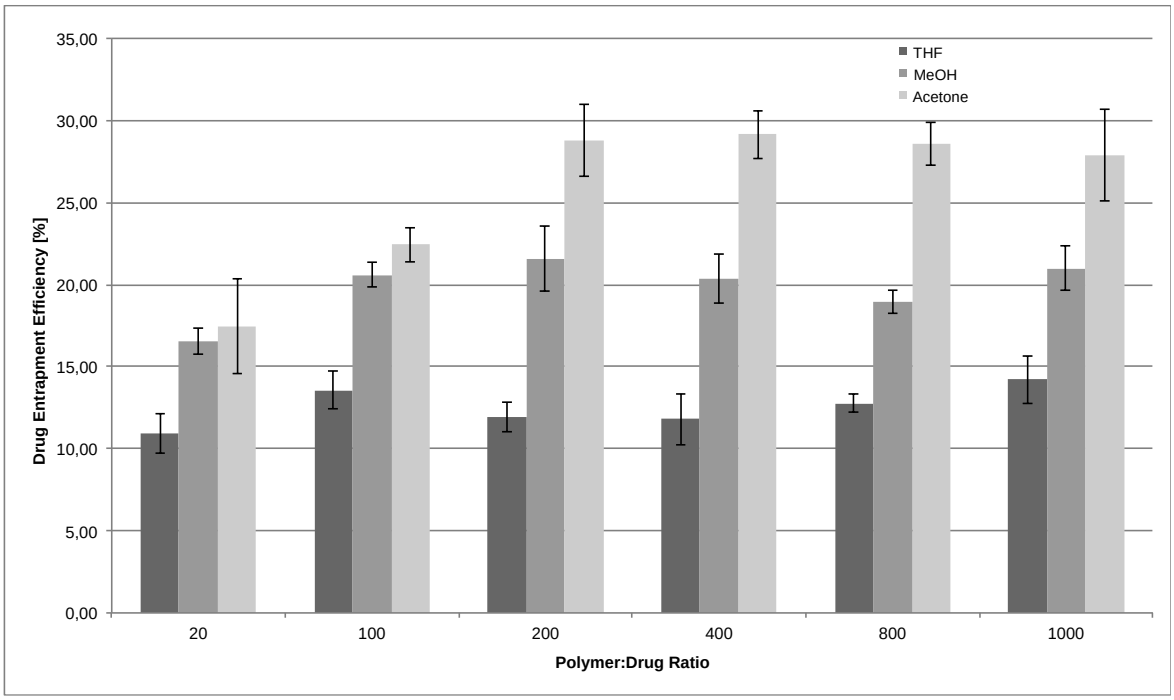

Fig. 3-5 Effect of polymer:drug ratio and solvent on drug entrapment efficiency in Gliclazide/Eudragit S100 nanoparticles.

3.2. Results of the experiments with the second microjet reactor set-up

Following the establishment of the second setup of the microjet reactor Gliclazide/Eudragit S100 and Danazol/HPMCP HP50 nanoparticles were prepared with different parameters that would affect the particle size, size distribution and drug loading efficiency. For all the particles prepared, the ZETA potential was also determined but did not show any differences depending on different parameters since it is a property of the polymer used. Both for Eudragit S100 and HPMCP HP50 polymers showed the required ZETA potential of < 30 mv (-45 mv and -55 mv respectively) which is required for stability of the nanoparticles.

3.2.1. Effect of polymer:drug ratio on the second microjet reactor setup

Gliclazide/Eudragit S100 nanoparticles

Polymer:drug ratios changing from 1 to 200 were used for the preparation of Gliclazide/Eudragit S100 nanoparticles according to Tab. 3-9. Furthermore the flow rate of the solvent was changed in the range of 1-200 ml/min.

Tab. 3-9 Parameters of the experimental setup for the evaluation of effect of the polymer:drug ratios.

Drug	Gliclazide
Polymer	Eudragit S100
Microjet reactor [µm]	300
Aqueous phase	Water
Organic phase	MeOH
Temperature [ºC]	80
Gas flow (bar)	0,1
Total solid content [mg•mL^{-1}]	2
Polymer:drug ratio	**1, 2, 5, 10, 20, 50, 100, 200**
Flow rate solvent [mL•min^{-1}]	**0.5, 2, 5, 10**
Flow rate non-solvent [mL•min^{-1}]	10

Tab. 3-10 Effect of polymer:drug ratio on drug entrapment efficiency in Gliclazide/Eudragit S100 nanoparticles

		Drug entrapment efficiency [%]			
	Nonsolvent Flow Rate [mL/min]	**10.0**	**10.0**	**10.0**	**10.0**
	Solvent Flow Rate [mL/min]	**10.0**	**5.0**	**2.0**	**0.5**
polymer:drug ratio	**2**	1.2	2.1	3.2	2.8
		0.8	1.8	2.8	3.2
		0.5	2.6	3.4	3.7
	AVG	**0.8**	**2.2**	**3.1**	**3.2**
	SD	**0.4**	**0.4**	**0.3**	**0.5**
	RSD%	**42.1**	**18.7**	**9.8**	**13.9**
	5	1.5	2.9	2.7	3.9
		1.2	2.1	2.9	3.7
		1.9	2.6	3.2	3.6
	AVG	**1.5**	**2.5**	**2.9**	**3.7**
	SD	**0.4**	**0.4**	**0.3**	**0.2**
	RSD%	**22.9**	**16.0**	**8.6**	**4.1**
	10	5.2	5.9	6.9	7.8
		4.8	5.7	7.5	7.2
		5.9	5.8	7.9	6.9
	AVG	**5.3**	**5.8**	**7.4**	**7.3**
	SD	**0.6**	**0.1**	**0.5**	**0.5**
	RSD%	**10.5**	**1.7**	**6.8**	**6.3**
	20	14.3	16.4	19.9	19.5
		16.5	15.9	18.9	20.1
		15.8	17.9	18.5	20.9
	AVG	**15.5**	**16.7**	**19.1**	**20.2**
	SD	**1.1**	**1.0**	**0.7**	**0.7**
	RSD%	**7.2**	**6.2**	**3.8**	**3.5**
	50	43.6	43.6	46.2	53.6
		42.9	44.6	42.5	55.2
		43.8	45.2	50.1	54.5
	AVG	**43.4**	**44.5**	**46.3**	**54.4**
	SD	**0.5**	**0.8**	**3.8**	**0.8**
	RSD%	**1.1**	**1.8**	**8.2**	**1.5**
	100	43.1	43.2	48.1	72.4
		46.7	44.5	49.6	68.9
		47	45.6	48.5	70.1
	AVG	**45.6**	**44.4**	**48.7**	**70.5**
	SD	**2.2**	**1.2**	**0.8**	**1.8**
	RSD%	**4.8**	**2.7**	**1.6**	**2.5**
	200	47.2	54.7	92	97.6
		49.5	58.7	88.6	95.5
		50.2	58.6	90.6	96.6
	AVG	**49.0**	**57.3**	**90.4**	**96.6**
	SD	**1.6**	**2.3**	**1.7**	**1.1**
	RSD%	**3.2**	**4.0**	**1.9**	**1.1**

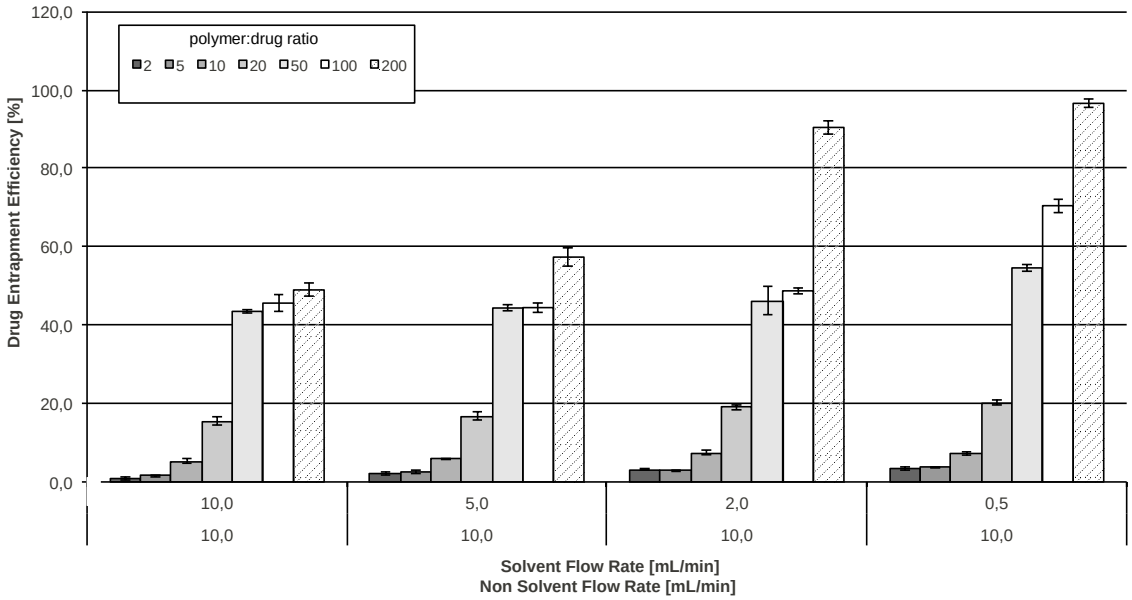

Fig. 3-6 Effect of polymer:drug ratio on drug entrapment efficiency in Gliclazide/Eudragit S100 nanoparticles.

High drug loading efficiencies (92,0 %, 97,6 %) were achieved when polymer:drug ratio was adjusted to 200 and the non-solvent/solvent ratio was higher than 5.

Danazol/HPMCP HP50 nanoparticles

Polymer:drug ratios changing from 1 to 20 were used for the preparation of Danazol/HPMCP HP 50 nanoparticles using solvent flow rates in the range of 0.5-10 ml/min according to Tab. 3-11.

Tab. 3-11 Parameters of the experimental setup for the evaluation of effect of polymer:drug ratios.

Drug	Danazol
Polymer	HPMCP HP50
Microjet reactor [µm]	300
Aqueous phase	Water
Organic phase	Acetone
Temperature [ºC]	80
Gas flow (bar)	0,1
Total solid content [mg•mL^{-1}]	2
Polymer:drug ratio	**1, 2, 5, 10, 20**
Flow rate solvent [mL•min^{-1}]	**0.5, 2, 5, 10**
Flow rate non-solvent [mL•min^{-1}]	10

As seen in Tab. 3-12 and Fig. 3-7, high drug loading efficiencies were gathered with polymer:drug ratios of 20 independent of the non-solvent/solvent ratio.

Tab. 3-12 Effect of polymer:drug ratio an drug entrapment efficiency in Danazol/HPMCP HP50 nanoparticles

		Drug entrapment efficiency [%]			
	Nonsolvent Flow Rate [mL/min]	**10.0**	**10.0**	**10.0**	**10.0**
	Solvent Flow Rate [mL/min]	**10.0**	**5.0**	**2.0**	**0.5**
polymer:drug ratio	**20**	100.5	100.4	100.2	106.4
		99.8	95.6	96.5	100.6
		102.3	99.8	98.4	99.6
	AVG	**100.9**	**98.6**	**98.4**	**102.2**
	SD	**1.3**	**2.6**	**1.9**	**3.7**
	RSD%	**1.3**	**2.7**	**1.9**	**3.6**
	10	33.9	51.4	70.6	80.7
		32.4	49.7	68.9	78.4
		29.7	52.4	69.3	82.4
	AVG	**32.0**	**51.2**	**69.6**	**80.5**
	SD	**2.1**	**1.4**	**0.9**	**2.0**
	RSD%	**6.7**	**2.7**	**1.3**	**2.5**
	5	14.4	11	27.9	42.5
		13.7	12.5	25.6	39.4
		12.5	14.9	26.9	44.6
	AVG	**13.5**	**12.8**	**26.8**	**42.2**
	SD	**1.0**	**2.0**	**1.2**	**2.6**
	RSD%	**7.1**	**15.4**	**4.3**	**6.2**
	2	9.7	8.6	12.6	15.4
		8.6	10.2	13.9	14.2
		7.9	9.5	15.4	12.6
	AVG	**8.7**	**9.4**	**14.0**	**14.1**
	SD	**0.9**	**0.8**	**1.4**	**1.4**
	RSD%	**10.4**	**8.5**	**10.0**	**10.0**
	1	4.2	5.9	11.5	23.6
		5.4	6.9	10.5	22.5
		3.9	8.5	14.9	25.9
	AVG	**4.5**	**7.1**	**12.3**	**24.0**
	SD	**0.8**	**1.3**	**2.3**	**1.7**
	RSD%	**17.6**	**18.5**	**18.8**	**7.2**

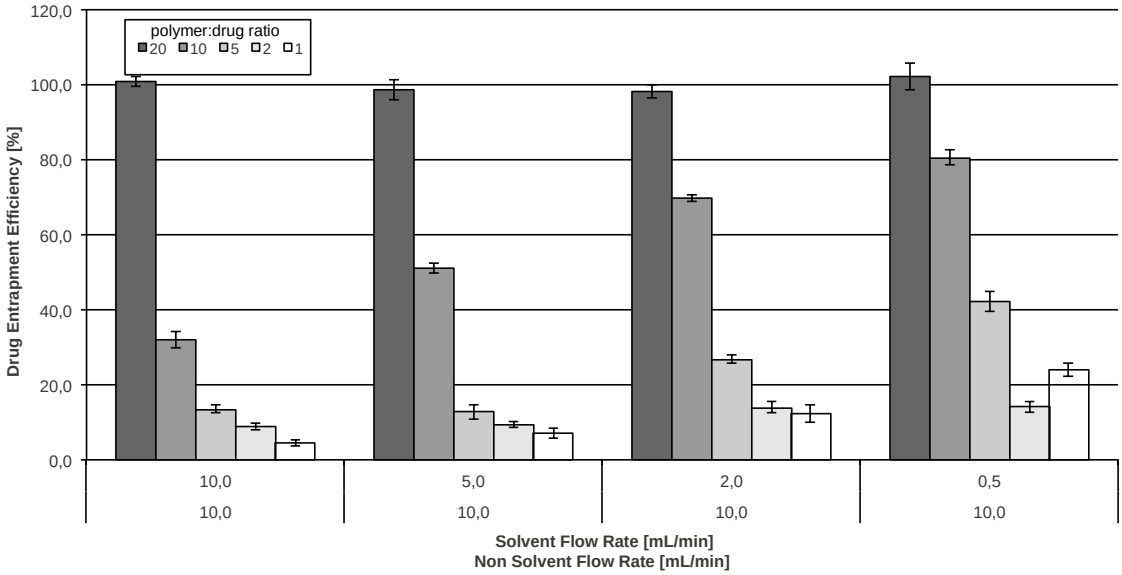

Fig. 3-7 Effect of polymer:drug on ratio drug entrapment efficiency in Danazol/HPMCP HP50 nanoparticles.

3.2.2. Effect of temperature and pressure on the second microjet reactor setup

Gliclazide/Eudragit S100 nanoparticles

Temperatures in the range of 40 to 100 °C were used for the preparation of Gliclazide/Eudragit S100 nanoparticles according toTab. 3-13. Furthermore gas pressure was adjusted to 0.1 or 1 bar and solvent flow rate was adjusted in the range of 0.5-10 mL/min.

Tab. 3-13 Parameters of the experimental setup for the evaluation of effect of temperature and pressure

Drug	Gliclazide
Polymer	Eudragit S100
Microjet reactor [µm]	300
Aqueous phase	Water
Organic phase	MeOH
Temperature [ºC]	**40, 60, 80, 100**
Gas flow (bar)	**0,1, 1**
Total solid content [mg•mL^{-1}]	2
Polymer:drug ratio	200
Flow rate solvent [mL•min^{-1}]	**0,5, 2, 5, 10**
Flow rate non-solvent [mL•min^{-1}]	10

There is no major change in the drug loading capacity with increasing temperature as seen in Tab. 3-14 and Fig 3-8. This sets an advantage for the entrapment of heat sensitive drugs with the ability to prepare the nanoparticles at low temperatures. Furthermore gas pressure did also not play a significant role on the drug loading efficiencies.

Tab. 3-14 Effect of temperature and pressure on drug entrapment efficiency in Gliclazide/Eudragit S100 nanoparticles

		Drug entrapment efficiency [%]			
	Nonsolvent Flow Rate [mL/min]	**10.0**	**10.0**	**10.0**	**10.0**
	Solvent Flow Rate [mL/min]	**10.0**	**5.0**	**2.0**	**0.5**
Temperature (°C) / Pressure (bar)	**40/0.1**	40.5	52.0	96.3	93.4
		38.7	50.9	94.6	95.6
		42.6	54.7	89.6	98.7
	AVG	**40.6**	**52.5**	**93.5**	**95.9**
	SD	**2.0**	**2.0**	**3.5**	**2.7**
	RSD%	**4.8**	**3.7**	**3.7**	**2.8**
	40/1	39.7	50.8	97.4	95.0
		35.6	55.6	99.8	92.9
		32.4	60.4	64.9	96.5
	AVG	**35.9**	**55.6**	**87.4**	**94.8**
	SD	**3.7**	**4.8**	**19.5**	**1.8**
	RSD%	**10.2**	**8.6**	**22.3**	**1.9**
	60/0.1	61.5	67.5	93.1	92.3
		58.6	62.7	90.5	98.6
		55.7	69.3	95.4	95.6
	AVG	**58.6**	**66.5**	**93.0**	**95.5**
	SD	**2.9**	**3.4**	**2.5**	**3.2**
	RSD%	**4.9**	**5.1**	**2.6**	**3.3**
	60/1	33.5	66.4	73.6	81.4
		32.5	61.7	75.6	78.9
		37.9	62.8	77.3	83.6
	AVG	**34.6**	**63.6**	**75.5**	**81.3**
	SD	**2.9**	**2.5**	**1.9**	**2.4**
	RSD%	**8.3**	**3.9**	**2.5**	**2.9**
	80/0.1	69.2	72.9	95.6	98.4
		64.9	75.4	92.5	95.4
		70.5	77.1	97.9	92.6
	AVG	**68.2**	**75.1**	**95.3**	**95.5**
	SD	**2.9**	**2.1**	**2.7**	**2.9**
	RSD%	**4.3**	**2.8**	**2.8**	**3.0**
	80/1	69.2	72.9	95.6	98.4
		64.9	75.4	92.5	95.4
		70.5	77.1	97.9	92.6
	AVG	**68.2**	**75.1**	**95.3**	**95.5**
	SD	**2.9**	**2.1**	**2.7**	**2.9**
	RSD%	**4.3**	**2.8**	**2.8**	**3.0**
	100/0.1	75.8	78.0	84.0	91.6
		82.4	86.4	85.6	95.6
		77.5	88.9	99.4	97.1
	AVG	**78.6**	**84.4**	**89.7**	**94.8**
	SD	**3.4**	**5.7**	**8.5**	**2.8**
	RSD%	**4.4**	**6.8**	**9.4**	**3.0**
	100/1	78.3	87.1	80.4	85.7
		75.6	88.6	78.6	88.6
		72.9	82.1	72.6	89.4
	AVG	**75.6**	**85.9**	**77.2**	**87.9**
	SD	**2.7**	**3.4**	**4.1**	**1.9**
	RSD%	**3.6**	**4.0**	**5.3**	**2.2**

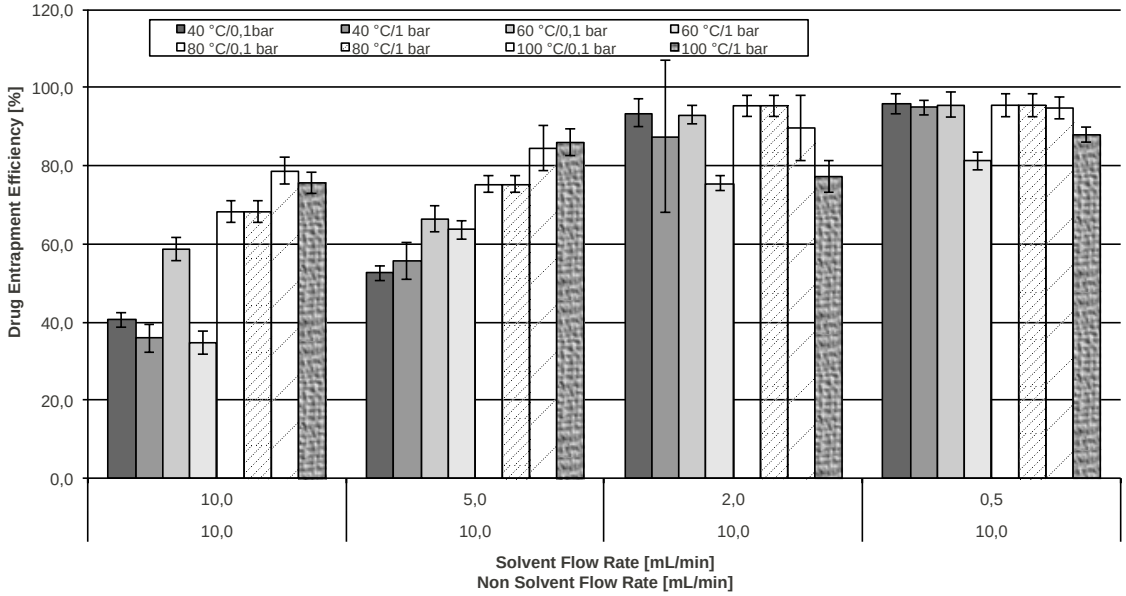

Fig. 3-8 Effect of temperature and pressure on drug entrapment efficiency in Gliclazide/Eudragit S100 nanoparticles

The results of the particle size analyses are presented in Fig. 3-9 and Tab. 3-15. It was observed that an increase in the temperature or pressure resulted in an increase in the particle size. Changes in these parameters enabled to gather particles ranging from 205 to 756 nm.

Tab. 3-15 Effect of temperature and pressure on particle size of Gliclazide/Eudragit S100 nanoparticles

Temperature [°C] / Pressure [bar]	Nonsolvent Flow Rate [mL/min]	10.0		10.0		10.0		10.0	
	Solvent Flow Rate [mL/min]	10.0		5.0		2.0		0.5	
		Particle Size [nm]	PDI	Particle Size [nm]	PDI	Particle Size [nm]	PDI	Particle Size [nm]	PDI
	40/0.1	260.9	0.237	243.8	0.281	223.5	0.245	205.3	0.337
		250.7	0.326	234.9	0.371	211.5	0.389	195.4	0.192
		255.4	0.340	239.1	0.365	229.7	0.177	196.4	0.210
	AVG	**255.7**	**0.301**	**239.3**	**0.339**	**221.6**	**0.270**	**199.0**	**0.246**
	SD	**5.1**	**0.056**	**4.5**	**0.050**	**9.3**	**0.108**	**5.5**	**0.079**
	RSD%	**2.0**	**18.560**	**1.9**	**14.843**	**4.2**	**40.042**	**2.7**	**32.084**
	40/1	431.6	0.323	364.3	0.243	214.9	0.153	181.1	0.204
		428.7	0.459	358.7	0.311	200.9	0.130	186.4	0.359
		422.1	0.331	360.4	0.277	210.1	0.180	196.7	0.328
	AVG	**427.5**	**0.371**	**361.1**	**0.277**	**208.6**	**0.154**	**188.1**	**0.297**
	SD	**4.9**	**0.076**	**2.9**	**0.034**	**7.1**	**0.025**	**7.9**	**0.082**
	RSD%	**1.1**	**20.570**	**0.8**	**12.274**	**3.4**	**16.216**	**4.2**	**27.616**
	60/0.1	272.7	0.375	255.1	0.411	233.5	0.439	216.6	0.365
		264.5	0.361	250.4	0.457	230.5	0.496	200.3	0.389
		276.1	0.451	259.1	0.020	250.4	0.100	210.4	0.146
	AVG	**271.1**	**0.396**	**254.9**	**0.296**	**238.1**	**0.345**	**209.1**	**0.300**
	SD	**6.0**	**0.048**	**4.4**	**0.240**	**10.7**	**0.214**	**8.2**	**0.134**
	RSD%	**2.2**	**12.240**	**1.7**	**81.124**	**4.5**	**62.053**	**3.9**	**44.636**
	60/1	435.3	0.296	437.7	0.244	389.5	0.239	380.8	0.261
		428.9	0.332	412.6	0.274	392.6	0.208	370.5	0.600
		430.7	0.123	430.7	0.223	395.4	0.220	369.7	0.175
	AVG	**431.6**	**0.250**	**427.0**	**0.247**	**392.5**	**0.222**	**373.7**	**0.345**
	SD	**3.3**	**0.112**	**13.0**	**0.026**	**3.0**	**0.016**	**6.2**	**0.225**
	RSD%	**0.8**	**44.634**	**3.0**	**10.377**	**0.8**	**7.031**	**1.7**	**65.068**
	80/0.1	306.6	0.190	273.3	0.209	248.3	0.207	232.6	0.155
		316.2	0.172	285.6	0.136	252.4	0.231	235.6	0.236
		310.5	0.250	274.6	0.179	250.6	0.160	248.9	0.219
	AVG	**311.1**	**0.204**	**277.8**	**0.175**	**250.4**	**0.199**	**239.0**	**0.203**
	SD	**4.8**	**0.041**	**6.8**	**0.037**	**2.1**	**0.036**	**8.7**	**0.043**
	RSD%	**1.6**	**20.020**	**2.4**	**21.007**	**0.8**	**18.118**	**3.6**	**21.006**
	80/1	468.2	0.395	542.1	0.262	395.0	0.188	399.2	0.319
		450.3	0.275	569.4	0.207	390.5	0.165	399.9	0.289
		440.9	0.188	556.4	0.216	410.2	0.203	386.5	0.245
	AVG	**453.1**	**0.286**	**556.0**	**0.228**	**398.6**	**0.185**	**395.2**	**0.284**
	SD	**13.9**	**0.104**	**13.7**	**0.030**	**10.3**	**0.019**	**7.5**	**0.037**
	RSD%	**3.1**	**36.342**	**2.5**	**12.920**	**2.6**	**10.327**	**1.9**	**13.090**
	100/0.1	438.7	0.256	410.2	0.248	386.6	0.289	325.6	0.278
		430.2	0.178	390.6	0.521	375.6	0.344	310.5	0.255
		459.6	0.169	389.4	0.036	380.5	0.298	298.6	0.246
	AVG	**442.8**	**0.201**	**396.7**	**0.268**	**380.9**	**0.310**	**311.6**	**0.260**
	SD	**15.1**	**0.048**	**11.7**	**0.243**	**5.5**	**0.030**	**13.5**	**0.017**
	RSD%	**3.4**	**23.803**	**2.9**	**90.611**	**1.4**	**9.506**	**4.3**	**6.355**
	100/1	758.6	0.200	638.7	0.180	540.7	0.250	405.0	0.198
		770.9	0.250	615.0	0.489	510.6	0.264	375.6	0.201
		760.5	0.230	625.7	0.159	530.9	0.287	390.4	0.222
	AVG	**763.3**	**0.227**	**626.5**	**0.276**	**527.4**	**0.267**	**390.3**	**0.207**
	SD	**6.6**	**0.025**	**11.9**	**0.185**	**15.4**	**0.019**	**14.7**	**0.013**
	RSD%	**0.9**	**11.103**	**1.9**	**66.943**	**2.9**	**6.997**	**3.8**	**6.317**

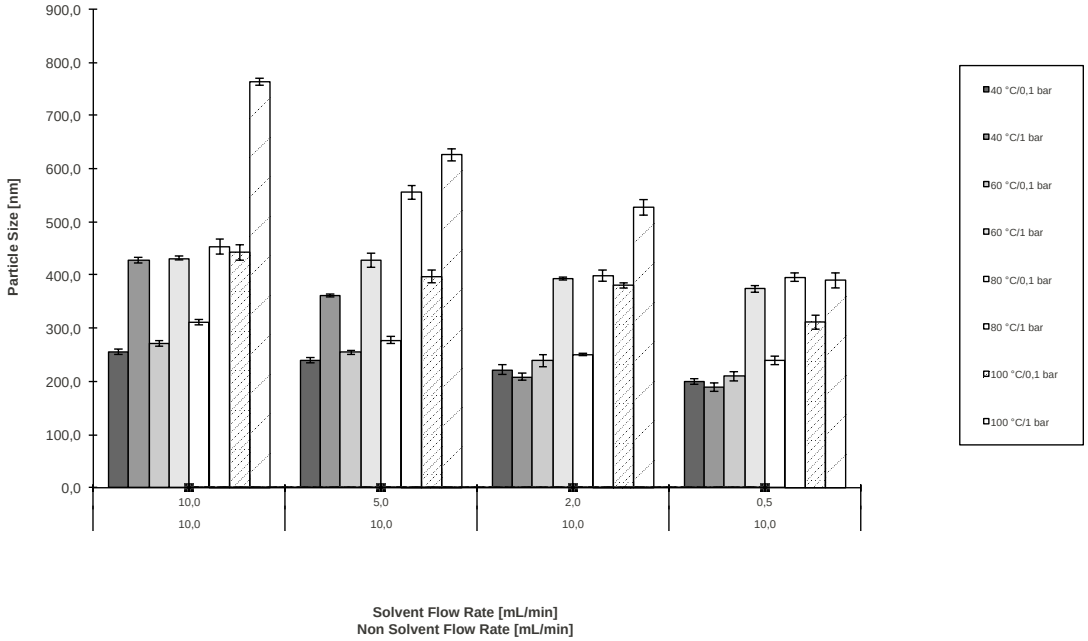

Fig. 3-9 Effect of temperature and pressure on particle size of Gliclazide/Eudragit S100 nanoparticles

Danazol/HPMCP HP50 nanoparticles

Temperatures in the range of 40 to 100 °C were used for the preparation of Danazol/HPMCP HP50 nanoparticles according to Tab. 3-16. Furthermore gas pressure was adjusted to 0.1 or 1 bar and solvent flow rate was adjusted in the range of 0.5-10 mL/min

Tab. 3-16 Parameters of the experimental setup for the evaluation of effect of temperature and pressure.

Drug	Danazol
Polymer	HPMCP HP50
Microjet reactor [µm]	300
Aqueous phase	Water
Organic phase	Acetone
Temperature [ºC]	**40, 60, 80, 100**
Gas flow (bar)	**0.1, 1**
Total solid content [mg•mL^{-1}]	2
Polymer:drug ratio	50
Flow rate solvent [mL•min^{-1}]	**0.5, 2, 5, 10**
Flow rate non-solvent [mL•min^{-1}]	10

The results of drug loading efficiency studies are presented in Tab. 3-17 and Fig. 3-10. There was a major change in the drug loading capacity with increasing temperature. At 80 and 100 °C maximum drug loading was achieved. On the other hand when pressure increased to 1 bar it was not possible to obtain any nanoparticles due to high crystallization. This high crystallization was most probably due to sudden evaporation of the solvent together with very low solubility of Danazol in aqueous media.

Tab. 3-17 Effect of temperature and pressure on drug entrapment efficiency in Danazol/HPMCP HP50 nanoparticles.

		Drug entrapment efficiency [%]			
	Nonsolvent Flow Rate [mL/min]	**10.0**	**10.0**	**10.0**	**10.0**
	Solvent Flow Rate [mL/min]	**10.0**	**5.0**	**2.0**	**0.5**
Temperature [^{0}C] / Pressure [bar]	**40/0.1**	25.3	39.3	55.4	64.7
		20.4	37.4	52.1	60.3
		22.6	36.5	48.9	57.9
	AVG	**22.8**	**37.7**	**52.1**	**61.0**
	SD	**2.5**	**1.4**	**3.3**	**3.4**
	RSD%	**10.8**	**3.8**	**6.2**	**5.7**
	40/1	na	na	na	na
		na	na	na	na
		na	na	na	na
	AVG	**na**	**na**	**na**	**na**
	SD	**na**	**na**	**na**	**na**
	RSD%	**na**	**na**	**na**	**na**
	60/0.1	27.3	38.0	58.3	75.5
		29.5	42.1	56.5	78.9
		30.2	45.9	52.4	72.4
	AVG	**29.0**	**42.0**	**55.7**	**75.6**
	SD	**1.5**	**4.0**	**3.0**	**3.3**
	RSD%	**5.2**	**9.4**	**5.4**	**4.3**
	60/1	na	na	na	na
		na	na	na	na
		na	na	na	na
	AVG	**na**	**na**	**na**	**na**
	SD	**na**	**na**	**na**	**na**
	RSD%	**na**	**na**	**na**	**na**
	80/0.1	35.1	48.4	68.3	90.2
		39.6	53.6	72.5	95.6
		42.5	52.4	75.9	89.7
	AVG	**39.1**	**51.5**	**72.2**	**91.8**
	SD	**3.7**	**2.7**	**3.8**	**3.3**
	RSD%	**9.5**	**5.3**	**5.3**	**3.6**
	80/1	na	na	na	na
		na	na	na	na
		na	na	na	na
	AVG	**na**	**na**	**na**	**na**
	SD	**na**	**na**	**na**	**na**
	RSD%	**na**	**na**	**na**	**na**
	100/0.1	42.0	57.6	77.2	98.5
		46.9	58.9	75.1	92.4
		48.7	60.2	79.4	95.4
	AVG	**45.9**	**58.9**	**77.2**	**95.4**
	SD	**3.5**	**1.3**	**2.2**	**3.1**
	RSD%	**7.6**	**2.2**	**2.8**	**3.2**
	100/1	na	na	na	na
		na	na	na	na
		na	na	na	na
	AVG	**na**	**na**	**na**	**na**
	SD	**na**	**na**	**na**	**na**
	RSD%	**na**	**na**	**na**	**na**

na: not applicable

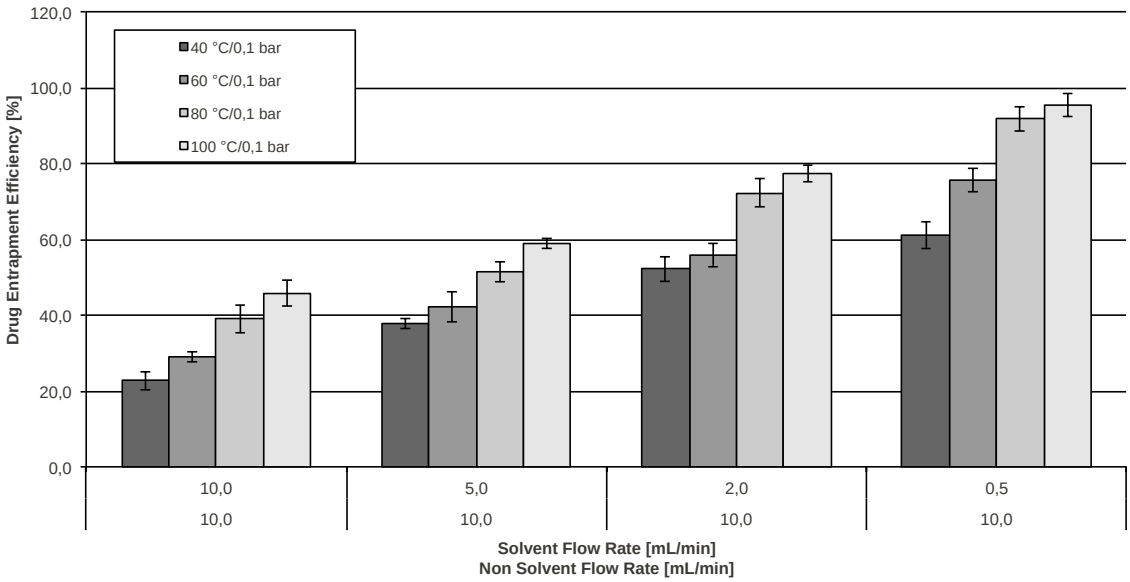

Fig. 3-10 Effect of temperature and pressure on drug entrapment efficiency in Danazol/HPMCP HP50 nanoparticles

It was observed that an increase in the temperature and in pressure resulted in the increase in the particle size as presented in Tab. 3-18 and Fig. 3-11. Changes in these parameters enabled to gather particles ranging from 30 to 275 nm. The effect of pressure was not included in Fig. 3-11 since higher pressure of 1 bar resulted in agglomeration of the particles where particle size analyses was not conducted.

Tab. 3-18 Effect of temperature and pressure on particle size of Danazol/HPMCP HP50 nanoparticles

Temperature [°C] / Pressure [bar]	Nonsolvent Flow Rate [mL/min]	10.0		10.0		10.0		10.0	
	Solvent Flow Rate [mL/min]	10.0		5.0		2.0		0.5	
		Particle Size [nm]	PDI	Particle Size [nm]	PDI	Particle Size [nm]	PDI	Particle Size [nm]	PDI
	40/0.1	102.4	0.299	91.7	0.204	74.3	0.105	31.7	0.132
		112.5	0.203	85.6	0.251	67.5	0.199	42.5	0.170
		102.6	0.290	97.4	0.215	89.5	0.124	36.1	0.161
	AVG	**105.8**	**0.264**	**91.6**	**0.223**	**77.1**	**0.143**	**36.8**	**0.154**
	SD	**5.8**	**0.053**	**5.9**	**0.025**	**11.3**	**0.050**	**5.4**	**0.020**
	RSD%	**5.5**	**20.083**	**6.4**	**11.007**	**14.6**	**34.838**	**14.8**	**12.867**
	40/1	na	na	na	na	na	na	na	na
		na	na	na	na	na	na	na	na
		na	na	na	na	na	na	na	na
	AVG	**na**	**na**	**na**	**na**	**na**	**na**	**na**	**na**
	SD	**na**	**na**	**na**	**na**	**na**	**na**	**na**	**na**
	RSD%	**na**	**na**	**na**	**na**	**na**	**na**	**na**	**na**
	60/0.1	122.1	0.284	87.1	0.274	70.6	0.204	41.3	0.117
		132.5	0.258	88.4	0.207	74.6	0.248	45.0	0.181
		127.9	0.272	92.6	0.240	79.8	0.273	47.3	0.189
	AVG	**127.5**	**0.271**	**89.4**	**0.240**	**75.0**	**0.242**	**44.5**	**0.162**
	SD	**5.2**	**0.013**	**2.9**	**0.034**	**4.6**	**0.035**	**3.0**	**0.039**
	RSD%	**4.1**	**4.796**	**3.2**	**13.939**	**6.2**	**14.455**	**6.8**	**24.310**
	60/1	na	na	na	na	na	na	na	na
		na	na	na	na	na	na	na	na
		na	na	na	na	na	na	na	na
	AVG	**na**	**na**	**na**	**na**	**na**	**na**	**na**	**na**
	SD	**na**	**na**	**na**	**na**	**na**	**na**	**na**	**na**
	RSD%	**na**	**na**	**na**	**na**	**na**	**na**	**na**	**na**
	80/0.1	218.5	0.222	109.6	0.225	104.6	0.226	89.2	0.148
		229.5	0.259	107.5	0.232	92.4	0.234	87.6	0.198
		235.4	0.280	100.0	0.311	88.5	0.247	88.2	0.138
	AVG	**227.8**	**0.254**	**105.7**	**0.256**	**95.2**	**0.236**	**88.3**	**0.161**
	SD	**8.6**	**0.029**	**5.0**	**0.048**	**8.4**	**0.011**	**0.8**	**0.032**
	RSD%	**3.8**	**11.576**	**4.8**	**18.656**	**8.8**	**4.497**	**0.9**	**19.925**
	80/1	na	na	na	na	na	na	na	na
		na	na	na	na	na	na	na	na
		na	na	na	na	na	na	na	na
	AVG	**na**	**na**	**na**	**na**	**na**	**na**	**na**	**na**
	SD	**na**	**na**	**na**	**na**	**na**	**na**	**na**	**na**
	RSD%	**na**	**na**	**na**	**na**	**na**	**na**	**na**	**na**
	100/0.1	275.4	0.227	173.6	0.293	136.4	0.286	90.1	0.230
		266.9	0.223	185.2	0.224	116.5	0.291	95.6	0.195
		287.1	0.231	199.3	0.229	126.4	0.301	99.9	0.177
	AVG	**276.5**	**0.227**	**186.0**	**0.249**	**126.4**	**0.293**	**95.2**	**0.201**
	SD	**10.1**	**0.004**	**12.9**	**0.038**	**10.0**	**0.008**	**4.9**	**0.027**
	RSD%	**3.7**	**1.762**	**6.9**	**15.473**	**7.9**	**2.610**	**5.2**	**13.431**
	100/1	na	na	na	na	na	na	na	na
		na	na	na	na	na	na	na	na
		na	na	na	na	na	na	na	na
	AVG	**na**	**na**	**na**	**na**	**na**	**na**	**na**	**na**
	SD	**na**	**na**	**na**	**na**	**na**	**na**	**na**	**na**
	RSD%	**na**	**na**	**na**	**na**	**na**	**na**	**na**	**na**

na: not applicable

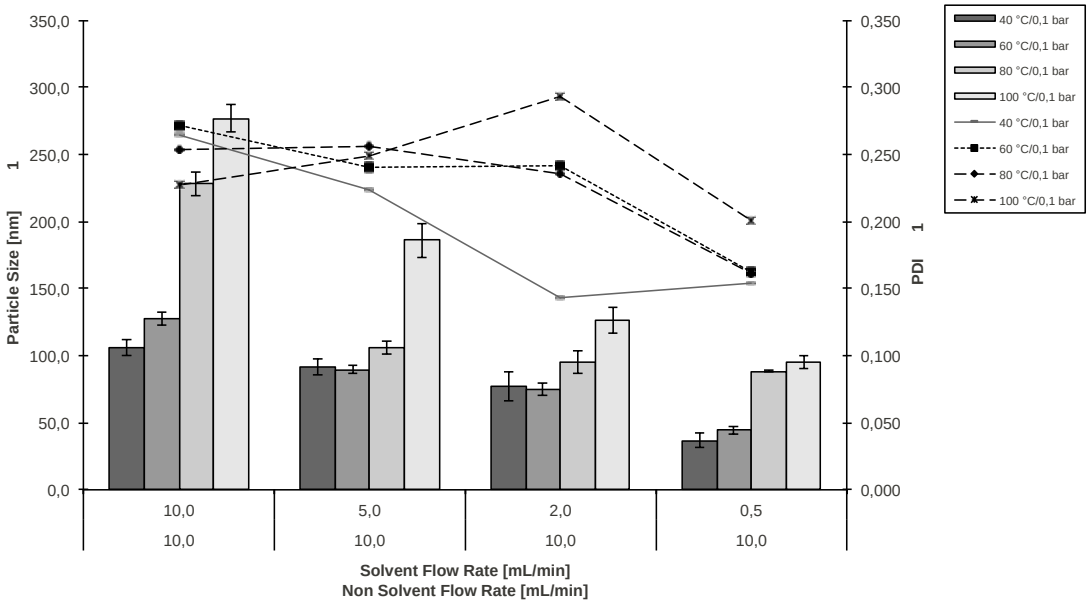

Fig. 3-11 Effect of temperature and pressure on particle size of HPMCP HP50/Danazol nanoparticles

3.2.3. Effect of total solid content and solvent on the second microjet reactor setup

Gliclazide/Eudragit S100 nanoparticles

Total solid contents (total concentration of polymer and drug in solution) in the range of 2 to 8 mg•mL^{-1} were used for the preparation of Gliclazide/Eudragit S100 nanoparticles with solvents MeOH, Acetone and THF according to Tab. 3-19. Additionally the flow rate of the solvent was varied in the range of 0.5-10 mL/min.

Tab. 3-19 Parameters of the experimental setup for the evaluation of total solid content and solvent

Drug	Gliclazide
Polymer	Eudragit S100
Microjet reactor [µm]	300
Aqueous phase	Water
Organic phase	**MeOH, Acetone, THF**
Temperature [ºC]	60
Gas flow (bar)	0,1
Total solid content [mg•mL^{-1}]	**2, 3, 5, 8**
Polymer:drug ratio	200
Flow rate solvent [mL•min^{-1}]	**0,5, 2, 5, 10**
Flow rate non-solvent [mL•min^{-1}]	10

In Tab. 3-20 to Tab. 3-22 drug entrapment efficiencies for THF, MeOH and acetone are listed based on the total solid concentration and solvent/non-solvent flow rate ratios.

Tab. 3-20 Drug entrapment efficiency in Gliclazide/Eudragit S100 nanoparticles in THF

		Drug entrapment efficiency [%]			
	Nonsolvent Flow Rate [mL/min]	**10.0**	**10.0**	**10.0**	**10.0**
	Solvent Flow Rate [mL/min]	**10.0**	**5.0**	**2.0**	**0.5**
Total Solid Concentration [mg/mL]	**2**	58.3	58.9	60.0	77.3
		56.4	50.4	65.4	70.5
		54.3	51.2	66.9	72.6
	AVG	**56.3**	**53.5**	**64.1**	**73.5**
	SD	**2.0**	**4.7**	**3.6**	**3.5**
	RSD%	**3.6**	**8.8**	**5.7**	**4.7**
	3	42.9	45.5	49.9	60.1
		45.6	40.6	55.7	65.6
		49.8	48.4	57.6	66.9
	AVG	**46.1**	**44.8**	**54.4**	**64.2**
	SD	**3.5**	**3.9**	**4.0**	**3.6**
	RSD%	**7.5**	**8.8**	**7.4**	**5.6**
	5	47.2	49.9	52.8	58.3
		46.5	47.5	55.6	65.7
		48.7	46.9	59.7	67.9
	AVG	**47.5**	**48.1**	**56.0**	**64.0**
	SD	**1.1**	**1.6**	**3.5**	**5.0**
	RSD%	**2.4**	**3.3**	**6.2**	**7.9**
	8	49.5	52.9	54.3	54.1
		49.6	51.9	52.4	56.9
		51.2	50.1	61.9	55.9
	AVG	**50.1**	**51.6**	**56.2**	**55.6**
	SD	**1.0**	**1.4**	**5.0**	**1.4**
	RSD%	**1.9**	**2.7**	**8.9**	**2.6**

Tab. 3-21 Drug entrapment efficiency in Gliclazide/Eudragit S100 nanoparticles in acetone

		Drug entrapment efficiency [%]			
	Nonsolvent Flow Rate [mL/min]	**10.0**	**10.0**	**10.0**	**10.0**
	Solvent Flow Rate [mL/min]	**10.0**	**5.0**	**2.0**	**0.5**
Total Solid Concentration [mg/mL]	**2**	36.0	42.8	49.7	55.9
		34.9	39.7	52.6	50.2
		42.5	35.1	50.9	49.6
	AVG	**37.8**	**39.2**	**51.1**	**51.9**
	SD	**4.1**	**3.9**	**1.5**	**3.5**
	RSD%	**10.9**	**9.9**	**2.9**	**6.7**
	3	38.2	48.9	41.0	55.9
		35.1	45.9	39.5	50.1
		39.8	40.9	37.6	48.9
	AVG	**37.7**	**45.2**	**39.4**	**51.6**
	SD	**2.4**	**4.0**	**1.7**	**3.7**
	RSD%	**6.3**	**8.9**	**4.3**	**7.3**
	5	38.8	48.2	41.8	59.6
		35.1	45.9	40.2	50.9
		32.9	52.6	41.9	52.9
	AVG	**35.6**	**48.9**	**41.3**	**54.5**
	SD	**3.0**	**3.4**	**1.0**	**4.6**
	RSD%	**8.4**	**7.0**	**2.3**	**8.4**
	8	39.8	48.4	40.6	55.6
		31.0	42.5	37.9	50.1
		42.9	45.9	35.7	52.4
	AVG	**37.9**	**45.6**	**38.1**	**52.7**
	SD	**6.2**	**3.0**	**2.5**	**2.8**
	RSD%	**16.3**	**6.5**	**6.4**	**5.2**

Tab. 3-22 Drug entrapment efficiency in Gliclazide/Eudragit S100 nanoparticles in methanol

		Drug entrapment efficiency [%]			
	Nonsolvent Flow Rate [mL/min]	**10.0**	**10.0**	**10.0**	**10.0**
	Solvent Flow Rate [mL/min]	**10.0**	**5.0**	**2.0**	**0.5**
Total Solid Concentration [mg/mL]	**2**	28.9	33.6	38.9	49.5
		25.9	30.7	35.1	45.9
		22.9	35.9	32.6	42.1
	AVG	**25.9**	**33.4**	**35.5**	**45.8**
	SD	**3.0**	**2.6**	**3.2**	**3.7**
	RSD%	**11.6**	**7.8**	**8.9**	**8.1**
	3	24.0	39.7	33.9	45.1
		20.1	32.6	37.8	40.6
		22.6	34.9	36.4	49.7
	AVG	**22.2**	**35.7**	**36.0**	**45.1**
	SD	**2.0**	**3.6**	**2.0**	**4.6**
	RSD%	**8.9**	**10.1**	**5.5**	**10.1**
	5	28.8	39.8	33.0	45.0
		25.4	30.9	30.2	42.5
		22.4	35.5	29.4	40.1
	AVG	**25.5**	**35.4**	**30.9**	**42.5**
	SD	**3.2**	**4.5**	**1.9**	**2.5**
	RSD%	**12.5**	**12.6**	**6.1**	**5.8**
	8	26.7	36.5	39.0	49.1
		25.9	33.6	32.6	45.9
		20.7	39.4	30.1	42.7
	AVG	**24.4**	**36.5**	**33.9**	**45.9**
	SD	**3.3**	**2.9**	**4.6**	**3.2**
	RSD%	**13.3**	**7.9**	**13.5**	**7.0**

The drug loading increased in the order THF>Acetone>MeOH which is the same order of the solubility of the polymer which indicates that higher the affinity of the polymer to the solvent, the higher the drug loading. This is most probably due to marangoni effect which effects the ability of diffusion of polymer to the non-solvent phase together with the solvent

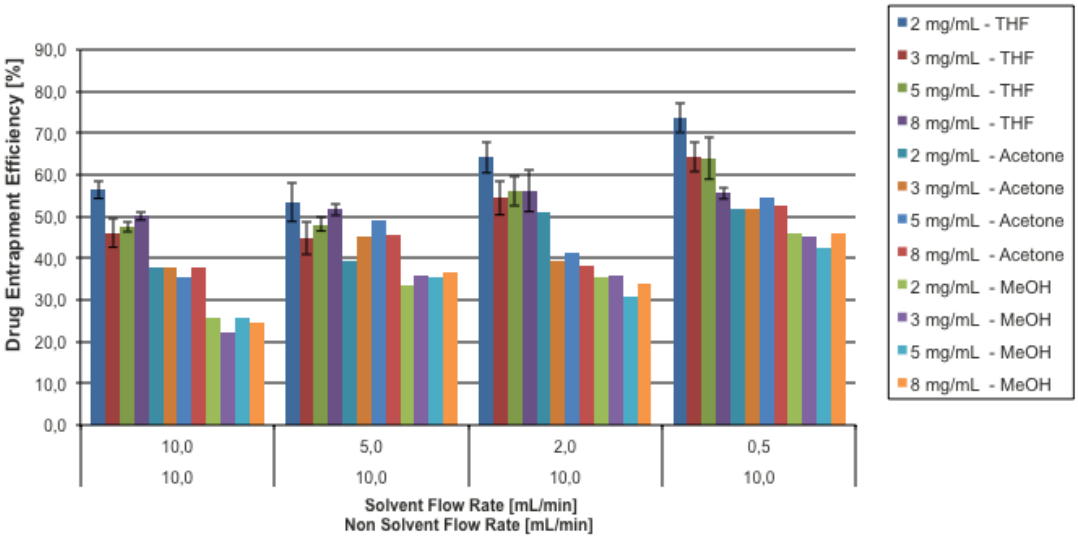

Fig. 3-12 Effect of total solid contents and solvent on drug entrapment efficiency in Gliclazide/Eudragit S100 nanoparticles.

Particle size and PDI analyses were conducted with different solvents, total solid contents and flow rate ratios. The results of these analyses are given in Tab. 3-23 to Tab. 3-25 and Fig. 3-13.

Tab. 3-23 Particle size of Gliclazide/Eudragit S100 nanoparticles in THF

	Nonsolvent Flow Rate [mL/min]	**10.0**		**10.0**		**10.0**		**10.0**	
	Solvent Flow Rate [mL/min]	**10.0**		**5.0**		**2.0**		**0.5**	
		Particle Size [nm]	**PDI**	**Particle Size [nm]**	**PDI**	**Particle Size [nm]**	**PDI**	**Particle Size [nm]**	**PDI**
Total Solid Concentration [mg/mL]	**2**	210.1	0.215	100.2	0.200	90.2	0.196	75.2	0.147
		219.4	0.225	90.7	0.245	80.4	0.201	70.6	0.162
		205.4	0.200	95.6	0.212	85.2	0.175	69.9	0.187
	AVG	**211.6**	**0.213**	**95.5**	**0.219**	**85.3**	**0.191**	**71.9**	**0.165**
	SD	**7.1**	**0.013**	**4.8**	**0.023**	**4.9**	**0.014**	**2.9**	**0.020**
	RSD%	**3.4**	**5.898**	**5.0**	**10.640**	**5.7**	**7.236**	**4.0**	**12.222**
	3	255.6	0.321	111.6	0.249	106.4	0.147	80.0	0.173
		240.9	0.295	100.9	0.265	125.6	0.192	85.9	0.185
		235.6	0.245	110.5	0.278	116.4	0.201	90.2	0.149
	AVG	**244.0**	**0.287**	**107.7**	**0.264**	**116.1**	**0.180**	**85.4**	**0.169**
	SD	**10.4**	**0.039**	**5.9**	**0.015**	**9.6**	**0.029**	**5.1**	**0.018**
	RSD%	**4.2**	**13.459**	**5.5**	**5.502**	**8.3**	**16.073**	**6.0**	**10.846**
	5	253.1	0.222	234.6	0.254	159.2	0.198	113.5	0.175
		250.9	0.265	222.0	0.222	150.9	0.204	90.6	0.198
		246.4	0.214	229.6	0.239	165.4	0.232	100.5	0.111
	AVG	**250.1**	**0.234**	**228.7**	**0.238**	**158.5**	**0.211**	**101.5**	**0.161**
	SD	**3.4**	**0.027**	**6.3**	**0.016**	**7.3**	**0.018**	**11.5**	**0.045**
	RSD%	**1.4**	**11.738**	**2.8**	**6.718**	**4.6**	**8.613**	**11.3**	**27.943**
	8	277.4	0.152	254.4	0.278	170.5	0.281	152.9	0.214
		289.6	0.177	250.6	0.250	186.2	0.244	149.7	0.222
		299.6	0.178	241.1	0.281	180.9	0.233	123.6	0.195
	AVG	**288.9**	**0.169**	**248.7**	**0.270**	**179.2**	**0.253**	**142.1**	**0.210**
	SD	**11.1**	**0.015**	**6.9**	**0.017**	**8.0**	**0.025**	**16.1**	**0.014**
	RSD%	**3.8**	**8.717**	**2.8**	**6.340**	**4.5**	**9.952**	**11.3**	**6.594**

Tab. 3-24 Particle size of Gliclazide/Eudragit S100 nanoparticles in Acetone

	Nonsolvent Flow Rate [mL/min]	**10.0**		**10.0**		**10.0**		**10.0**	
	Solvent Flow Rate [mL/min]	**10.0**		**5.0**		**2.0**		**0.5**	
		Particle Size [nm]	**PDI**	**Particle Size [nm]**	**PDI**	**Particle Size [nm]**	**PDI**	**Particle Size [nm]**	**PDI**
Total Solid Concentration [mg/mL]	**2**	112.5	0.301	100.5	0.264	92.6	0.244	70.2	0.195
		110.5	0.365	90.2	0.210	90.1	0.198	60.5	0.201
		125.6	0.332	90.1	0.236	85.9	0.123	65.7	0.251
	AVG	**116.2**	**0.333**	**93.6**	**0.237**	**89.5**	**0.188**	**65.5**	**0.216**
	SD	**8.2**	**0.032**	**6.0**	**0.027**	**3.4**	**0.061**	**4.9**	**0.031**
	RSD%	**7.1**	**9.621**	**6.4**	**11.411**	**3.8**	**32.430**	**7.4**	**14.256**
	3	128.5	0.322	105.2	0.185	97.2	0.175	80.7	0.198
		118.5	0.295	103.5	0.189	90.6	0.169	70.6	0.206
		110.6	0.289	115.9	0.245	82.6	0.199	75.4	0.154
	AVG	**119.2**	**0.302**	**108.2**	**0.206**	**90.1**	**0.181**	**75.6**	**0.186**
	SD	**9.0**	**0.018**	**6.7**	**0.034**	**7.3**	**0.016**	**5.0**	**0.028**
	RSD%	**7.5**	**5.821**	**6.2**	**16.258**	**8.1**	**8.770**	**6.7**	**15.054**
	5	147.5	0.365	128.3	0.265	109.6	0.206	82.6	0.195
		130.7	0.302	115.6	0.278	90.6	0.242	89.6	0.184
		135.6	0.249	110.4	0.224	95.6	0.241	90.5	0.179
	AVG	**137.9**	**0.305**	**118.1**	**0.256**	**98.6**	**0.230**	**87.6**	**0.186**
	SD	**8.6**	**0.058**	**9.2**	**0.028**	**9.8**	**0.021**	**4.4**	**0.008**
	RSD%	**6.3**	**19.019**	**7.8**	**11.024**	**10.0**	**8.927**	**5.0**	**4.401**
	8	156.7	0.215	132.6	0.154	105.1	0.198	95.7	0.201
		166.5	0.245	120.6	0.167	100.2	0.175	99.5	0.157
		175.6	0.200	115.6	0.149	99.6	0.154	100.4	0.164
	AVG	**166.3**	**0.220**	**122.9**	**0.157**	**101.6**	**0.176**	**98.5**	**0.174**
	SD	**9.5**	**0.023**	**8.7**	**0.009**	**3.0**	**0.022**	**2.5**	**0.024**
	RSD%	**5.7**	**10.415**	**7.1**	**5.931**	**3.0**	**12.528**	**2.5**	**13.588**

Tab. 3-25 Particle size of Gliclazide/Eudragit S100 nanoparticles in MeOH

	Nonsolvent Flow Rate [mL/min]	10.0		10.0		10.0		10.0	
	Solvent Flow Rate [mL/min]	10.0		5.0		2.0		0.5	
		Particle Size [nm]	PDI	Particle Size [nm]	PDI	Particle Size [nm]	PDI	Particle Size [nm]	PDI
Total Solid Concentration [mg/mL]	2	272.7	0.247	255.1	0.198	233.5	0.194	216.6	0.127
		289.1	0.237	250.1	0.243	220.6	0.154	200.6	0.159
		264.3	0.224	241.9	0.264	211.6	0.198	195.6	0.167
	AVG	**275.4**	**0.236**	**249.0**	**0.235**	**221.9**	**0.182**	**204.3**	**0.151**
	SD	**12.6**	**0.012**	**6.7**	**0.034**	**11.0**	**0.024**	**11.0**	**0.021**
	RSD%	**4.6**	**4.887**	**2.7**	**14.349**	**5.0**	**13.369**	**5.4**	**14.017**
	3	280.7	0.345	275.8	0.219	272.9	0.147	270.8	0.199
		289.4	0.247	260.3	0.229	289.6	0.165	250.7	0.198
		290.6	0.298	280.6	0.276	260.4	0.199	260.7	0.135
	AVG	**286.9**	**0.297**	**272.2**	**0.241**	**274.3**	**0.170**	**260.7**	**0.177**
	SD	**5.4**	**0.049**	**10.6**	**0.030**	**14.7**	**0.026**	**10.1**	**0.037**
	RSD%	**1.9**	**16.521**	**3.9**	**12.611**	**5.3**	**15.503**	**3.9**	**20.676**
	5	284.6	0.247	282.5	0.245	280.8	0.154	275.8	0.148
		299.6	0.261	280.4	0.239	270.1	0.178	280.9	0.134
		300.1	0.278	260.3	0.220	275.6	0.201	270.4	0.158
	AVG	**294.8**	**0.262**	**274.4**	**0.235**	**275.5**	**0.178**	**275.7**	**0.147**
	SD	**8.8**	**0.016**	**12.3**	**0.013**	**5.4**	**0.024**	**5.3**	**0.012**
	RSD%	**3.0**	**5.925**	**4.5**	**5.562**	**1.9**	**13.228**	**1.9**	**8.220**
	8	297.6	0.274	288.9	0.298	282.8	0.222	277.9	0.199
		310.9	0.200	299.63	0.257	270.1	0.247	260.5	0.198
		305.6	0.234	298.4	0.299	275.1	0.201	255.1	0.176
	AVG	**304.7**	**0.236**	**295.6**	**0.285**	**276.0**	**0.223**	**264.5**	**0.191**
	SD	**6.7**	**0.037**	**5.9**	**0.024**	**6.4**	**0.023**	**11.9**	**0.013**
	RSD%	**2.2**	**15.695**	**2.0**	**8.419**	**2.3**	**10.311**	**4.5**	**6.806**

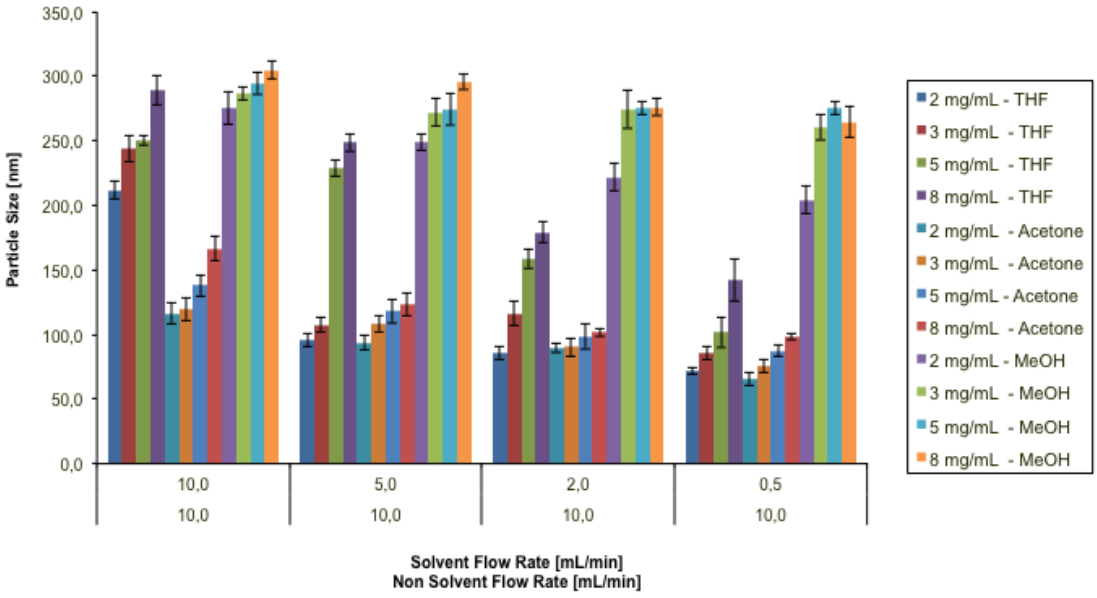

Fig. 3-13 Effect of total solids content and solvent on particle size of Gliclazide/Eudragit S100 nano-particles

It was observed that the particle size increases with an increase in the total solids content. The order of the mean size in different solvents were MeOH>THF>Acetone. As a result with the change in these parameters a particle size range of 70-300 nm is covered.

Danazol/HPMCP HP50 nanoparticles

Total solid contents in the range of 3 to 8 mg•mL^{-1} was used for the preparation of Danazol/HPMCP HP50 nanoparticles with solvents acetone:EtOH 50:50 (w/w %), acetone, EtOH:water 95:5 (w/w %) according toTab. 3-26.

Tab. 3-26 Parameters of the experimental setup for the evaluation of effect of total solid content and solvent.

Drug	Danazol
Polymer	HPMCP HP50
Microjet reactor [µm]	300
Aqueous phase	Water
Organic phase	**Acetone:EtOH, Acetone, EtOH:Water**
Temperature [ºC]	60
Gas flow (bar)	0,1
Total solid content [mg•mL^{-1}]	**3, 5, 8**
Polymer:drug ratio	50
Flow rate solvent [mL•min^{-1}]	**0,5, 2, 5, 10**
Flow rate non-solvent [mL•min^{-1}]	10

The following results (Tab. 3-27) of drug entrapment efficiencies were gathered with using different solvents such as acetone:EtOH 50:50 (w/w %), acetone, EtOH:water 95:5 (w/w %) and aditionally with total solids concentration range of 3-8 mg/mL and solvent flow rate of 10-0.5 mL/min.

Tab. 3-27 Drug entrapment efficiency in Danazol/HPMCP HP50 nanoparticles in acetone

		Drug entrapment efficiency [%]			
	Nonsolvent Flow Rate [mL/min]	**10.0**	**10.0**	**10.0**	**10.0**
	Solvent Flow Rate [mL/min]	**10.0**	**5.0**	**2.0**	**0.5**
Total Solid Concentration [mg/mL]	**3**	38.9	44.3	54.9	64
		35.6	45.9	59.1	69.1
		33.4	50.2	60.5	65.9
	AVG	**36.0**	**46.8**	**58.2**	**66.3**
	SD	**2.8**	**3.1**	**2.9**	**2.6**
	RSD%	**7.7**	**6.5**	**5.0**	**3.9**
	5	33.4	50.3	55.0	61.9
		35.1	49.1	50.2	59.1
		39.6	45.9	59.4	69.5
	AVG	**36.0**	**48.4**	**54.9**	**63.5**
	SD	**3.2**	**2.3**	**4.6**	**5.4**
	RSD%	**8.9**	**4.7**	**8.4**	**8.5**
	8	60.8	60.9	66.4	70.7
		59.4	65.2	65.6	75.6
		55.6	60.9	67.9	79.6
	AVG	**58.6**	**62.3**	**66.6**	**75.3**
	SD	**2.7**	**2.5**	**1.2**	**4.5**
	RSD%	**4.6**	**4.0**	**1.8**	**5.9**

Tab. 3-28 Drug entrapment efficiency in Danazol/HPMCP HP50 nanoparticles in EtOH:Water 95:5 (w/w)

		Drug entrapment efficiency [%]			
	Nonsolvent Flow Rate [mL/min]	**10.0**	**10.0**	**10.0**	**10.0**
	Solvent Flow Rate [mL/min]	**10.0**	**5.0**	**2.0**	**0.5**
Total Solid Concentration [mg/mL]	**3**	50.8	52.6	56.2	72.2
		45.6	48	62.6	68.9
		42.1	51.2	65.4	62.4
	AVG	46.2	50.6	61.4	67.8
	SD	4.4	2.4	4.7	5.0
	RSD%	9.5	4.7	7.7	7.4
	5	48.8	49.9	54.2	71.4
		49.6	55.6	59.4	65.9
		50.2	59.1	62.5	75.6
	AVG	49.5	54.9	58.7	71.0
	SD	0.7	4.6	4.2	4.9
	RSD%	1.4	8.5	7.1	6.9
	8	52.0	57.4	55.3	71.0
		50.3	59.6	59.6	78.4
		48.4	52.3	75.4	75.1
	AVG	50.2	56.4	63.4	74.8
	SD	1.8	3.7	10.6	3.7
	RSD%	3.6	6.6	16.7	5.0

Tab. 3-29 Drug entrapment efficiency in Danazol/HPMCP HP50 nanoparticles in acetone: EtOH 50:50 (w/w)

		Drug entrapment efficiency [%]			
	Nonsolvent Flow Rate [mL/min]	**10.0**	**10.0**	**10.0**	**10.0**
	Solvent Flow Rate [mL/min]	**10.0**	**5.0**	**2.0**	**0.5**
Total Solid Concentration [mg/mL]	**3**	35.5	44.5	50.2	60.7
		39.6	49.6	45.2	50.2
		30.2	45.2	52.6	55.9
	AVG	35.1	46.4	49.3	55.6
	SD	4.7	2.8	3.8	5.3
	RSD%	13.4	6.0	7.7	9.5
	5	37.4	45.6	47.6	57.4
		35.1	48.9	47.6	65.7
		32.6	50.2	49.7	55.1
	AVG	35.0	48.2	48.3	59.4
	SD	2.4	2.4	1.2	5.6
	RSD%	6.9	4.9	2.5	9.4
	8	57.6	60.0	60.5	61.5
		50.4	65.6	55.6	59.6
		45.6	68.2	65.9	61.2
	AVG	51.2	64.6	60.7	60.8
	SD	6.0	4.2	5.2	1.0
	RSD%	11.8	6.5	8.5	1.7

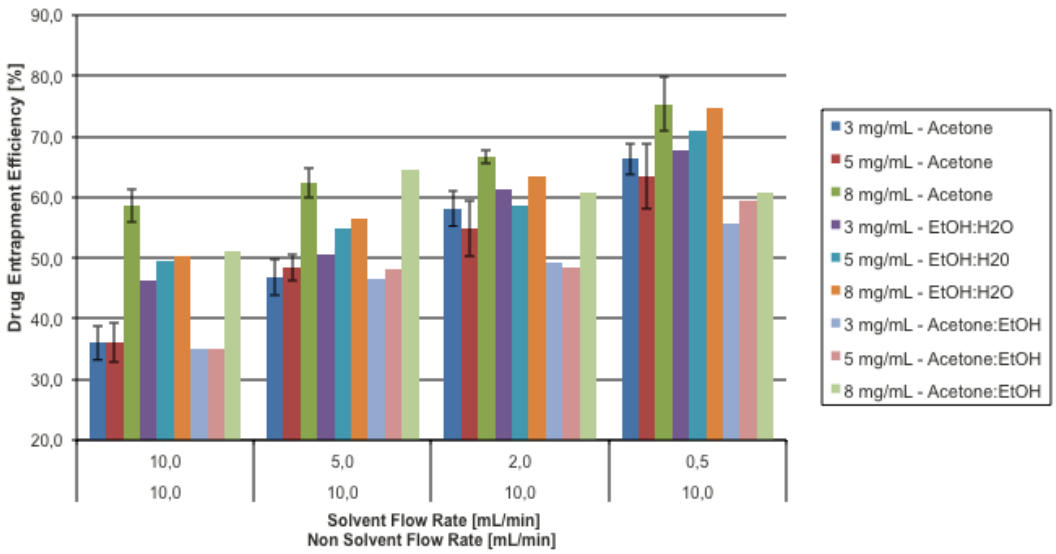

Fig. 3-14 Effects of total solid concentrations and solvent on drug entrapment efficiency in Danazol/HPMCP HP50 nanoparticles

There was no major change in the drug entrapment efficiency with different solvents or different total solid contents. This is most probably due to the good solubility of HPMCP HP50 in all the solvents tested. Furthermore particle size and PDI analyses were conducted with these samples. The results are given in Tab. 3-30 to Tab. 3-32.

Tab. 3-30 Particle size of Danazol/HPMCP HP50 nanoparticles in acetone

	Nonsolvent Flow Rate [mL/min]	10.0		10.0		10.0		10.0	
	Solvent Flow Rate [mL/min]	10.0		5.0		2.0		0.5	
		Particle Size [nm]	PDI	Particle Size [nm]	PDI	Particle Size [nm]	PDI	Particle Size [nm]	PDI
Total Solid Concentration [mg/mL]	3	115.7	0.121	98.1	0.165	91.8	0.280	57.7	0.323
		125.6	0.219	90.5	0.197	85.1	0.240	50.7	0.370
		110.2	0.180	95.6	0.260	88.3	0.340	55.1	0.250
	AVG	117.2	0.173	94.7	0.207	88.4	0.287	54.5	0.314
	SD	7.8	0.049	3.9	0.048	3.4	0.050	3.5	0.060
	RSD%	6.7	28.465	4.1	23.313	3.8	17.558	6.5	19.237
	5	128.0	0.299	153.6	0.386	129.3	0.349	58.2	0.250
		115.6	0.240	135.9	0.240	110.9	0.320	62.6	0.150
		110.6	0.180	144.1	0.190	119.1	0.290	62.7	0.190
	AVG	118.1	0.240	144.5	0.272	119.8	0.320	61.2	0.197
	SD	9.0	0.060	8.9	0.102	9.2	0.030	2.6	0.050
	RSD%	7.6	24.826	6.1	37.442	7.7	9.229	4.2	25.593
	8	132.9	0.350	201.7	0.280	150.1	0.140	74.0	0.290
		148.5	0.390	215.3	0.210	142.3	0.160	70.1	0.240
		130.6	0.400	222.2	0.260	152.1	0.250	71.9	0.210
	AVG	137.3	0.380	213.1	0.250	148.2	0.183	72.0	0.247
	SD	9.7	0.026	10.4	0.036	5.2	0.059	2.0	0.040
	RSD%	7.1	6.963	4.9	14.422	3.5	31.961	2.7	16.384

Tab. 3-31 Particle size of Danazol/HPMCP HP50 nanoparticles in EtOH:Water 95:5 (w/w)

	Nonsolvent Flow Rate [mL/min]	10.0		10.0		10.0		10.0	
	Solvent Flow Rate [mL/min]	10.0		5.0		2.0		0.5	
		Particle Size [nm]	PDI	Particle Size [nm]	PDI	Particle Size [nm]	PDI	Particle Size [nm]	PDI
Total Solid Concentration [mg/mL]	3	272.3	0.368	139.8	0.325	87.6	0.320	80.6	0.270
		278.4	0.237	112.6	0.262	89.1	0.341	79.1	0.390
		255.6	0.240	146.9	0.200	85.2	0.290	70.9	0.210
	AVG	268.8	0.282	133.1	0.262	87.3	0.317	76.9	0.290
	SD	11.8	0.075	18.1	0.063	2.0	0.026	5.2	0.092
	RSD%	4.4	26.550	13.6	23.825	2.3	8.086	6.8	31.604
	5	298.5	0.229	156.6	0.346	98.7	0.320	77.26	0.190
		302.1	0.350	150.9	0.290	95.4	0.300	70.9	0.210
		312.9	0.320	157.4	0.350	93.2	0.350	75.1	0.280
	AVG	304.5	0.300	155.0	0.329	95.8	0.323	74.4	0.227
	SD	7.5	0.063	3.5	0.034	2.8	0.025	3.2	0.047
	RSD%	2.5	21.027	2.3	10.207	2.9	7.783	4.3	20.849
	8	325.8	0.340	298.2	0.290	123.6	0.180	98.6	0.170
		333.6	0.390	285.6	0.270	110.4	0.190	84.63	0.140
		342.9	0.370	280.4	0.250	123.9	0.240	102.9	0.160
	AVG	334.1	0.367	288.1	0.270	119.3	0.203	95.4	0.157
	SD	8.6	0.025	9.2	0.020	7.7	0.032	9.6	0.015
	RSD%	2.6	6.863	3.2	7.407	6.5	15.809	10.0	9.750

Tab. 3-32 Particle size of Danazol/HPMCP HP50 nanoparticles in acetone: EtOH 50:50 (w/w)

	Nonsolvent Flow Rate [mL/min]	10.0		10.0		10.0		10.0	
	Solvent Flow Rate [mL/min]	10.0		5.0		2.0		0.5	
		Particle Size [nm]	PDI	Particle Size [nm]	PDI	Particle Size [nm]	PDI	Particle Size [nm]	PDI
Total Solid Concentration [mg/mL]	3	100.5	0.330	80	0.358	56.9	0.256	34.9	0.237
		99.5	0.229	75.6	0.294	50.1	0.326	30.2	0.120
		105.2	0.270	70.9	0.230	55.9	0.390	32.9	0.150
	AVG	101.7	0.276	75.5	0.294	54.3	0.324	32.7	0.169
	SD	3.0	0.051	4.6	0.064	3.7	0.067	2.4	0.061
	RSD%	3.0	18.383	6.0	21.769	6.8	20.686	7.2	35.959
	5	106.4	0.321	89.1	0.306	78.2	0.308	57.2	0.210
		115.9	0.240	92.6	0.390	82.5	0.240	67.9	0.180
		110.7	0.290	95.1	0.350	88.6	0.210	60.2	0.170
	AVG	111.0	0.284	92.3	0.349	83.1	0.253	61.8	0.187
	SD	4.8	0.041	3.0	0.042	5.2	0.050	5.5	0.021
	RSD%	4.3	14.408	3.3	12.050	6.3	19.873	8.9	11.152
	8	120.3	0.340	109	0.290	89.5	0.180	68.6	0.170
		110.2	0.390	102.3	0.270	85.1	0.190	60.4	0.140
		112.6	0.370	120.1	0.250	97.5	0.240	65.1	0.160
	AVG	114.4	0.367	110.5	0.270	90.7	0.203	64.7	0.157
	SD	5.3	0.025	9.0	0.020	6.3	0.032	4.1	0.015
	RSD%	4.6	6.863	8.1	7.407	6.9	15.809	6.4	9.750

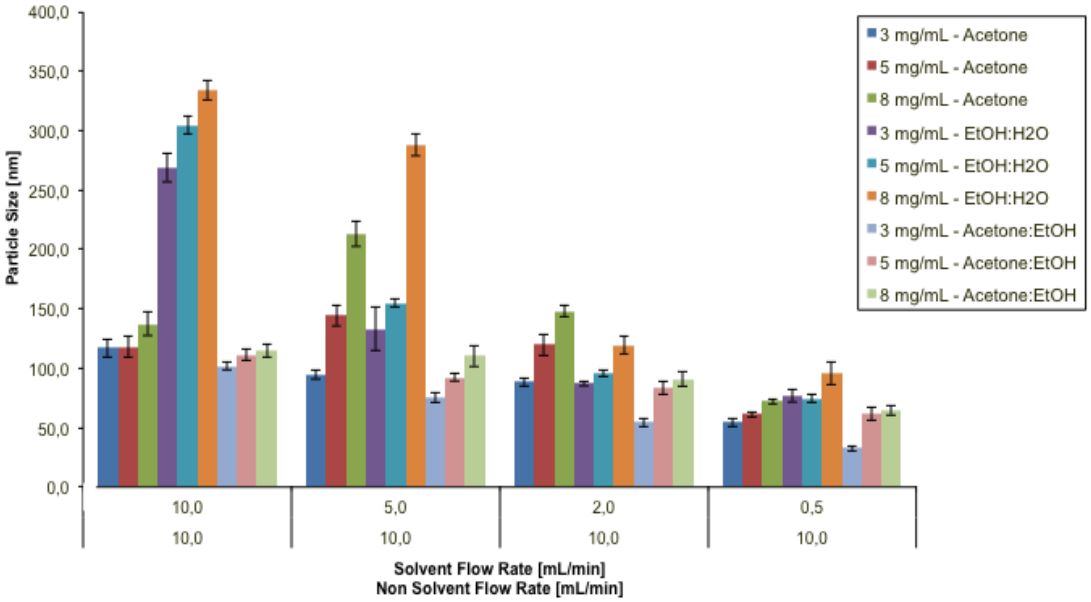

Fig. 3-15 Effect of total solid concentration and solvent on particle size of HPMCP HP50/Danazol nanoparticles

It was observed that the particle size increases with the increase in the total solid content. The order of the mean size in different solvents were EtOH:Water>Acetone>Acetone:EtOH. As a result with the change in these parameters a particle size range of 38-325 nm is covered.

3.2.4. Drug release of Gliclazide/Eudragit S100 and Danazol/HPMCP HP50 nanoparticles

Gliclazide/Eudragit S100 and Danazol/HPMCP HP50 nanoparticles were characterized in terms of drug release using SGF, SIF as medium and furthermore with two stage dissolution methodology as described in Chapter 2.2. The media was supplemented with 0.5 % Tween 20 for Gliclazide nanoparticles and 1% Tween 20 for Danazol nanoparticles.

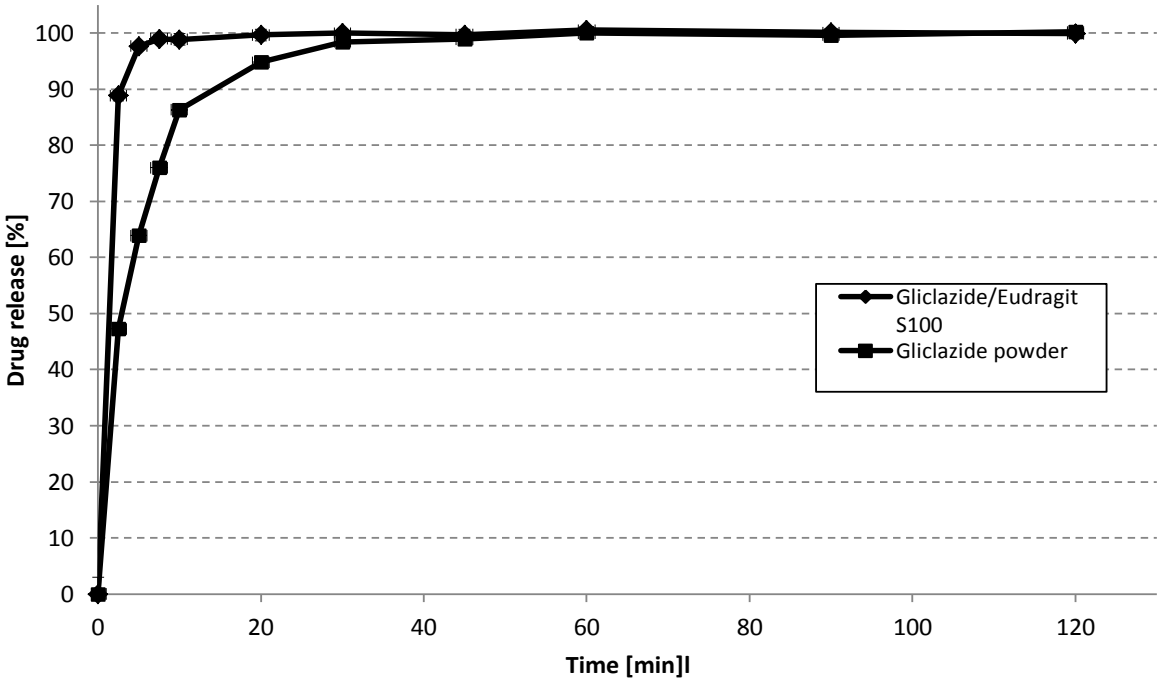

Fig. 3-16 Drug release from Gliclazide powder and Gliclazide/Eudragit S100 nanoparticles using simulated intestinal fluid supplemented with 0.5 % Tween 20

In the case of nanoparticles drug release was completed within 10 minutes whereas for Gliclazide powder with a volume weighted diameter of 3.683 µm, it was more than 60 minutes.

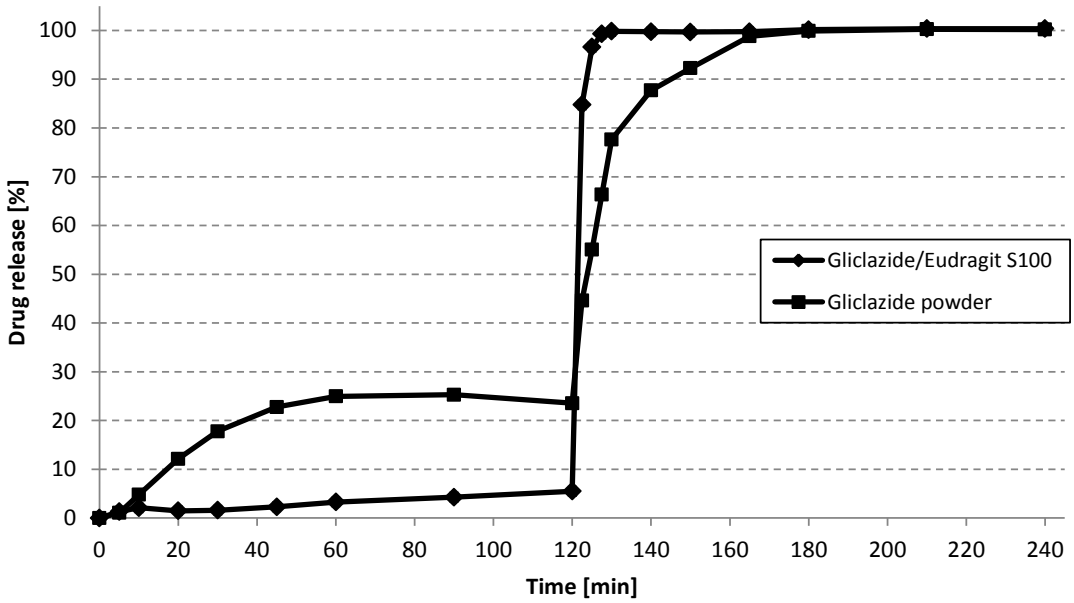

Fig. 3-17 Drug release from Gliclazide powder and Gliclazide/Eudragit S100 nanoparticles using two stage methodology

Enteric coating of Gliclazide /Eudragit S100 nanoparticles was shown in the acid stage of the drug release studies. Furthermore, with the increase in the pH, 100 % drug release was reached within 10 minutes.

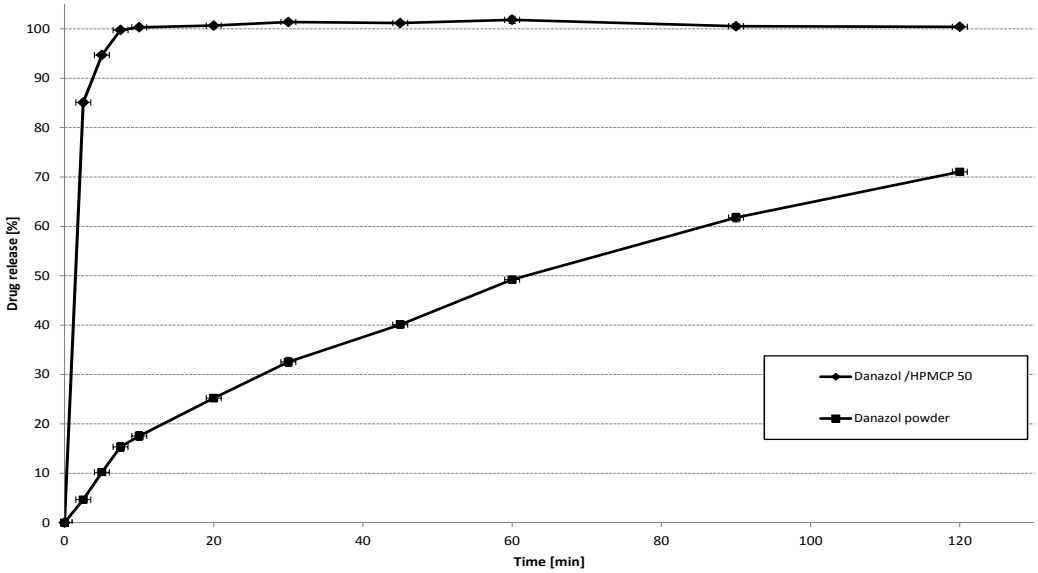

Fig. 3-18 Drug release from Danazol powder and Danazol/HPMCP HP50 nanoparticles using simulated intestinal fluid supplemented with 1 % Tween 20

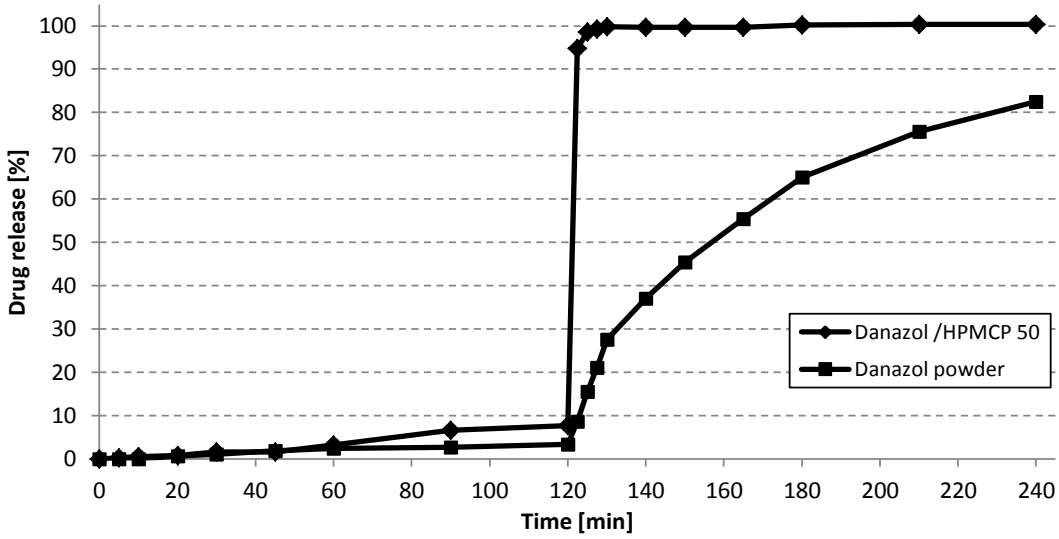

Fig. 3-19 Drug release from Danazol powder and Danazol/HPMCP HP50 nanoparticles using two stage methodology

With both drug release studies enteric resistance of Danazol nanoparticles and increase in the drug release rate was shown also for Danazol/HPMCP HP50 nanoparticles.

3.2.5. DSC studies with Gliclazide/Eudragit S100 and Danazol/HPMCP HP50 nanoparticles

DSC studies were conducted with nanoparticles prepared as described in chapter 2.2.4 in order to prove the encapsulation of Gliclazide and Danazol resulting in amorph API.

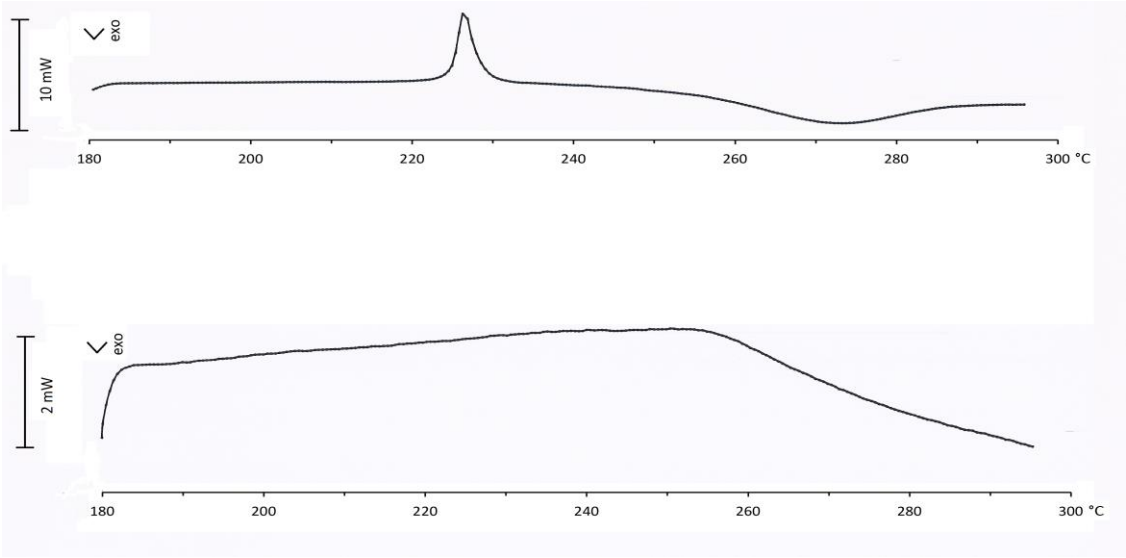

Fig. 3-20 DSC diagram of Danazol powder and Danazol/HPMCP HP50 nanoparticles

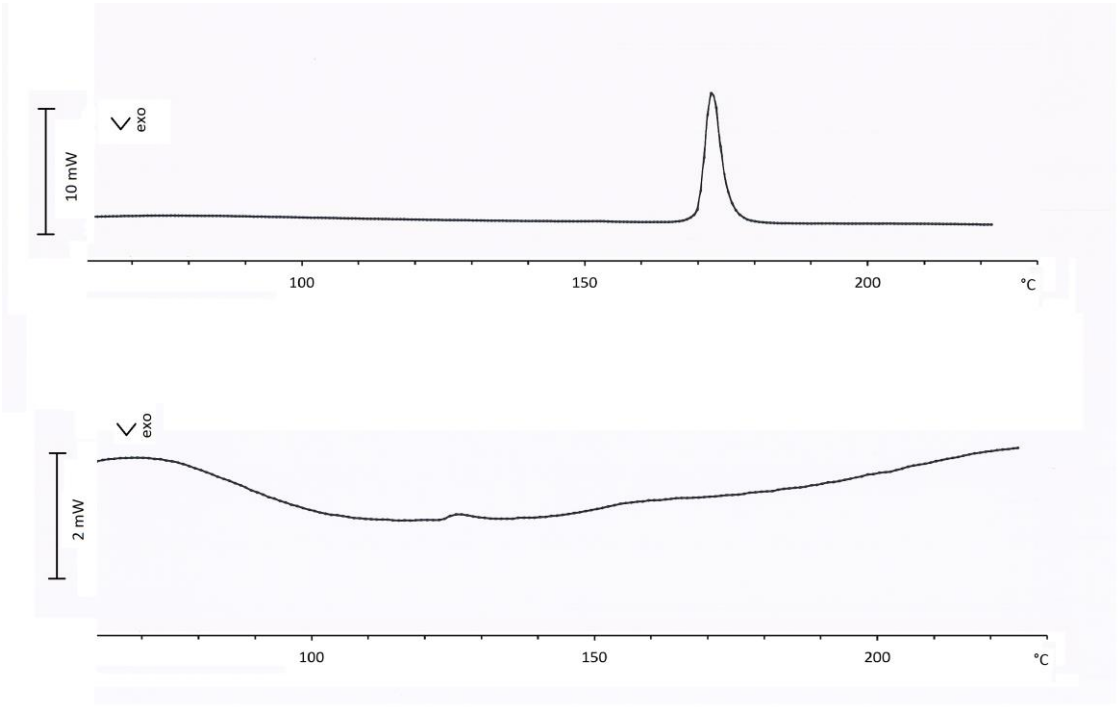

Fig. 3-21 DSC diagram of Gliclazide powder and Gliclazide/Eudragit S100 nanoparticles

As seen in both diagrams melting curves of Danazol and Gliclazide could not be observed for nanoparticle formulations indicating encapsulation of Danazol and Gliclazide in the used polymer resulting in amorphous API.

3.3. Preparation of pH selective positively loaded nanoparticles for oral applications

Fenofibrate was used as the model drug and HPMCP HP50 /chitosan polymer system was used for the preparation of pH selective and positively loaded particles. First HPMCP HP50/chitosan system was established. Thereafter fenofibrate was loaded in these particles. Design of experiments was applied for these experiments.

3.3.1. Establishment of HPMCP HP50/chitosan system

Determination of HPMCP HP50/chitosan concentrations

The aim of this part of the study was to find the right concentration ratio between HPMCP HP50 and chitosan that will result in positively charged particles with a particle size between 100-200 nm. As the reaction takes place in the microjet reactor it is expected that depending on the concentration ratio of the polymers there would be remaining either amine or carboxylic acid groups.

The results of particle size and ZETA potential changes depending on the concentrations of HPMCP HP50 and chitosan are given in Tab. 3-33, Tab. 3-34 and Fig. 3-22 . Statistical analyses of the change in particle size and ZETA potential are given in Tab. 3-33 and Tab. 3-34. IR spectra are represented in Fig. 3-23 to Fig. 3-26 to prove the changes in the molecular structure through neutralization of amine group of chitosan with carboxylic acid group of HPMCP HP50.

Tab. 3-33 Results of the particle size determinations of nanoparticles prepared using different concentrations of HPMCP HP50 (3, 5, 8, 10 mg/mL) and chitosan (0.01, 0.02, 0.05, 0.1, 0.5, 1, 1.5, 2, 3 mg/mL). n=3.

HPMCP HP50 Concentration (mg/mL)	Chitosan concentration (mg/mL)									
	0.01	0.02	0.05	0.1	0.2	0.5	1	1.5	2	3
	Particle size (nm)									
3_1	160.2	126.8	129.8	614.0	586.2	1431.0	157.1	266.3	224.8	582.8
3_2	154.2	115.6	137.5	596.3	593.5	1358.0	148.7	266.2	219.3	575.5
3_3	165.8	120.6	129.6	600.4	564.3	1565.9	164.5	258.6	222.4	596.3
Average	**160.1**	**121.0**	**132.3**	**603.6**	**581.3**	**1451.6**	**156.8**	**263.7**	**222.2**	**584.9**
SD	**5.8**	**5.6**	**4.5**	**9.3**	**15.2**	**105.5**	**7.9**	**4.4**	**2.8**	**10.6**
5_1	174.6	146.6	147.7	145.8	248.6	1291.0	190.5	287.4	271.9	689.2
5_2	168.5	153.7	153.8	155.9	238.5	1365.6	183.9	278.9	265.6	689.9
5_3	182.4	155.9	150.6	140.5	250.2	1389.6	187.6	288.5	266.8	695.3
Average	**175.2**	**152.1**	**150.7**	**147.4**	**245.8**	**1348.7**	**187.3**	**284.9**	**268.1**	**691.5**
SD	**7.0**	**4.9**	**3.1**	**7.8**	**6.3**	**51.4**	**3.3**	**5.3**	**3.3**	**3.3**
8_1	160.7	156.6	179.0	176.6	163.0	573.0	302.2	327.1	345.9	750.8
8_2	165.5	148.7	170.5	165.3	162.5	565.3	299.6	319.4	333.5	730.6
8_3	164.3	149.6	177.5	185.6	163.5	582.6	310.8	325.6	340.9	823.6
Average	**163.5**	**151.6**	**175.7**	**175.8**	**163.0**	**573.6**	**304.2**	**324.0**	**340.1**	**768.3**
SD	**2.5**	**4.3**	**4.5**	**10.2**	**0.5**	**8.7**	**5.9**	**4.1**	**6.2**	**48.9**
10_1	180.5	182.1	198.9	202.5	186.8	348.8	1268.0	964.0	393.1	798.3
10_2	178.5	176.9	198.6	212.6	195.6	358.9	1158.6	965.9	400.5	756.6
10_3	185.6	189.5	195.6	210.9	177.6	361.5	1222.5	947.6	389.6	885.6
Average	**181.5**	**182.8**	**197.7**	**208.7**	**186.7**	**356.4**	**1216.4**	**959.2**	**394.4**	**813.5**
SD	**3.7**	**6.3**	**1.8**	**5.4**	**9.0**	**6.7**	**55.0**	**10.1**	**5.6**	**65.8**

Tab. 3-34: Results of the ZETA potential determinations of nanoparticles prepared using different concentrations of HPMCP HP50 (3, 5, 8, 10 mg/mL) and chitosan (0.01, 0.02, 0.05, 0.1, 0.5, 1, 1.5, 2, 3 mg/mL). n=3

HPMCP HP50 Concentration (mg/mL)	Chitosan concentration (mg/mL)									
	0.01	0.02	0.05	0.1	0.2	0.5	1	1.5	2	3
	ZETA potential (mV)									
3_1	-37.4	-31.5	-30.8	-18.5	-10.8	-2.3	19.1	22.0	34.8	40.3
3_2	-30.6	-29.5	-20.9	-19.6	-9.5	-1.0	20.5	23.5	32.5	45.6
3_3	-43.6	-22.6	-20.4	-20.1	-15.5	-3.6	17.5	26.9	39.6	48.3
Average	**-37.2**	**-27.9**	**-24.0**	**-19.4**	**-11.9**	**-2.3**	**19.0**	**24.1**	**35.6**	**44.7**
SD	**6.5**	**4.7**	**5.9**	**0.8**	**3.2**	**1.3**	**1.5**	**2.5**	**3.6**	**4.1**
5_1	-39.6	-32.1	-31.4	-23.8	-16.1	-6.6	13.0	18.5	30.6	36.4
5_2	-40.5	-29.6	-25.4	-22.5	-15.4	-5.8	22.3	23.5	32.6	38.6
5_3	-39.6	-28.4	-22.5	-25.9	-16.5	-3.4	15.4	24.9	28.6	35.9
Average	**-39.9**	**-30.0**	**-26.4**	**-24.1**	**-16.0**	**-5.3**	**16.9**	**22.3**	**30.6**	**37.0**
SD	**0.5**	**1.9**	**4.5**	**1.7**	**0.6**	**1.7**	**4.8**	**3.4**	**2.0**	**1.4**
8_1	-42.5	-36.9	-32.4	-26.4	-18.3	-11.0	10.5	14.3	26.5	34.5
8_2	-44.6	-32.6	-30.4	-23.6	-19.4	-12.5	9.5	12.4	28.9	32.4
8_3	-49.5	-33.5	-28.9	-25.6	-20.3	-10.9	12.6	15.6	22.3	30.5
Average	**-45.5**	**-34.3**	**-30.6**	**-25.2**	**-19.3**	**-11.5**	**10.9**	**14.1**	**25.9**	**32.5**
SD	**3.6**	**2.3**	**1.8**	**1.4**	**1.0**	**0.9**	**1.6**	**1.6**	**3.3**	**2.0**
10_1	-45.6	-39.4	-38.4	-29.2	-23.5	-14.2	1.0	9.1	24.2	29.5
10_2	-46.9	-38.6	-32.5	-25.6	-26.4	-12.9	5.0	7.9	18.5	27.9
10_3	-48.9	-40.2	-32.6	-26.9	-20.4	-18.5	8.0	10.5	21.4	26.4
Average	**-47.1**	**-39.4**	**-34.5**	**-27.2**	**-23.4**	**-15.2**	**4.7**	**9.2**	**21.4**	**27.9**
SD	**1.7**	**0.8**	**3.4**	**1.8**	**3.0**	**2.9**	**3.5**	**1.3**	**2.9**	**1.6**

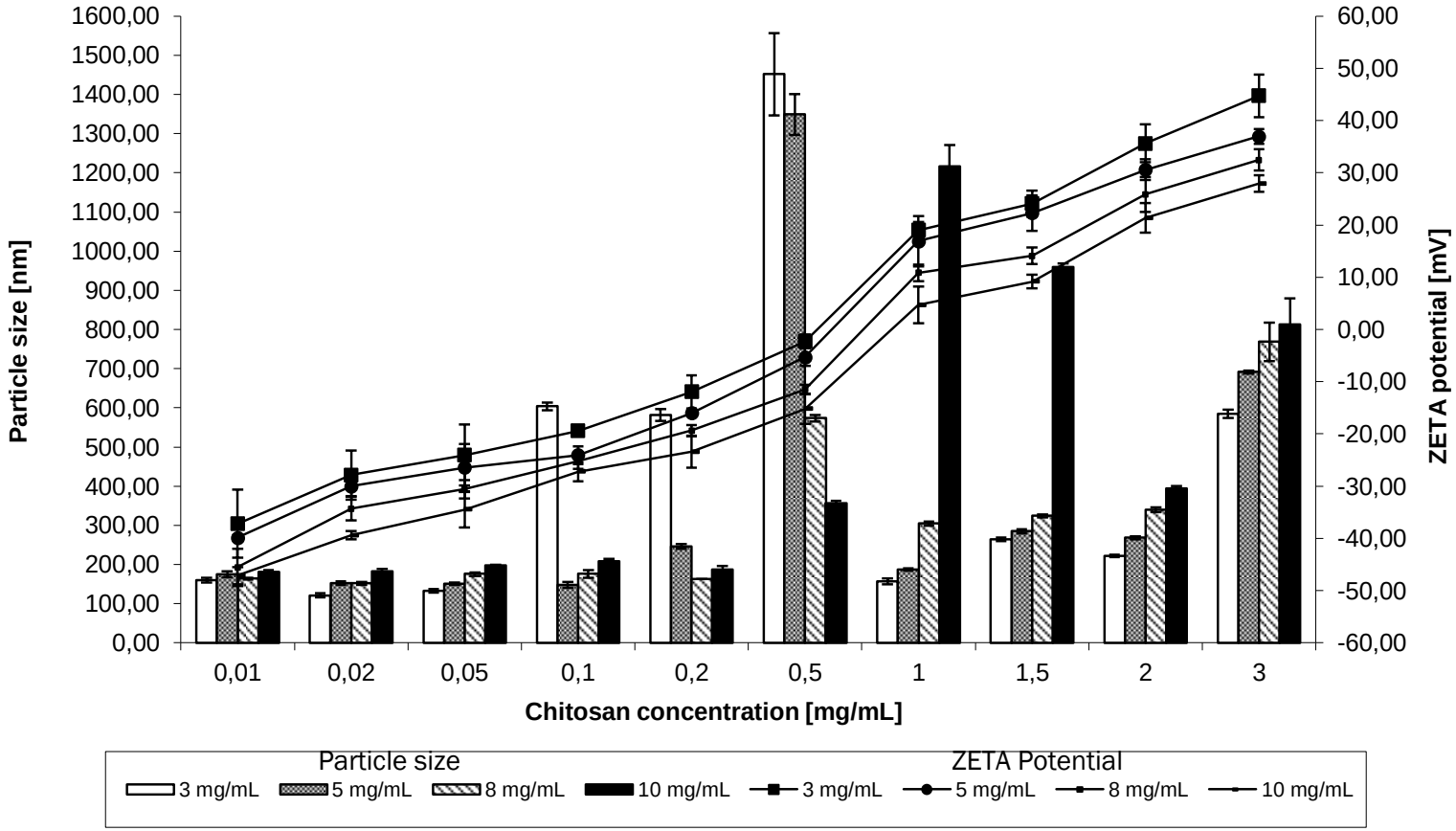

Fig. 3-22 Changes in the particle size and ZETA potential of nanoparticles prepared using different concentrations of HPMCP HP50 (3, 5, 8, 10 mg/mL) and chitosan (0.01, 0.02, 0.05, 0.1, 0.5, 1, 1.5, 2, 3 mg/mL). Results are given as average of n= 3. (Bars represent the particle size on the left axis, lines represent the ZETA potential on the right axis).

PDI (polydispersity index) values were for all cases lower than 0.3 indicating homogenous dispersion of the particles.

The proof of concept is shown above with the significant increase of the ZETA potential with the increase in chitosan concentration for all the tested concentrations of HPMCP HP50. Also increase in HPMCP HP50 concentration resulted in the significant decrease in the ZETA potential for all the tested concentrations of chitosan.

ANOVA statistics was applied for each HPMCP HP50 concentration to investigate the significance of difference in ZETA potential with an increase in the chitosan concentration. Results are presented in Tab. 3-35 . Furthermore Bonferroni correction was applied to investigate the differences between groups based on the chitosan concentration.

Tab. 3-35 ANOVA statistics of significance of increase in the ZETA potential with the increase in the chitosan concentration (0.01, 0.02, 0.05, 0.1, 0.5, 1, 1.5, 2, 3 mg/mL) for all concentrations of HPMCP HP50 (3, 5, 8, 10 mg/mL) tested.

HPMCP HP50 concentration [mg/mL]	Degree of Freedom (DF)	Sum of Squares (SS)	Mean Squares (MS)	F	P
3 mg/mL	9	22432.4210	2492.4910	167.2210	<0.001
5 mg/mL	9	21058.3050	2339.8120	328.8250	<0.001
8 mg/mL	9	20033.7400	2225.9710	491.6740	<0.001
10 mg/mL	9	18890.3070	2098.9230	348.1760	<0.001

As seen in the table above the results are found to be significant with p values all smaller than 0.001

Tab. 3-36 ANOVA statistics of significance with the Bonferroni correction of the decrease in the ZETA potential with an increase in the HPMCP HP50 concentrations (3, 5, 8, 10 mg/mL) for all the concentrations of chitosan (0.01, 0.02, 0.05, 0.1, 0.5, 1, 1.5, 2, 3 mg/mL) tested

Chitosan concentration [mg/mL]	DF	SS	MS	F	P
0.01	3	196.5160	65.5050	4.5010	0.0390
0.02	3	282.4000	94.1360	13.5170	0.0020
0.05	3	395.6760	131.8920	10.2990	0.0040
0.10	3	99.1690	33.0560	14.6650	0.0010
0.20	3	215.0420	71.6810	14.1380	0.0010
0.50	3	307.7160	102.5720	29.6090	<0.001
1.00	3	376.6070	125.5360	12.4290	0.0020
1.50	3	444.0690	148.0230	27.0280	<0.001
2.00	3	338.6290	112.8760	12.4020	0.0020
3.00	3	461.5760	153.8590	24.5850	<0.001

All P values are in agreement with the significance of results since $p < 0.05$ points out the significance of the differences.

As demonstrated with the results when the chitosan concentrations were lower than 0.5 mg/mL nanoparticles were negatively charged. When the ZETA potential was within the limits -10.0 to +10.0, electrostatic charges were not strong enough to stabilize the nanoparticles which results in formation of microparticles through particle aggregation. This is also closely related to the concentration of polymers used and their ratio which directly determines the ZETA potential. When the ZETA potential was higher than +10.0 the increase in the concentrations of any of the polymers results in increase in the particle size due to the increase in the density of nanoparticles. The structures of the nanoparticles were proved with the following IR profiles of chitosan, HPMCP HP50 and Chitosan/HPMCP HP50 nanoparticles.

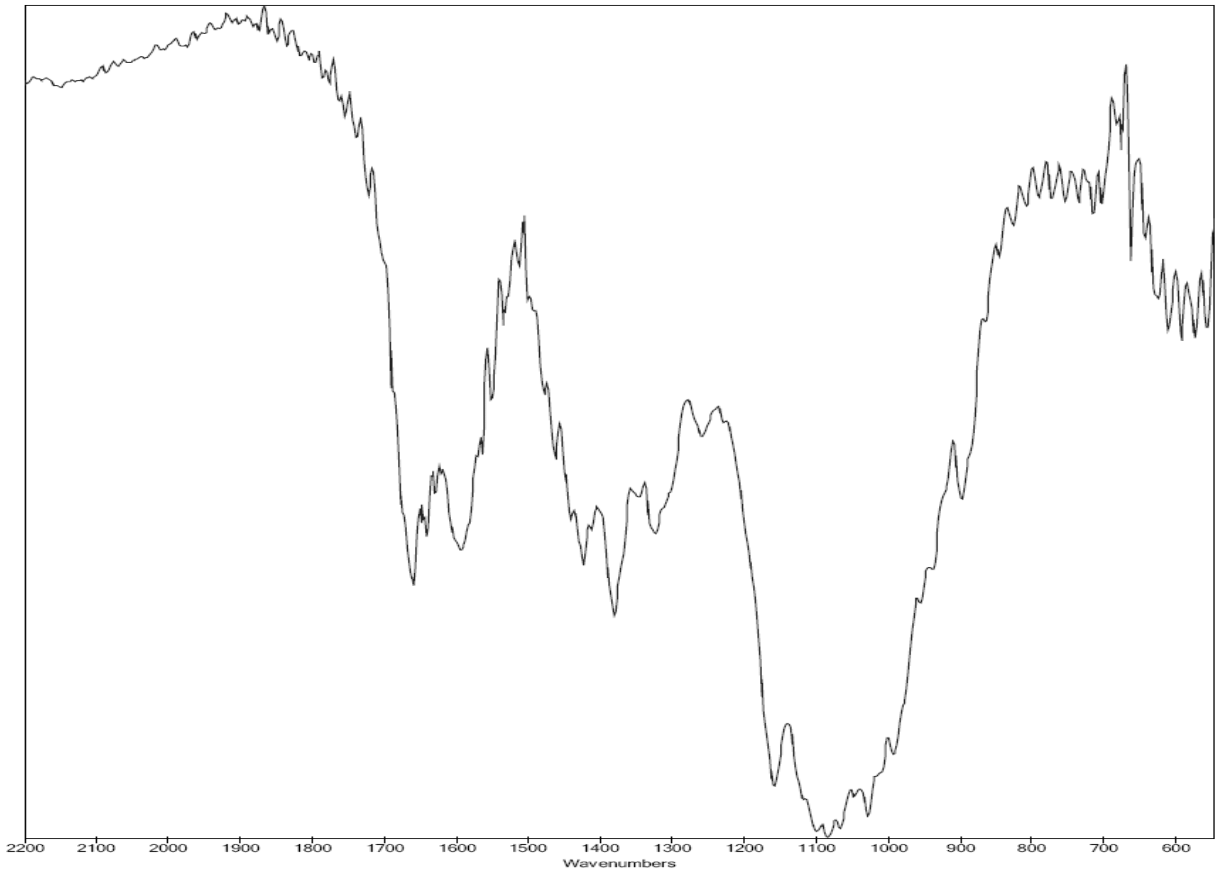

Fig. 3-23 IR profile of chitosan

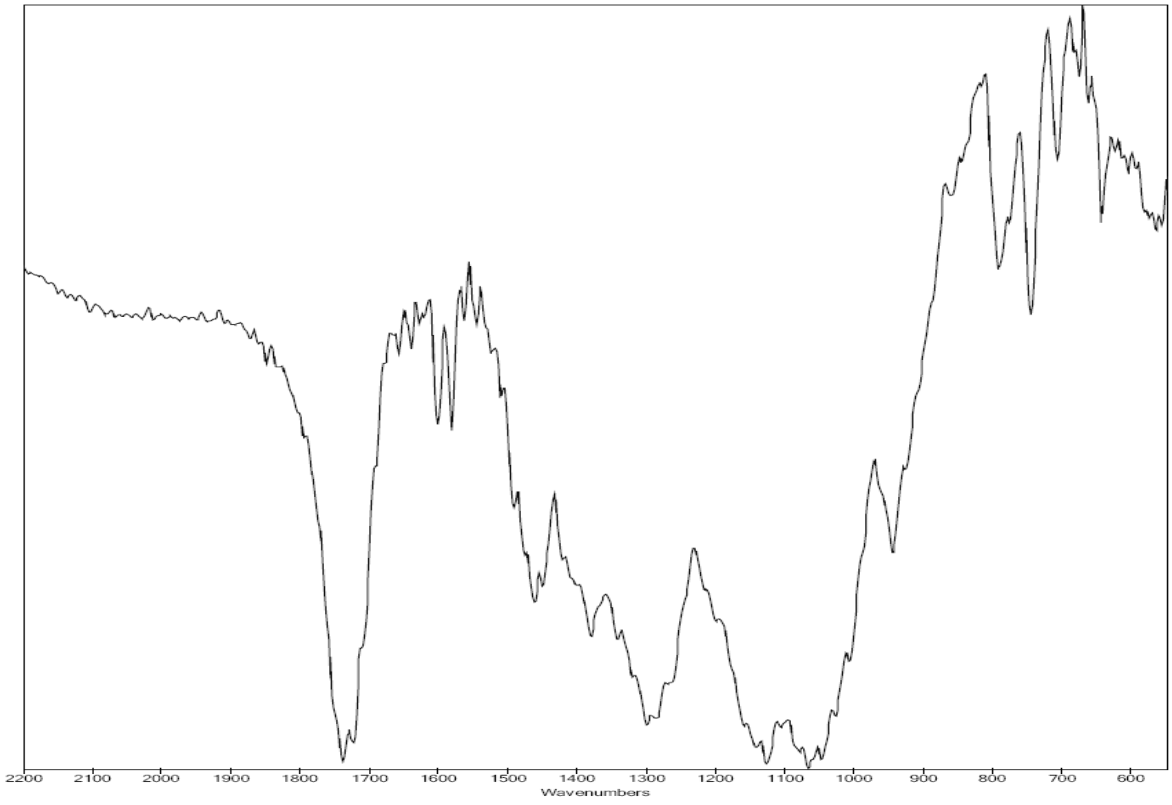

Fig. 3-24 IR profile of HPMCP HP50

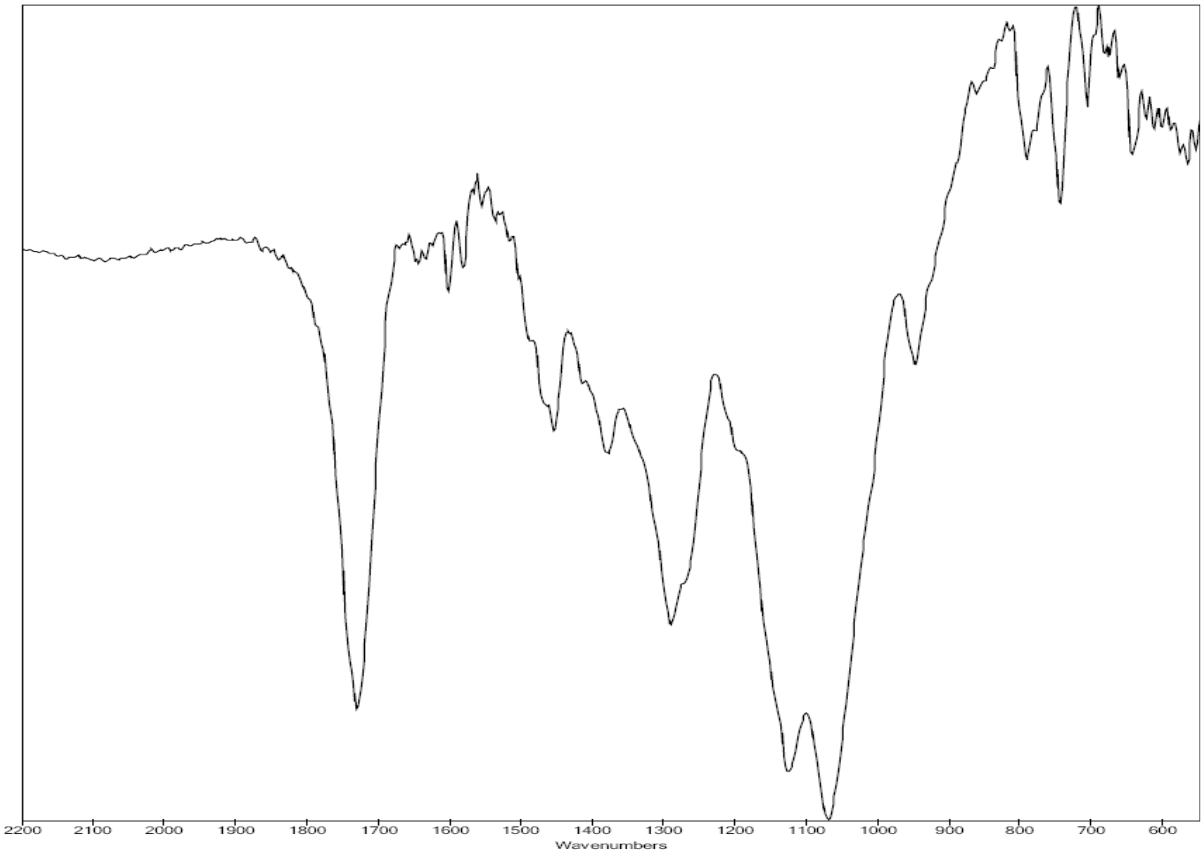

Fig. 3-25 IR profile of Chitosan/HPMCP HP50 nanoparticles

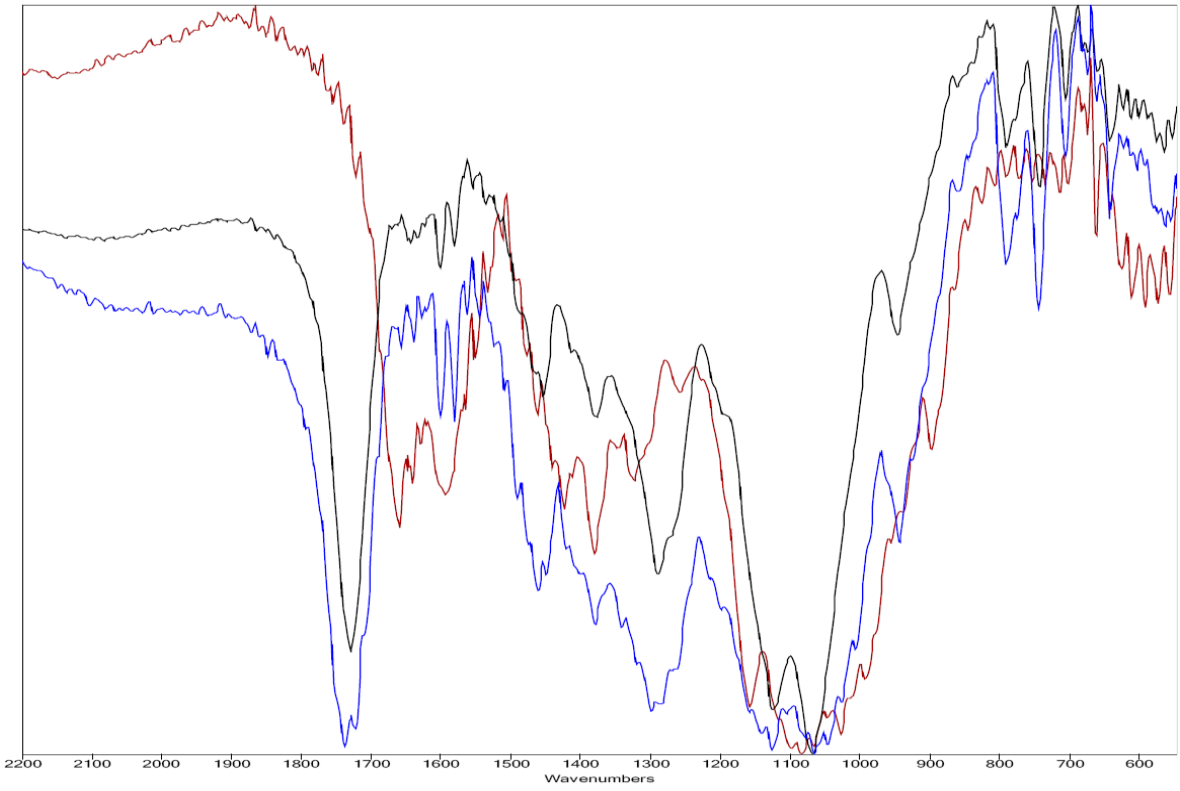

Fig. 3-26 IR profile of overlay of HPMCP HP50/chitosan nanoparticles (black), chitosan (red), HPMCP HP50 (blue).

IR profiles of HPMCP HP50 and Chitosan/HPMCP HP50 nanoparticles were found to be similar due to the high ration of HPMCP HP50 in the nanoparticles (5.3:1).

Two signals are taken into consideration in the IR profile of chitosan. First one is the –NH bending band at 1593 cm^{-1} and the second one is the absorption peak of $–NH_2$ at 1158 cm^{-1}

HPMCP HP50 showed the characteristic C=O stretching bands at 1737 cm^{-1} (-COOH) and 1722 cm^{-1} (-COOR)

Although IR profile of Chitosan/HPMCP HP50 nanoparticles are similar to the IR profile of HPMCP HP50 due to the high HPMCP HP50 content in the nanoparticle formation it is still possible to point out the interaction between $–NH_2$ group of chitosan and –COOH group of HPMCP HP50. $–NH_3^+$ bending bands are seen at 1545 cm^{-1} and 1638 cm^{-1} On the contrary C=O stretching band at 1735 cm^{-1} (-COOH) and 1718 cm^{-1} (-COOR) are shifted to 1730 cm^{-1} as a single band.

Selection of the steric stabilization agent

Efficiency of the surfactant coating was evaluated with the increase in the particle size, decrease in the ZETA potential and also electron microscope analyses. The result of the size determinations are given in Tab. 3-33 with the statistical evaluation of the change in the particle size to prove the significant difference of the surfactant coated particles compared to the surfactant free particles. Furthermore the decrease in the ZETA potentials depending on the surfactant used and its concentration are shown in Tab. 3-34.

The pictures of SEM and TEM were also included to prove the measurements done with DLS method and also for the presentation of surfactant coating.

The coating of nanoparticles using different surfactant molecules were proven with the increase in the particle size. It was found that there is significant difference ($p<0.001$) between the particle sizes of different formulations. Anova analyses were further evaluated with Bonferroni t-test for the comparison of individual groups with the Chitosan/HPMCP HP50 nanoparticles which is given as control.

Tab. 3-37 Particle sizes of Chitosan/HPMCP50 nanoparticles in the presence of PVA, PVP, HPC, Pluronic F127, HPMC.

Nanoparticle composition	Particle size	Standard deviation	PDI
Chitosan/HPMCP50	130.7	3.2	0.104
Chitosan/HPMCP50 0.5 % PVA	127.0	5.6	0.129
Chitosan/HPMCP50 1.0 % PVA	141.4	2.5	0.121
Chitosan/HPMCP50 0.5 % PVP	133.8	7.3	0.117
Chitosan/HPMCP50 1.0 % PVP	142.2	6.8	0.148
Chitosan/HPMCP50 0.5 % HPC	152.3	4.5	0.090
Chitosan/HPMCP50 0.5 % Pluronic F127	153.4	3.9	0.004
Chitosan/HPMCP50 1.0 % Pluronic F127	268.4	2.9	0.004
Chitosan/HPMCP50 0.5 % HPMC	175.5	6.5	0.195
Chitosan/HPMCP50 1.0 % HPMC	204.0	7.8	0.202

Tab. 3-38 Comparison between Chitosan/HPMCP50 nanoparticles prepared without any surfactant and Chitosan/HPMCP50 nanoparticles prepared using PVA, PVP, HPC, Pluronic F127, HPMC with Bonferroni test.

Comparison	Difference of means	t	P
Row 1 vs. Row 8	137.700	31.085	<0.001
Row 1 vs. Row 10	73.700	16.638	<0.001
Row 1 vs. Row 9	44.800	10.113	<0.001
Row 1 vs. Row 7	22.700	5.124	<0.001
Row 1 vs. Row 6	21.600	4.876	<0.001
Row 1 vs. Row 5	11.500	2.596	0.155
Row 1 vs. Row 3	10.700	2.415	0.229
Row 1 vs. Row 2	3.700	0.835	1.000
Row 1 vs. Row 4	3.100	0.700	1.000

The results summarized in table 8 revealed that there is no significant difference of nanoparticles prepared with PVA and PVP in comparison to control in terms of particle sizes. The most significant difference was observed in the nanoparticles coated with Pluronic F127. Thus when particle size is taken into consideration PVP and PVA were not able to interact with the nanoparticle surface to form

micelle like structures. On the other hand it was possible to coat the nanoparticles with HPC, Pluronic F127, HPMC in both concentrations 0.5% and 1.0% with increasing intensities.

Efficiency of coating process was also proven with the decrease in the ZETA potential. As the nanoparticles are coated with the surfactant molecules the interaction between the charged groups on the nanoparticle surface and the ions present in the medium are effected resulting in the decrease in the ZETA potential.

Tab. 3-39 ZETA potentials of Chitosan/HPMCP50 nanoparticles in the presence of PVA, PVP, HPC, Pluronic F127, HPMC

Nanoparticle composition	ZETA potential	Standard deviation
Chitosan/HPMCP50	23.8	4.29
Chitosan/HPMCP50 0.5 % PVA	20.2	4.05
Chitosan/HPMCP50 1.0 % PVA	18.5	6.66
Chitosan/HPMCP50 0.5 % PVP	23.2	8.58
Chitosan/HPMCP50 1.0 % PVP	19.2	9.42
Chitosan/HPMCP50 0.5 % HPC	5.43	6.26
Chitosan/HPMCP50 0.5 % Pluronic F127	14.1	4.84
Chitosan/HPMCP50 1.0 % Pluronic F127	9.1	9.75
Chitosan/HPMCP50 0.5 % HPMC	19.5	5.08
Chitosan/HPMCP50 1.0 % HPMC	16.4	5.74

The concentration dependent trend in decrease of the ZETA potential is clearly shown when nanoparticles are coated with Pluronic F127. As the concentration increases the ZETA potential is decreasing. Anova analyses also revealed a significant difference between nanoparticles formulation without any surfactant molecule and the ones that are coated with Pluronic F127 ($p<0.01$)

SEM analyses

SEM analyses were conducted in order to prove the DLS particle size measurements and also to get information on the structure of nanoparticles.

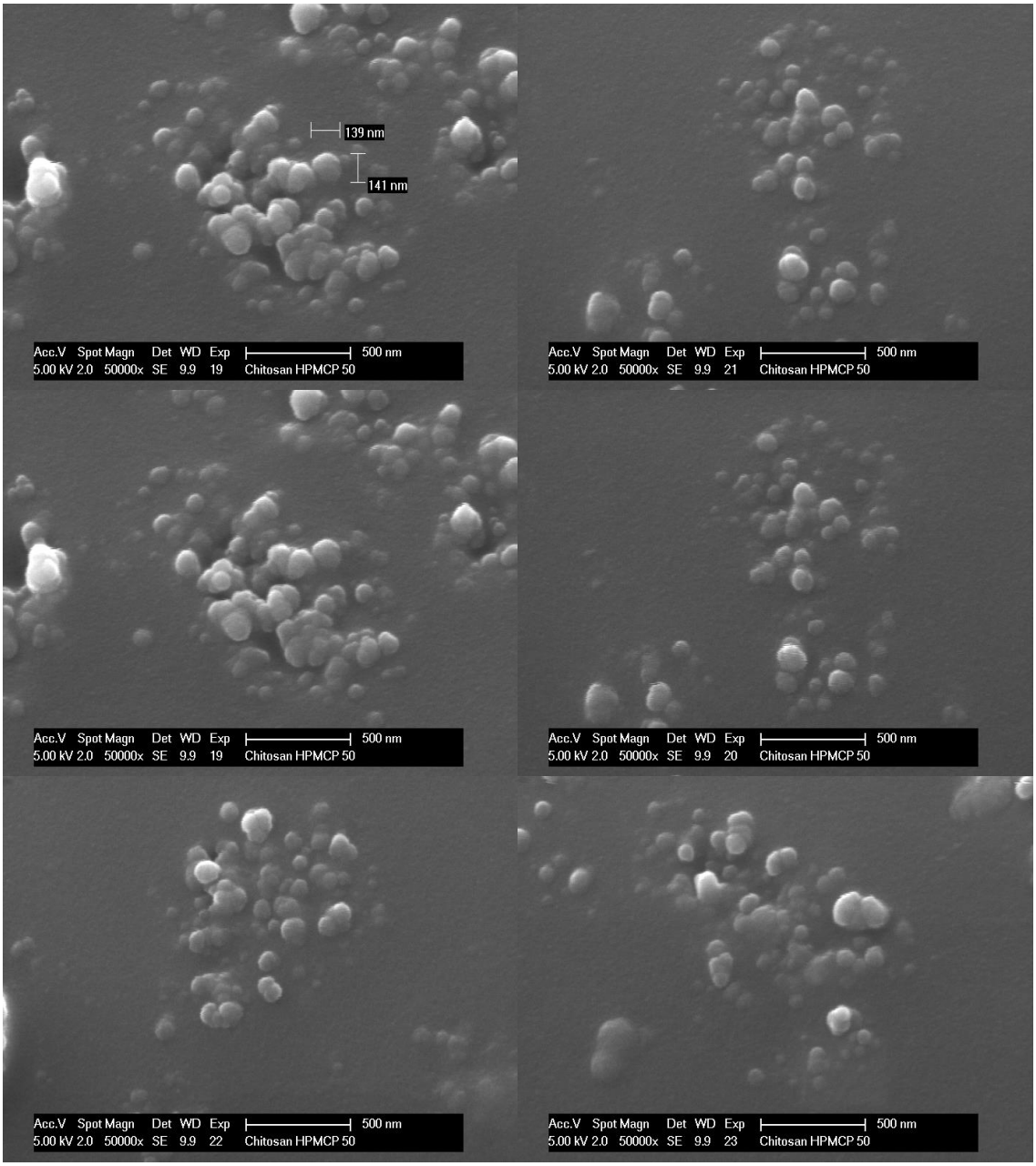

Fig. 3-27 SEM pictures of Chitosan/HPMCP HP50 nanoparticles coated with HPMC 0.5 %(Scales indicates 500 nm)

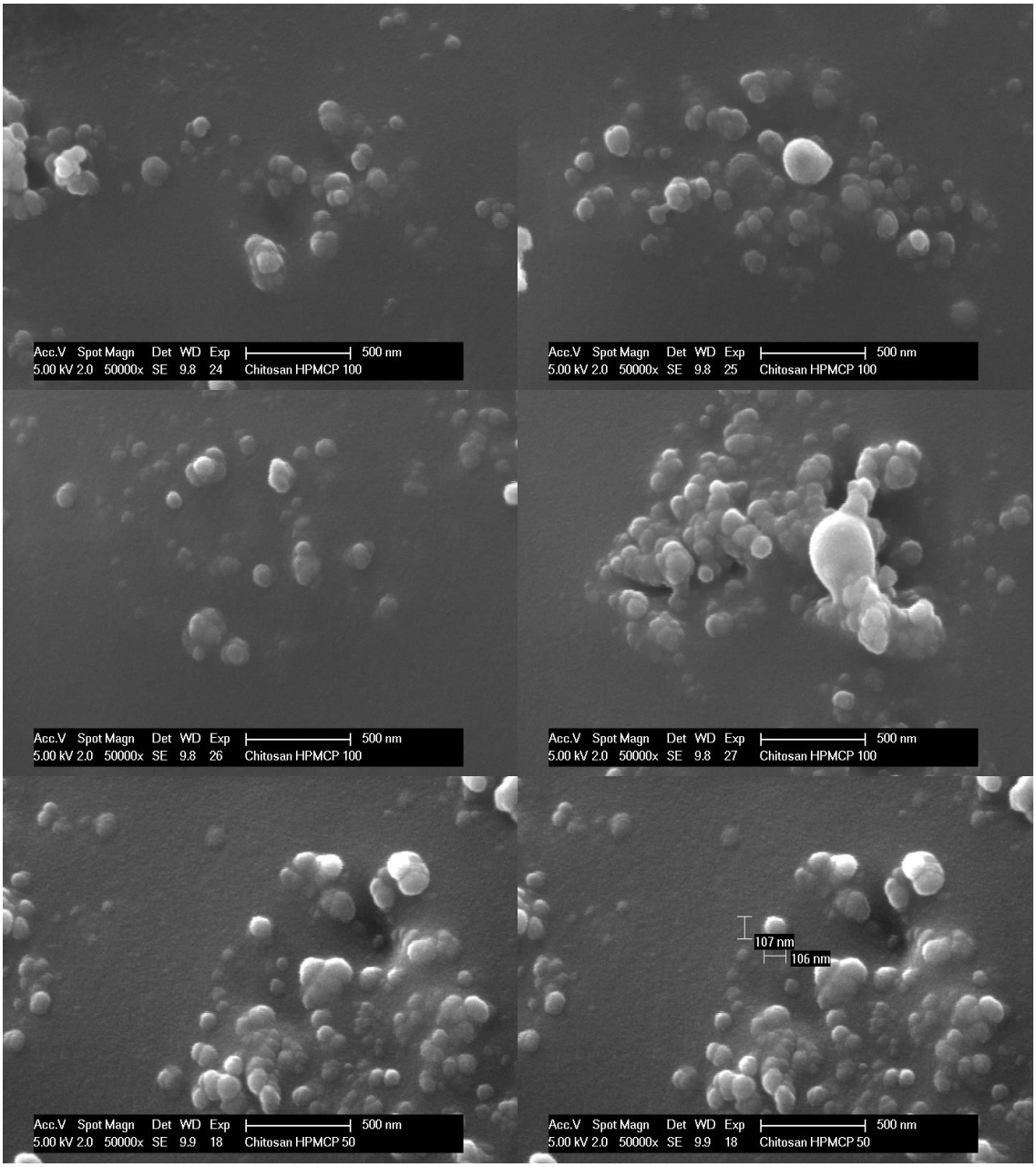

Fig. 3-28 **SEM pictures of Chitosan/HPMCP HP50 nanoparticles coated with Pluronic F127 0.5 %. (Scales indicates 500 nm)**

SEM investigations were in agreement with the particle size determinations done with DLS. The particles were tend to aggregate due to the sample pretreatment and SEM conditions but it was possible to identify single particles and measure the particle size. SEM investigations were in agreement with the particle size determinations done with DLS with a particle size range of 100-200 nm. Furthermore the produced nanoparticles were spherical.

TEM analyses

The results of the TEM analyses were in agreement with DLS and SEM measurements in regards to the particle size of 100-200 nm. There was no aggregation present between the particles.

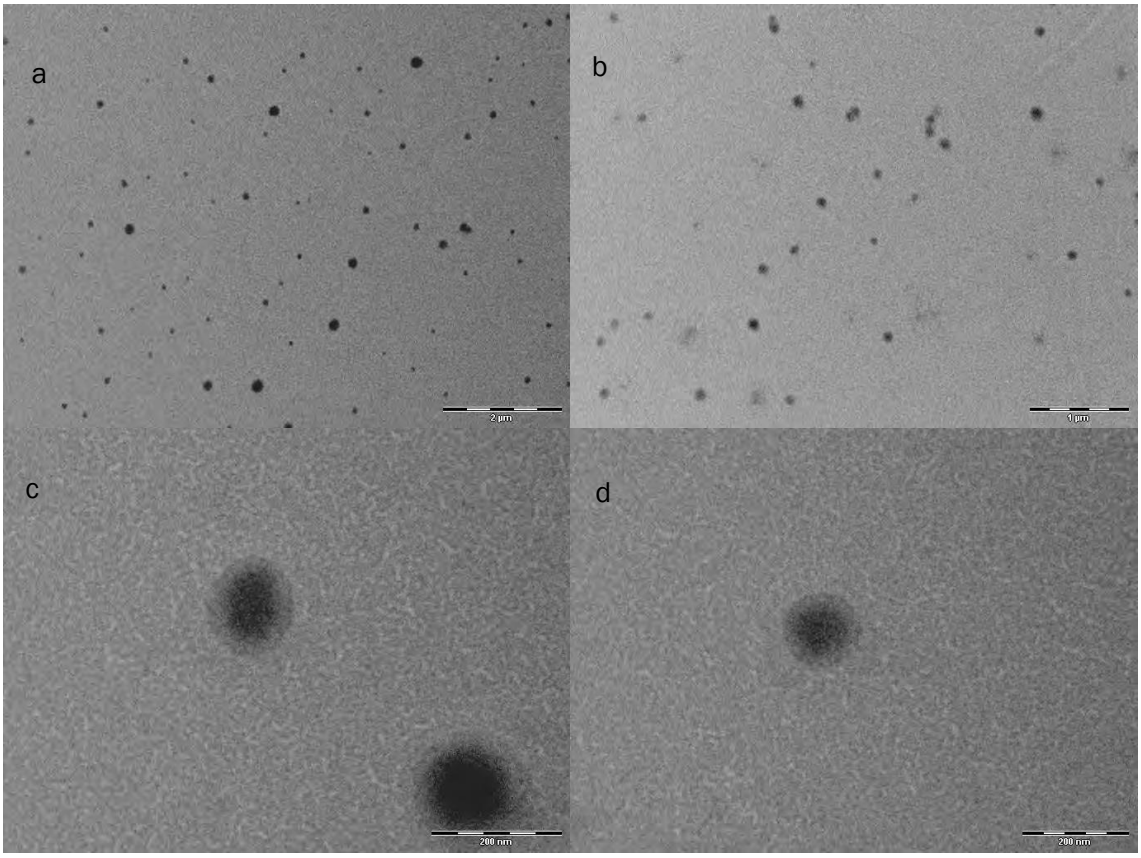

Fig. 3-29 TEM of pictures of Chitosan/HPMCP HP50 nanoparticles coated with Pluronic F127 0.5 % (Scales represent 2 µm, 1 µm, 200 nm, 200 nm for a, b, c and d respectively)

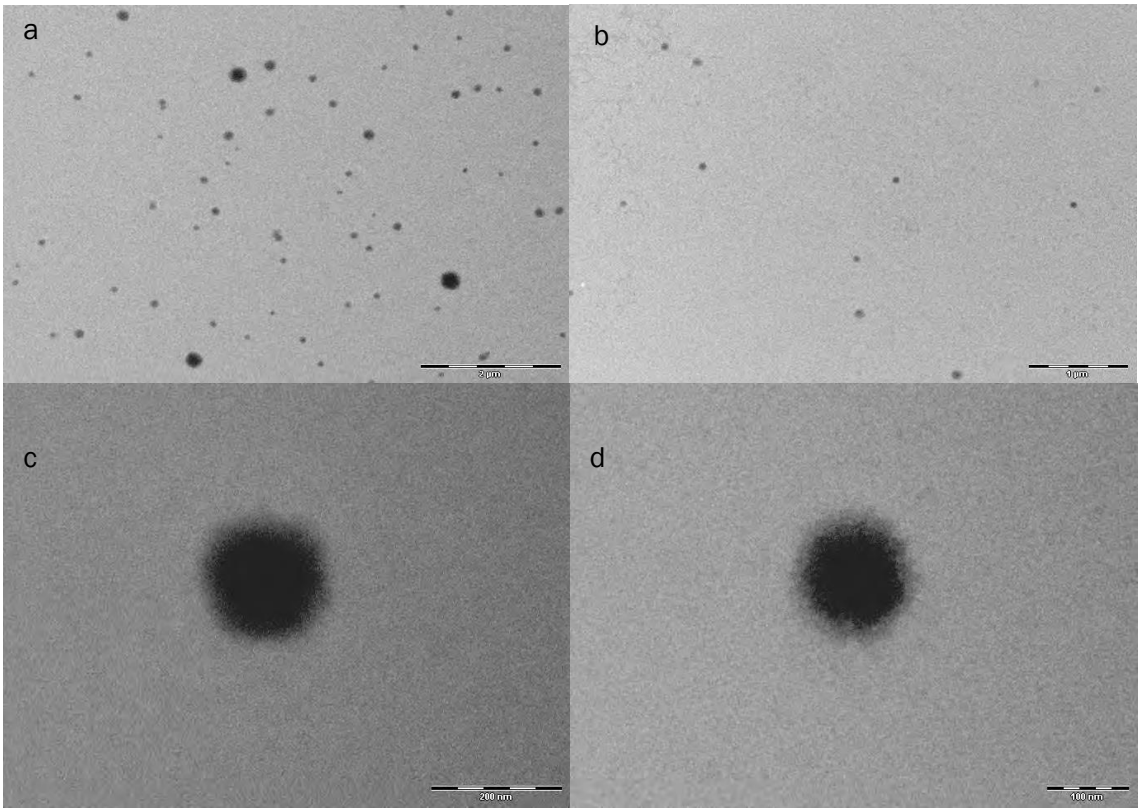

Fig. 3-30 TEM of pictures of Chitosan/HPMCP HP50 nanoparticles coated with HPMC 0.5 % (Scales represent 2 µm, 1 µm, 200 nm, 100 nm for a, b, c and d respectively)

It was also possible to see the coating around the nanoparticles formed by the surfactant molecule Pluronic F127 and HPMC. The thickness of the coating was around 25 nm which is also the difference between the uncoated and 0,5 % Pluronic F127 coated nanoparticles which have the particle sizes of 130.7 nm and 153.4 nm respectively determined using DSL technique.

The results above demonstrated the efficiency of Pluronic F127 in coating the Chitosan/HPMCP50 nanoparticles. There was a significant increase in the particle size and decrease in ZETA potential in concentration dependent manner. Furthermore the particle size and the efficiency of coating were proved with SEM and TEM pictures.

3.3.2. Drug loading into pH selective positively loaded nanoparticles for oral applications

Optimization of production parameters using orthogonal design

30 experiments were conducted to ensure the rotatable orthogonality in response surface. 8 experiments contained extreme values (-2, +2). Repeatability was ensured with 6 central points and these points are statistically evaluated for deviations.

The data was analysed separately for all the dependent factors (particle size, PDI and drug loading) using ANOVA. Correlation of predicted values with the real values is given for the sake of repeatability. Furthermore the normality of the data and the Box-Cox transformation analyses were conducted.

Lastly the graphics of response surface is constructed for the presentation of acquired data and the predictions.

Degrees of freedom values were evaluated for the selected factors and the values. The evaluation is summarized in Tab. 3-40.

Tab. 3-40 Evaluation of degrees of freedom for the rotatable orthogonal design

Parameter	Degrees of freedom
Model	14
Residuals	15
Lack of Fit	10
Pure Error	5
Corr. Total	29

A recommendation is a minimum of 3 lack of fit degrees of freedom and 4 degrees of freedom for pure error. This ensures a valid lack of fit test. Fewer degrees of freedom will lead to a test that may

not detect lack of fit. Below in Tab**. 3-41** and Tab. 3-42 particle size, PDI, drug load of nanoparticles are presented.

Tab. 3-41 **Coded values of factors flow rate, solvent, gas pressure, temperature and corresponding real values gathered from experiments conducted with the given run order.**

Run order	Flow rate (mL/min)	Solvent	Gas pressure (bar)	Temperature (ºC)	Particle Size (nm)	PDI	Drug load (µg/mL)
1	1.00	1.00	-1.00	1.00	319.7	0.26	131.80
2	0.00	0.00	0.00	0.00	196.4	0.14	72.50
3	-1.00	-1.00	1.00	1.00	396.2	0.29	49.20
4	-1.00	1.00	-1.00	1.00	419.7	0.27	100.90
5	0.00	0.00	0.00	0.00	202.2	0.14	79.00
6	1.00	-1.00	1.00	-1.00	174.8	0.14	85.10
7	-1.00	-1.00	-1.00	-1.00	176.1	0.16	71.60
8	0.00	0.00	0.00	0.00	190.4	0.15	81.90
9	0.00	0.00	0.00	0.00	198.7	0.14	76.00
10	0.00	0.00	-2.00	0.00	136.3	0.17	103.00
11	-1.00	-1.00	-1.00	1.00	277.3	0.16	69.70
12	0.00	0.00	0.00	-2.00	219.8	0.21	107.10
13	-1.00	1.00	1.00	1.00	456.2	0.34	54.70
14	1.00	-1.00	-1.00	-1.00	165.1	0.17	101.50
15	1.00	1.00	1.00	-1.00	267.2	0.27	93.30
16	0.00	-2.00	0.00	0.00	170.0	0.13	45.00
17	-2.00	0.00	0.00	0.00	408.3	0.27	30.60
18	1.00	1.00	1.00	1.00	243.9	0.33	74.70
19	0.00	0.00	2.00	0.00	248.3	0.24	54.30
20	0.00	0.00	0.00	0.00	199.5	0.15	70.70
21	1.00	-1.00	-1.00	1.00	202.3	0.12	87.90
22	0.00	0.00	0.00	2.00	446.8	0.28	91.10
23	-1.00	1.00	1.00	-1.00	358.3	0.30	58.20
24	1.00	-1.00	1.00	1.00	219.8	0.19	51.60
25	-1.00	1.00	-1.00	-1.00	325.9	0.22	74.40
26	-1.00	-1.00	1.00	-1.00	198.1	0.19	68.00
27	1.00	1.00	-1.00	-1.00	266.1	0.25	152.90
28	0.00	2.00	0.00	0.00	305.6	0.29	63.20
29	0.00	0.00	0.00	0.00	208.3	0.15	81.40
30	2.00	0.00	0.00	0.00	169.4	0.17	101.40

Tab. 3-42 Actual values of factors flow rate, solvent, gas pressure, temperature and corresponding real values gathered from experiments conducted with the given run order.

Run order	Flow rate (mL/min)	Solvent	Gas pressure (bar)	Temperature (ºC)	Particle Size (nm)	PDI	Drug load (µg/mL)
1	8.00	11.22	0.50	75.00	319.7	0.26	131.80
2	6.00	7.56	1.00	58.00	196.4	0.14	72.50
3	4.00	3.89	1.50	75.00	396.2	0.29	49.20
4	4.00	11.22	0.50	75.00	419.7	0.27	100.90
5	6.00	7.56	1.00	58.00	202.2	0.14	79.00
6	8.00	3.89	1.50	40.00	174.8	0.14	85.10
7	4.00	3.89	0.50	40.00	176.1	0.16	71.60
8	6.00	7.56	1.00	58.00	190.4	0.15	81.90
9	6.00	7.56	1.00	58.00	198.7	0.14	76.00
10	6.00	7.56	0.00	58.00	136.3	0.17	103.00
11	4.00	3.89	0.50	75.00	277.3	0.16	69.70
12	6.00	7.56	1.00	23.00	219.8	0.21	107.10
13	4.00	11.22	1.50	75.00	456.2	0.34	54.70
14	8.00	3.89	0.50	40.00	165.1	0.17	101.50
15	8.00	11.22	1.50	40.00	267.2	0.27	93.30
16	6.00	0.23	1.00	58.00	170.0	0.13	45.00
17	2.00	7.56	1.00	58.00	408.3	0.27	30.60
18	8.00	11.22	1.50	75.00	243.9	0.33	74.70
19	6.00	7.56	2.00	58.00	248.3	0.24	54.30
20	6.00	7.56	1.00	58.00	199.5	0.15	70.70
21	8.00	3.89	0.50	75.00	202.3	0.12	87.90
22	6.00	7.56	1.00	93.00	446.8	0.28	91.10
23	4.00	11.22	1.50	40.00	358.3	0.30	58.20
24	8.00	3.89	1.50	75.00	219.8	0.19	51.60
25	4.00	11.22	0.50	40.00	325.9	0.22	74.40
26	4.00	3.89	1.50	40.00	198.1	0.19	68.00
27	8.00	11.22	0.50	40.00	266.1	0.25	152.90
28	6.00	14.89	1.00	58.00	305.6	0.29	63.20
29	6.00	7.56	1.00	58.00	208.3	0.15	81.40
30	10.00	7.56	1.00	58.00	169.4	0.17	101.40

Statistical evaluations of the results were carried out with ANOVA statistics to evaluate the significance of the model as well as the factors.

Tab. 3-43 ANOVA analyses of the model itself together with the separate factors regarding particle size

ANOVA for Response Surface Quadratic Model Analysis of variance table [Partial sum of squares - Type III]					
Source	**Sum of Squares**	**df**	**Mean Square**	**F Value**	**p-value Prob > F**
Model	235400.00	14	16814.96	20.93	< 0.0001
A-Flow rate	62699.70	1	62699.70	78.04	< 0.0001
B-Solvent	52126.76	1	52126.76	64.88	< 0.0001
C-Gas flow	6217.82	1	6217.82	7.74	0.0100
D-Temperature	46596.09	1	46596.09	58.00	< 0.0001

Tab. 3-44 ANOVA analyses of the model itself together with the separate factors regarding PDI

ANOVA for Response Surface Quadratic Model Analysis of variance table [Partial sum of squares - Type III]					
Source	**Sum of Squares**	**df**	**Mean Square**	**F Value**	**p-value Prob > F**
Model	0.12	14	0.01	27.13	< 0.0001
A-Flow rate	0.01	1	0.01	17.66	0.0008
B-Solvent	0.05	1	0.05	165.28	< 0.0001
C-Gas flow	0.02	1	0.02	45.86	< 0.0001
D-Temperature	0.01	1	0.01	20.82	0.0004

Tab. 3-45 ANOVA analyses of the model itself together with the separate factors regarding drug loading

ANOVA for Response Surface Quadratic Model Analysis of variance table [Partial sum of squares - Type III]					
Source	**Sum of Squares**	**df**	**Mean Square**	**F Value**	**p-value Prob > F**
Model	17992.68	14	1285.19	18.66	< 0.0001
A-Flow rate	5828.37	1	5828.37	84.61	< 0.0001
B-Solvent	1545.03	1	1545.03	22.43	0.0003
C-Gas flow	5197.23	1	5197.23	75.45	< 0.0001
D-Temperature	566.07	1	566.07	8.22	0.0118

The model F-value of 20.93, 27.13 and 18.66 for particle size, PDI and drug loading respectively implies that the model is significant. There is only a 0.01% change that a Model F-value this large could occur due to noise. Additionally with p values less than 0.05 all factors were to be significant.

Tab. 3-46 Regression coefficients of the predicted and actual values for particle size, PDI and drug loading.

Coefficient	Particle Size	PDI	Drug load
R-Squared	0.9513	0.9620	0.9457
Adj R-Squared	0.9058	0.9265	0.8950
Pred R-Squared	0.7226	0.7866	0.7117
Adeq Precision	15.7540	19.1810	16.8300

The "Pred R-Squared" of 0.7226, 0.7866, 07117 is in reasonable agreement with the "Adj R-Squared" of 0.9058, 0.9265, 0.8950 for particle size, PDI and drug loading respectively indicating that there is neither a block effect nor there is a need in model reduction. Adeq Precision measures the signal to noise ratio. A ratio greater than 4 is desirable. All ratios indicate an adequate signal. This model can be used to navigate the design space for all of the tested parameters. Using above created design space the following equations were generated to be used in the further calculations of parameters for the required particle size, PDI and drug loading.

Tab. 3-47 Final equations in terms of coded factors for particle size, PDI and drug loading. Each cell represents the coefficient for the coded factors and their combinations.

Factor	Coefficients		
	Particle size =	PDI =	Drug loading =
	199.25	0.1400	76.90
A	-51.11	-0.0160	15.58
B	46.60	0.0480	8.02
C	16.10	0.0250	-14.72
D	44.06	0.0170	-4.86
AB	-11.09	0.0100	6.05
AC	-16.08	-0.0120	-5.18
AD	-23.66	-0.0072	-5.57
BC	-10.87	0.0029	-6.38
BD	-9.97	0.0036	3.20
CD	1.99	0.0160	-4.01
A^2	25.08	0.0200	-1.32
B^2	12.32	0.0170	-4.31
C^2	0.950	0.0170	1.830
D^2	36.20	0.0270	6.95

Tab. 3-48 Final equations in terms of actual factors for particle size, PDI and drug loading. Each cell represents the coefficient for the actual factors and their combinations

Factor	Coefficients		
	Particle size =	**PDI =**	**Drug loading =**
	254.73	0.6588	31.64
Flow rate	-34.43	-0.0550	19.85
Solvent	22.80	-0.0188	2.70
Gas pressure	152.81	-0.1265	39.62
Temperature	-6.07	-0.0102	-1.85
Flow rate*Solvent	-1.51	0.0014	0.83
Flow rate*Gas pres.	-16.08	-0.0121	-5.18
Flow rate*Temperature	-0.68	-0.0002	-0.16
Solvent*Gas press.	-5.93	0.0016	-3.48
Solvent*Temperature	-0.16	0.0001	0.05
Gas press.*Temperature	0.23	0.0018	-0.46
Flow rate^2	6.27	0.0050	-0.33
Solvent^2	0.92	0.0012	-0.32
Gas pressure^2	3.79	0.0673	7.33
Temperature^2	0.12	0.0001	0.02

Correlation plots that are represented in Fig. 3-31 to Fig. 3-33 containing the predicted values calculated using equations that are represented in Tab. 3-47 and Tab. 3-48 and their correlation with measured values gathered throughout the 30 experiments conducted.

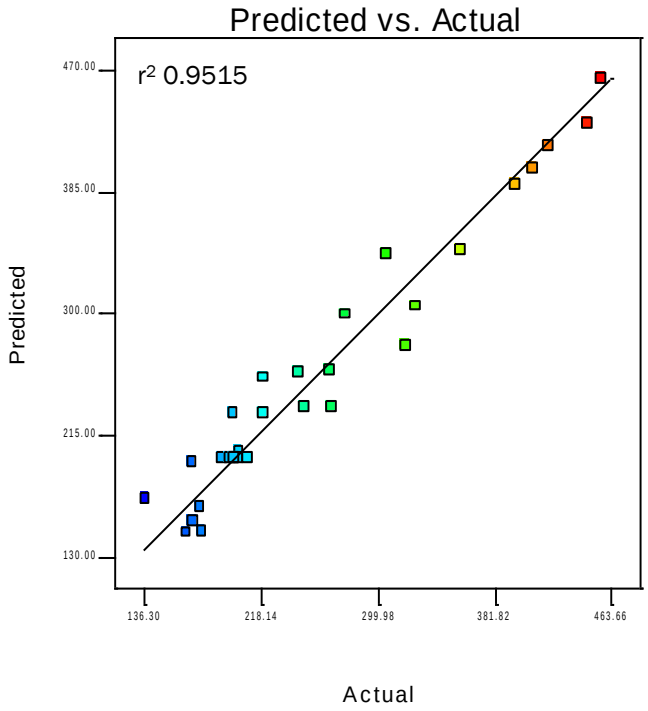

Fig. 3-31 Correlation of predicted values with actual values for particle size

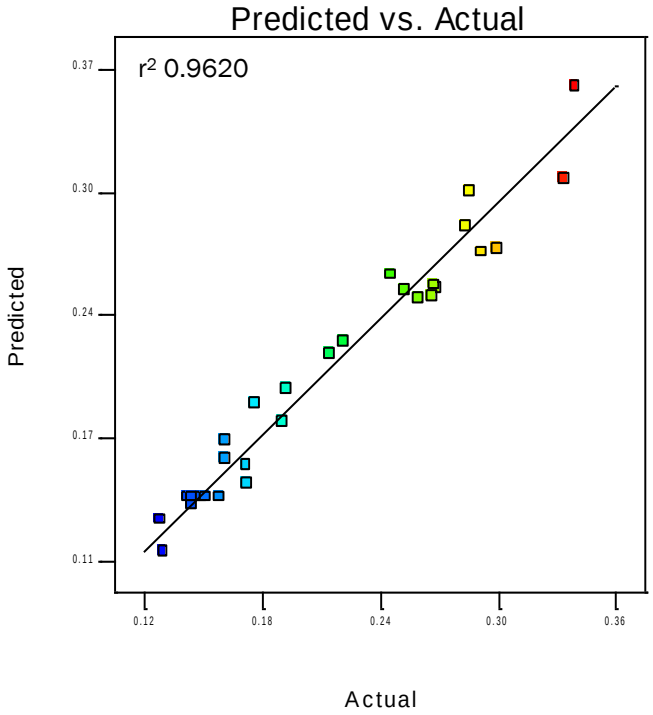

Fig. 3-32 Correlation of predicted values with actual values for PDI

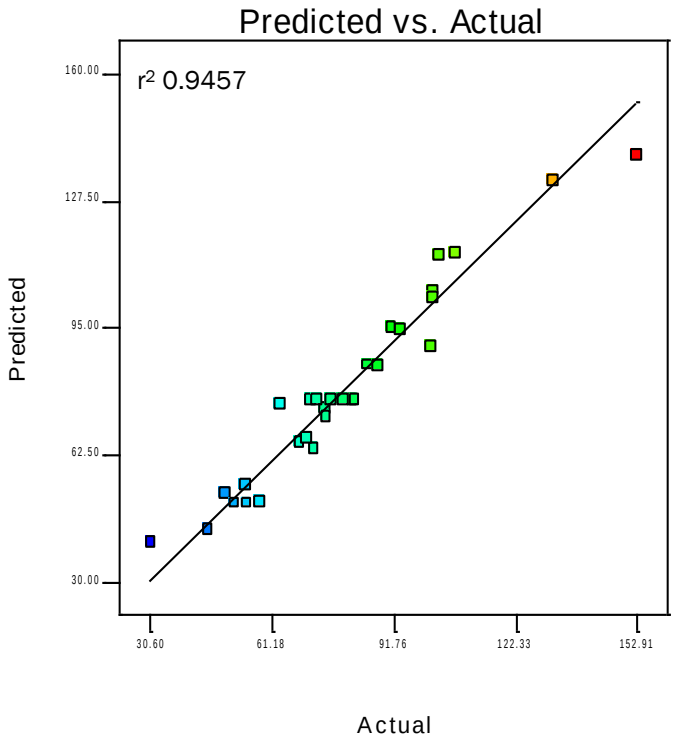

Fig. 3-33 Correlation of predicted values with actual values for drug loading efficiency.

As shown by the above graphics of correlation of predicted values with actual values and correlation coefficients of 0.9515, 0.9620 and 0.9457 for particle size, PDI and drug loading respectively showing that it was possible to establish a good correlation indicating that equations can be used for prediction of the effects of the factors solvent, flow rate, gas pressure and temperature on particle size, PDI and drug loading.

Above model is further analyzed with normal probability plot of studentized residuals to check for normal distribution of residuals, studentized residuals versus predicted values to check for constant error, externally studentized residuals to look for outliers and lastly Box-Cox plot to determine if transformation of the data is needed for better quadratic analyses and establishment of the correlation.

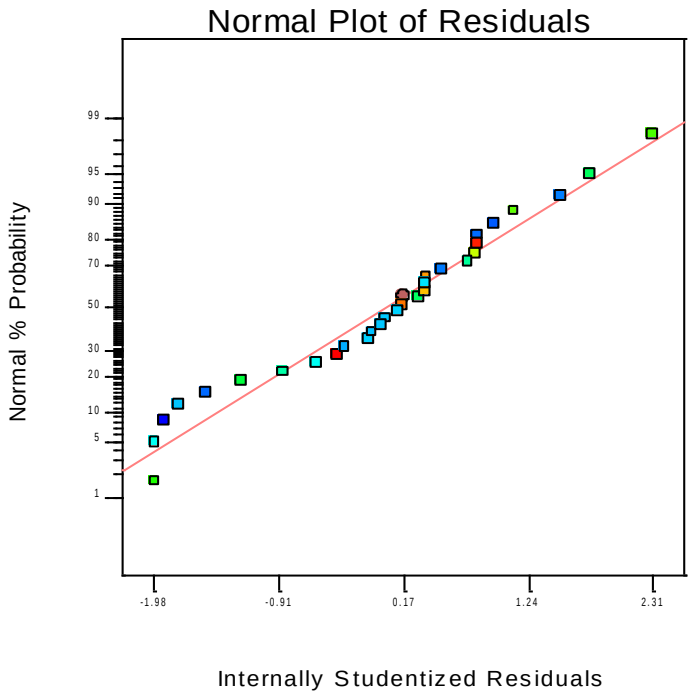

Fig. 3-34 **Normal plot of residuals for particle size for each of the 30 run performed for each of the 30 run performed in the experimental design.**

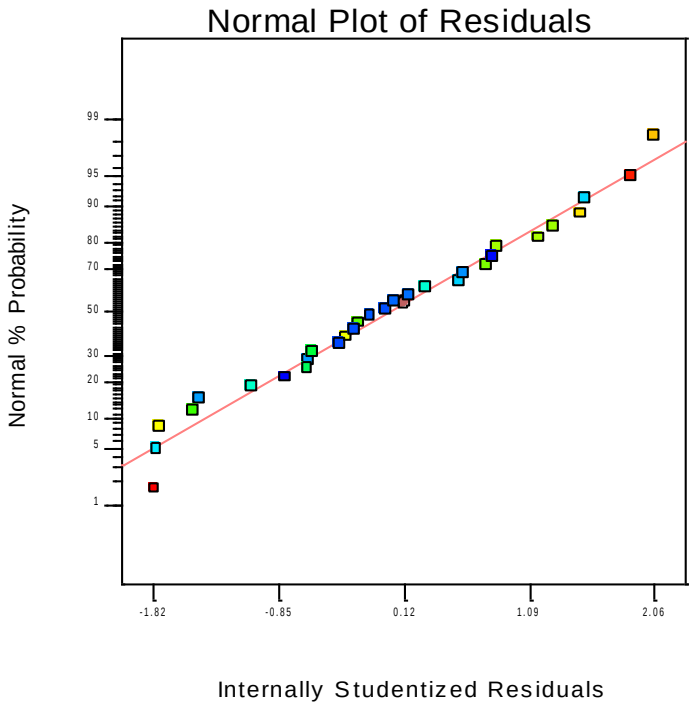

Fig. 3-35 Normal plot of residuals for PDI for each of the 30 run performed in the experimental design.

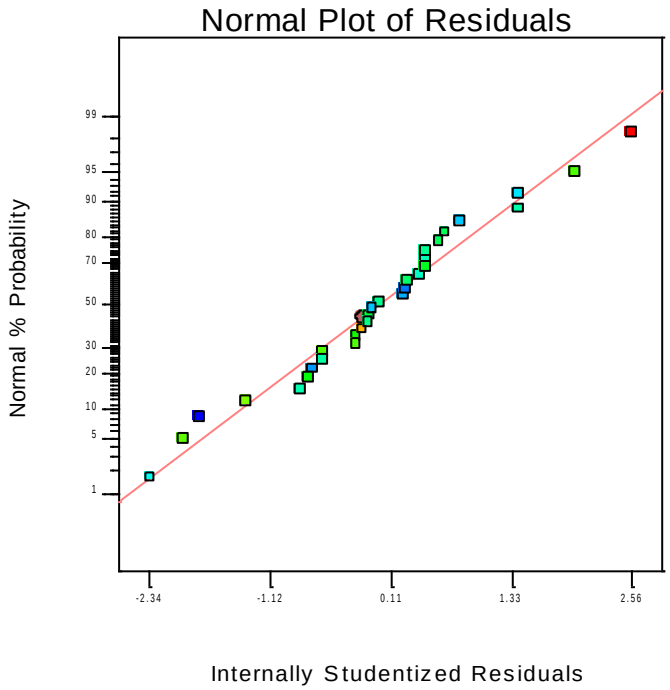

Fig. 3-36 **Normal plot of residuals for drug load for each of the 30 run performed in the experimental design.**

Normality plot was drawn with internally studentized residuals which are calculated by dividing the residuals by a estimation of its own standard deviation. As seen in the graph above points follow a straight line with no major deviations from the line along with the random placement of the points not following any pattern which will require transformation of data, thus showing the normality of residuals.

Further analyses were carried out with studentized residuals versus predicted values. Fig. 3-37 to Fig. 3-39 are showing the relationship between the studentized residuals with predicted.

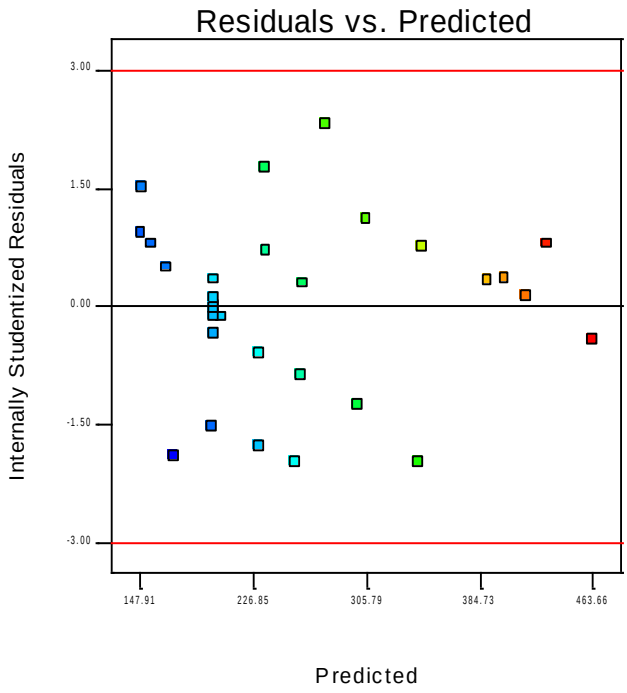

Fig. 3-37 **Internally studentized residuals of particle size compared with predicted values for each 30 run performed in the experimental design.**

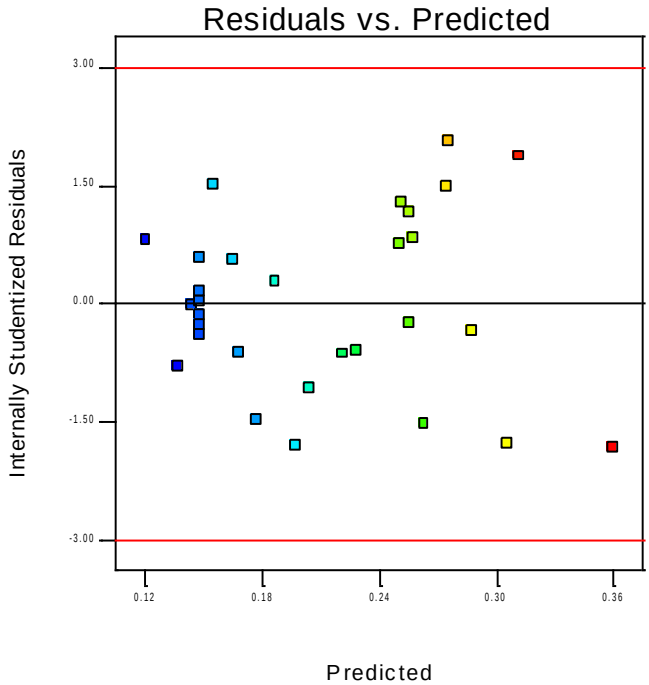

Fig. 3-38 Internally studentized residuals of PDI compared with predicted values for each 30 run performed in the experimental design.

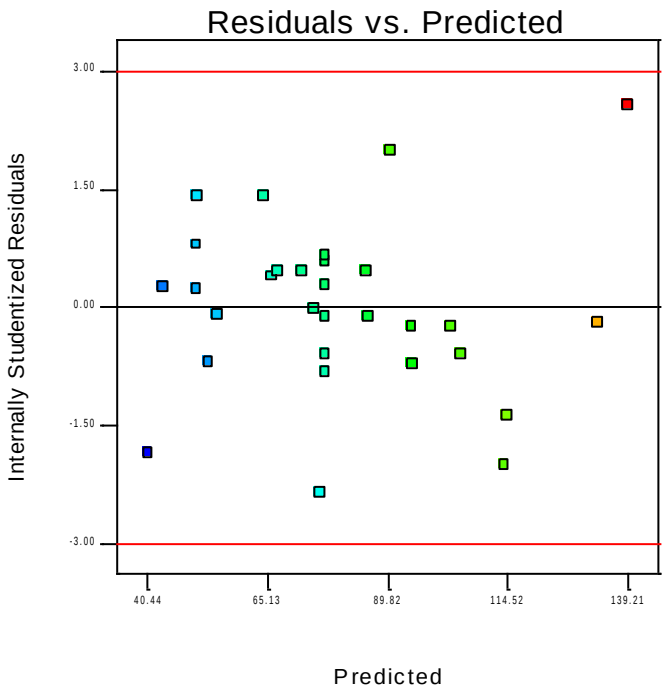

Fig. 3-39 Internally studentized residuals of drug load compared with predicted values for each 30 run performed in the experimental design.

Points are scattered evenly above and below the 0 point which is showing the points under the curve as negative and points over the curve as positive values. There is no grouping at any point where the internally studentized residuals are only positive or negative. This shows that there is no constant error for the predicted data. The limits – 3.0 and +3.0 were selected according to the 95% confidence interval.

Externally studentized residuals were used to determine the outliners. As seen in Fig. 3-40 to Fig. 3-42 there are no points above or below the red lines indicating that there is no data point that can be considered as outliner. The limits -3.88 and +3.88 were determined according to the 95% confidence interval.

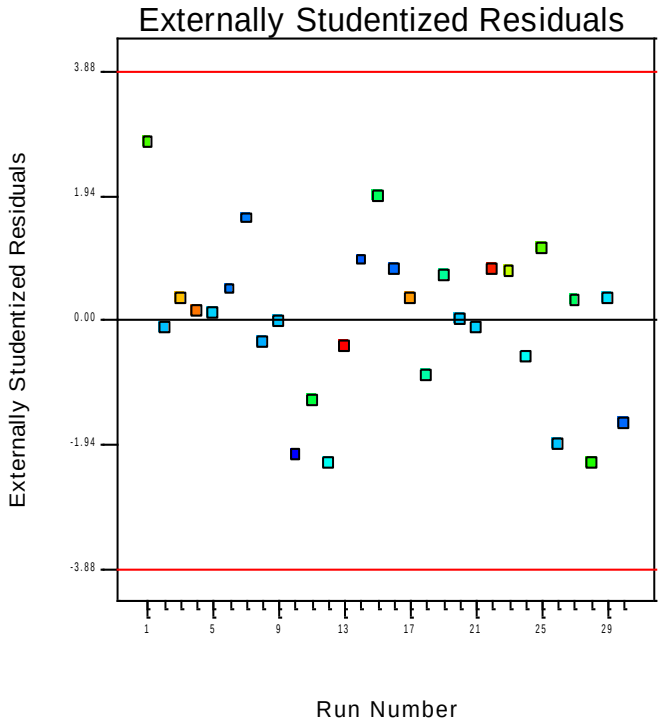

Fig. 3-40 Externally studentized residuals of particle size for each 30 runs

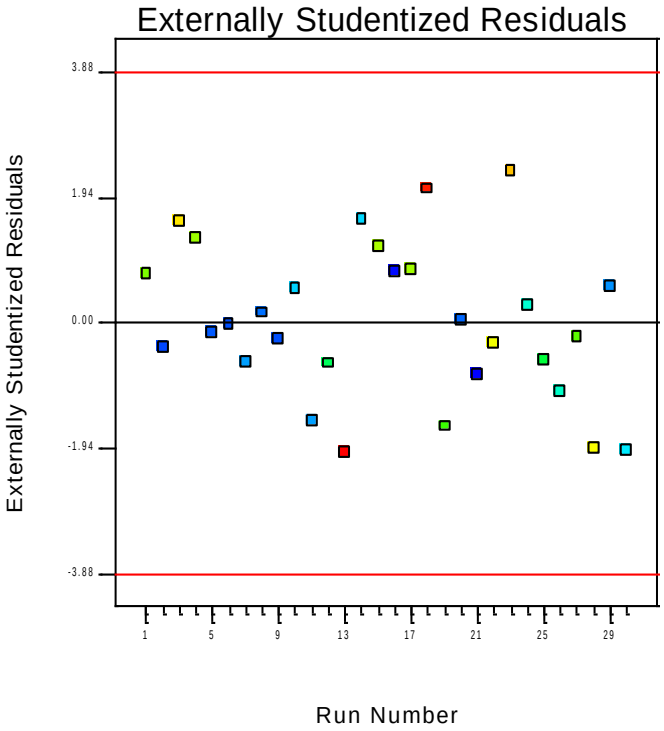

Fig. 3-41 Externally studentized residuals of PDI for each 30 runs

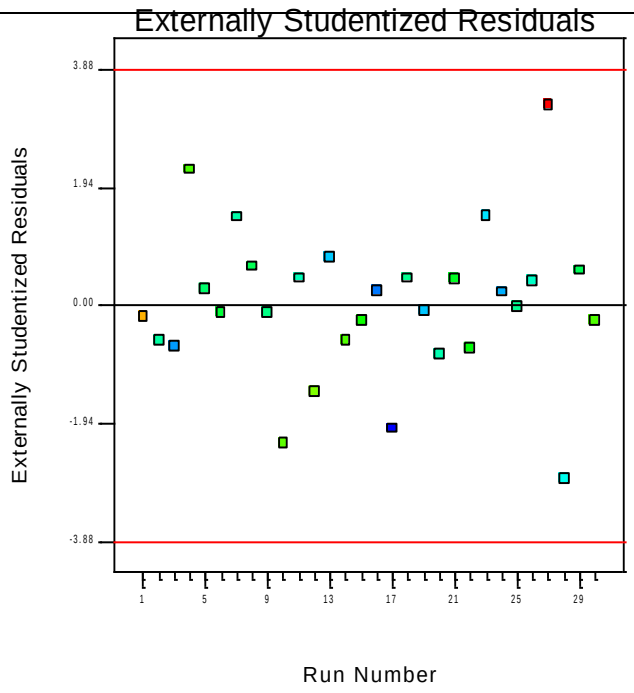

Fig. 3-42 Externally studentized residuals of drug loading for each runs

Lastly Box-Cox plot was evaluated in order to calculate lambda values for the conclusion if the data in model needs any transformations.

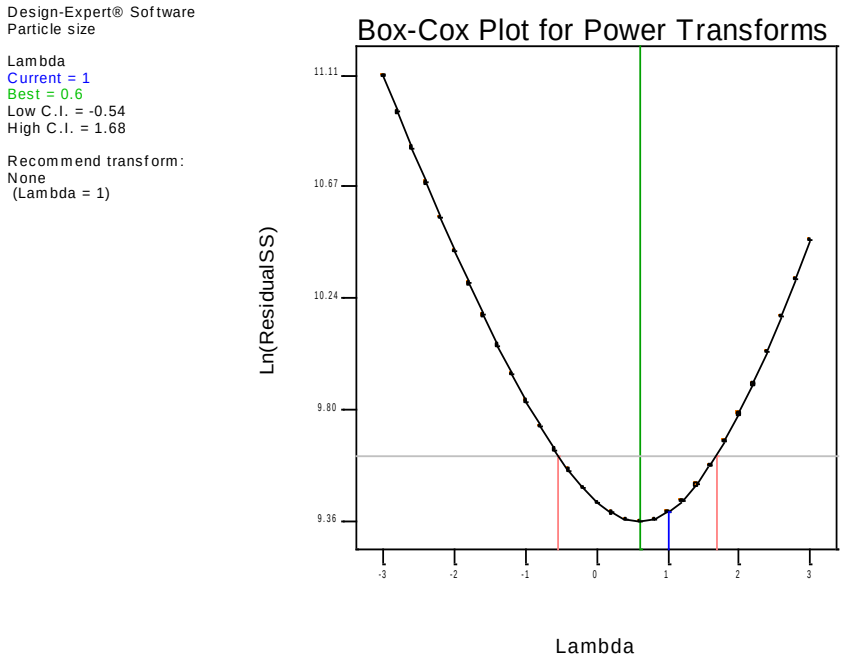

Fig. 3-43 Box-Cox plot for particle size

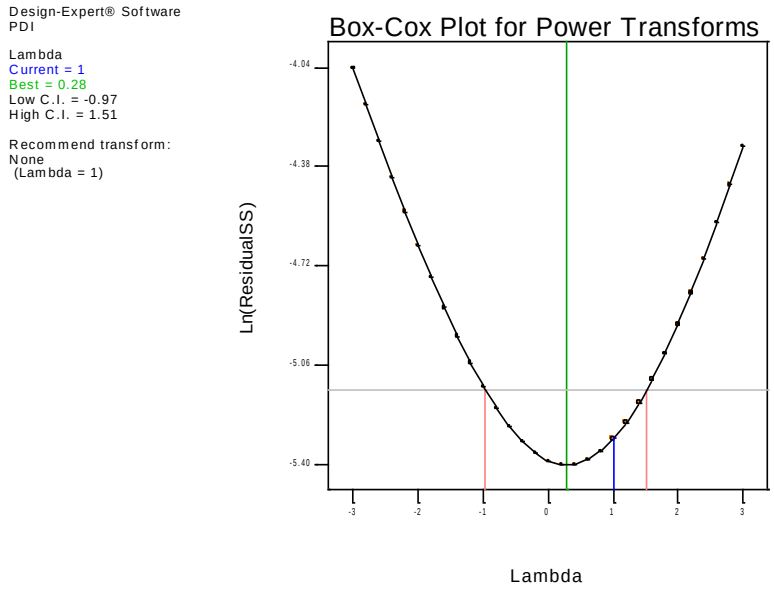

Fig. 3-44 Box-Cox plot for PDI

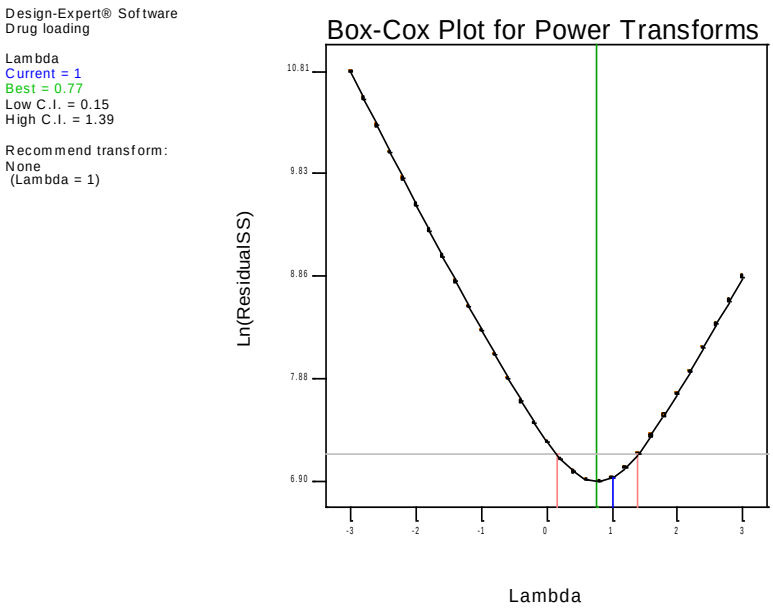

Fig. 3-45 Box-Cox plot for drug loading

95 % confidence limits for the lambda at the lowest Ln(ResidualsSS) value was calculated. Since the confidence limits include the value of lambda 1 for all the plots above, a transformation is not required for the data to ensure the normality or homogeneity of the data.

Data and equation were controlled with the above stated methods for the appropriateness of data for creating the design space. Since the results met all the expected criteria the data were used to create surface diagrams to evaluate the effects of the chosen factors more closely.

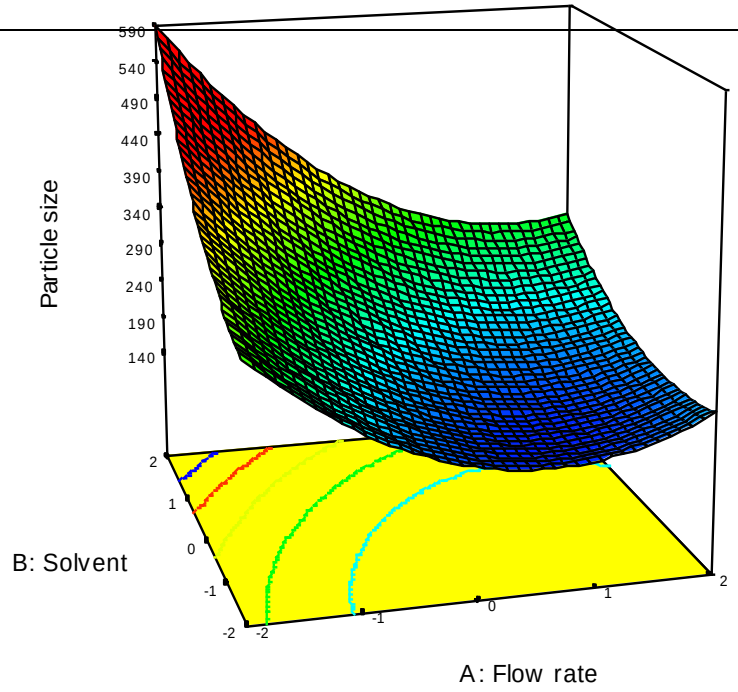

Fig. 3-46 3D surface graph of effect of flow rate and solvent on particle size. Factors, gas pressure and temperature were kept constant at center point

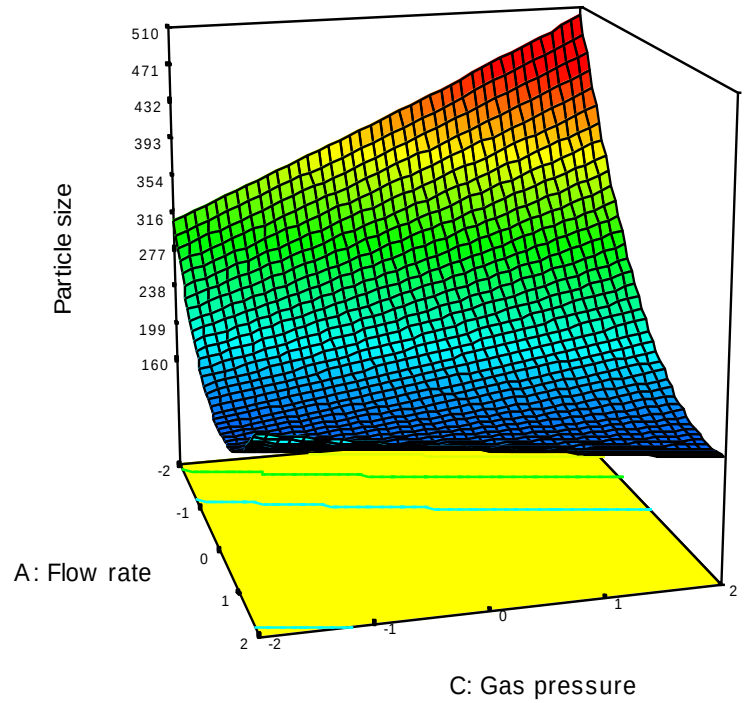

Fig. 3-47 3D surface graph of effect of flow rate and gas pressure on particle size. Factors, solvent and temperature were kept constant at center point

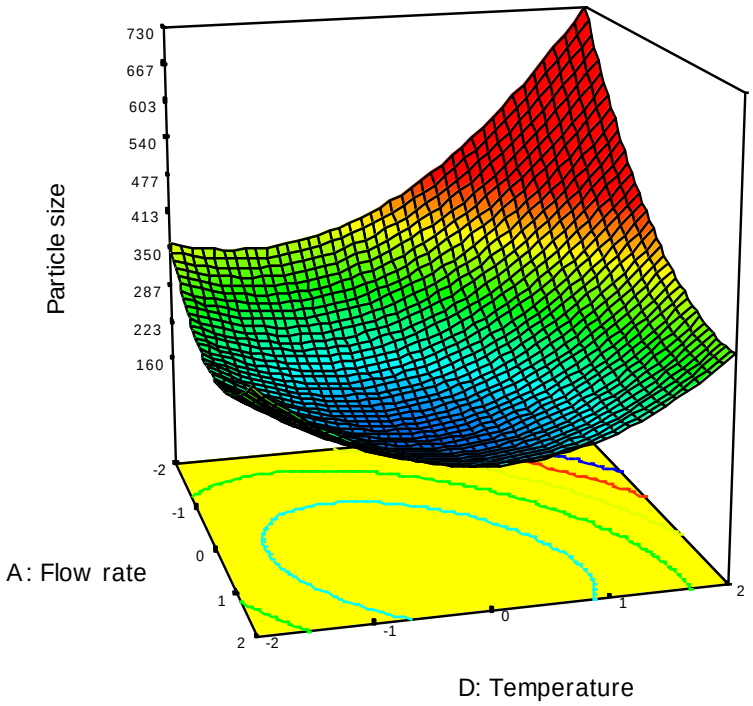

Fig. 3-48 3D surface graph of effect of flow rate and temperature on particle size. Factors, solvent and gas pressure were kept constant at center point

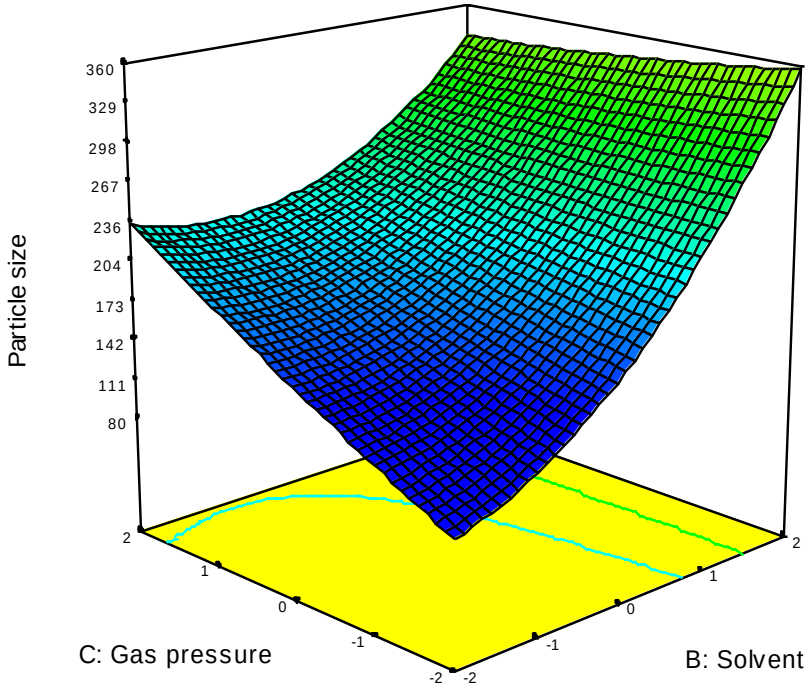

Fig. 3-49 3D surface graph of effect of gas pressure and solvent on particle size. Factors, flow rate and temperature were kept constant at center point

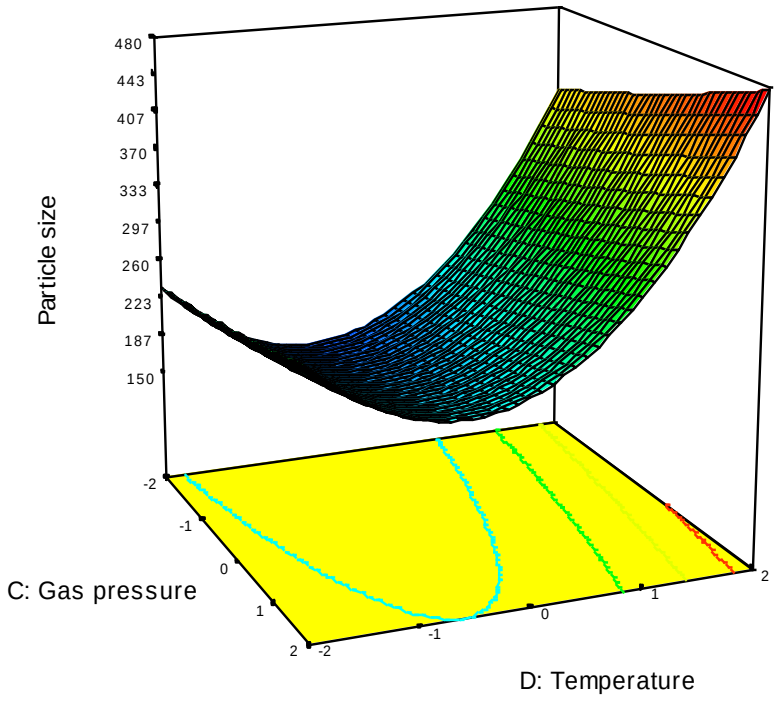

Fig. 3-50 3D surface graph of effect of gas pressure and temperature on particle size. Gas pressure, flow rate and temperature were kept constant at center point

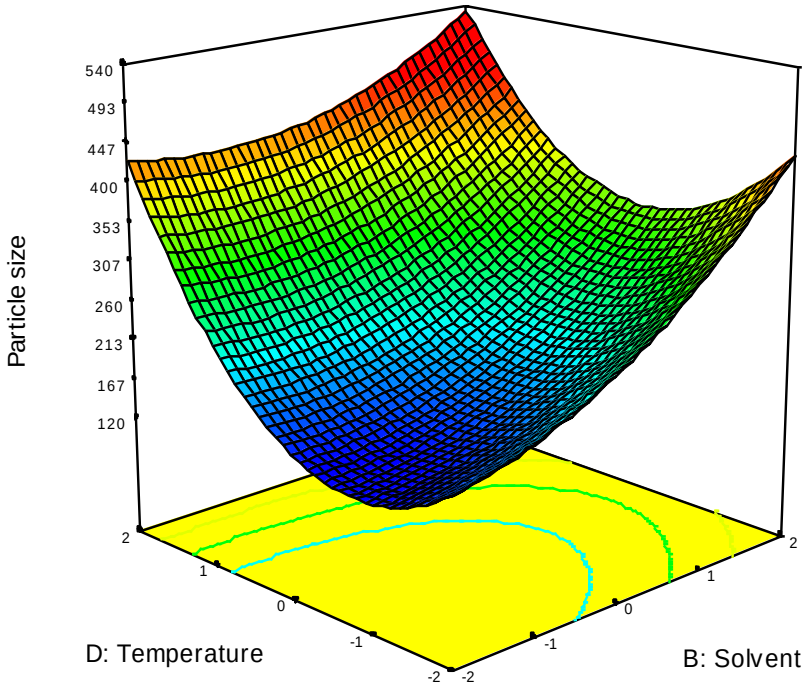

Fig. 3-51 3D surface graph of effect of solvent and temperature on particle size. Gas pressure and flow rate were kept constant at center point

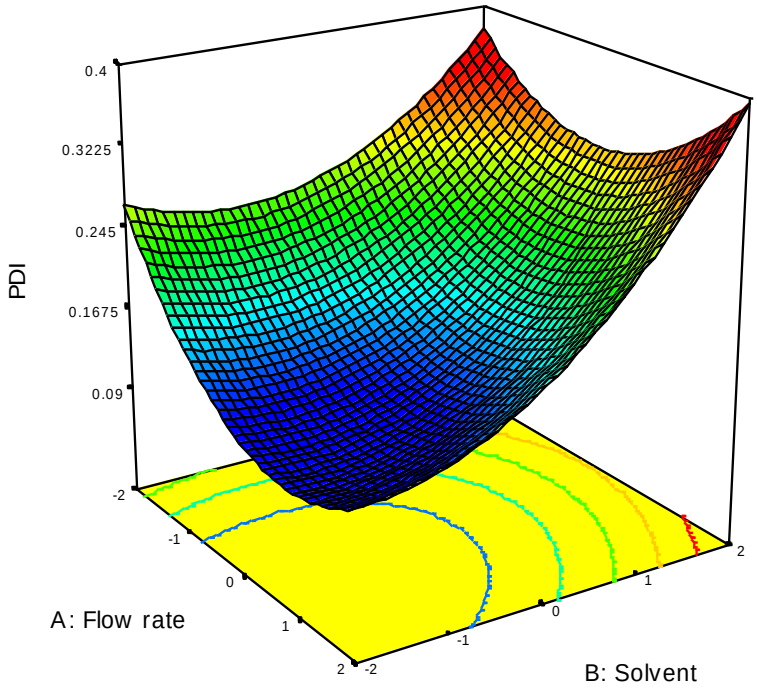

Fig. 3-52 3D surface graph of effect of flow rate and solvent on PDI. Gas pressure and temperature were kept constant at center point

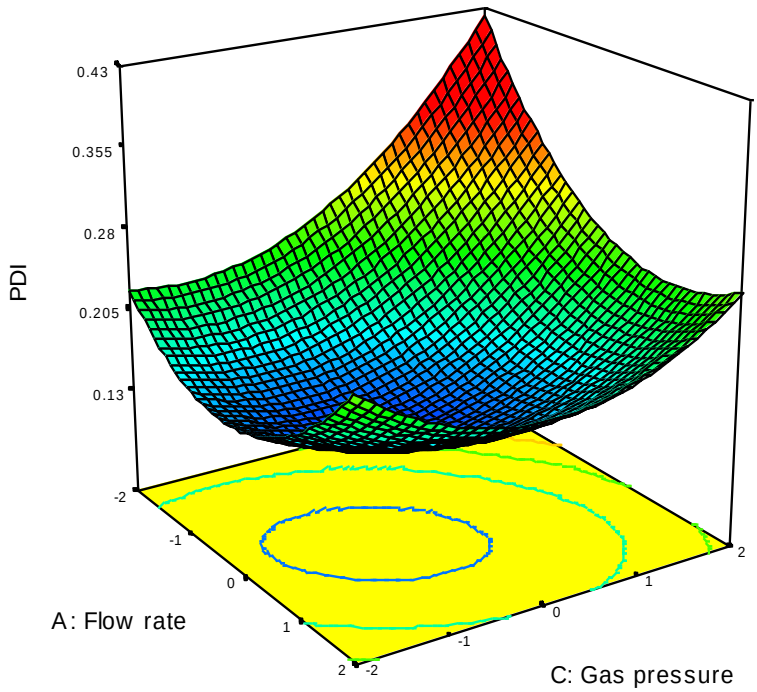

Fig. 3-53 3D surface graph of effect of flow rate and gas pressure on PDI. Solvent and temperature were kept constant at center point

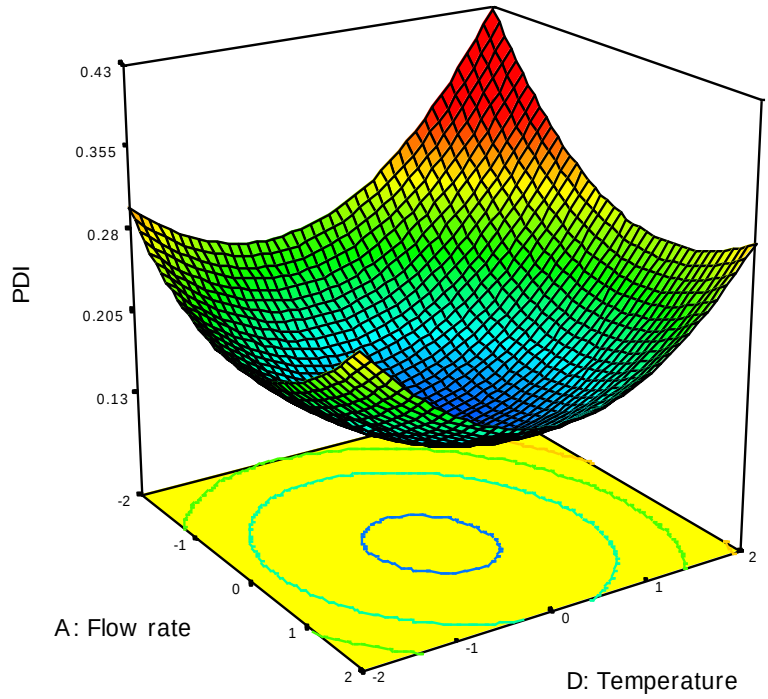

Fig. 3-54 3D surface graph of effect of flow rate and temperature on PDI. Solvent and gas pressure were kept constant at center point

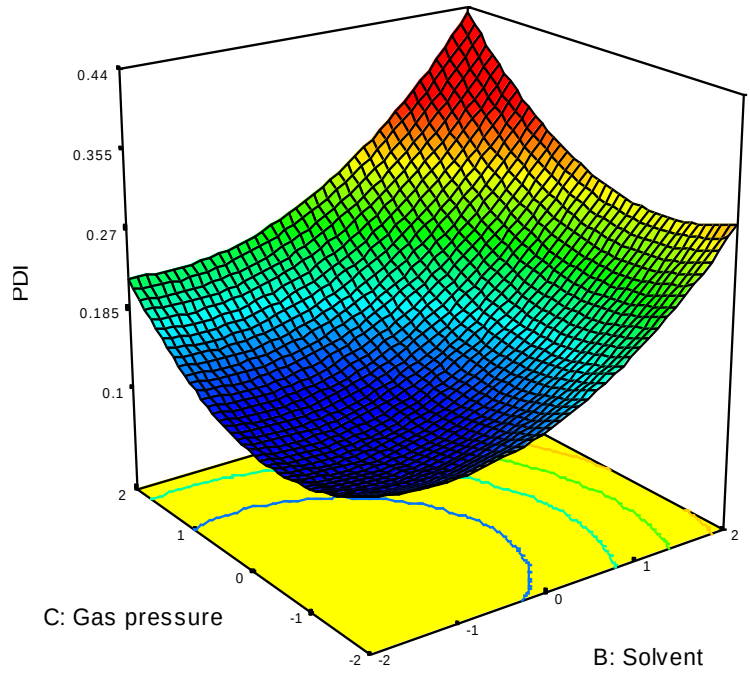

Fig. 3-55 3D surface graph of effect of gas pressure and solvent on PDI. Flow rate and temperature were kept constant at center point

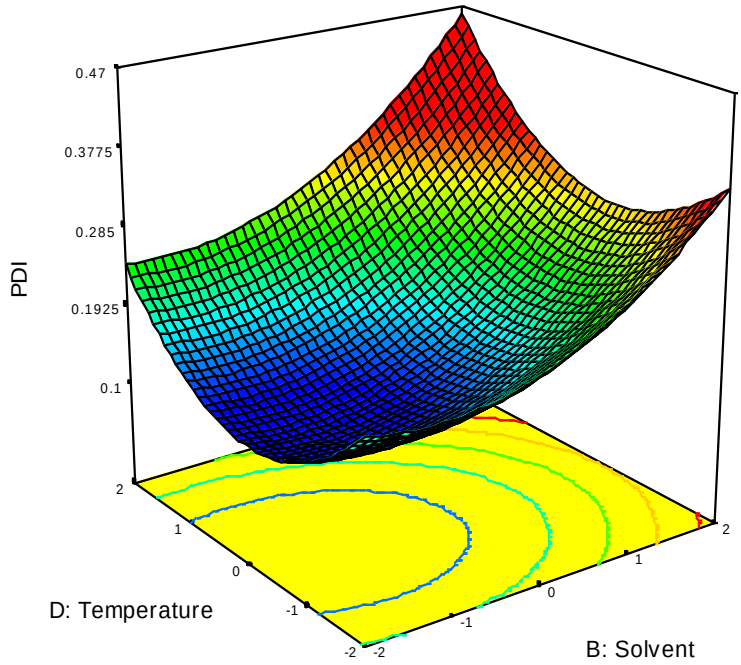

Fig. 3-56 3D surface graph of effect of temperature and solvent on PDI. Flow rate and gas pressure were kept constant at center point

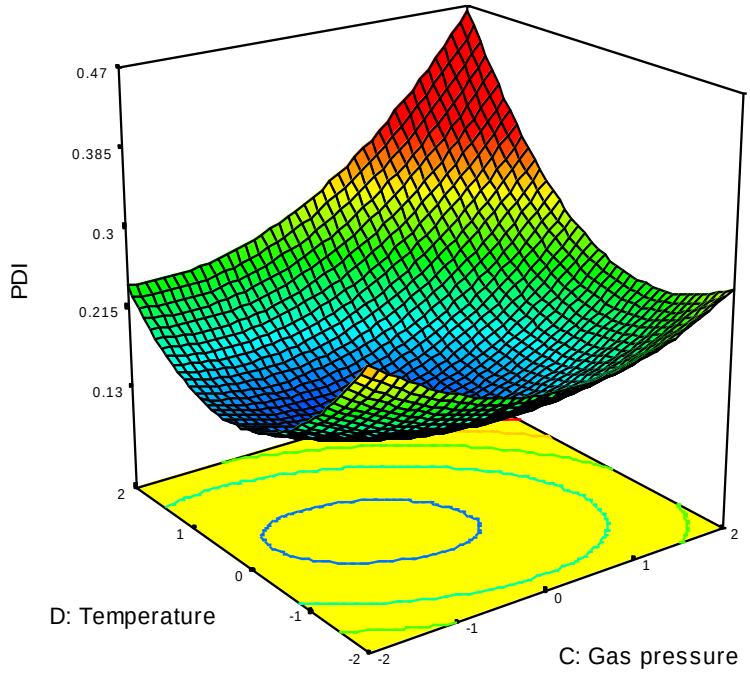

Fig. 3-57 3D surface graph of effect of temperature and gas pressure on PDI. Flow rate and temperature were kept constant at center point

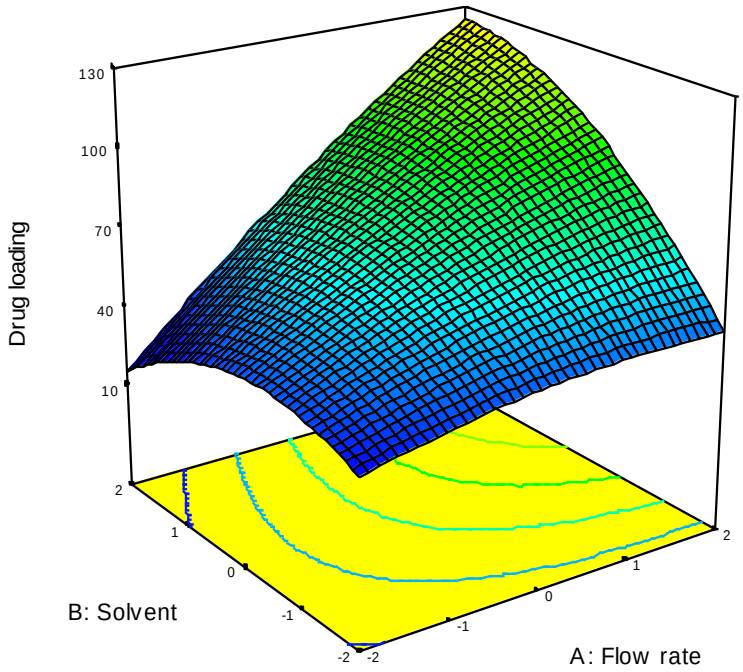

Fig. 3-58 3D surface graph of effect of solvent and flow rate on drug loading efficiency. Temperature and gas pressure were kept constant at center point

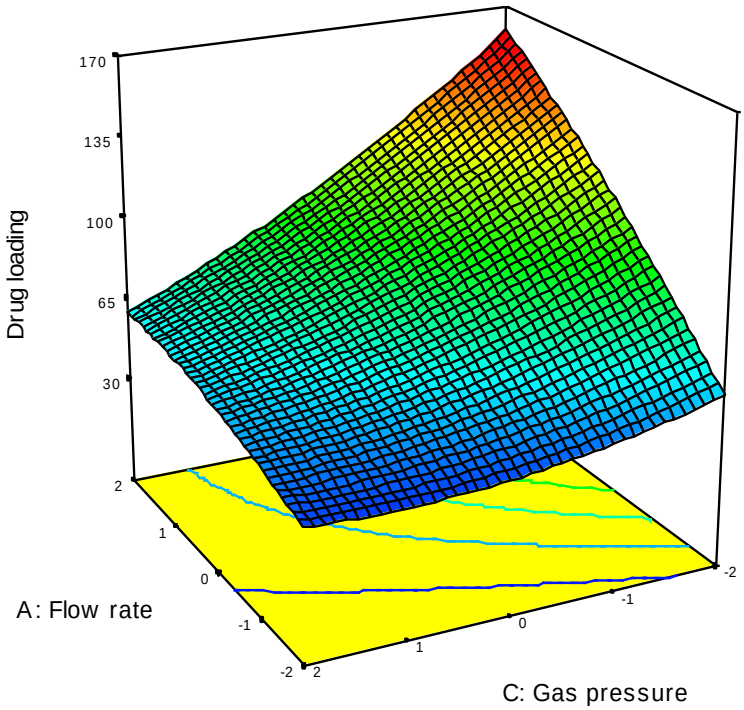

Fig. 3-59 3D surface graph of effect of gas pressure and flow rate on drug loading efficiency. Temperature and solvent were kept constant at center point

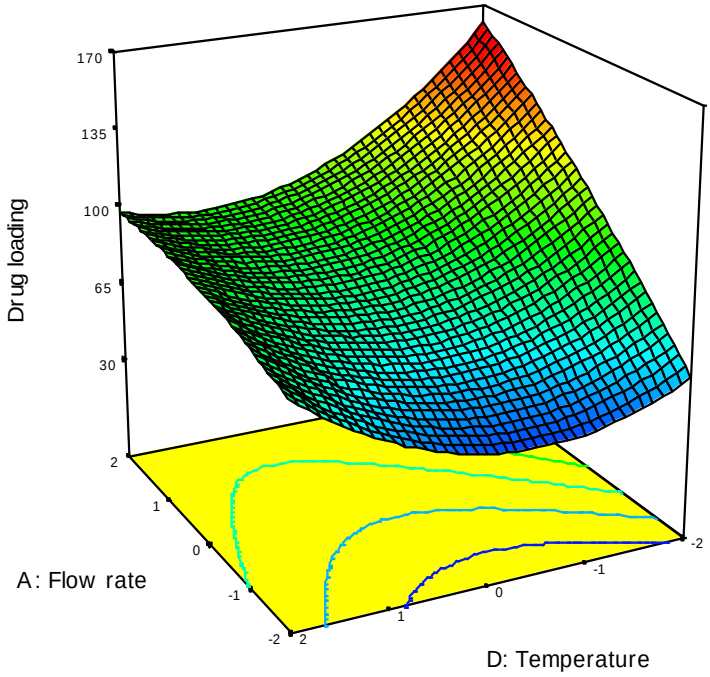

Fig. 3-60 3D surface graph of effect of temperature and flow rate on drug loading efficiency. Gas pressure and solvent were kept constant at center point

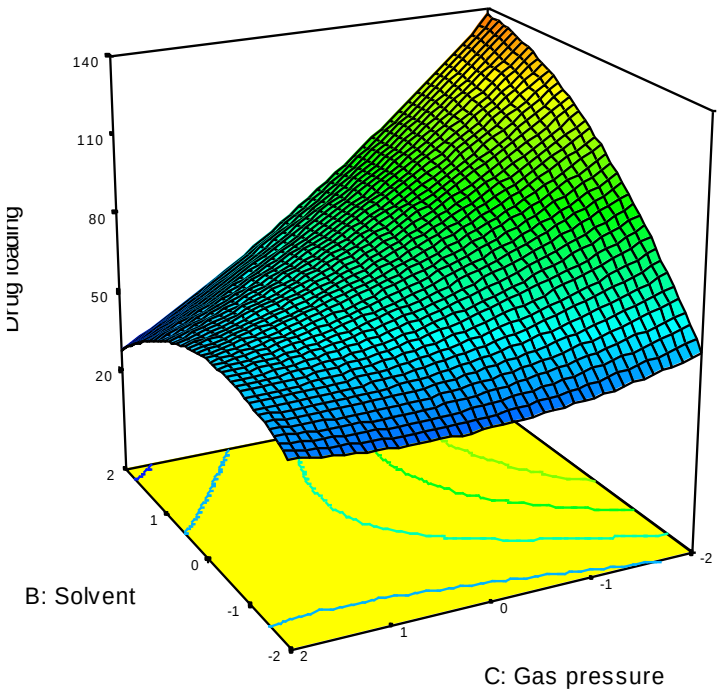

Fig. 3-61 3D surface graph of effect of gas pressure and solvent on drug loading efficiency. Temperature and flow rate were kept constant at center point

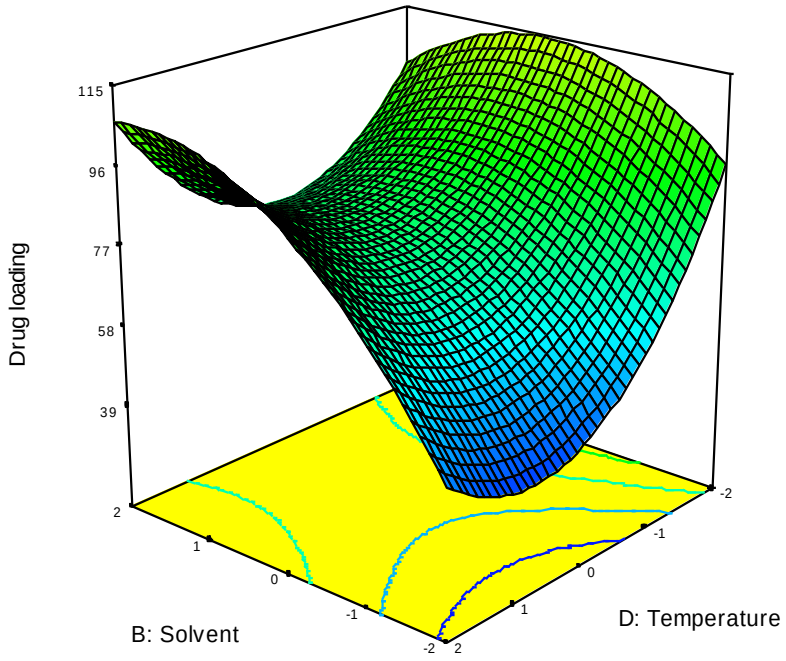

Fig. 3-62 3D surface graph of effect of temperature and solvent on drug loading efficiency. Gas pressure and flow rate were kept constant at center point

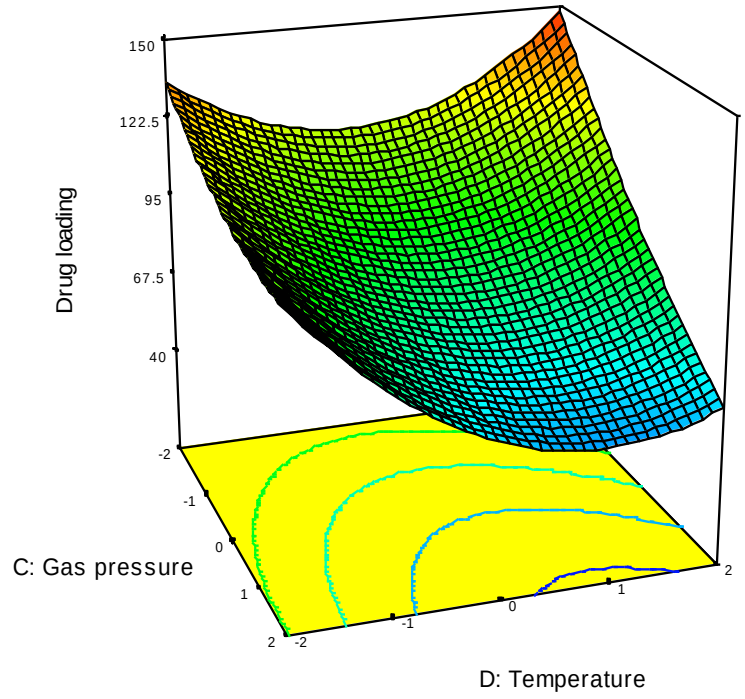

Fig. 3-63 3D surface graph of effect of temperature and gas pressure on drug loading efficiency. Solvent and flow rate were kept constant at center point

Optimization of the system parameters were carried out with Design Expert software. Using the equations and design spaces given at tables 18-20 and figures 26-43 the operating conditions of the

microjet reactor is determined for the production of particles in the range of 100-200 nm, a PDI value of lower than 0.2 and maximum drug loading efficiency. The constraints applied is given below

Tab. 3-49 Requirements for the optimization

Lower Name	Upper Goal	Lower Limit	Upper Limit	Weight	Weight	Importance
Flow rate	is in range	-2	2	1	1	3
Solvent	is in range	-2	2	1	1	3
Gas pressure	is in range	-2	2	1	1	3
Temperature	is in range	-2	2	1	1	3
Particle size	is in range	100	200	1	1	3
PDI	is in range	0	0	1	1	3
Drug loading	maximize	31	500	1	1	3

The solutions calculated from design space for the above stated system are presented in Tab. 3-50:

Tab. 3-50 Solutions using the equations and design space for a particle size of 100-200, PDI of lower than 0.2 and maximum drug loading efficiency

Solution Number	Flow rate (mL/min)	Solvent	Gas pressure (bar)	Temperature (ºC)	Particle size (nm)	PDI	Drug load (µg/mL)	Desirability
1.00	8.00	8.18	0.10	64.00	200.00	0.20	144.96	0.24
2.00	8.00	8.18	0.01	64.00	199.00	0.20	144.78	0.24
3.00	8.00	8.44	0.00	63.00	200.00	0.20	144.68	0.24
4.00	8.00	7.72	0.00	65.00	200.00	0.20	144.46	0.24
5.00	8.00	7.86	0.03	63.00	197.00	0.20	143.71	0.24
6.00	8.00	8.48	0.02	61.00	196.00	0.20	143.68	0.24
7.00	8.00	8.49	0.08	61.00	198.00	0.20	142.81	0.24
8.00	8.00	8.48	0.00	57.00	189.00	0.20	142.30	0.24
9.00	8.00	8.65	0.03	57.00	192.00	0.20	142.02	0.24
10.00	8.00	8.13	0.07	56.00	188.00	0.20	141.72	0.24
11.00	9.00	7.65	0.09	61.00	195.00	0.20	141.72	0.24
12.00	9.00	7.32	0.07	58.00	188.00	0.20	140.84	0.24
13.00	9.00	7.92	0.27	49.00	193.00	0.20	137.08	0.23
14.00	9.00	6.73	0.27	45.00	189.00	0.20	135.00	0.22
15.00	9.00	6.28	0.13	58.00	193.00	0.20	134.97	0.22
16.00	9.00	6.87	0.33	44.00	194.00	0.20	134.65	0.22
17.00	9.00	6.43	0.42	41.00	200.00	0.20	132.84	0.22
18.00	8.00	6.16	0.00	71.00	200.00	0.18	132.28	0.22
19.00	8.00	7.02	0.44	35.00	199.00	0.20	129.68	0.21
20.00	8.00	5.99	0.52	31.00	200.00	0.20	128.15	0.21
21.00	8.00	6.26	0.51	31.00	200.00	0.20	127.73	0.21
22.00	8.00	7.13	0.50	34.00	200.00	0.20	127.62	0.21
23.00	7.00	3.58	0.80	23.00	200.00	0.20	117.59	0.19
24.00	7.00	3.10	0.98	23.00	200.00	0.19	113.50	0.18
25.00	8.00	4.19	1.07	30.00	200.00	0.17	113.20	0.18
26.00	10.00	7.36	1.00	49.00	200.00	0.19	109.97	0.17
27.00	7.00	1.91	1.20	23.00	200.00	0.19	108.53	0.17
28.00	8.00	5.47	1.39	33.00	200.00	0.17	107.67	0.16
29.00	7.00	1.43	1.65	27.00	200.00	0.18	99.90	0.15

The Design Expert software calculated 29 possible solutions showing optimum microjet reactor setup parameters for the production of the nanoparticles. The solutions are listed in Tab. 3-50. In the first solution 8 mL/min, 8.18, 64 ºC are given for flow rate, solvent, gas pressure and temperature which will result in nanoparticles with the particle size of 200 nm, PDI of 0.2 and drug loading efficiency of 144.96 µg/mL. This first solution was used for the further experiments.

Validation of solution number 1 was done in terms of repeatability. Nanoparticles were prepared with the given factors of 8 mL/min, 8.18, 64 ºC are given for flow rate, solvent, gas pressure and temperature respectively and assayed for particle size, PDI, drug loading efficiency.

Tab. 3-51 Validation of the solution proposed by design of experiments conducted for the optimization of microjet reactor parameters.

Trial number	Paricle size [nm]	PDI	Drug loading efficiency [%]
1	195.8	0.18	158.84
2	192.9	0.22	142.65
3	201.4	0.14	144.54
Average	**196.70**	**0.18**	**148.68**
SD	**4.32**	**0.04**	**8.85**
RSD %	**2.20**	**22.22**	**5.95**

Further experiments were carried out using this setup of the microjet reactor. A second design of experiments was conducted in order to optimize the formulation parameters. For this purpose a mixture design, D- optimal design was selected.

D-optimal design for optimization of formulation content

D-optimal design had 20 runs for 4 factors in single block design since it was possible to run all experiments with the same material in the same day. The data is analyzed separately for the dependent factors; particle size, PDI, ZETA potential, drug loading efficiency, mucoadhessiveness and drug release in 0.1 N HCl using ANOVA analyses. Furthermore normality of results were evaluated using normal plot of residuals, predicted values vs internally studentized residuals, run number vs internally studentized residuals and box-cox transformation analyses. Furthermore correlations between predicted and real values were analyzed for the sake of repeatability. Lastly the graphics of response surface is constructed for the presentation of acquired data and the predictions.

Tab. 3-52 Experimental D-optimal design for the optimization of nanoparticle formulation together with the particle size, PDI, ZETA, drug loading efficiency, mucoadhesiveness and drug release in pH 1.2 results of 20 runs

			Component 1	Component 2	Component 3	Component 4	Response 1	Response 2	Response 3	Response 4	Response 5	Response 6
Std	Run	Block	A:HPMCP HP50	B:Chitosan	C:Pluronic F127	D:Fenofibrate	Particle size	PDI	ZETA	Drug loading	Turbidity	Drug release pH 1.2
			mg/mL	mg/mL	mg/mL	mg/mL	nm		mV	µg/mL	NTU	%
6	5	Block 1	5.8	0.5	1.0	4.8	420.0	0.2	-5.9	266.2	64.9	11.4
13	3	Block 1	7.8	0.9	1.0	2.2	401.9	0.2	5.2	342.5	85.1	13.9
8	9	Block 1	9.2	1.3	1.0	0.5	270.1	0.0	4.8	118.9	115.5	7.7
19	11	Block 1	9.2	1.3	1.0	0.5	319.3	0.0	3.4	126.6	110.8	6.0
4	8	Block 1	10.0	0.2	1.0	0.8	282.0	0.1	-20.1	14.5	45.1	1.1
15	10	Block 1	7.1	0.2	1.0	3.7	233.6	0.3	-14.9	145.3	47.9	4.9
5	16	Block 1	3.4	1.5	2.1	5.0	285.4	0.2	15.3	84.6	93.5	31.3
16	20	Block 1	3.4	1.5	2.1	5.0	298.0	0.2	13.6	71.2	92.3	30.2
7	19	Block 1	6.1	1.5	2.2	2.2	303.7	0.2	14.4	258.8	115.0	20.5
11	4	Block 1	8.6	0.2	2.4	0.8	490.6	0.2	-16.9	209.3	50.9	2.4
12	6	Block 1	5.1	0.2	3.0	3.7	321.0	0.3	-10.6	230.9	51.2	10.0
10	15	Block 1	7.2	0.7	3.6	0.5	759.0	0.2	0.8	419.1	72.9	5.9
20	1	Block 1	3.2	0.2	3.6	5.0	198.9	0.2	-8.5	101.0	54.2	15.0
9	12	Block 1	3.2	0.2	3.6	5.0	188.9	0.2	-8.5	69.6	52.6	16.0
14	7	Block 1	5.8	0.2	4.2	1.8	528.0	0.2	-10.4	286.2	59.6	8.4
18	13	Block 1	3.0	1.1	5.0	3.0	174.6	0.0	17.6	212.2	67.0	31.0
1	14	Block 1	3.0	1.1	5.0	3.0	178.4	0.0	16.1	141.2	65.0	28.2
17	17	Block 1	4.8	1.5	5.0	0.7	287.6	0.1	15.2	161.8	100.0	15.4
3	18	Block 1	4.8	1.5	5.0	0.7	282.0	0.0	14.5	163.0	102.0	16.9
2	2	Block 1	4.1	0.3	5.0	2.7	305.4	0.1	-8.8	220.8	53.6	11.5

Statistical evaluation of the results was carried out with ANOVA statistics to evaluate the significance of the model as well as the factors.

Tab. 3-53 ANOVA analyses of the model itself together with the separate factors regarding particle size

ANOVA for Response Surface Quadratic Model Analysis of variance table [Partial sum of squares - Type III]					
Source	**Sum of Squares**	**df**	**Mean Square**	**F Value**	**p-value Prob > F**
Model	3.66E+005	9	40635.21	93.33	< 0.0001
Linear mixture	8.69E+004	3	28975.99	66.55	< 0.0001
AB	65070.72	1	65070.72	149.45	< 0.0001
AC	40335.31	1	40335.31	92.64	< 0.0001
AD	5085.28	1	5085.28	11.68	0.0066
BC	45162.85	1	45162.85	103.73	< 0.0001
BD	70528.98	1	70528.98	161.98	< 0.0001
CD	4146.8	1	4146.8	9.52	0.0115
Residual	4354.09	10	435.41	9.52	0.0115
Lack of fit	2991.49	5	598.3	2.2	0.2042

Tab. 3-54 ANOVA analyses of the model itself together with the separate factors regarding PDI

ANOVA for Response Surface Quadratic Model Analysis of variance table [Partial sum of squares - Type III]					
Source	**Sum of Squares**	**df**	**Mean Square**	**F Value**	**p-value Prob > F**
Model	0.15	9	0.016	95.82	< 0.0001
Linear mixture	0.063	3	0.021	123.98	< 0.0001
AB	2.79E-004	1	2.79E-004	1.66	0.2272
AC	2.60E-002	1	2.60E-002	153.3	< 0.0001
AD	0.023	1	0.023	136.4	< 0.0001
BC	1.32E-004	1	1.32E-004	0.78	0.3971
BD	1.47E-004	1	1.47E-004	0.87	0.3721
CD	7.88E-003	1	7.88E-003	46.71	< 0.0001
Residual	1.69E-003	10	1.69E-004	46.71	< 0.0001
Lack of fit	1.19E-003	5	2.38E-004	2.38	0.1816

Tab. 3-55 ANOVA analyses of the model itself together with the separate factors regarding ZETA poptential

ANOVA for Response Surface Quadratic Model Analysis of variance table [Partial sum of squares - Type III]					
Source	**Sum of Squares**	**df**	**Mean Square**	**F Value**	**p-value Prob > F**
Model	3064.04	9	340.45	346.44	< 0.0001
Linear mixture	2904.33	3	968.11	985.14	< 0.0001
AB	109.59	1	109.59	111.52	< 0.0001
AC	13.83	1	13.83	14.08	0.0038
AD	21.77	1	21.77	22.16	0.0008
BC	109.65	1	109.65	111.58	< 0.0001
BD	116.25	1	116.25	118.3	< 0.0001
CD	23.97	1	23.97	24.39	0.0006
Residual	9.83	10	0.98		
Lack of fit	6.1	5	1.22	1.64	0.301

Tab. 3-56 ANOVA analyses of the model itself together with the separate factors regarding drug loading efficiency

ANOVA for Response Surface Quadratic Model Analysis of variance table [Partial sum of squares - Type III]					
Source	**Sum of Squares**	**df**	**Mean Square**	**F Value**	**p-value Prob > F**
Model	1.86E+005	9	20624	37.03	< 0.0001
Linear mixture	19940.1	3	6646.7	11.93	0.0012
AB	61955.74	1	61955.74	111.24	< 0.0001
AC	28097.59	1	28097.59	50.45	< 0.0001
AD	25607.03	1	25607.03	45.98	< 0.0001
BC	47411.73	1	47411.73	85.13	< 0.0001
BD	62131.95	1	62131.95	111.56	< 0.0001
CD	3729.54	1	3729.54	6.7	0.0271
Residual	5569.42	10	556.94		
Lack of fit	2439	5	487.8	0.78	0.6046

Tab. 3-57 ANOVA analyses of the model itself together with the separate factors for mucoadhesiveness.

ANOVA for Response Surface Quadratic Model Analysis of variance table [Partial sum of squares - Type III]					
Source	**Sum of Squares**	**df**	**Mean Square**	**F Value**	**p-value Prob > F**
Model	10426.16	9	1158.46	354.87	< 0.0001
Linear mixture	9119.1	3	3039.7	931.15	< 0.0001
AB	63.31	1	63.31	19.39	0.0013
AC	47.27	1	47.27	14.48	0.0035
AD	53.06	1	53.06	16.25	0.0024
BC	113.26	1	113.26	34.7	0.0002
BD	141.39	1	141.39	43.31	< 0.0001
CD	4.98	1	4.98	1.52	0.2452
Residual	32.64	10	3.26		
Lack of fit	15.6	5	3.12	0.92	0.5375

Tab. 3-58 ANOVA analyses of the model itself together with the separate factors regarding drug release in HCl buffer pH 1.2

ANOVA for Response Surface Quadratic Model Analysis of variance table [Partial sum of squares - Type III]					
Source	**Sum of Squares**	**df**	**Mean Square**	**F Value**	**p-value Prob > F**
Model	1703.01	9	189.22	113.94	< 0.0001
Linear mixture	1521.64	3	507.21	305.41	< 0.0001
AB	14.42	1	14.42	8.68	0.0146
AC	0.98	1	0.98	0.59	0.4593
AD	14.51	1	14.51	8.74	0.0144
BC	20.36	1	20.36	12.26	0.0057
BD	30.16	1	30.16	18.16	0.0017
CD	27.75	1	27.75	16.71	0.0022
Residual	16.61	10	1.66		
Lack of fit	9.23	5	1.85	1.25	0.4059

The model F-value of 93.33, 118.30, 37.03, 95.82, 346.44, 37.03 for particle size, PDI, ZETA potential and drug loading efficiency, mucoadhesiveness and drug release in HCl buffer pH 1.2 respectively implies that the model is significant. There is only a 0.01% change that a Model F-value this large could occur due to noise. Additionally with p values less than 0.05 all factors were to be significant.

Tab. 3-59 Regression coefficients of the predicted and actual values for particle size, PDI, ZETA potential and drug loading efficiency, mucoadhesiveness and drug release in HCl buffer pH 1.2.

Coefficient	Particle Size	PDI	ZETA potential	Drug loading efficiency	Muco-adhesiveness	Drug release
R-Squared	0.9882	0.9885	0.9968	0.9709	0.9969	0.9903
Adj R-Squared	0.9776	0.9782	0.9939	0.9447	0.9941	0.9817
Pred R-Squared	0.941	0.9478	0.9869	0.8835	0.9886	0.9551
Adeq Precision	38.833	27.158	52.794	25.366	55.914	32.625

The "Pred R-Squared is found to be in reasonable agreement with the "Adj R-Squared" for all the parameters tested indicating that there is neither a block effect nor there is a need in model reduction. Adequate Precision measures the signal to noise ratio. A ratio greater than 4 is desirable. All ratios indicate an adequate signal. This model can be used to navigate the design space for all of the tested parameters. Using above created design space, equations for each factor is created. Final equations are given in terms of L-pseudo components.

Tab. 3-60 Final equations in terms of coded factors for particle size, PDI, ZETA potential and drug loading efficiency, mucoadhesiveness and drug release in HCl buffer pH 1.2.. Each cell represents the coefficient for the coded factors and their combinations.

Factor	Coefficients					
	Particle size	PDI	ZETA potential	Drug loading efficiency	Muco-adhesiveness	Drug release
A	260.63	0.017	-21.4	-38.45	42.17	0.33
B	17924.46	1.39	-609.98	-16905.2	1081.72	-230.81
C	227.77	-0.5	-30.87	-186.7	35.41	-6.36
D	489.07	0.01	-24.31	-155.67	50.71	-1.69
AB	21748.99	-1.42	892.57	21222.03	-678.39	323.81
AC	1957.18	1.57	36.24	1633.52	67	9.67
AD	-466.8	0.99	30.54	1047.5	47.68	24.93
BC	20071.06	-1.09	988.96	20564.7	-1005.13	426.21
BD	22542.09	-1.03	915.2	21157.67	-1009.28	466.13
CD	-981.36	1.35	74.61	930.68	33.99	80.28

Further statistical analyses were conducted such as normal probability plot of the studentized residuals to check for normality of residuals, studentized residuals versus predicted values to check for constant error and Box-Cox plot for power transformations.

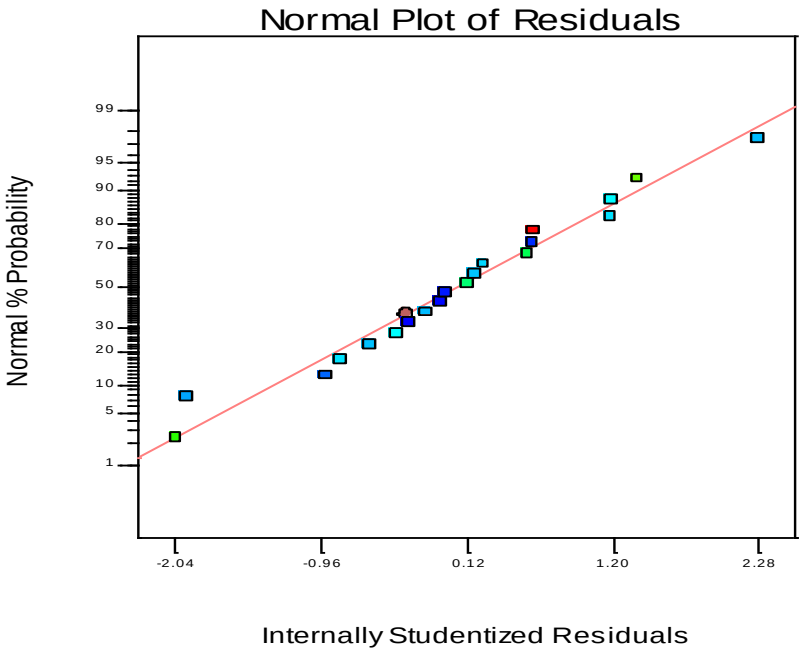

Fig. 3-64 Normal plot of residuals for particle size

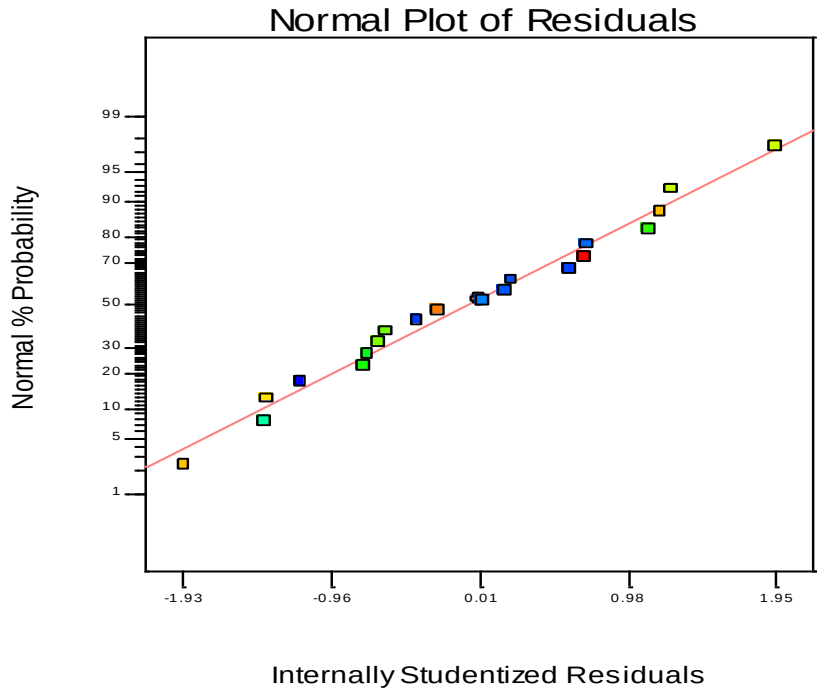

Fig. 3-65 Normal plot of residuals for PDI

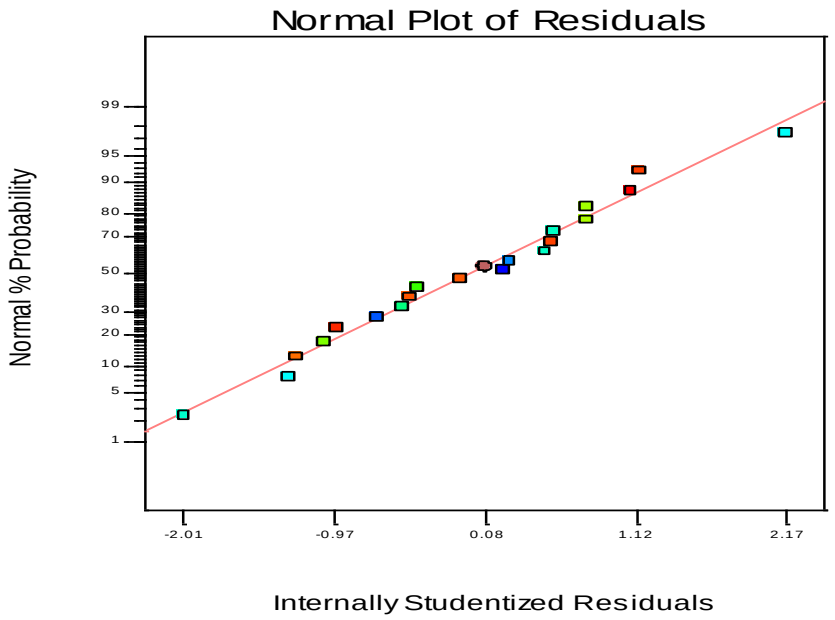

Fig. 3-66 Normal plot of residuals for ZETA potential

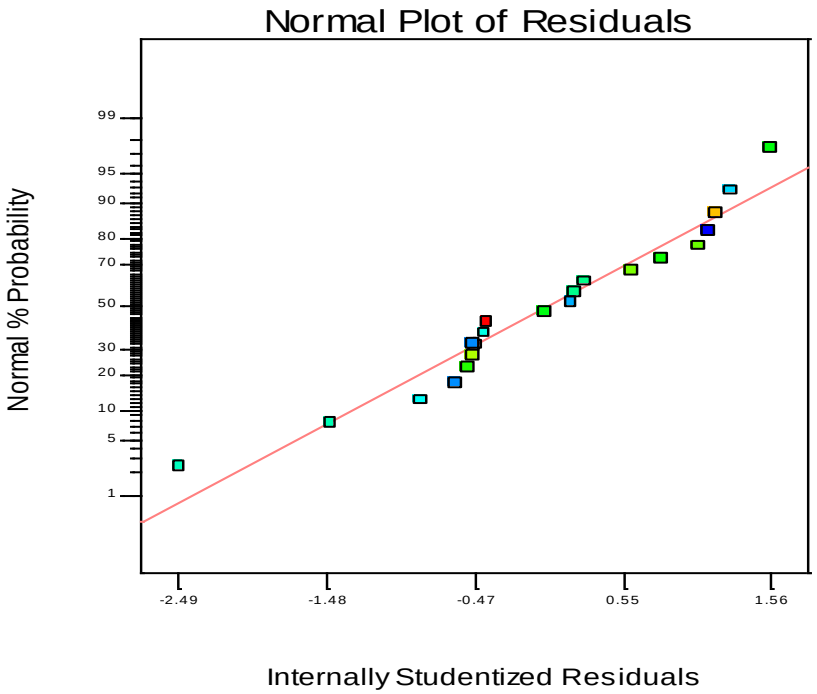

Fig. 3-67 Normal plot of residuals for drug loading efficiency

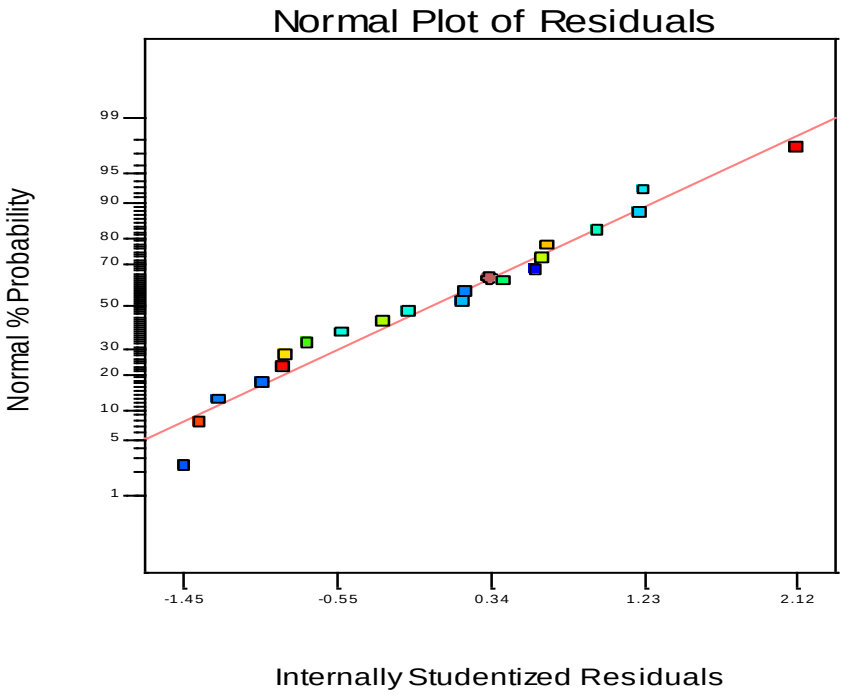

Fig. 3-68 Normal plot of residuals for mucoadhesiveness.

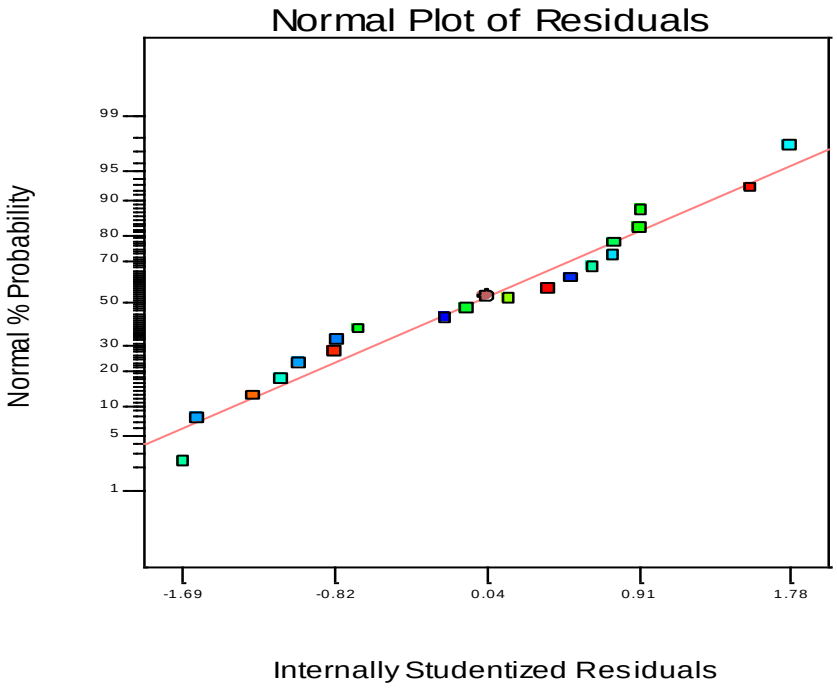

Fig. 3-69 Normal plot of residuals for drug release in 0.1 N HCl buffer pH 1.2

Normality plot was drawn with internally studentized residuals which are calculated by dividing the residuals by a estimation of its own standard deviation. As seen in the graph above points follow a straight line with no major deviations from the line along with the random placement of the points not following any pattern which will require transformation of data, thus showing the normality of residuals.

Further analyses were carried out with studentized residuals versus predicted values.

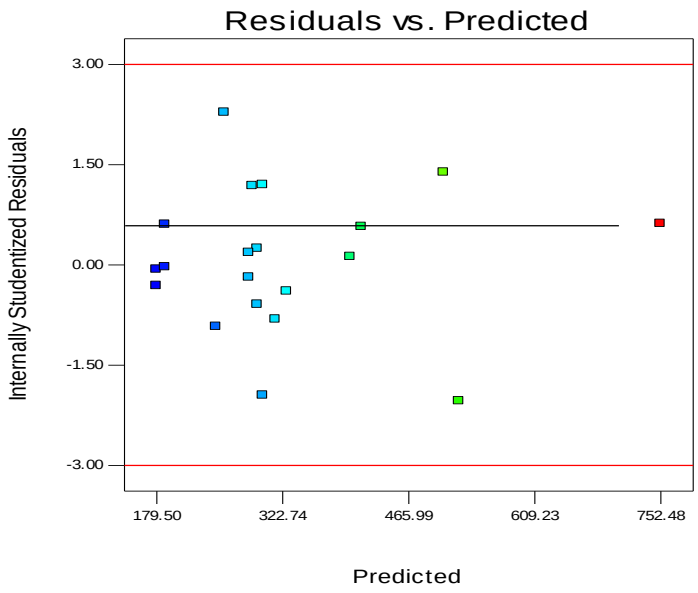

Fig. 3-70 Internally studentized residuals of particle size compared with predicted values for each 30 run performed in the experimental design.

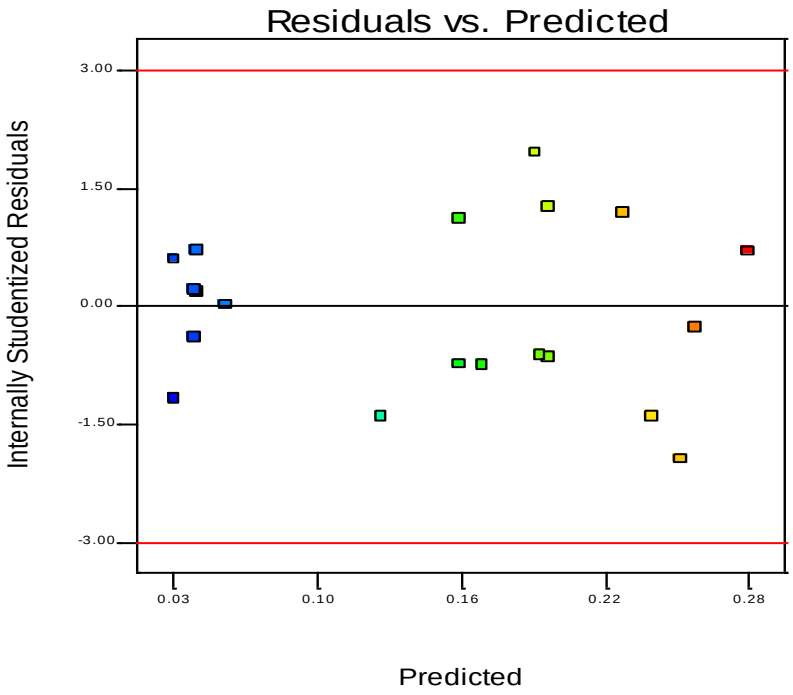

Fig. 3-71 Internally studentized residuals of PDI compared with predicted values for each 30 run performed in the experimental design.

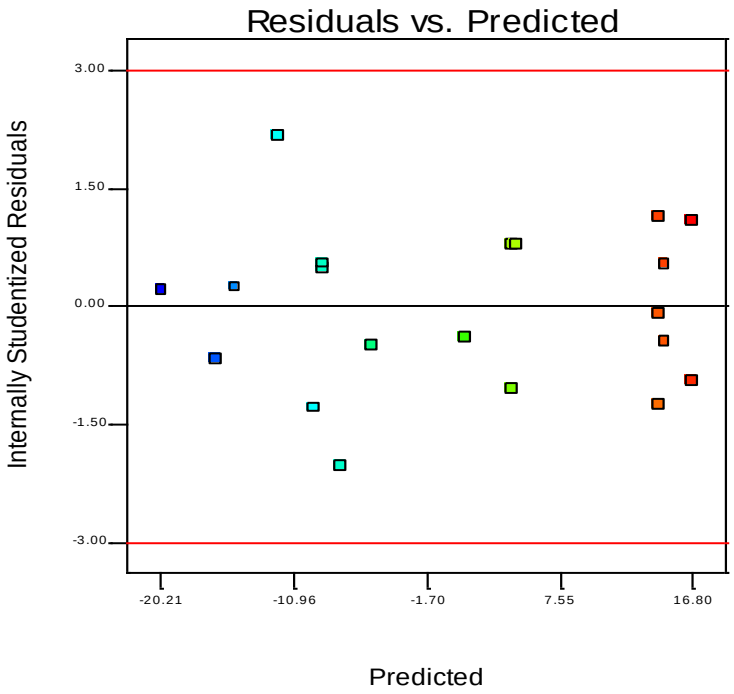

Fig. 3-72 Internally studentized residuals of ZETA potential compared with predicted values for each 30 run performed in the experimental design.

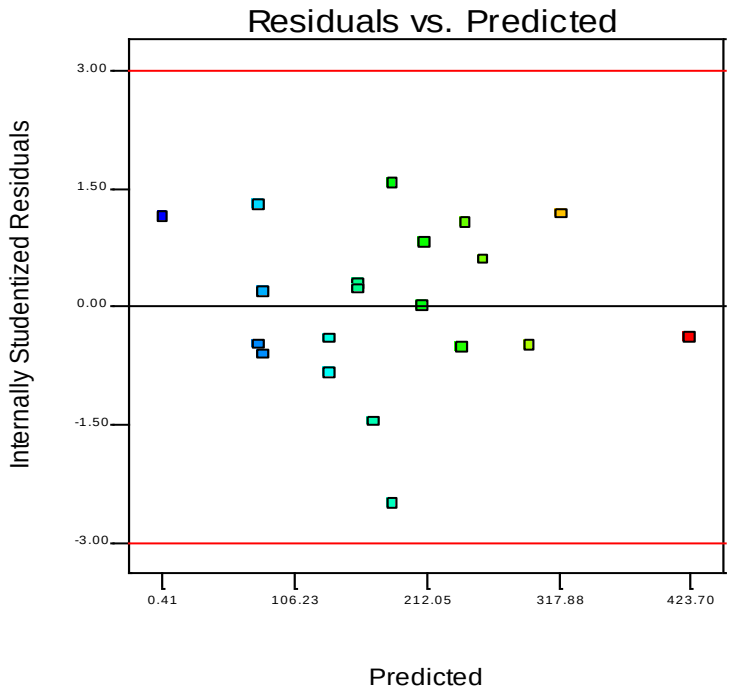

Fig. 3-73 Internally studentized residuals of drug loading efficiency compared with predicted values for each 30 run performed in the experimental design

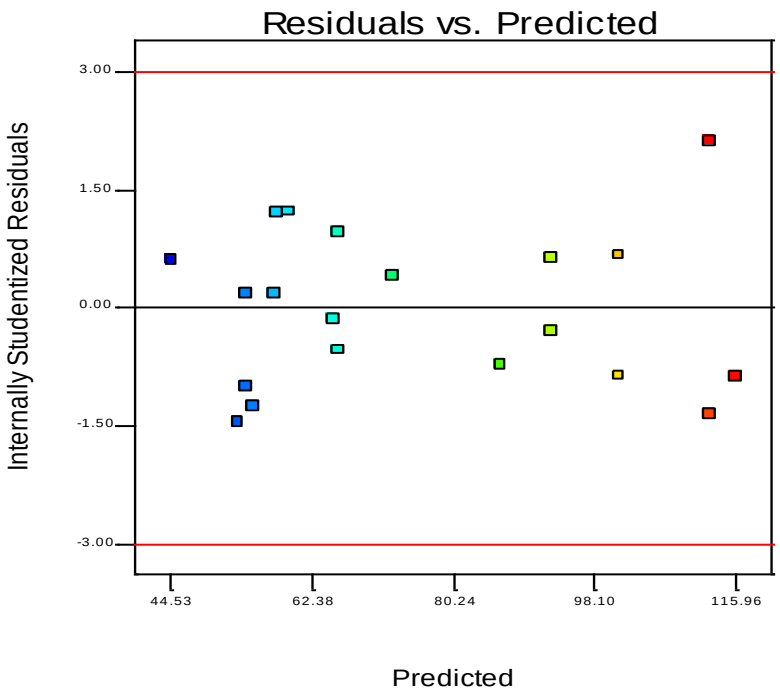

Fig. 3-74 Internally studentized residuals of mucoadhesiveness efficiency compared with predicted values for each 30 run performed in the experimental design

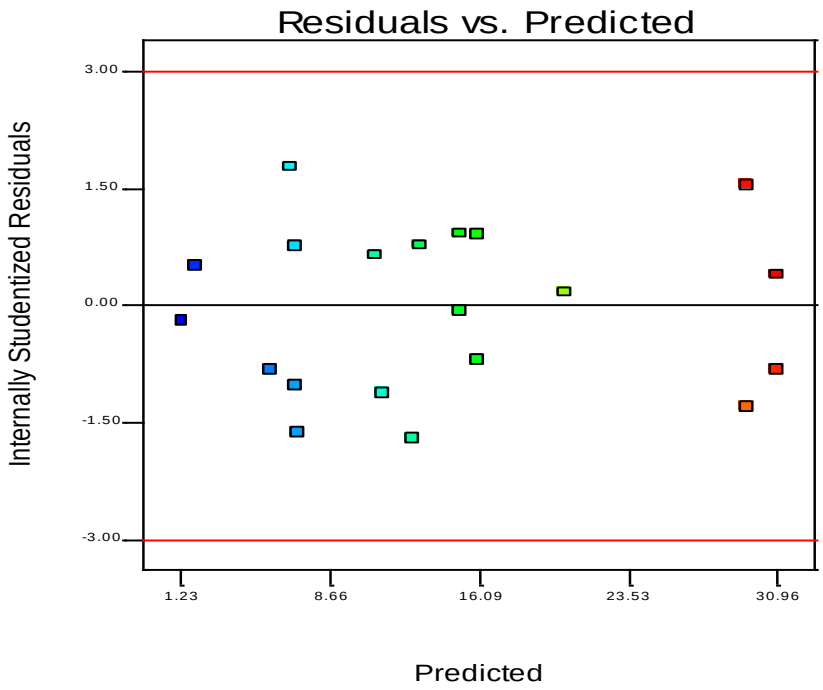

Fig. 3-75 Internally studentized residuals of drug release in 0.1 N HCl buffer pH 1.2 compared with predicted values for each 30 run performed in the experimental design

The points are scattered evenly above and below the 0 point which is showing the points under the curve as negative and points over the curve as positive values. There is no grouping at any point where the internally studentized residuals are only positive or negative. This shows that there is no constant error for the predicted data. The limits – 3.0 and +3.0 were selected according to the 95% confidence interval.

Lastly Box-Cox plot was evaluated in order to calculate lambda values for the conclusion if the data in model needs any transformations.

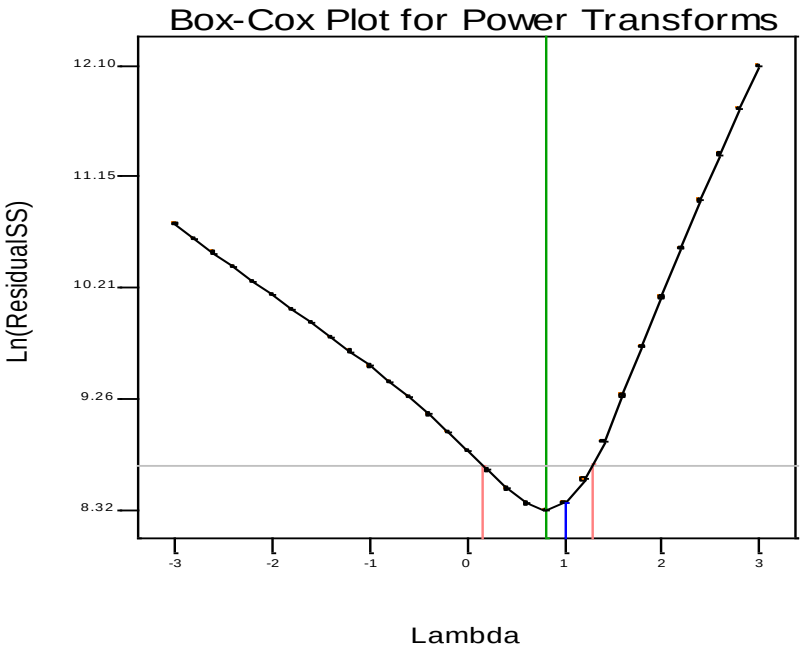

Fig. 3-76 Box-Cox plot for particle size

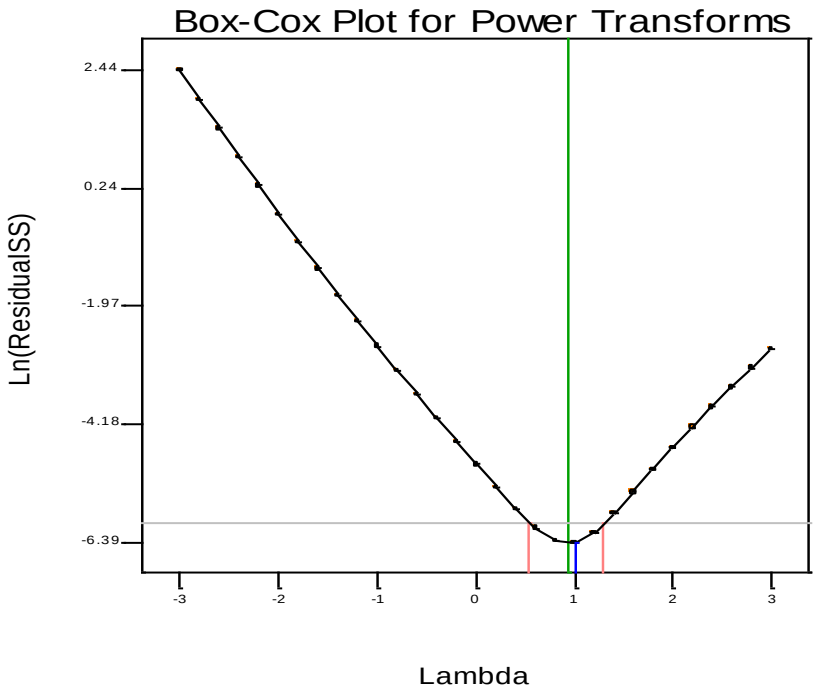

Fig. 3-77 Box-Cox plot for PDI

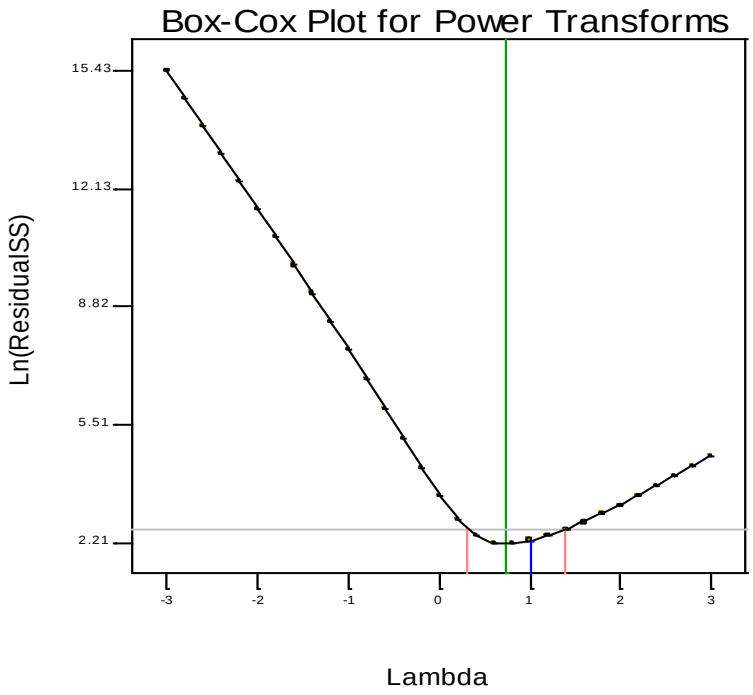

Fig. 3-78 Box-Cox plot for ZETA potential

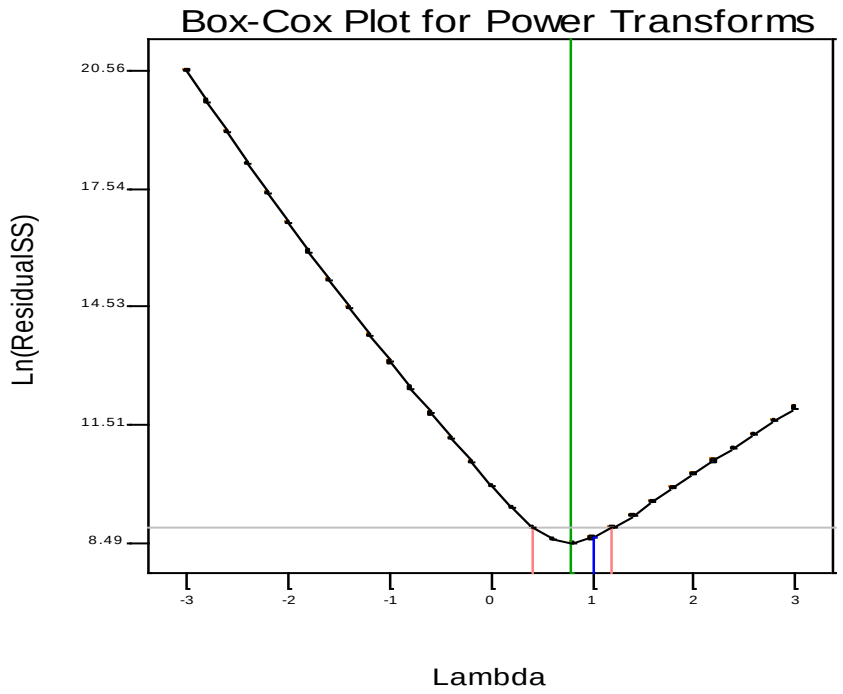

Fig. 3-79 Box-Cox plot for drug loading efficiency

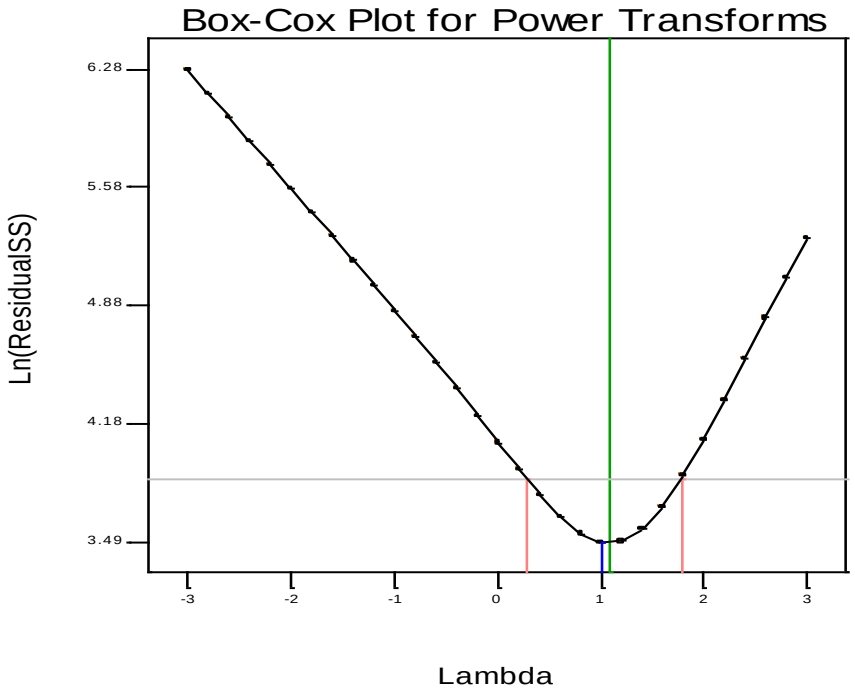

Fig. 3-80 Box-Cox plot for mucoadhesiveness

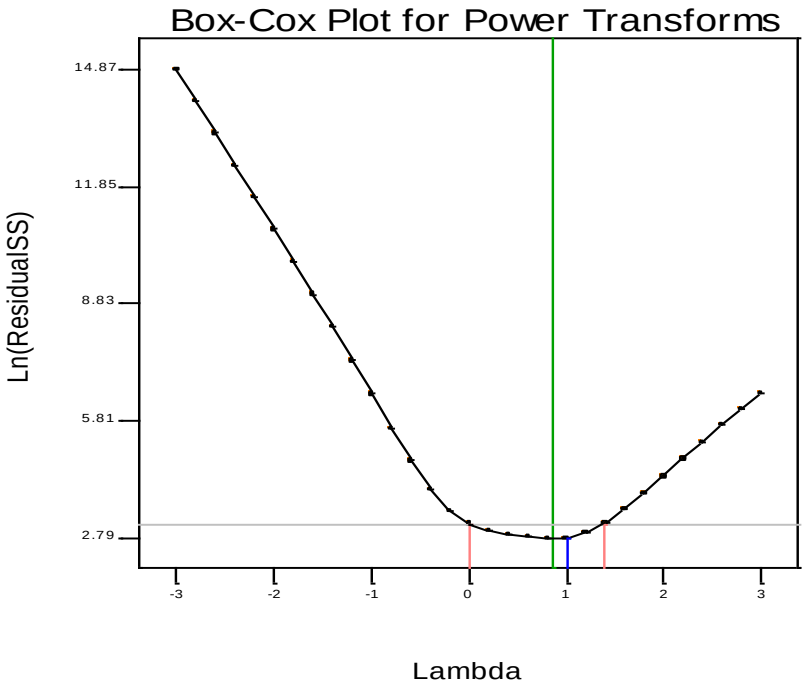

Fig. 3-81 Box-Cox plot for drug release in 0.1 N HCl buffer pH 1.2

95 % confidence limits for the lambda at the lowest Ln(ResidualsSS) value were calculated. Since the confidence limits include the value of lambda 1 for all the plots above, a transformation is not required for the data to ensure the normality or homogeneity of the data.

Data and equation were controlled with the above stated methods for the appropriateness of data for creating the design space. Since the results met all the expected criteria the data were used to create surface diagrams to evaluate the effects of the chosen factors more closely.

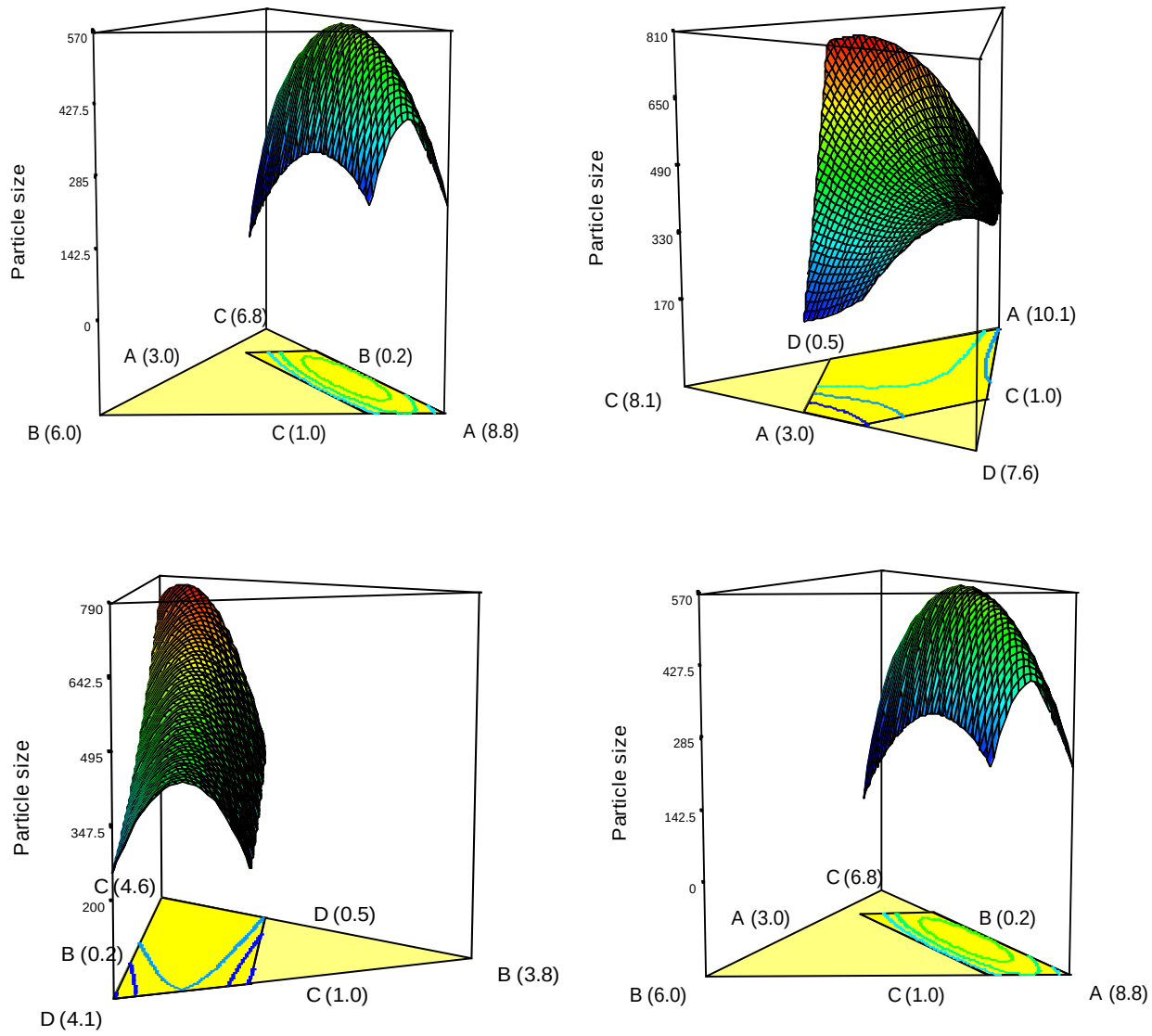

Fig. 3-82 3D surface graph of formulation parameters on particle size. Amount of Fenofibrate was kept constant at center point for a, amount of chitosan was kept constant at center point for b, amount of HPMCP HP50 was kept constant at center point for c and amount of Pluronic F127 was kept constant at center point for d.

As seen in the graphs above particle size of the nanoparticles are closely related with the amount and ratio of the polymers involved in the formulation. When HPMCP HP50 and chitosan is evaluated the ratio is even more dominant in determination of the particle size as the single amount of the polymers in the formulation. It is due to the fact that the ratio between these two polymers determines the ZETA potential of the particle, which plays role in the stabilization of the particles and inhibits particle growth during preparation process. Furthermore as the Pluronic F127 amount increases the particle size decreases due to the

lowering of surface tension of solvent and non solvent resulting in the more efficient mixing of these two.

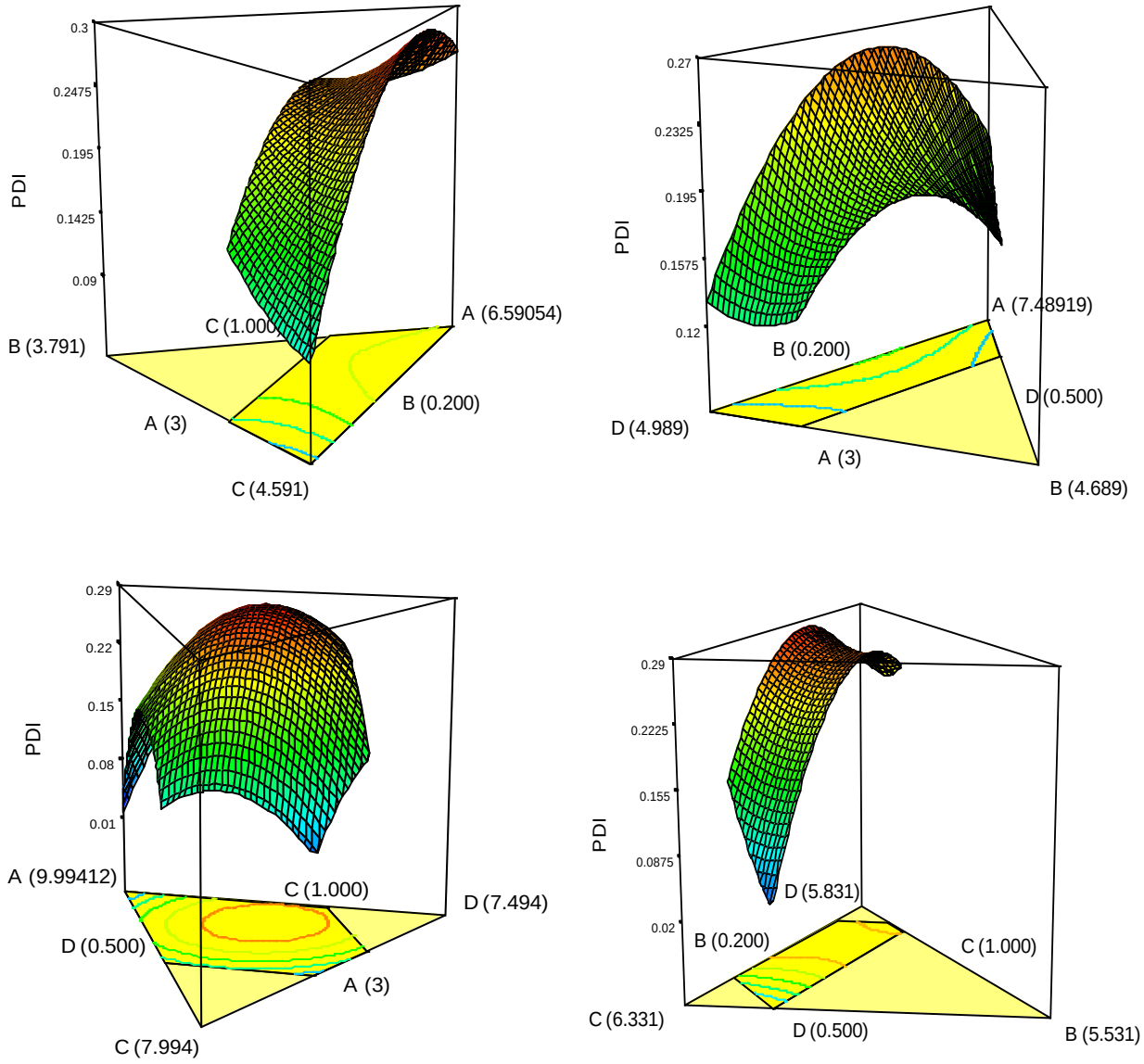

Fig. 3-83 3D surface graph of formulation parameters on PDI. Amount of Fenofibrate was kept constant at center point for a, amount of Pluronic F127 was kept constant at center point for b, amount of chitosan was kept constant at center point for c and amount of HPMCP HP50 was kept constant at center point for d.

The same principle for the particle size works also for the PDI. PDI gets smaller as the particle agglomeration can be avoided which is directly related to the ratio of the chitosan and HPMCP HP50 and the amount of Pluronic F127. Higher PDI values are gathered from the uncontrolled growth of the particles after the production values which can be overcome with steric or electrostatic stabilization.

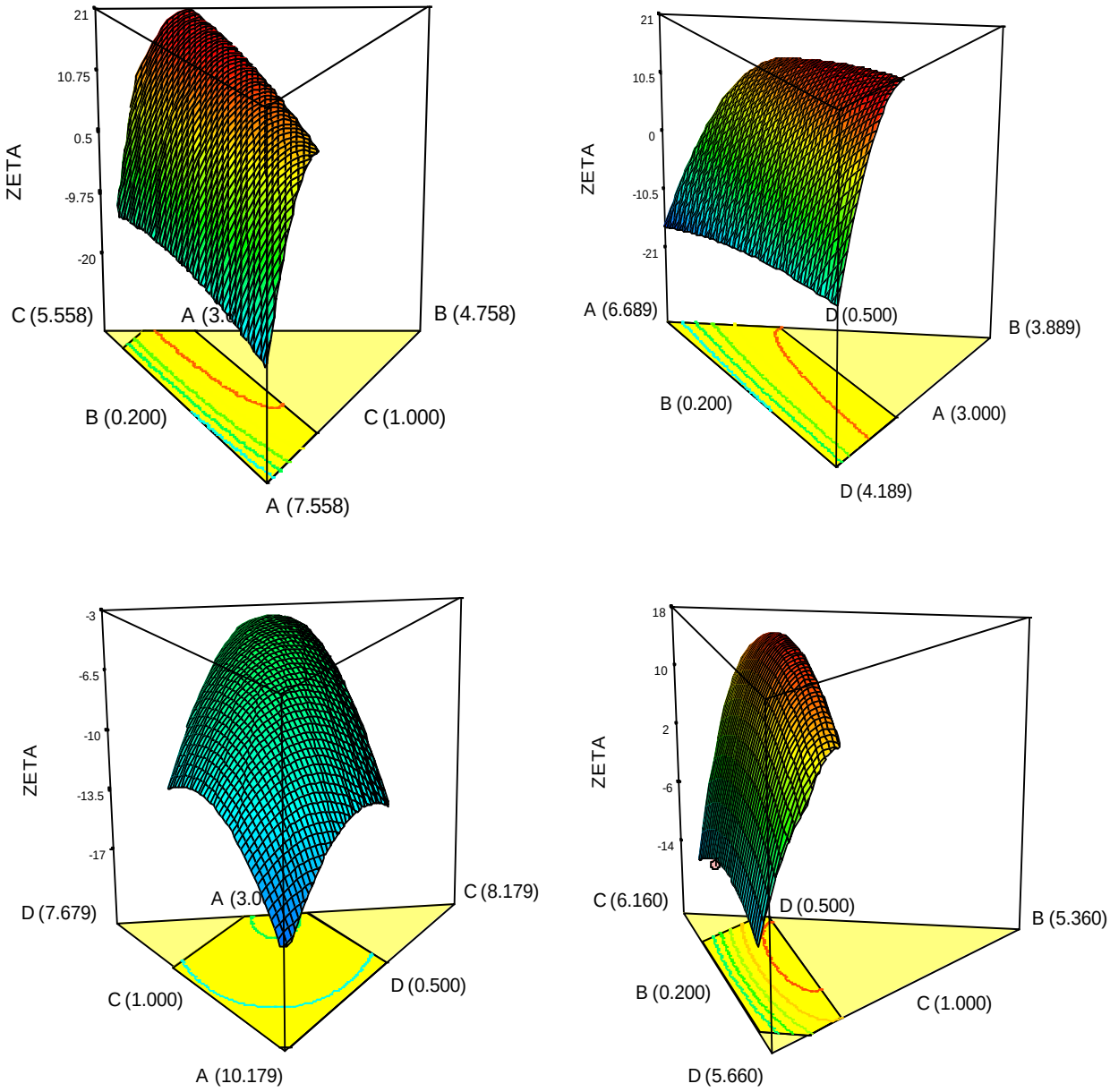

Fig. 3-84 3D surface graph of formulation parameters on particle size. Amount of Fenofibrate was kept constant at center point for a, amount of Pluronic F127 was kept constant at center point for b, amount of chitosan was kept constant at center point for c and amount of HPMCP HP50 was kept constant at center point for d.

The aim for the formulation was to develop positively charged particle which will increase the mucoadhesiveness. As expected with the decreasing amount of HPMCP HP50 and increasing amount of chitosan, increase in the ZETA potential was observed.

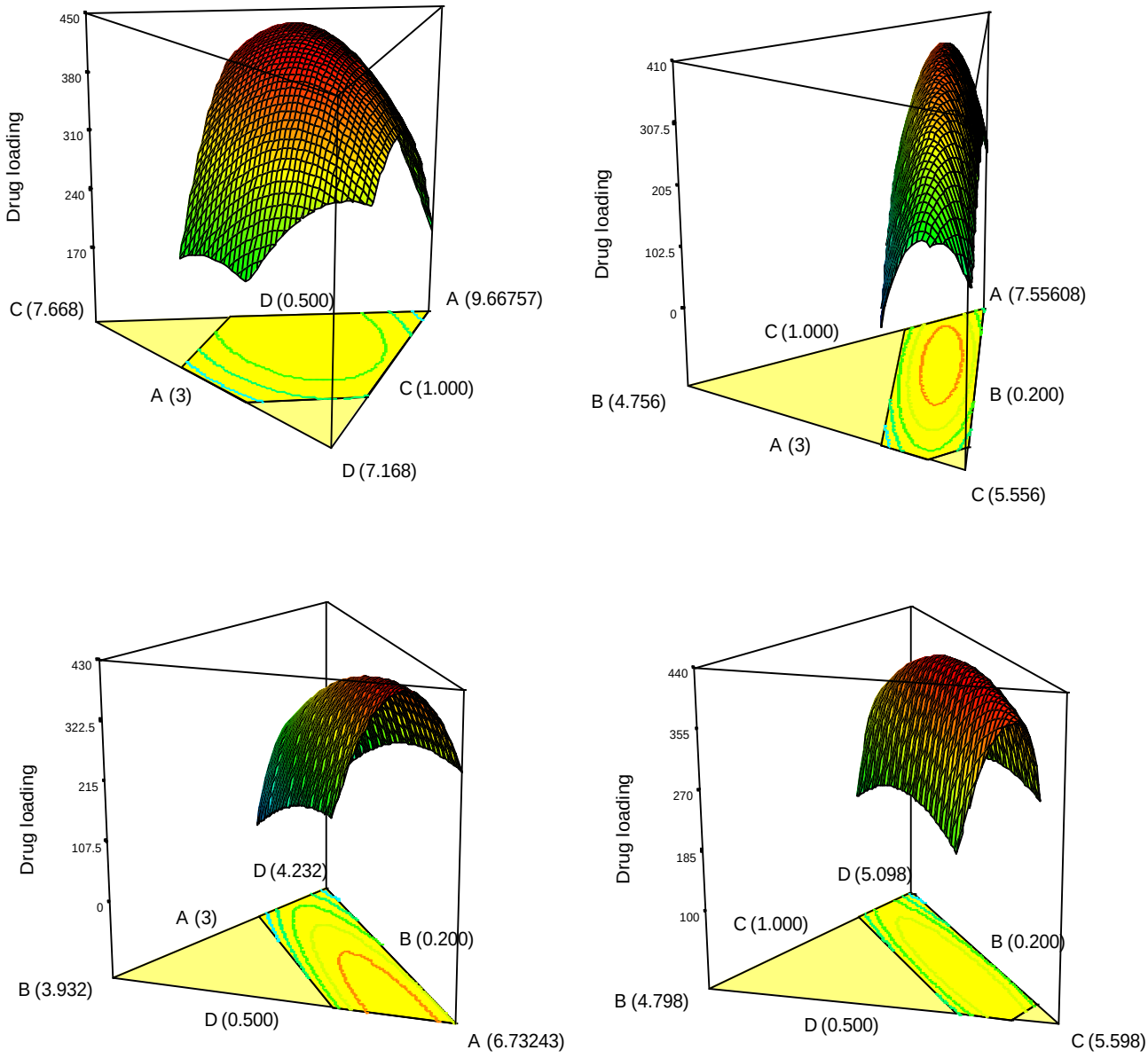

Fig. 3-85 3D surface graph of formulation parameters on drug loading efficiency. Amount of Fenofibrate was kept constant at center point for a, amount of Pluronic F127 was kept constant at center point for b, amount of chitosan was kept constant at center point for c and amount of HPMCP HP50 was kept constant at center point for d.

Drug loading efficiency is directly correlated with the total solid content and the amount of the surfactant in the solution upto a certain concentration. Higher surfactant concentrations increase the solubility of Fenofibrate in the solvent- non solvent mixture thus resulting in the decrease in drug loading efficiency. Furthermore increase in the total solid content results in

the increase in the particle size which upto certain point results in formation of microparticles and crystallization of Fenofibrate.

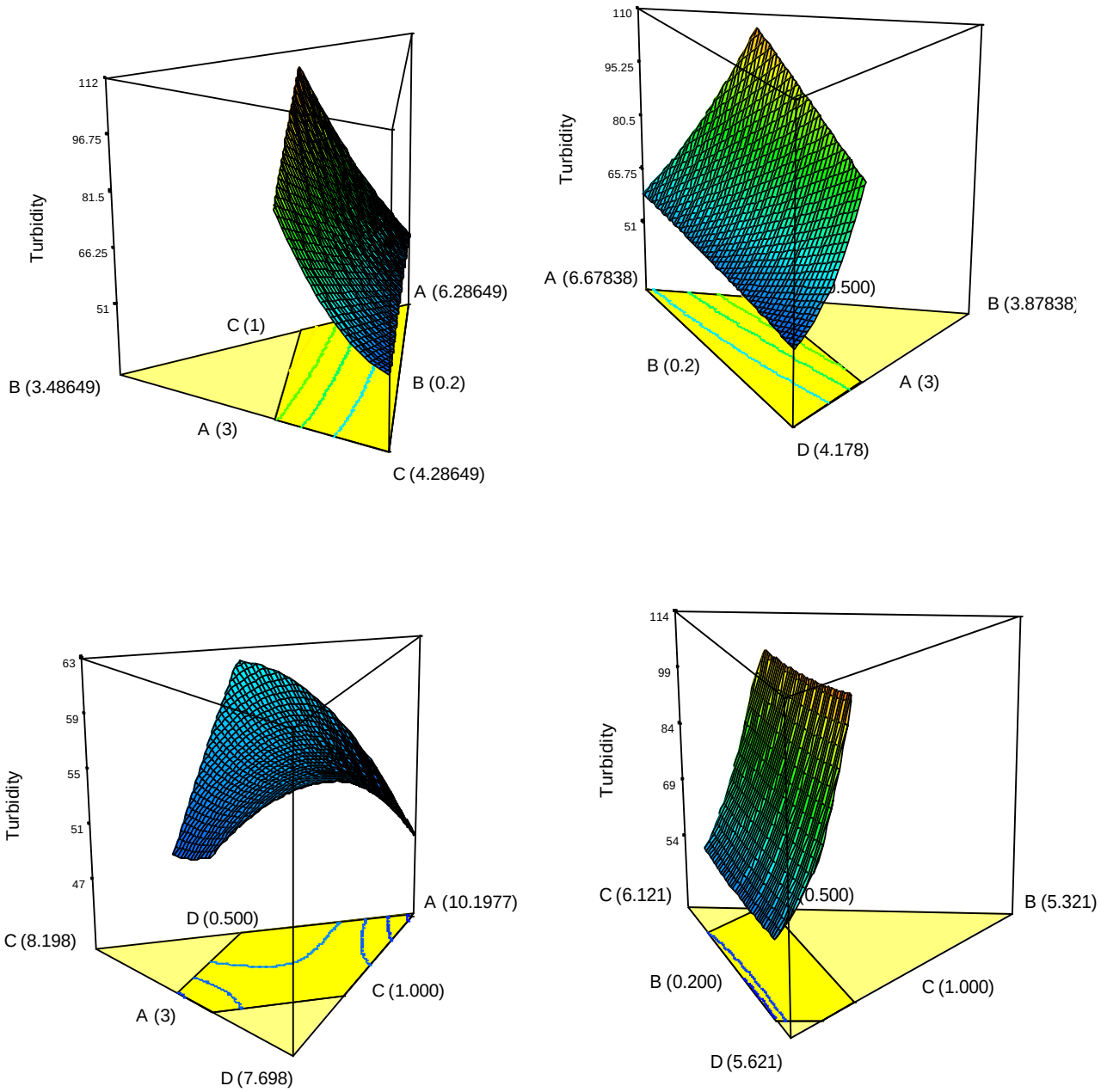

Fig. 3-86 3D surface graph of formulation parameters on mucoadhesivity. Amount of Fenofibrate was kept constant at center point for a, amount of Pluronic F127 was kept constant at center point for b, amount of chitosan was kept constant at center point for c and amount of HPMCP HP50 was kept constant at center point for d.

Turbidity in order words mucoadhesiveness is directly correlated with the amount of chitosan, HPMCP HP50 and Pluronic F127. With the increasing amount of chitosan and decreasing amount of HPMCP HP50 there is an increase in the turbidity due to the higher positive charge on the nanoparticle surface which interacts with the negative charge of mucus. Furthermore with the increase in the surfactant concentration the surface charge of the nanoparticles decrease due to the absorbance of the polymer on the nanoparticle surface which causes in decrease of mucoadhesiveness.

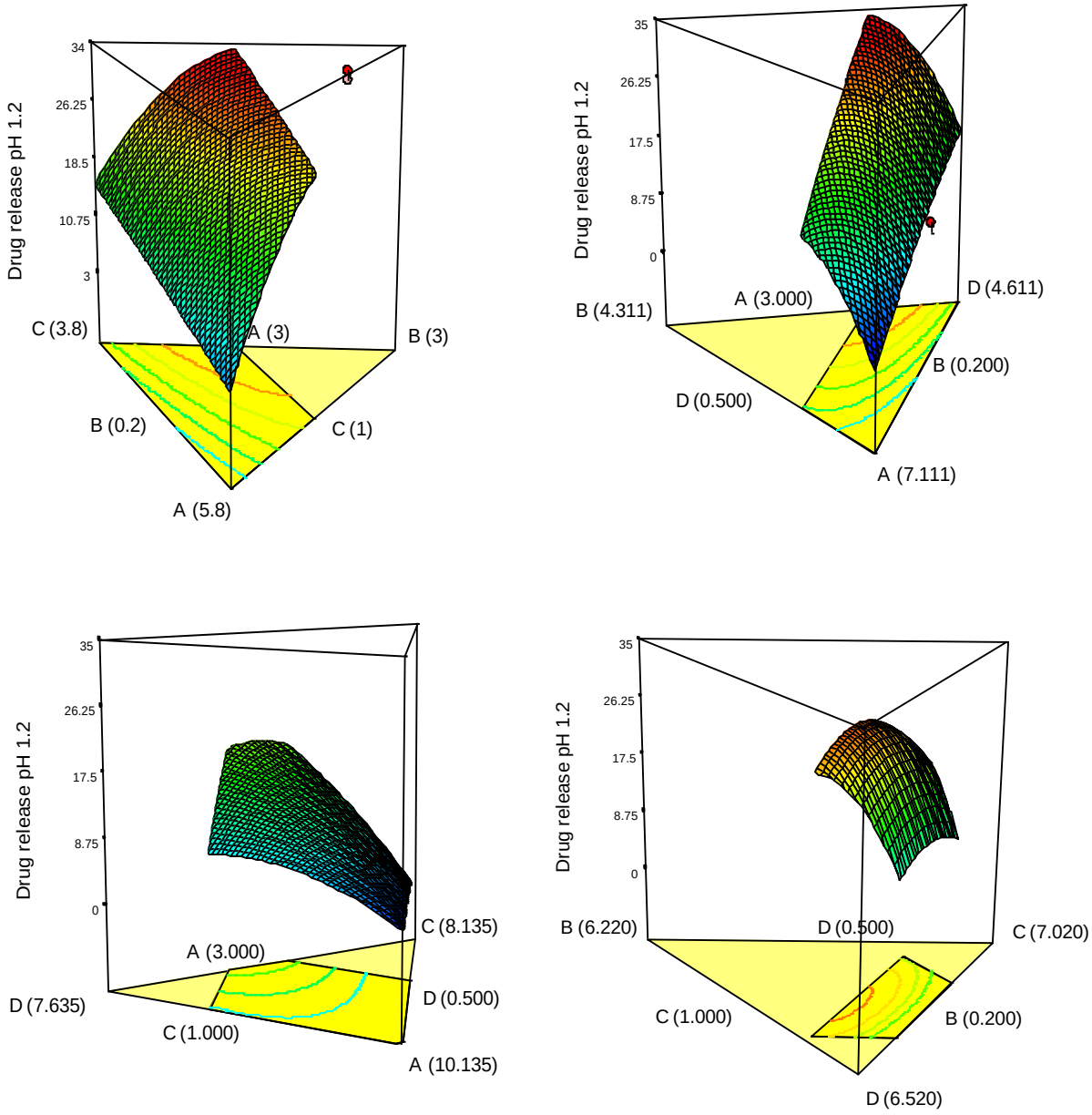

Fig. 3-87 3D surface graph of formulation parameters on drug release in pH 1.2 HCl buffer. Amount of Fenofibrate was kept constant at center point for a, amount of Pluronic F127 was kept constant at center point for b, amount of chitosan was kept constant at center point for c and amount of HPMCP HP50 was kept constant at center point for d.

Enteric coating of the nanoparticles was realized with HPMCP HP50. Thus drug release in acidic media is directly correlated with the amount of HPMCP HP50 in nanoparticle.

After design spaces were created for different parameters optimization of formulation was further carried out with Design Expert software. In the formulation optimization, following parameters were used as requirements:

Tab. 3-61 Requirements for the optimization

Lower Name	Goal	Lower Limit	Upper Limit
HPMCP HP50	is in range	3.000	10.000
Chitosan	is in range	0.200	1.500
Pluronic F127	is in range	0100	5.000
Fenofibrate	minimize	0.500	5.000
Particle size	minimize	174.000	300.000
PDI	minimize	0.022	0.290
ZETA	maximize	0.000	17.600
Drug loading	maximize	200.000	419.052
Turbidity	maximize	45.100	115.500
Drug release pH 1.2	is in range	1.097	11.000

The solution calculated from design space for the above stated system was as follows:

Tab. 3-62 Solutions using the equations and design space calculated based on the requirements given above

HPMCP HP50	Chitosan	Pluron-ic F127	Feno-fibrate	Particle size [nm]	PDI	ZETA [mV]	Drug loading efficiency [µg/mL]	Turbidity	Drug re-lease pH 1.2 [%]
8.421	1.312	1	1.267	199.00	0.13	6.63	402.81	111.71	10.94

DSC studies were conducted with the nanoparticles prepared in according to Tab. 3-62. These nanoparticles were characterized in terms of particle size, ZETA potential and drug loading efficiency. Particle size was found to be 196.6 with a PDI value of 0.13 whereas ZETA potential was 6.78 mV. Particle had a drug loading efficiency of 404.92 µg/mL. These data were in agreement with the proposed solution of Design Expert software. Further characterization of particles was done with DSC measurements. Before DSC measurement nanoparticles were dried until complete dryness.

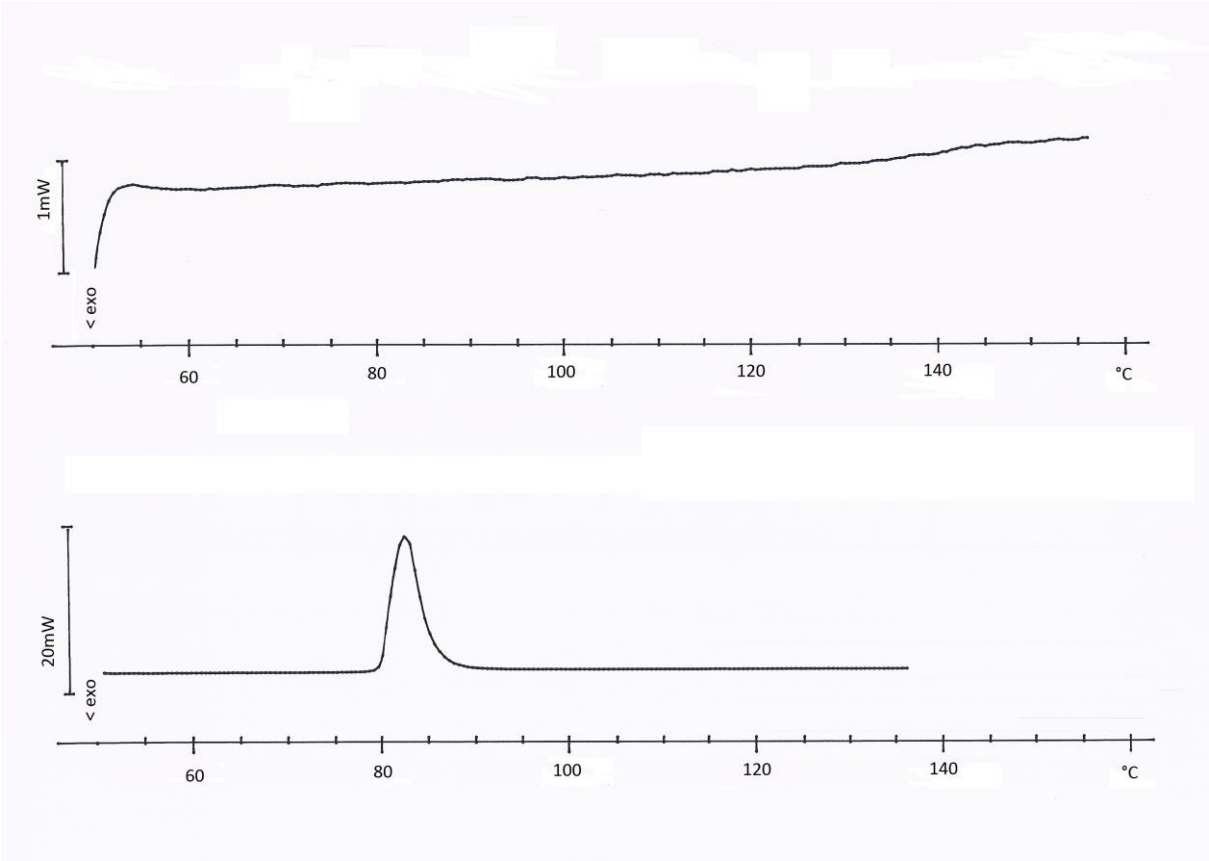

Fig. 3-88 DSC measurements of Fenofibrate nanoparticles prepared with HPMCP HP50 and chitosan. The first spectra represents nanoparticles and the second spectra represents fenofibrate.

As seen in the DSC measurements melting peak of Fenofibrate was completely disappeared indicating that Fenofibrate was fully encapsulated in an amorphous stage in HPMCP HP50/chitosan polymers.

Stability studies were conducted with the nanoparticles produced with in Tab. 3-62 given formulation parameters. Nanoparticles were freeze dried prior to stability studies. Particle size, PDI and drug release properties were investigated in a period of 6 months at 25 °C.

Tab. 3-63: Particle size and PDI analyses of Fenofibrate nanoparticles prepared with HPMCP HP50/chitosan in regard to stability at room temperature

	Particle size [nm]	PDI
0.month	196.6	0.134
1.month	206.2	0.081
2.month	193.2	0.161
3.month	191.3	0.123
6.month	190.6	0.164
Average	195.58	0.13
SD	6.38	0.03
RSD %	3.26	25.43

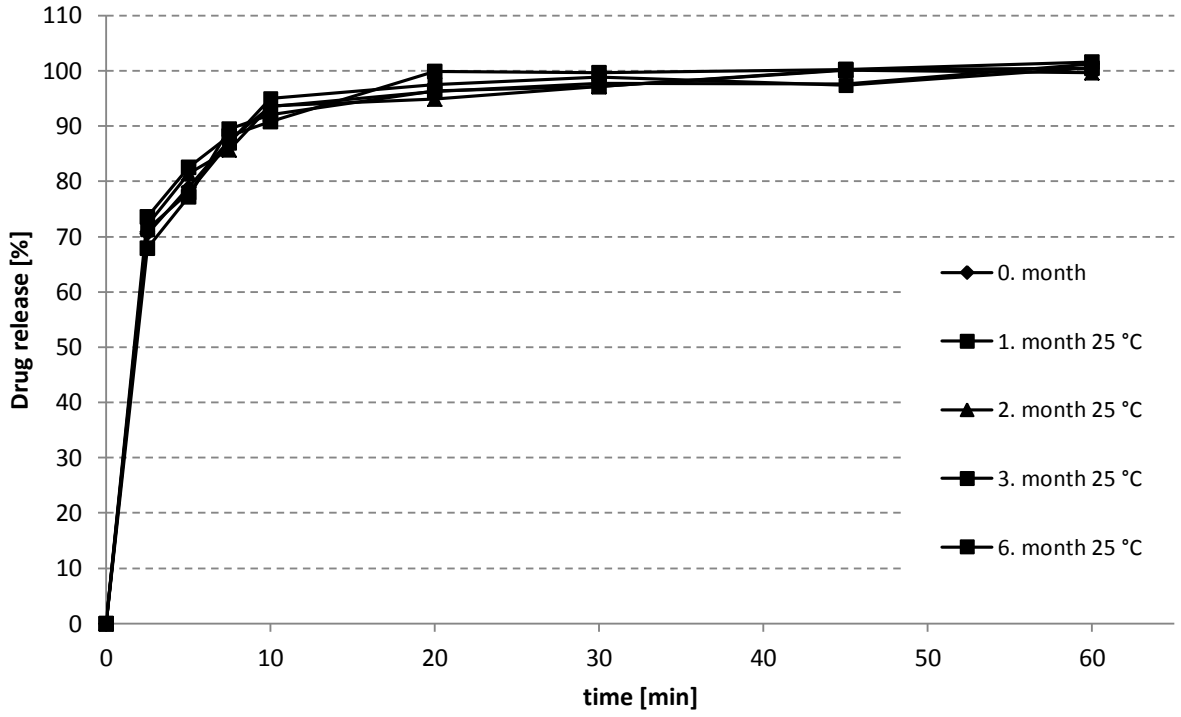

Fig. 3-89 Drug release studies using SIF medium supplemented with 1% tween 20 for the stability tests of Fenofibrate nanoparticles prepared with HPMCP HP50 and chitosan

Results indicated that freeze dried Fenofibrate nanoparticles were stable for a period of 6 months in room temperature conditions. Drug release curves of stored samples did not differentiate from 0 month samples indicating that no crystallization happened throughout the storage.

3.3.3. Comparative evaluation of Fenofibrate nanoparticles

Preparation and characterization of nanoparticles

Particle size is one of the factors that strongly influence the drug release and permeation properties. Thus particle size measurements were conducted together with the ZETA potential for the nanoparticle preparations FN, FHN and FHCN.

Tab. 3-64: Results of the particle size, PDI and Zeta potential analyses for FN, FHN, FHCN nanoparticles prepared using microjet reactor technology

Nanoparticle	Particle size [nm] (n=3)	SD	PDI (n=3)	SD	ZETA potential [mV] (n=3)
FN	286.3	21.2	0.05	0.02	-
FHN	185.4	18.2	0.07	0.04	-12.5
FHCN	211.9	14.9	0.12	0.03	13.1

As seen in the results from Tab. 3-64 it was possible to prepare Fenofibrate nanoparticles in different formulations with comparable particle sizes. Furthermore Fenofibrate particles did not have any surface charge and corresponding ZETA potential whereas FHN nanoparticles had a negative ZETA potential due to the presence of HPMCP HP50and FHCN nanoparticles had a positive ZETA potential due to the presence of chitosan in addition to the HPMCP HP50 which neutralizes the –COOH groups of HPMCP HP50 and furthermore loads the particles positively due to the excess amount of chitosan. Thus the effect of surface properties on drug release and permeation of nanoparticles can also be evaluated using these formulations.

Drug encapsulation efficiencies of the nanoparticles were determined for FHN and FHCN, and the concentration of Fenofibrate was determined for the FN. Finally drug concentrations were adjusted to 400 µg/mL for all formulations by dilution with distilled water.

Drug release studies

Drug release studies with Fenofibrate and the nanoparticle formulations containing Fenofibrate were conducted using different buffers in order to evaluate and interpret the performance of nanoparticle formulations and furthermore to compare the performance with Fenofibrate.

i. Two stage drug release

Two stage drug release studies were conducted in order to evaluate the effectiveness of pH resistance of FHN and FHCN nanoparticles. Furthermore FN nanoparticles were included for comparison reasons.

In the acid stage of the drug release, no drug release is expected since the FHN and FHCN nanoparticles are enteric coated. As seen in the table below there was no remarkable drug release for any of the formulations. Due to the low solubility of Fenofibrate there was also no dissolution observed for Fenofibrate and FN nanoparticles. But one of the observations was that FN nanoparticles agglomerated forming larger microparticles since the stabilizing effect of Pluronic F127 did not exist anymore due to the dilution in 0.1 N HCL

Tab. 3-65 : Cumulative drug release profiles of Fenofibrate, FHN and FHCN formulations in 0.1 N HCl (n=3)

Time [min]	Cumulative drug release [%]							
	5	10	20	30	45	60	90	120
Fenofibrate	0.00	0.00	0.01	0.02	0.09	0.14	0.23	0.33
SD	0.0002	0.0039	0.0094	0.00807	0.0116	0.0076	0.02147	0.015
FN	0.03	0.05	0.07	0.09	0.15	0.27	0.62	0.85
SD	0.005	0.004	0.008	0.003	0.009	0.04	0.009	0.004
FHN	0.02	0.02	0.02	0.04	0.05	0.05	0.05	0.05
SD	0.0002	0.004	0.008	0.007	0.02	0.01	0.015	0.02
FHCN	0.01	0.04	0.01	0.02	0.03	0.03	0.03	0.04
SD	0.0002	0.0491	0.0009	0.00354	0.0058	0.0058	0.01518	0.0058

After 120 minutes the pH of the medium was increased to pH 6.8 with the addition of 0.2 M tribasic sodium phosphate buffer supplemented with 4% tween 20. Since 250 mL of buffer was added to 750 mL of 0.1 N HCl, the resulting tween 20 concentration in the vessel was 1 %.

Tab. 3-66 Cumulative drug release profiles of Fenofibrate, FHN and FHCN formulations in buffer stage in the presence of 1 % Tween 20 (n=3)

Time [min]	Cumulative drug release [%]									
	2.5	5	7.5	10	20	30	45	60	90	120
Fenofibrate	2.3	3.9	4.5	6.1	8.4	11.8	16.3	21.1	26.8	34.9
SD	0.1	0.1	0.1	0.1	0.3	0.3	2.1	0.6	0.8	2.0
FN	10.90	15.80	21.90	25.70	32.90	37.90	45.70	52.60	62.70	69.80
SD	2.10	1.40	1.90	3.10	1.90	3.10	1.60	2.50	3.20	2.90
FHN	82.5	96.0	99.2	99.6	99.2	99.5	99.2	99.8	99.4	99.9
SD	3.5	3.1	1.1	2.5	3.0	2.1	2.2	1.8	2.4	1.6
FHCN	68.4	77.2	80.8	89.1	99.1	99.3	99.4	100.1	99.9	100.8
SD	3.1	2.3	2.6	0.5	1.6	1.2	0.5	07	0.3	1.2

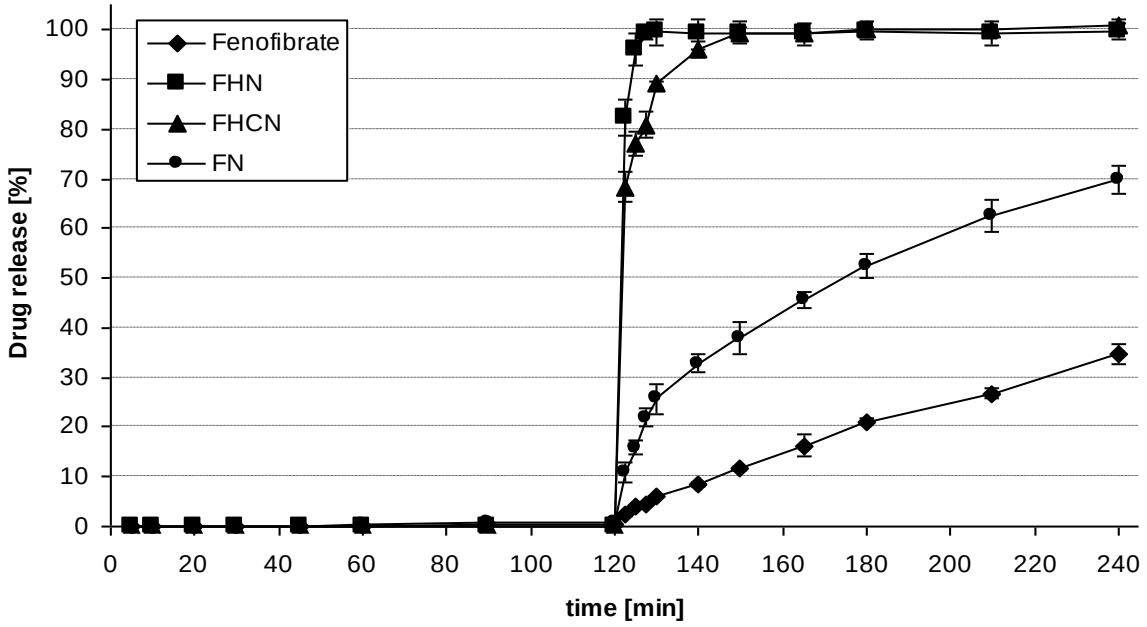

Fig. 3-90: 2 stage drug release profiles of Fenofibrate, FHN and FHCN using USP apparatus II at a speed of 50 rpm (n=3)

ii. Drug release studies with simulated intestinal fluid

Drug release studies for Fenofibrate, FN, FHN and FHCN was done using SIF buffer supplemented with either 1 % tween 20 or 1 % SDS.

Tab. 3-67 : Cumulative drug release profiles of Fenofibrate, FN, FHN and FHCN formulations in SIF buffer in the presence of 1 % Tween 20 (n=3)

	Cumulative drug release [%]									
Time [min]	**2.5**	**5**	**7.5**	**10**	**20**	**30**	**45**	**60**	**90**	**120**
Fenofibrate	0.9	1.7	2.7	3.6	6.6	9.5	13.7	17.8	25.4	31.8
SD	0.0	0.0	0.1	0.2	0.4	0.4	0.6	0.9	1.4	1.3
FN	89.2	94.0	96.0	96.3	98.6	100.2	100.7	100.3	100.6	100.5
SD	0.8	0.4	0.7	1.9	0.6	1.1	0.2	1.8	0.3	0.3
FHN	91.5	93.3	95.9	97.9	99.7	101.0	100.9	100.5	100.5	100.5
SD	0.4	0.3	0.4	0.5	0.7	0.5	0.5	0.3	0.3	0.4
FHCN	70.5	80.9	87.4	90.9	99.6	99.1	100.3	101.3	101.0	101.1
SD	2.2	2.6	1.9	1.6	1.3	0.2	1.7	0.6	0.9	1.1

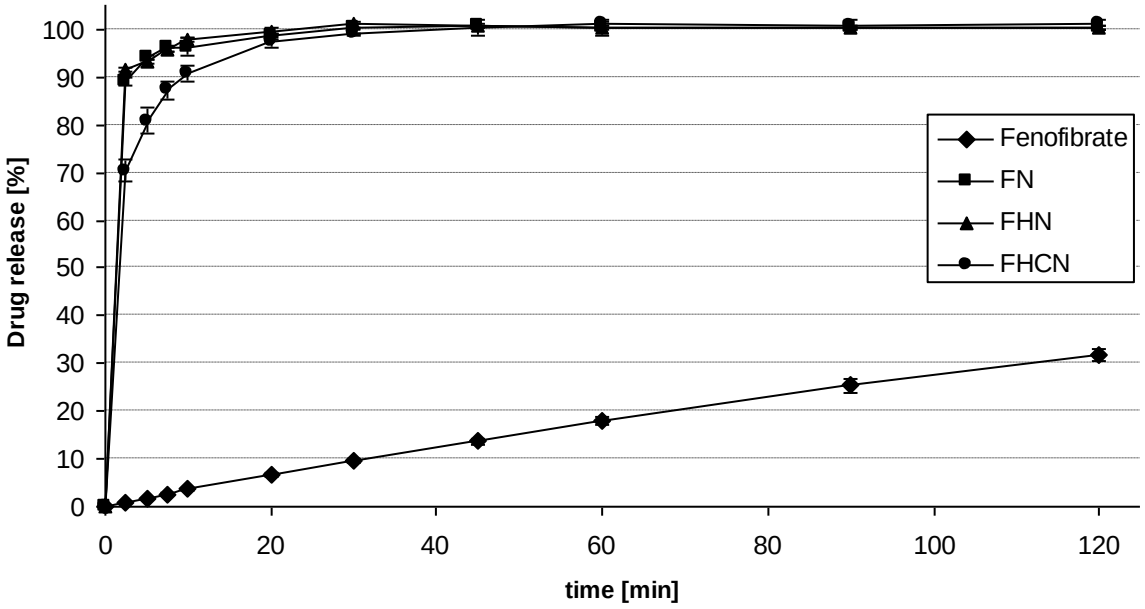

Fig. 3-91 Drug release profiles of Fenofibrate, FN, FHN and FHCN in SIF buffer pH 6.8 supplemented with 1 % tween 20 using USP apparatus II at a speed of 50 rpm (n=3)

It was observed that the dissolution of Fenofibrate was not complete at the end of 2 hours even in the presence of tween 20. Whereas nanoparticle formulations released the drug immediately where 100 % was reached within 20 minutes. It was again observed that initial burst was lower in the case of FHCN due to the presence of chitosan.

Further experiments were conducted in SIF buffer supplemented with 1 % SDS to ensure the 100 % dissolution of Fenofibrate within 2 hours.

Tab. 3-68 : Cumulative drug release profiles of Fenofibrate, FN, FHN and FHCN formulations in SIF buffer in the presence of 1 % SDS (n=3)

	Cumulative drug release [%]									
Time [min]	**2.5**	**5**	**7.5**	**10**	**20**	**30**	**45**	**60**	**90**	**120**
Fenofibrate	4.5	9.1	14.0	18.6	34.9	47.9	63.3	72.8	85.9	92.5
SD	0.1	0.2	0.3	0.4	0.4	0.7	1.6	2.8	0.3	2.2
FN	96.2	99.5	100.5	100.2	100.3	100.2	100.6	100.5	100.5	100.7
SD	0.5	0.6	0.9	0.3	1.0	0.5	0.2	0.5	0.8	0.5
FHN	98.2	99.8	101.0	100.6	100.5	100.8	100.6	100.8	100.6	100.8
SD	0.5	0.8	0.8	0.5	1.0	0.4	0.5	0.7	0.6	0.5
FHCN	89.8	94.4	96.8	98.7	100.0	100.4	100.9	101.6	100.8	99.5
SD	1.9	2.1	1.5	1.4	1.7	1.6	1.4	1.5	1.3	0.8

Fig. 3-92: Drug release profiles of Fenofibrate, FN, FHN and FHCN in SIF buffer pH 6.8 supplemented with 1 % SDS using USP apparatus II at a speed of 50 rpm (n=3)

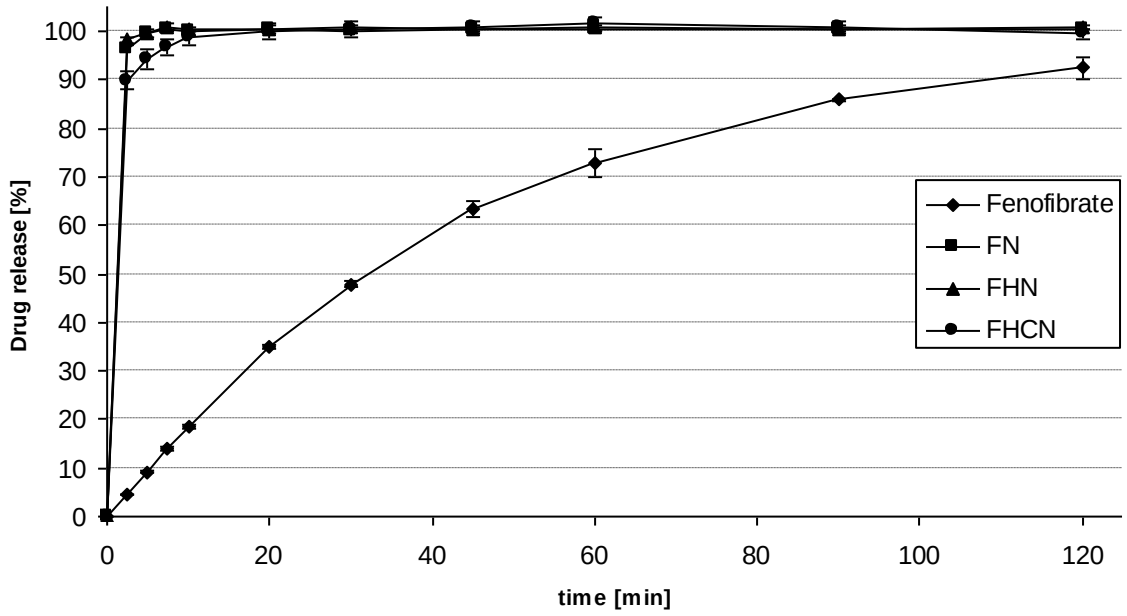

iii. Drug release studies with FASSIF and FESSIF

It is known that there is a significant difference between the bioavailability of Fenofibrate in fed and fasted states. This difference is due to the low solubility of Fenofibrate and the dissolution rate changing due to the bile salt contents of fed or fasted state.

Tab. 3-69 : Cumulative drug release profiles of Fenofibrate, FN, FHN and FHCN formulations in FESSIF buffer (n=3)

	Cumulative drug release [%]									
Time [min]	**2.5**	**5**	**7.5**	**10**	**20**	**30**	**45**	**60**	**90**	**120**
Fenofibrate	3.1	5.5	6.8	7.4	14.5	21.3	30.9	39.5	53.8	70.2
SD	0.3	0.6	0.1	0.4	1.2	2.4	3.0	2.5	2.9	4.4
FN	96.3	98.6	100.2	100.7	100.3	100.6	100.5	100.3	100.6	100.5
SD	1.9	0.6	1.1	0.2	1.8	0.3	0.3	1.8	0.3	0.3
FHN	91.0	96.0	99.6	99.5	99.8	100.0	100.1	100.0	100.3	100.5
SD	0.3	0.7	0.4	0.3	0.1	0.8	0.8	0.6	0.3	0.1
FHCN	85.8	91.2	94.3	97.5	99.8	99.7	100.2	99.8	99.1	99.7
SD	1.5	1.0	1.7	1.0	0.8	0.8	0.8	0.8	0.8	0.8

Tab. 3-70 : Cumulative drug release profiles of Fenofibrate, FN, FHN and FHCN formulations in FASSIF buffer (n=3)

	Cumulative drug release [%]									
Time [min]	**2.5**	**5**	**7.5**	**10**	**20**	**30**	**45**	**60**	**90**	**120**
Fenofibrate	1.1	1.2	2.3	3.6	7.6	11.3	16.3	22.9	30.3	43.4
SD	0.3	0.0	0.1	0.2	0.5	0.2	1.6	1.7	1.7	3.8
FN	31.5	41.8	52.3	55.1	66.2	74.0	79.8	83.0	85.2	85.3
SD	1.0	1.4	1.9	1.9	2.1	1.3	1.6	4.1	2.6	1.2
FHN	36.7	48.1	58.7	63.6	75.0	81.1	82.9	84.3	84.3	85.0
SD	1.3	0.8	0.4	2.3	4.6	0.9	1.5	1.1	2.5	1.3
FHCN	34.0	46.3	57.7	68.8	77.8	80.2	80.3	80.5	82.2	82.8
SD	1.7	3.7	0.7	1.2	1.9	0.2	1.8	1.8	1.5	0.3

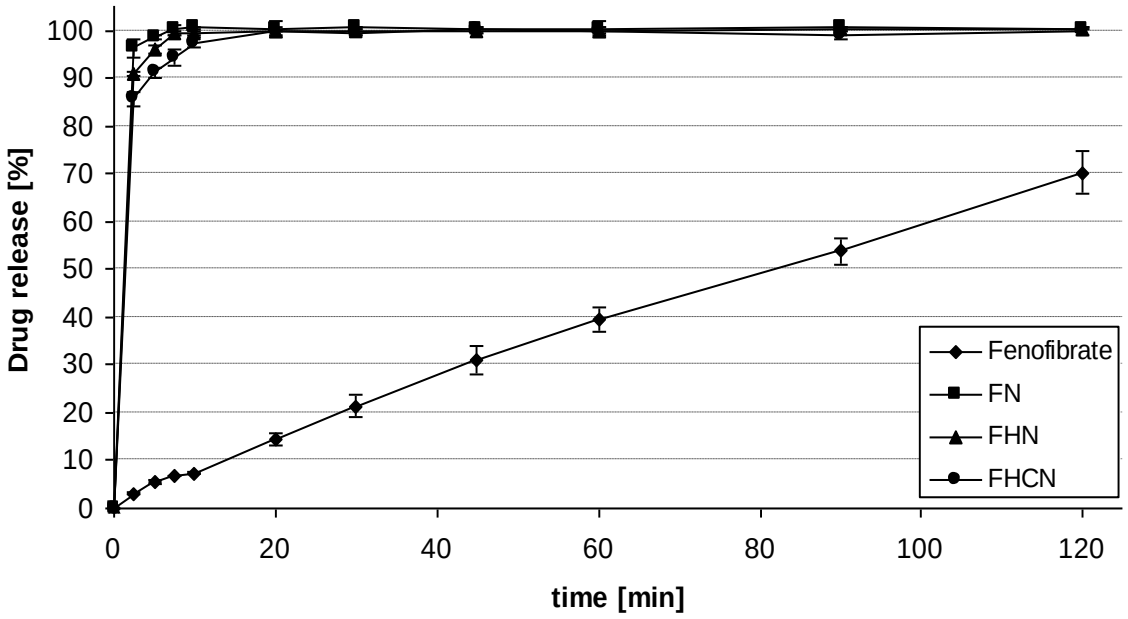

Fig. 3-93: Drug release profiles of Fenofibrate, FN, FHN and FHCN in FESSIF using USP apparatus II at a speed of 50 rpm (n=3)

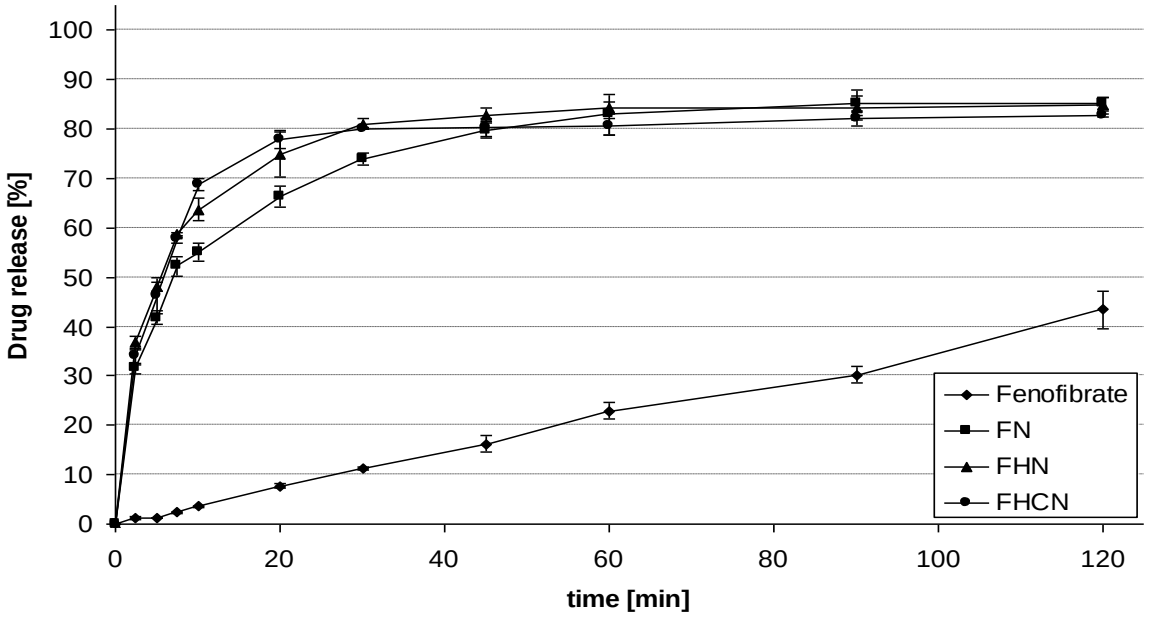

Fig. 3-94: Drug release profiles of Fenofibrate, FN, FHN and FHCN in FaSSIF using USP apparatus II at a speed of 50 rpm (n=3)

In general nanoparticle formulations did not show any dramatic differences between the drug release profiles in FESSIF and FASSIF which would affect the absorption and bioavailability of Fenofibrate if it is taken with meals or not. Furthermore as seen in the drug release profiles of Fenofibrate there is more than 2 fold difference between the drug release percent in FASSIF and FESSIF. This affects the later bioavailability of API resulting in very low bioavailability if not taken together with meals.

In-vitro mucoahesiveness test

FN, FHN and FHCN nanoparticles were investigated for their affinity to mucin. The investigations were carried out in mucin dispersions containing the nanoparticles. If the nanoparticles attached to mucin it is expected that the turbidity of the solution increases and stays stable for a period of 3 hours. Furthermore for positively charged particles there should be a decrease in the ZETA potential due to interaction with negative loaded mucin.

Before the start of turbidity experiments nanoparticle suspension were diluted with water in the same ratio (1:25) as they are diluted with mucin to control the difference in the turbidity and furthermore mucin dispersion was used as blank which has a turbidity of 43.9 NTU. The turbidity increase when nanoparticles were added to water was also added to the blank value and this value

was subtracted from the measurements at every time point. The blank values for FN, FHN and FHCN nanoparticles were 48.9, 50.2 and 50.3 respectively.

Tab. 3-71 Turbidity of the mucin solution containing FN, FHN and FHCN over a period of 3 hours (n=3)

Time [min]	Turbidity [NTU]					
	30	**60**	**90**	**120**	**150**	**180**
FN	0.8	0.5	0.7	2	2.3	1
SD	4.2	2.7	3.4	4.1	7.9	6.4
FHN	6.3	3.9	4.1	1.7	0.3	5.6
SD	3.4	2.7	4.9	3.4	6.2	4.3
FHCN	81.1	77.1	81.1	85.1	87.1	78.1
SD	3.4	5.5	4.8	4.2	6.3	6.7

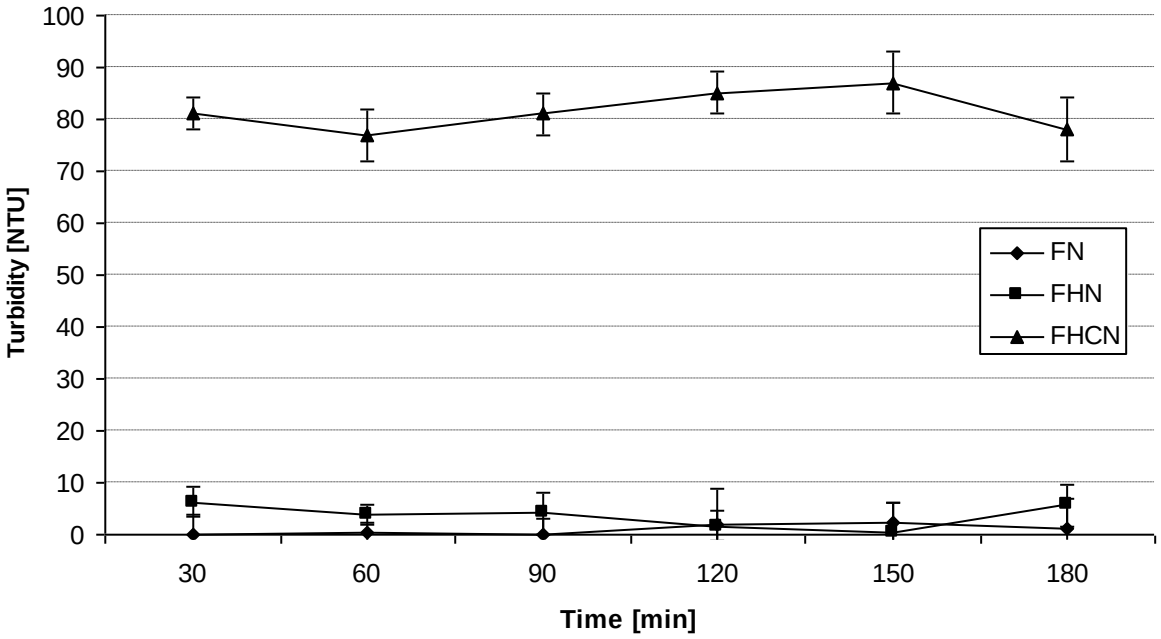

Fig. 3-95: Turbidity of the mucin solution containing FN, FHN and FHCN over a period of 3 hours (n=3)

ZETA analyses were performed first with FN, FHN and FHCN nanoparticles 1:25 diluted in water. Furthermore ZETA potential of mucin was determined which was -6.14 mV. The 0 minute values indicate the ZETA potential of nanoparticles diluted in water.

Tab. 3-72 ZETA potential of the mucin dispersion containing FN, FHN and FHCN over a period of 3 hours (n=3)

Time [min]	ZETA Potential [mV]						
	0	**30**	**60**	**90**	**120**	**150**	**180**
FN	0.2	-5.2	-6.4	-4.9	-5.9	-6.3	-6.9
SD	0.4	2.1	4.9	6.7	8.1	4.3	5.2
FHN	-12.5	-13.5	-15.6	-17.5	-14.9	-13.5	-13.7
SD	3.2	2.7	4.9	3.4	6.9	5.7	4.6
FHCN	13.1	-2.45	-3.45	-4.25	-3.98	-3.54	-3.2
SD	4.6	3.4	6.7	4.6	5.9	4.6	3.9

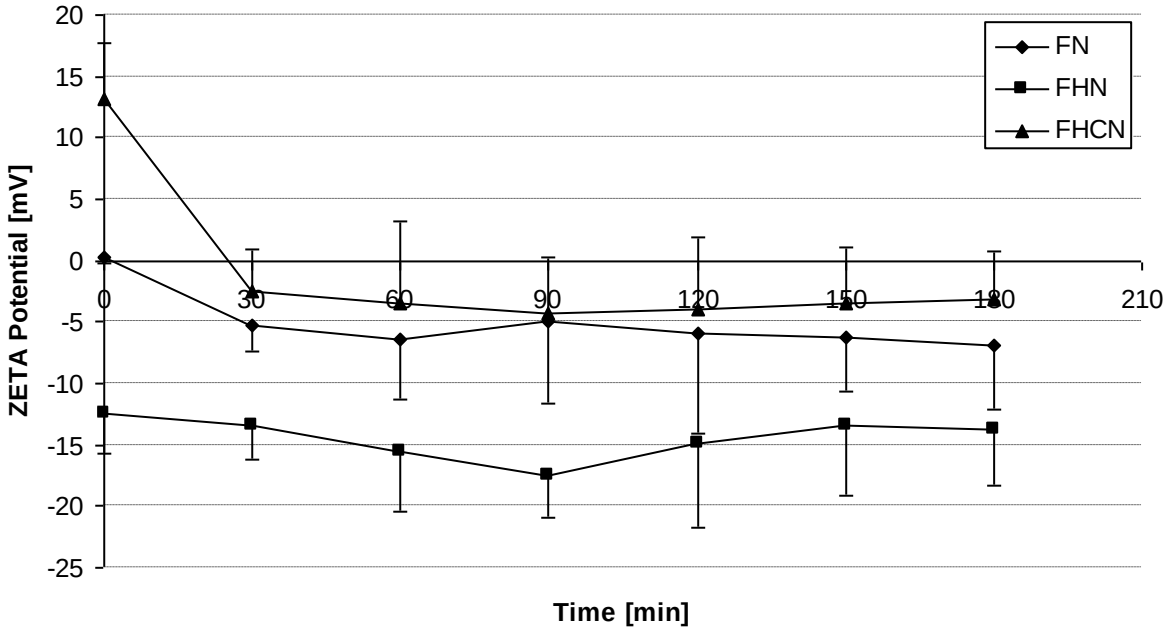

Fig. 3-96 ZETA potential of the mucin solution containing FN, FHN and FHCN over a period of 3 hours (n=3)

ZETA potential of FHCN nanoparticles decreased dramatically after addition to mucin dispersion showing the interaction of mucin with these particles. Furthermore this interaction was stable throughout the period of 180 minutes.

Caco-2 permeability studies

Caco-2 permeation studies were conducted for the evaluation of possible differences between the amount absorbed when FASSIF or FESSIF was used as the transport medium. Nanosuspensions and Fenofibrate were applied to each well in an amount of 7 µg/well to be able to observe the differences dependent on the solubility of the substance together with the surface properties of the nanoparticles.

Tab. 3-73 Amount of Fenofibrate dissolved in FASSIF and FASSIF determined from the donor samples (n=3)

Formulation	FASSIF [µg/mL]	FESSIF [µg/mL]	Ratio FASSIF/FESSIF
Fenofibrate	0.4 ± 0.03	1.2±1.34	10.5
FN	1.6±0.40	2.8±0.37	1.8
FHN	1.4±0.06	2.4±0.06	1.7
FHCN	1.5±0.23	2.5±0.38	1.7

The ratio of FASSIF/FESSIF solubilities was approximately 10 in the case of Fenofibrate powder. Whereas this difference decreases down to 1.8, 1.7 and 1.7 for FN, FHN and FHCN respectively.

Tab. 3-74 Cumulative percentage absorbed of Fenofibrate, FN, FHN and FHCN in Caco-2 experiments using FASSIF as transport buffer (n=3)

Time [min]	% Cumulative permeation/SD			
	Fenofibrate	**FN**	**FHN**	**FHCN**
30	0.1±0.05	1.4±0.19	0.8±0.16	1.2±0.23
60	0.3±0.04	1.8±0.24	1.3±0.36	1.7±0.34
90	0.3±0.01	2.1±0.19	1.7±0.24	2.4±0.20
120	0.3±0.03	2.3±0.25	2.5±0.09	3.0±0.16

The permeability of Fenofibrate is limited with its solubility. It was revealed that in case of FN, FHN and FHCN the % cumulative permeability is significantly ($p<0.01$) higher than that of Fenofibrate.

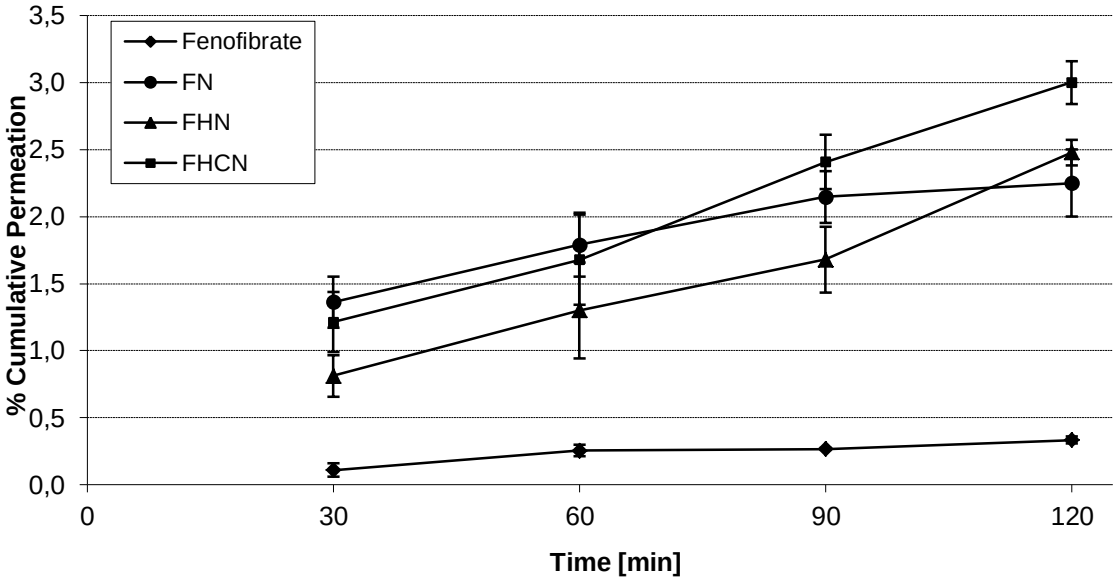

Fig. 3-97 Cumulative percentage absorbed of Fenofibrate, FN, FHN and FHCN in Caco-2 experiments using FASSIF as transport buffer (n=3)

Furthermore in order to compare the differences between the FN, FHN, FHCN % cumulative permeability one way ANOVA test was run with Bonferroni correction. One way ANOVA test revealed the significant difference between all three groups with a p value of 0.08, furthermore the % cumulative permeation of FHCN was found to be different from FN and FHN with p values of 0.009 and 0.042 respectively. In the same test no significant difference was observed between FN and FHN particles.

Permeation experiments with FESSIF as the transport buffer revealed following results shown in Tab 3-75:

Tab. 3-75 Cumulative percentage absorbed of Fenofibrate, FN, FHN and FHCN in Caco-2 experiments using FESSIF as transport buffer (n=3)

Time [min]	% Cumulative permeation/SD			
	Fenofibrate	FN	FHN	FHCN
30	0.4±0.1	1.1±0.3	1.4±0.2	1.4±0.2
60	0.6±0.1	2.8±0.6	2.6±0.2	2.9±0.5
90	0.7±0.2	4.0±0.4	3.8±0.3	4.2±0.5
120	0.9±0.1	4.7±0.2	4.5±0.1	5.2±0.2

There was found to be a significant difference between Fenofibrate, FN, FHN and FHCN ($p<0.01$).

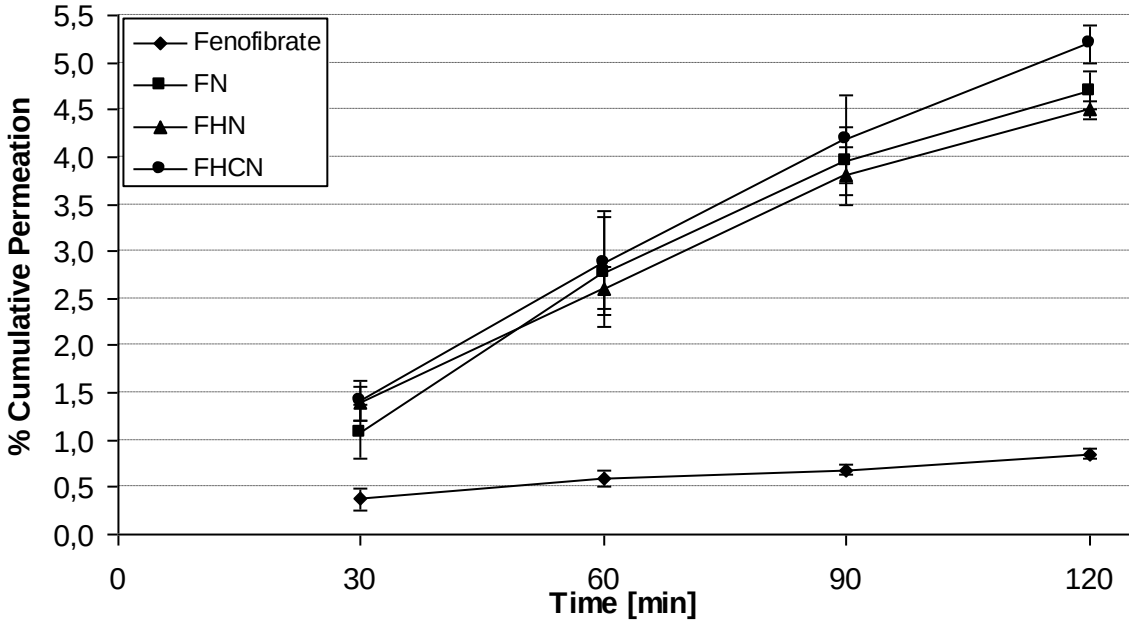

Fig. 3-98 Cumulative percentage absorbed of Fenofibrate, FN, FHN and FHCN in Caco-2 experiments using FESSIF as transport buffer (n=3)

Furthermore in order to compare the differences between the FN, FHN, FHCN % cumulative permeability one way ANOVA test was run with Bonferroni correction. One way ANOVA test revealed the significant difference between all three groups with a p value of 0.019, furthermore the % cumulative permeation of FHCN was found to be different from FN and FHN with p values of 0.036 and 0.023 respectively. In the same test no significant difference was observed between FN and FHN particles.

Furthermore the % doses absorbed at the time of 120 minutes were compared for FESSIF and FASSIF.

Tab. 3-76 Comparison of percentage absorbed of Fenofibrate, FN, FHN and FHCN in Caco-2 experiments using FESSIF and FASSIF as transport buffers (n=3)

Formulation	FASSIF [%]	FESSIF[%]	Ratio FESSIF/FASSIF
Fenofibrate	0.3±0.03	0.9±0.1	3.0
FN	2.3±0.25	4.7±0.2	2.0
FHN	2.5±0.09	4.5±0.1	1.8
FHCN	3.0±0.16	5.2±0.2	1.7

As the ratio gets closer to 1 the difference between fed and fasted state bioavailability of Fenofibrate gets lower. Thus in the case of nanoformulations FN, FHN and FHCN it might be concluded that the difference in fed and fasted state bioavailabilities will be significantly lower than that of Fenofibrate.

4. Discussion

4.1. Construction and feasibility of microjet reactor for preparation of nanoparticles

In the first part of this study two different setups of microjet reactor were evaluated in order to optimize its construction to enable the control of particle properties such as particle size and drug loading efficiency. Combination of different parameters such as flow rate, temperature, pressure, organic solvent, concentrations of substances was tested for the evaluation of these two constructions.

Results revealed that none of the parameters changed was sufficient in increasing the drug loading to more than 30% for both Gliclazide/Eudragit S100 and Danazol/HPMCP HP50 systems. There was also no clear trend in the particle size with the changed parameters which in other words makes the control on the particle size in order to be able to create the desired particle size impossible. At this point the second set-up of the microjet reactor was established. There were two major changes in the new set up. The first one is to decrease the inner diameter of the stainless steel tubings in order to observe the effect of flow rates more clearly on drug loading efficiency as well as the particles size. The second major change was to immerge the microjet reactor into the water bath for the better control of the temperature during nanoparticle production since in the first setup although the nitrogen gas was preheated, temperature decreases down to 4 °C due to evaporation of the organic solvent in the microjet reactor.

First the effect of polymer:drug ratio in combination with non-solvent/solvent ratio was evaluated. Drug loading into the polymer is highly related to the molecular solubility of the drug in the polymer. Thus, for the entrapment of relatively hydrophilic molecule Gliclazide polymer:drug ratios of 200 were required but in the case of Danazol polymer:drug ratio of 20 was enough for the efficient entrapment of the substance in HPMCP HP50 nanoparticles since the more lipophilic substance, Danazol, has a higher molecular solubility in the lipophilic matrix compared to Gliclazide. In the case of Danazol nanoparticles flow rate ratio had no effect on the drug loading efficiency but in case of Gliclazide high drug loading efficiencies were gathered using 5:1 non-solvent/solvent ratio. This is again due to the higher solubility of Gliclazide in aqueous systems, which limits the drug loading efficiency in higher solvent concentrations due to solubilization of Gliclazide in solvent and non-solvent mixture.

Secondly the effect of temperature and gas pressure on particle size and drug loading ratio was investigated. It was observed for both of the systems that an increase in temperature resulted in an increase in mean particle size. Possible explanations can be as follows:

Metastability zone plays an important role for the control of particle size in precipitation process since duration of the metastability zone is directly related to the growth of particles. Metastability zone is the point where supersaturation occurs due to the mixing of solvent and nonsolvent resulting in an unstable system where precipitation as nanoparticles occurs. In case this zone can be narrowed either by efficient mixing or lowering the solubility of the substance depending on the temperature, particle growth can be inhibited resulting in smaller particles. At low temperature the drug solubility is decreased and the metastability zone become narrow, thus, it is easily reached to high supersaturation when solution was infused into non-solvent resulting in small particles [115].

Furthermore considering the nucleation, free energy of the solution phase is greater than the sum of free energies of the nuclei thus the nucleating process is a process of free energy decrease and heat release, thus, it favors to from the high nucleation rate at low temperature. High nucleation rate is also another factor, which narrows the metastability zone resulting in smaller particles [115].

It was also found that as the temperature increased the particle size and degree of aggregation also increased, this could be attributed to the closer position of the polymer to its glass transition temperature as the temperature increased [116]. When temperature is close to the glass transition temperature of the polymer they tend to be adhesive due to the partial solubility of the polymer which increases the aggregation of nanoparticles resulting in an increase in the particle size

For Gliclazide/Eudragit S100 nanoparticles it was observed that an increase in the pressure resulted in an increase in the particle size whereas in Danazol/HPMCP HP50 system precipitation as nanoparticles did not occur due to the high rate of crystallization. Nanoprecipitation is a diffusion limited process. High pressures would decrease the diffusion rate by interacting with the formed diffusion layers resulting in the bigger nanoparticles and accordingly in some cases increased crystal growth rate. Furthermore high pressures in the gas flow may result in sudden evaporation of solvent and lead to crystallization especially in the case of Danazol/HPMCP HP50 nanoparticles due to the lower aqueous solubility of Danazol in comparison to Gliclazide.

Furthermore the effect of total solid content and solvent selection was investigated. The mechanism of nanoparticle formation can be described based on the water-solvent, water-polymer and solvent-polymer interactions. In all cases increasing the polymer concentration in the organic phase resulted

in an increase of the particle mean size. This phenomenon is also favored by the fact that increasing polymer concentration increases polymer-polymer interactions which means that more polymer chains remain associated during the diffusion process. On the other hand the influence of polymer concentration on the viscosity of the organic phase must be taken into account. At increasing polymer concentration a more viscous organic phase is obtained which provides a higher mass transfer resistance; thus, the diffusion of solvent-polymer phase into external aqueous phase is reduced and larger nanoparticles are formed [35]

Due to differences in the polymer solvent and water solvent interactions, it was supposed that the diffusion process might be altered; thus, inducing changes in the mean size. Considering that water-solvent interactions play an important role during the diffusion stranding process, the solubility parameters of the solvents were initially used to explain this tendency. It is well known that the most widely used application of solubility parameters is to predict the solubility of a substance in a solvent. In effect they express the affinity between like molecules. A first requirement of mutual solubility is that the solubility parameter of the solute (δ solute) and that of solvent (δ solvent) do not differ too much. The smaller the difference, the higher the affinity. The relationship between the mean sizes of NP produced with different solvents and the solvent-water affinity is highly dependent on the water-solvent interaction parameter which is calculated with Eq. 2-3 [35, 117].

The lower Χwater-solvent of the solvent the smaller the NP mean size. Solvents having high affinity for water which is evidenced by low Χwater-solvent values tend to promote solvent diffusion and polymer chain partition into the aqueous phase. This leads to formation of smaller nanoparticles. Moreover, using different solvents to prepare NP, it is possible to modify not only the particle mean size but also the internal mean size and also the internal and external structure of the NP (porosity and roughness). All of these NP properties lead to improve the drug loading efficiency and control of the release kinetics and eventually change the biological behaviour of nanoparticle [35, 117].

Acetone, MeOH, and THF were used for the preparation of the Gliclazide nanoparticles. These solvents have 73,98, 40,55, 81,09 as molar volumes and 19,7, 29,7, 18,5 $(Mpa)^{1/2}$ as Hildebrand solubility parameters respectively [118]. Thus Χwater-solvent parameters for acetone, MeOH, THF is calculated as 23,7, 5,48, 28,86 at 25 °C with δ water =48 $(Mpa)^{1/2}$. In this sense the nanoparticle mean particle sizes should be in the order MeOH<acetone<THF. However, results of the experiments revealed the order of the mean particle size as acetone<THF<MeOH. The results of THF and acetone are in consistency with the phenomena above although the nanoparticles prepared with MeOH showed the biggest particle size under every condition. This may be due to the fact that methanol

interacts with Eudragit S100 as a poor solvent in contrast to the other solvents that interact as good solvents. This fact was evidenced by the turbid aspect of the organic phase constituted by methanol and polymer. In a good solution polymer chains are more disentangled from one another and hence are extensively solvated. Converse in a poor solvent chains of polymer are more shrunken and their solvation is limited. Logically because solvent diffusion occurs differently for a good solvent and a poor solvent, it is highly probable that MeOH will not behave like the other solvents [35, 117].

Danazol/HPMCP HP50 nanoparticles are prepared with acetone, acetone:EtOH 50:50 (w/w %) and EtOH:water 95:5 (w/w %). Using the above equation χwater-solvent parameter for EtOH is calculated as 11.19 using the molar volume of 58.39 and Hildebrand parameter of 26.2 $(Mpa)^{1/2}$. It means that since acetones' χwater-solvent parameter is found to be 23.7 and the χwater-solvent parameter for EtOH:water will be smaller than χwater-solvent parameter for EtOH due to the addition of 5% water in the solution, the order of the mean particle size should be EtOH:water<acetone:EtOH<acetone. The experiment revealed the mean particle size in the order of acetone:EtOH<acetone<EtOH:water. The mean particles sizes are in agreement with the phenomena for acetone and acetone:EtOH but not with EtOH:water due to the low solubility of HPMCP HP50 in EtOH:water as explained above.

With the decrease in the solvent/non-solvent ratio a decrease is observed in the mean particle size. This can be explained by 3 factors:

First the number of nuclei formed on the solvent/non-solvent interface. The large number of the nuclei formed in the interface of two phases leads to aggregates and thus formation of larger nanoparticles. Simultaneously those nuclei decrease the diffusion from solvent to non-solvent which limited nanoparticles formation and decrease the yield [115].

Second the instantaneous supersaturation level of the solution due to the lower solubility of the substance in a non-solvent enriched mixture was greatly increased due to the reduction of the solvent concentration by the enhancement of the Non-Solvent/solvent ratio when the solvent and the deionized water is mixed, which leads to smaller particles.

Third the crystal growth rate (dl/dt) can be expressed by

$$\frac{dl}{dt} = Kg(Ci\text{-}C^*)^b$$

Eq. 4-1

Where Kg is the crystal growth rate constant; Ci and C* are the solute concentration at the crystal/solution interface and the saturation concentration respectively. Solute concentration at the crystal/solution interface is a function of diffusion from crystal structure to the solution. The value of the parameter b is usually between 1 and 3. Solute concentration at the crystal/solution interface is a function of diffusion from crystal structure to the solution. The increased non-solvent volume virtually decreases the solute concentration on the formed polymer crystal surface. Therefore decreased value of Ci-C* results in a lower crystal growth rate of the polymer crystal embryo, thereby resulting in smaller ultimate particle size [73].

Drug release properties of Gliclazide/Eudragit S100 and Danazol/HPMCP HP50 nanoparticles were characterized using SIF supplemented with 0.5 % Tween 20 and SIF supplemented with 1 % Tween 20 respectively and compared with drug release of powder forms of the substances in the same media. In both cases increase in the drug release rate was clearly observed where nanoparticle preparations reached 100 % within 10 minutes. Since Eudragit S100 and HPMCP HP 50 are both polymeric systems used for enteric coating, enteric resistance of nanoparticle formulations were tested using two stage dissolution studies. During the acid stage for two hours there was no remarkable drug release from both formulations whereas when the pH was increased 100 % was reached within 15 minutes for both formulations. Lack of drug release in acidic stage proves the efficiency of enteric resistance of nanoparticles and furthermore immediate drug release when the pH was increased, shows the gastric stability of nanoparticles and absence of agglomeration in acidic medium which would have adversely affected the drug release rate.

Morphology of nanoformulations was studied with DSC experiments where melting peaks of Danazol and Gliclazide were taken into consideration. Melting curves of Danazol and Gliclazide could not be observed for nanoparticle formulations indicating encapsulation of Danazol and Gliclazide in the used polymer resulting in amorphous and molecularly dissolved API.

4.2. Preparation of pH selective positively loaded nanoparticles for oral applications

HPMCP HP50 and chitosan were selected as the matrix for the preparation of positively loaded nanoparticles. Since positively charged particles are desired for the oral drug delivery applications, first the effect of ratio of HPMCP HP50 and chitosan concentrations on the particle surface properties were investigated. Due to the presence of carboxylic acid groups in the molecular structure of HPMCP HP50 and the presence of amine group in chitosan, the particles were expected to be negatively loaded until a definite chitosan concentration is reached and after this point increase in the chitosan concentration should result in positively loaded particles.

Proof of concept was shown were with the increase in chitosan concentration the negative surface charge of particles were decreasing and after the turnout point in the chitosan concentration positively loaded particles were produced. It was also observed that when the ZETA potential of the resulting particles was between -10 - +10 mV the particles tend to agglomerate due to the absence of steric stabilization where larger particle sizes were reached.

Furthermore IR analyses confirmed the interaction between the carboxylic group of HPMCP HP 50 and amino group of chitosan.

The intentions in the preparation of nanoparticles were that the nanoparticles are supposed to have a particle size of 100-200 nm and positively charged. It was shown that using HPMCP HP50 and chitosan, it is possible to prepare intended nanoparticles throughout the neutralization reactions. The most appropriate concentrations of HPMCP HP50 and chitosan were determined in respect to the above stated intentions and the structure was proven through IR analyses to show that the neutralization reaction took place between these 2 polymers. Different polymers for the steric stabilization of the nanoparticles were investigated as the next step. For this purpose PVA, PVP, HPC, Pluronic F127 and HPMC were tested. The effect of steric stabilization was investigated using ZETA potential and particle size analyses. The difference of particle sizes was investigated with Bonferroni test where particle sizes of the nanoparticles prepared with steric stabilization agents were compared with the particle size of nanoparticles without steric stabilization agent. As a result the most significant difference was recorded for Pluronic F127 which also showed ZETA potential of 14,1 for samples containing 0.5 % Pluronic F 127 and 9.1 for samples containing 1% Pluronic F127 whereas ZETA potential of Chitosan/HPMCP50 particles lacking steric stabilization agent was 28.3. The decrease in ZETA potential in concentration dependent manner demonstrated again the efficiency of Pluronic F127 in coating Chitosan/HPMC50 particles. Thus Pluronic F 127 was selected as steric stabilization

agent. Further analyses of Pluronic F127 coated nanoparticles were realised with TEM and SEM measurements. Both TEM and SEM results were in agreement with DLS measurement which indicated the particle size of 153.4 nm for nanoparticles coated in the presence of 0.5% Pluronic F127.

Drug loading studies in the developed particles were conducted using two different designs of experiments. In the first one orthogonal design was used for the optimization of flow rate, solvent type, gas pressure and temperature dependent on particle size, PDI and drug loading efficiency. The aim of this experiment was to determine the optimal conditions for highest drug loading efficiency with particles between 100-200 nm with the lowest possible PDI. The model was found to be significant and the equation resulting from the model was used for the determination of optimum parameters. The Design Expert software calculated 29 possible solutions showing optimum microjet reactor setup parameters for the production of the nanoparticles. In the first solution 8 mL/min, 8.18, 64 ºC are given for flow rate, solvent, gas pressure and temperature which will result in nanoparticles with the particle size of 200 nm, PDI of 0.2 and drug loading efficiency of 144.96 µg/mL. This solution was used for further validation experiments. Three separate preparations were conducted in order to validate the solution where the RSD % values were 2.2, 22.22 and 5.95 for particle size, PDI and drug loading efficiency respectively, showing the validity of method. Second design of experiments was conducted for the optimization of formulation contents where a D-optimal design was selected. In D-optimal design the total concentration of ingredients in the solutions used for preparation of nanoparticles were kept constant whereas ratios between the ingredients were changed to find the optimum combination of components. The evaluation was done using particle size, PDI, ZETA potential, mucoadhesiveness and drug release at pH 1.2. In this case the amounts of chitosan for mucoadhesiveness and amount of HPMCP HP50 for drug release at pH 1.2 was kept under control to be able to produce enteric coated nanoparticles with mucoadhesive properties. The model was found to be significant and used for the further calculations of optimum parameters using the equation created with the model. The requirements of the optimization was set to minimize the particle size and PDI to maximize the ZETA potential, drug loading efficiency and turbidity and finally to keep the drug release lower than 10 % in pH 1.2 HCl buffer. Resulting solution according to above stated criteria resulted in nanoparticles with a particle size of 199 nm, PDI of 0.13, ZETA potential of 6.63, drug loading efficiency of 402.81 µg/mL, turbidity of 111.71 and drug release in pH 0.1 medium 10.94%. These particles were prepared in order to assure the accuracy of the calculated parameter. Characterization of the particles revealed a particle size of 196.6 with a PDI value of 0.13 whereas ZETA potential was 6.78. Furthermore drug loading efficiency was found to be 404.92 µg/mL which is in agreement with the calculated results by the design of experiments software. Stability studies were conducted using the optimized particles. Stability studies included particle size measurements and dissolution studies during storage for 6 months at 25 °C. There was no change in the particle size as well as PDI during

six months of storage indicating that the particles were physically stable. Furthermore drug release studies revealed that drug release characteristics of Fenofibrate from the particles did not change in 6 months period.

4.3. Comparative evaluation of fenofibrate particles

Three different nanoparticle formulations were prepared to be used in the comparative evaluation of fenofibrate particles. These particles were FN (fenofibrate naked nanoparticles), FHN(fenofibrate entrapped in HPMCP HP 50) and FHCN(fenofibrate nanoparticles prepared with HPMCP HP50 and chitosan). As seen in the results from Tab. 3-64 it was possible to prepare Fenofibrate nanoparticles in different formulations with comparable particle sizes. Furthermore Fenofibrate particles did not have any surface charge and corresponding ZETA potential whereas FHN nanoparticles had a negative ZETA potential due to the presence of HPMCP HP50and FHCN nanoparticles had a positive ZETA potential due to the presence of chitosan in addition to the HPMCP HP50 which neutralizes the –COOH groups of HPMCP HP50 and furthermore charges the particles positively due to the excess amount of chitosan. Thus effect of surface properties on drug release and permeation of nanoparticles can also be evaluated using these formulations. Drug release studies were conducted with all 3 formulations in order to determine the differences in drug release characteristics. 5 different media were used for the drug release studies. These were 0.1 HCl and phosphate buffer pH 6.8 for two stage drug release studies, SIF, FASSIF and FESSIF. During the two stage dissolution in acid stage there was no remarkable difference in drug release profiles of Fenofibrate, FHN and FHCN nanoparticles. This is due to the low water solubility of Fenofibrate and due to the enteric coating on FHN and FHCN nanoparticles. But when the pH was increased to 6.8, the difference between the drug release profiles of Fenofibrate and FHN and FHCN nanoparticles was clearly observed. This is due to the fact that in acidic stage the nanoparticle formulations kept their integrity and particle properties upon the increase in the pH, the drug release were completed within 10 minutes for FHN and within 20 minutes for FHCN. The difference of the release kinetics between FHN and FHCN is due to the presence of chitosan which is only soluble at low pHs. It was observed that the drug release kinetics has two phase containing burst release as the first phase followed by a diffusion controlled release. Chitosan affects the initial burst release. 82.45 % of drug is released within 2.5 minutes from the FHN, chitosan lacking formulation whereas 68.39 % drug is released in the same time period from the FHCN, chitosan containing formulation. But in both cases drug release was significantly higher compared to the Fenofibrate. Furthermore, FN showed a higher dissolution compared to Fenofibrate but it was not as fast as the other nanoparticle formulations. This might be due to the fact that particle

size of Fenofibrate agglomerates was smaller than the Fenofibrate itself resulting in faster dissolution.

Drug release studies for Fenofibrate, FN, FHN and FHCN was done using SIF buffer supplemented with either 1 % tween 20 or 1 % SDS. SDS was used to achieve the complete dissolution of powder Fenofibrate within 2 hours, thus the drug release profiles can be more efficiently compared. It was observed that the dissolution of Fenofibrate was not complete at the end of 2 hours even in the presence of tween 20. Whereas nanoparticle formulations released the drug immediately where 100 % was reached within 20 minutes. It was again observed that initial burst was lower in the case of FHCN due to the presence of chitosan.

Further experiments were conducted in SIF buffer supplemented with 1 % SDS to ensure the 100 % dissolution of Fenofibrate within 2 hours. SDS increased significantly the solubility of Fenofibrate. In the presence of SDS dissolution of Fenofibrate reached up to 90 % within 2 hours. Furthermore when SDS used in the drug release medium the burst effects was significantly higher for the nanoparticle formulations due to the increase of the solubility of Fenofibrate and the fact that SDS increases also the dissolution of HPMCP HP50 used in the nanoparticle formulations.

Drug release studies in fed and fasted state were conducted in order to compare the drug release characteristics of the particles under the given conditions. It was observed that dissolution of Fenofibrate is complete using FESSIF as buffer in 20 minutes for nanoparticle formulations whereas Fenofibrate was dissolved only up to 70.2 % at the end of two hours in fed state. In fasted state due to the lower solubility of Fenofibrate only 43.40 % is dissolved within two hours whereas dissolution curves of nanoparticles reached up to 80 % in 30 minutes. Since in this dissolution study solubility is the rate limiting factor differences in nanoparticle formulations could be evaluated more efficiently. In previous drug release studies it was observed that drug release from FN and FHN were almost the same whereas FHCN nanoparticles released the drug slower in comparison to FN and FHN due to the presence of chitosan. But when FASSIF medium, in which solubility of Fenofibrate is limited, is used for the drug release studies drug release from FHN and FHCN particles are faster in comparison to FHCN particles. This may be due to the fact that Fenofibrate is molecularly dissolved in either HPMCP HP50 or HPMCP HP50/chitosan in a homogenous amorphous state when solubility is the limiting factor the diffusion process is easier and quicker in comparison to Fenofibrate nanoparticles alone. It was shown that there is no significant difference between the fed and fasted state drug release profiles of nanoparticle formulations indicating that there will be no differences in fed and fasted state bioavailability. Whereas there was as expected more than 2 fold difference in the case of fenofibrate.

Characterization studies were carried on using turbidity measurements in the presence of mucin solution. Increase in the turbidity was only observed for the FHCN nanoparticles as expected since these are the only nanoparticles that can get in interaction with negative mucin particles due to positive ZETA potential. Furthermore the interaction between mucin particles and FHCN was stable enough to be carried out over a period of 3 hour. These results were also controlled with ZETA potential measurements in the presence of mucin. ZETA potential of FHCN nanoparticles decreased dramatically after addition to mucin dispersion showing the interaction of mucin with these particles. Furthermore this interaction was stable throughout the period of 3 hours.

Caco-2 studies were conducted using FN, FHN and FHCN particles to determine the differences between amount absorbed when FASSIF or FESSIF was used as the transport medium. Although drug release profiles and solubility experiments with FASSIF and FESSIF did not show any significant difference when % absorbed doses are considered the values of FHCN was significantly higher compared to Fenofibrate and other formulations. This is most probably due to the positive charged particle surface which interacts the negative charged cell surface. This difference might be more obviously seen in the in-vivo experiments since mucus, which is not present in caco-2 cells, but is located on the intestinal cells in-vivo is also negatively charged which will result in the entrapment of positively charged nanoparticles in mucus.

5. Conclusion

A microjet reactor technology was developed for the preparation of pharmaceutical nanoparticles. In the development stage most critical parameters were found to be the temperature control, and the diameter of capillaries. In the first set up of the microjet reactor it was not possible to prepare nanoparticles in a controlled manner. This first setup was further developed with temperature control for solvent, non-solvent and microjet reactor itself and diameter of the capillaries was reduced. These changes resulted in a system which allows efficient control of particle properties such as particle size, PDI and drug loading efficiency.

Further parameters that might have an influence in the nanoparticle preparation process were tested using two model systems Danazol/HPMCP HP50 and Gliclazide/Eudragit S100 nanoparticles. Effects of flow rate, temperature, pressure, total solid concentration and type of solvent were tested on the particle size, PDI and drug loading efficiency to be able to determine the critical parameters to be used in design of experiments for the further optimization of the system. Functionality of these particles were tested with drug release studies where drug release profiles were investigated using pH 6.8 buffer and 2 stage dissolution were no significant drug release was observed in the acid stage and with the increase of the pH 100 % drug release was reached within minutes. Furthermore DSC measurements were conducted to ensure the molecular dispersion of the API in the polymer where for both of the model systems melting peak of the API was not observed in the nanoparticle samples. After determination of flow rate, temperature, pressure and solvent type as the most critical factors for the preparation of the pharmaceutical nanoparticles, a novel oral delivery system was developed using a microjet reactor.

The aim of the oral delivery system was development of pH controlled positively charged nanoparticles which show resistance to gastric conditions releasing the drug first in intestines and has an affinity to intestinal mucus due to negative charge of the mucus. For this purpose HPMCP HP50 and chitosan were used as polymers and Fenofibrate was used as the model API. First optimum ratio was determined for the preparation of HPMCP HP50/Chitosan nanoparticles to obtain positively charged stable nanoparticles and afterwards steric stabilization was ensured using a third polymer Pluronic F127. Fenofibrate containing HPMCP HP50/Chitosan nanoparticles were optimized using two different design of experiments. The rotatable orthogonal design was used for the optimization of microjet reactor parameters such as flow rate, temperature, pressure and solvent. In the second design which

was a D-optimal design formulation ingredients were optimized for the optimum particle size, PDI, drug loading efficiency and drug release properties at pH 1.2 HCl medium.

The advantages of this novel drug delivery system were shown in vitro in comparison to naked Fenofibrate nanoparticles and Fenofibrate/HPMCP HP50 nanoparticles. Drug release profiles were higher in case FHN and FHCN in comparison to FN where Fenofibrate is in crystalline state. Furthermore FHCN was the only nanoparticle formulation with mucus affinity. In Caco-2 trials FHCN showed significantly better performance in comparison to other nanoparticle formulations.

In conclusion a continuous production system using microjet reactor which is based on nanoprecipitation was developed for the preparation of pharmaceutical nanoparticles where efficient control of particle properties was possible. Using this method a novel oral drug delivery system was developed which showed superior characteristics in-vitro to the conventional nanoparticles.

6. Abstract

Production of nanoparticles for drug delivery requires simple and efficient methods yielding narrow size distributions within specified limits. In this study a novel method MicroJet reactor technology was developed to enable the custom preparation of nanoparticles. Another objective of the study was to prepare gastroresistant nanoparticles using hydroxypropyl methyl cellulose phthalate (HPMCP 50) and low molecular weight chitosan as matrix for the oral application of fenofibrate as model drug.

Danazol/HPMCP HP50 and Gliclazide/Eudragit S100 nanoparticles were used as model systems for the investigation of effects of process parameters and microjet reactor setup on the nanoparticle properties during the microjet reactor construction. Capillary diameter, microjet reactor nozzle size were investigated as microjet reactor parameters and flow rate and flow rate ratios, solvent type, temperature and pressure was investigated as process parameters. Following the feasibility study of the microjet reactor system, three different nanoparticle formulations were prepared using fenofibrate as model drug. Fenofibrate nanoparticles stabilized with poloxamer 407 (FN), fenofibrate nanoparticles in hydroxypropyl methyl cellulose phthalate (HPMCP) matrix (FHN) and fenofibrate nanoparticles in HPMCP and chitosan matrix (FHCN) were prepared under controlled precipitation using MicroJet reactor technology. Particle sizes of all the nanoparticle formulations were adjusted to 200-250 nm with the variations in production parameters such as flow rate, temperature and pressure. All nanoparticle formulations were characterized for particle size, drug loading efficiency, drug release, in-vitro mucoadhesiveness and Caco-2 permeation.

The right combination of construction parameters such as capillary diameter and the nozzle size allowed the effect of process parameters to be pronounced significantly in the case of Danazol/HPMCP HP50 and Gliclazide/Eudragit S100 nanoparticles. The changes in the experimental parameters altered the system thermodynamics resulting in the production of nanoparticles between 20-1000 nm (PDI<0.2) with high drug loading efficiencies (96.5% in 20:1 polymer:drug ratio) without need for using surfactant or toxic organic solvents.

Drug releases from all nanoparticle formulations were fast and complete after 15 minutes both in FaSSIF and FeSSIF medium whereas in mucodhesiveness tests, only FHCN formulation was found to be mucoadhesive. Results of the Caco-2 studies revealed that % dose absorbed values were significantly higher ($p<0.01$) for FHCN in both cases where FaSSIF and FeSSIF were used as transport buffer. Although no significant difference was observed in the drug release profiles, positively charged and mucoadhesive FHCN nanoparticles increased the absorption of fenofibrate more than other formulations.

7. Zusammenfassung

Die Produktion von Nanopartikeln für den gerichteten Wirkstofftransport erfordert einfache und effiziente Methoden, die in einer engen Partikelgrößenverteilung in vorgegebenen Grenzwerten münden. In der vorliegenden Arbeit wurde eine neuartige Methode entwickelt - die Mikrojetreaktor-Technologie - um die spezifische Herstellung von Nanopartikeln zu ermöglichen.

Ein weiteres Ziel der Arbeit war die Herstellung magensaftresistenter Nanopartikel der Modellsubstanz Fenofibrat zur oralen Applikation unter Verwendung von Hydroxypropyl-Methylcellulosephthalat (HPMCP 50) und niedermolekularem Chitosan als Matrixsubstanzen.

Danzol/HPMCP HP50 und Gliclazid/Eudragit S100 Nanopartikel wurden als Modellsysteme für die Untersuchung des Einflusses der verschiedenen Prozess- und konstruktionsbedingten Parameter am Mikrojetreaktor auf die Eigenschaften der Nanopartikel genutzt. Dabei wurden als konstruktionsbedingte Parameter am Mikrojetreaktor Kapillardurchmesser und Düsenweite untersucht, während sich die Untersuchung der Prozessparameter auf die Größen Flussrate, Flussratenverhältnis, Art des Lösungsmittels, Temperatur und Druck erstreckte.

Nach Abschluss einer initialen Machbarkeitsstudie am Mikrojetreaktorsystem wurden drei verschiedene Nanopartikelformulierungen unter Verwendung des Modellwirkstoffes Fenofibrat durch kontrollierte Fällung im Mikrojetreaktor hergestellt. Dies waren Fenofibrat Nanopartikel, stabilisiert mit Poloxamer 407 (FN), Fenofibrat Nanopartikel in einer Hydroxypropylmethylcellulosephthalat (HPMCP) Matrix (FHN) und Fenofibrat Nanopartikel in einer HPMCP/Chitosan Matrix (FHCN). Bei allen Formulierungen konnte die Partikelgröße durch die Variation einzelner Prozessparameter wie Flussrate, Temperatur und Druck auf 200-250 nm eingestellt werden. Alle Nanopartikelformulierungen wurden durch die Ermittlung der Partikelgröße, der Effizienz der Wirkstoffbeladung, der Wirkstofffreisetzung, einem in-vitro Mucoadhäsionstest sowie einem Caco-2 Permeationstest charakterisiert. Die richtige Kombination der konstruktionsbedingten Parameter am Mikrojetreaktor wie Kapillarduchmesser und Düsenweite zeigten im Falle der Danazol/HPMCP HP50 und Gliclazid/Eudragit S100 Nanopartikel einen signifikanten Einfluss bezüglich der Prozessparameter-Effekte.

Variationen der experimentellen Parameter resultierten in thermodynamischen Änderungen des Systems, welche die Herstellung von Nanopartikeln zwischen 20-1000nm (PDI <0,2) mit hohen Wirkstoffbeladungen (96,5% bei einem Polymer:Wirkstoff Verhältnis von 20:1) ohne die Verwendung von grenzflächenaktiven Substanzen oder toxischen organischen Lösungsmitteln erlaubten.

Fenofibrat Formulierungen zeichneten sich durch eine schnelle und vollständige Wirkstofffreisetzung in FaSSIF und FeSSIF Medien innerhalb von 15 Minuten aus. Die Mucoadhäsionstests ergaben nur für die FHCN Formulierung eine Mucoadhäsion. Die Caco-2 Studien zeigten sowohl bei der Nutzung von FaSSIF als auch FeSSIF Medien als Transportpuffersystem für FHCN signifikant höhere ($p<0,01$) pro-

zentuale Absorptionswerte. Obwohl in den Wirkstofffreisetzungsprofilen kein signifikanter Unterschied beobachtet werden konnte, erhöhten positiv geladene und mucoadhäsive FHCN Nanopartikel die Absorption von Fenofibrat stärker als die übrigen Formulierungen.

8. References

[1] C.A. Lipinski, Drug-like properties and the causes of poor solubility and poor permeability, Journal of pharmacological and toxicological methods, 44 (2000) 235-249.
[2] E.M. Merisko-Liversidge, G.G. Liversidge, Drug nanoparticles: formulating poorly water-soluble compounds, Toxicological Pathology, 36 (2008) 43-48.
[3] R.H. Müller, K. Peters, Nanosuspensions for the formulation of poorly soluble drugs I. Preparation by a size-reduction technique, International Journal of Pharmaceutics, 160 (1998) 229-237.
[4] X. Chen, J.M. Vaughn, M.J. Yacaman, R.O. Williams, 3rd, K.P. Johnston, Rapid dissolution of high-potency danazol particles produced by evaporative precipitation into aqueous solution, Journal of Pharmaceutical Sciences, 93 (2004) 1867-1878.
[5] E. Merisko-Liversidge, G.G. Merisko-Liversidge, Drug Nanoparticles: Formulating Poorly Water-Soluble Compounds, Toxicological Pathology 36 (2008) 43-48.
[6] G. Lövestam, H. Rauscher, G. Roebben, B.S. Klüttgen, N. Gibson, J. Putaud, H. Stamm, Considerations on a Definition of Nanomaterial for Regulatory Purposes, in: JRC Reference Reports, 2010, pp. 13.
[7] R. Bawa, Nanoparticle-based therapeutics in Humans: A survey, Nanotechnology Law&Bussiness 5(2008) 135-155.
[8] B.H. Bohm, R.H. Muller, Lab-scale production unit design for nanosuspensions of sparingly soluble cytotoxic drugs, Pharmaceutical Science & Technology Today, 2 (1999) 336-339.
[9] G.K. Bolhuis, K. Zuurman, G.H.P. te Wierik, Improvement of dissolution of poorly soluble drugs by solid deposition on a super disintegrant. II. The choice of super disintegrants and effect of granulation, European Journal of Pharmaceutical Sciences, 5 (1997) 63–69.
[10] J. Breitenbach, Melt extrusion: from process to drug delivery technology, European Journal of Pharmaceutics and Biopharmaceutics, 54 (2002) 107-117.
[11] L. Castro, Method of preparing stable drug nanoparticles, in, Nanosystems LLC, USA, 1996.
[12] Q. Chen, A.J. Rondinone, B.C. Chakoumakos, Z.J. John Zhang, Synthesis of superparamagnetic MgFe2O4 nanoparticles by coprecipitation, Journal of Magnetism and Magnetic Materials, 194 (1999) 1-7.
[13] M.J.A. Fernandez, P.C. Salve, C. Remunan-Lopez, J.L.V. Jato, Application of nanoparticles based on hydrophilic polymers as pharmaceutical forms, in, Universidade de Santiago de Compostela, USA, 2003.
[14] C. Fonseca, S. Simoes, R. Gaspar, Paclitaxel-loaded PLGA nanoparticles: preparation, physicochemical characterization and in vitro anti-tumoral activity, Journal of Controlled Release, 83 (2002) 273-286.
[15] K. Itoh, A. Pongpeerapat, Y. Tozuka, T. Oguchi, K. Yamamoto, Nanoparticle formation of poorly water-soluble drugs from ternary ground mixtures with PVP and SDS, Chemical & Pharmaceutical Bulletin, 51 (2003) 171-174.
[16] C. Jacobs, O. Kayser, R.H. Muller, Production and characterisation of mucoadhesive nanosuspensions for the formulation of bupravaquone, International Journal of Pharmaceutics, 214 (2001) 3-7.
[17] O.V. Kozyuk, Device and method for creating hydrodynamic cavitation in fluids, in, Five Star Technologies Inc., USA, 2007.
[18] G.G. Liversidge, C.K. Cundy, J.F. Bishop, D.A. Czekai, Surface modified drug nanoparticles, in, Sterling Drug Inc., USA, 1992.
[19] M.E. Matteucci, M.A. Hotze, K.P. Johnston, R.O. Williams, 3rd, Drug nanoparticles by antisolvent precipitation: mixing energy versus surfactant stabilization, Langmuir, 22 (2006) 8951-8959.

[20] R.H. Muller, K. Mader, S. Gohla, Solid lipid nanoparticles (SLN) for controlled drug delivery - a review of the state of the art, European Journal of Pharmaceutics and Biopharmaceutics, 50 (2000) 161-177.
[21] V. Rosenberger, N. Moldavski, M. Flasher-barak, I.E. Lerner, Nanoparticles for drug delivery, in, TEVA Pharmaceutical industries Ltd., IL, 2005.
[22] P.T. Vladimir, Nanoparticles as drug carriers, in, Imperial College Press, 2006.
[23] B.E. Rabinow, Nanosuspension in drug delivery, Nature Reviews, 3 (2004) 788-796
[24] W.H.D. Jong, P.J.A. Borm, Drug delivery and nanoparticles: Applications and hazards, International Jouornal of Nanomedicine, 3 (2008) 133-149.
[25] W. Ostwald, Studien uber die bildung und Umwandlung fester Korper, J Phys Chem B, 22 (1897) 289.
[26] M. Gaumet, A. Vargas, R. Gurny, F. Delie, Nanoparticles for drug delivery: the need for precision in reporting particle size parameters, European Journal of Pharmaceutics and Biopharmaceutics, 69 (2008) 1-9.
[27] T. Banerjee, S. Mitra, A.K. Singh, R.K. Shamara, A. Maitra, Preparation, characterization and biodistribution of ultrafine chitosan nanoparticles, International Journal of Pharmaceutics, 243 (2002).
[28] S.M. Moghimi, A.C. Hunter, J.C. Murray, Long-circulating and target-specific nanoparticles: theory to practice, Pharmacological Reviews, 53 (2001) 283-318.
[29] G. Strom, S.O. Belliot, T. Daemen, D.D. Lasic, Surface modification of nanoparticles to oppose uptake by the monoluclear phagocyte system, Advanced Drug Delivery Reviews, 17 (1995).
[30] K.S. Soppimath, T.M. Aminabhavi, A.R. Kulkarni, W.E. Rudzinski, Biodegradable polymeric nanoparticles as drug delivery devices, Journal of Controlled Release, 70 (2001) 1-20.
[31] J. Zhang, L. Wu, H.K. Chan, W. Watanabe, Formation, characterization and fate of inhaled drug nanoparticles, Advanced Drug Delivery Reviews, (2011) 441-455.
[32] C.L. De Castro, B.S. Mitchell, Chapter 1: Nanoparticles from Mechanical Attrition, American Scientific Publishers, 2002.
[33] R.H. Müller, C. Jacobs, O. Kayser, Nanosuspensions as particulate drug formulations in therapy Rationale for development and what we can expect for the future, Advanced Drug Delivery Reviews, 47 (2001) 3-19.
[34] G. Barrat, G. Courraze, C. Couvreur, E. Fattal, R. Gref, D. Labarre, P. Legrand, G. Ponchel, C. Vauthier, Polymeric Micro- and Nanoparticles as drug Carriers, 2 ed., 2000.
[35] S. Galindo-Rodriguez, E. Allemann, H. Fessi, E. Doelker, Physicochemical parameters associated with nanoparticle formation in the salting out, emulsification diffusion and nanoprecipitation methods, Pharmaceutical Research, 21 (2004).
[36] J. Hecq, M. Deleers, D. Fanara, H. Vranckx, K. Amighi, Preparation and characterization of nanocrystals for solubility and dissolution rate enhancement of nifedipine, International Journal of Pharmaceutics, 299 (2005) 167-177.
[37] L. Mu, S.S. Feng, PLGA/TPGS nanoparticles for controlled release of paclitaxel: effects of the emulsifier and drug loading ratio, Pharmaceutical Research, 20 (2003) 1864-1872.
[38] B. Seijo, E. Fattal, L. Roblot-Treupel, P. Couvreur, Design of nanoparticles of less than 50 nm diameter: preparation, characterization and drug loading, International Journal of Pharmaceutics, (1990) 1-7.
[39] G.G. Liversidge, P. Conzentino, Drug particle size reduction for decreasing gastric irritancy and enhancing absorption of naproxen in rats, International Journal of Pharmaceutics, 125 (1995) 309-313.
[40] M.F. Zambaux, F. Bonneaux, R. Gref, P. Maincent, E. Dellacherie, M.J. Alonso, P. Labrude, C. Vigneron, Influence of experimental parameters on the characteristics of poly(lactic acid) nanoparticles prepared by a double emulsion method, Journal of Controlled Release, 50 (1998) 31-40.
[41] R. Fernandez-Urrusuno, P. Calvo, R.-L. C., J.L. Vila-Jato, M.J. Alonso, Enhancement of nasal absortion of insulin using chitosan nanoparticles, Pharmaceutical Research, 16 (1999) 1576-1581.

[42] W. Tiyaboonchai, J. Woiszwillo, C.R. Middaugh, Formulation and characterization of amphotericin B-polyethylenimine-dextran sulfate nanoparticles, Journal of Pharmaceutical Sciences, 90 (2001) 902-914.
[43] P.D. Scholes, A.G.A. Coombesa, L. Illurn, S.S. Davisa, M. Vertb, M.C. Daviesa, The preparation of sub-200 nm poly (lactide-co-glycolide) microspheres for site-specific drug delivery, Journal of Controlled Release, 25 (1993) 145-153.
[44] G.G. Liversidge, C.C. Kenneth, Particle size reduction for improvement of oral bioavailability of hydrophobic drugs: I. Absolute oral bioavailability of nanocrystalline danazol in beagle dogs, International Journal of Pharmaceutics, 125 (1995) 91-97.
[45] C. Jacobs, O. Kayser, R.H. Müller, Nanosuspensions as a new approach for the formulation for the poorly soluble drug tarazepide, International Journal of Pharmaceutics, 196 (2000) 161-164.
[46] K. Ciftci, K. Süheyla, A.A. Hincal, T.M. Ercan, In vitro and in vivo evaluation of PLAGA (50/50) microspheres containing 5-fluorouracil prepared by a solvent evaporation method, International Journal of Pharmaceutics, 131 (1996) 73-82.
[47] P. York, Strategies for particle design using supercritical fluid technologies, PSTT, 2 (1999) 430-440.
[48] T.L. Rogers, A.C. Nelsen, M. Sarkari, T.J. Young, K.P. Johnston, R.O. Williams, 3rd, Enhanced aqueous dissolution of a poorly water soluble drug by novel particle engineering technology: spray-freezing into liquid with atmospheric freeze-drying, Pharmaceutical Research, 20 (2003) 485-493.
[49] R. Falka, T.W. Randolpha, J.D. Meyerb, M.R. Kellyb, Controlled release of ionic compounds from poly (L-lactide) microspheres produced by precipitation with a compressed antisolvent, Journal of Controlled Release, 44 (1997) 77-85.
[50] S. Yeob, E. Kirana, Formation of polymer particles with supercritical fluids: A review, Journal of Supercritical Fluids, 34 (2005) 287–308.
[51] K. Gong, R. Viboonkiat, I.U. Rehman, G. Buckton, J.A. Darr, Formation and characterization of porous indomethacin-PVP coprecipitates prepared using solvent-free supercritical fluid processing, Journal of Pharmaceutical Sciences, 94 (2005) 2583-2590.
[52] H. Fessi, J.P. Devissaguet, F. Puisieux, C. Thies, Process for the preparation of dispersible colloidal systems of a substance in the form of nanoparticles, in, USA, 1992.
[53] H. Fessi, F. Puisieux, J.P. Devissaguet, N. Ammoury, S. Benita, Nanocapsule formation by interfacial polymer deposition following solvent displacement, International Journal of Pharmaceutics, 55 (1989).
[54] U. Bilati, E. Allemann, E. Doelker, Development of a nanoprecipitation method intended for the entrapment of hydrophilic drugs into nanoparticles, European Journal of Pharmaceutical Sciences, 24 (2005) 67-75.
[55] S. Hornig, T. Heinze, C.R. Becer, U.S. Schubert, Synthetic polymeric nanoparticles by nanoprecipitation, Journal of Materials of Chemistry 19 (2009) 3838-3840.
[56] X. Chen, T.J. Young, M. Sarkari, R.O. Williams, 3rd, K.P. Johnston, Preparation of cyclosporine A nanoparticles by evaporative precipitation into aqueous solution, International Journal of Pharmaceutics, 242 (2002) 3-14.
[57] T. Govender, T. Riley, T. Ehtezazi, M.C. Garnett, S. Stolnik, L. Illum, S.S. Davis, Defining the drug incorporation properties of PLA-PEG nanoparticles, International Journal of Pharmaceutics, 199 (2000) 95-110.
[58] T. Govender, S. Stolnik, M.C. Garnett, L. Illum, S.S. Davis, PLGA nanoparticles prepared by nanoprecipitation: drug loading and release studies of a water soluble drug, Journal of Controlled Release, 57 (1999) 171-185.
[59] N. Rasenack, B.W. Muller, Dissolution rate enhancement by in situ micronization of poorly water-soluble drugs, Pharmaceutical Research, 19 (2002) 1894-1900.
[60] B.K. Johnson, R.K. Prud`homme, Flash Nanoprecipitation of Organic Actives and Block Copolymers using a Confined Impinging Jet Mixer, Australian Journal of Chemistry, (2003) 1021-1024.

[61] A.D. McNaught, Wilkinson. A, Compendium of Chemical Terminology, 2nd ed. (the "Gold Book"), Blackwell Scientific Publications, Oxforfd, 1997.
[62] H. Xie, Smith J.W., Fabrication of PLGA nanoparticles with a fluidic nanoprecipitation system, Journal of Nanobiotechnology (2010) 8-18.
[63] C.V. Sterling, L.E. Scriven, Interfacial Turbulence: Hydrodynamic instability and marangoni effect, AIChE Journal, (1959) 514-523.
[64] B.Y. Shekunov, P. Chattopadhyay, H.H.Y. Tong, H.L.C. Albert, Particle Size Analysis in Pharmaceutics: Principles, Methods and Applications, Pharmaceutical Research 24 (2006) 203-227.
[65] J. Holoubek, Some applications of light scattering in materials science, Journal of Quantitative Spectroscopy and Radiative Transfer, 106 (2007) 104-121.
[66] C.X. Zhao, L. He, S.Z. Qiao, A.P.J. Middelberg, Nanoparticle synthesis in microreactors, Chemical Engineering Science, 66 (2011) 1463-1479.
[67] L. Hung, A.P. Lee., Microfluidic Devices for the Synthesis of Nanoparticles and Biomaterials Journal of Medical and Biological Engineering, 27 (2007) 1-6.
[68] Y.J. Song, J. Hormes, C. Kumar, Microfluidic synthesis of nanomaterials, Small, 4 (2008) 698-711.
[69] K.B. Johnson, R.K. Prud'homme, Chemical processing and micromixing in confined impinging jets, AlChE Journal, 49 (2003) 2264-2282.
[70] S.W. Siddiqui, Y. Zhao, A. Kukukova, Kresta S. M., Characteristics of a Confined Impinging Jet Reactor: Energy Dissipation, Homogeneous and Heterogeneous Reaction Products, and Effect of Unequal Flow, Industrial & Engineering Chemistry Research 29 (2009) 7945-7958.
[71] F. Schwertfirm, J. Gradl, H. Schwarzer, W. Peukert, M. Manhart, The low Reynolds number turbulent flow and mixing in a confined impinging jet reactor, International Journal of Hear and Fluid Flow 28 (2008) 1429-1442.
[72] E. Schaer, P. Guichardon, L. Falk, E. Plasari, Determination of local energy dissipation rates in impinging jets by a chemical reaction method, Chemical Engineering Journal, 72 (1999) 125-138.
[73] H. Zhao, J. Wang, A.Q. Wang, J. Chen, J. Yun, Controlled liquid antisolvent precipitation of hyrophobic pharmaceutical nanoparticles in a microchannel reactor, Industrial & Engineering Chemistry Research 46 (2007).
[74] X.Q. Wang, J.D. Dai, Z. Chen, T. Zhang, G.M. Xia, T. Nagai, Q. Zhang, Bioavailability and pharmacokinetics of cyclosporine A-loaded pH-sensitive nanoparticles for oral administration, Journal of Controlled Release, 97 (2004) 421-429.
[75] P.S. Wong, L. Dong, R. Zhao, C. Pollock-dove, Controlled release nanoparticle active agent formulation dosage forms and methods, in, ALZA Cooperation, USA, 2006.
[76] H. Murakami, M. Kobayashi, H. Takeuchi, Y. Kawashima, Utilization of poly(DL-lactide-co-glycolide) nanoparticles for preparation of mini-depot tablets by direct compression, Journal of Controlled Release, 67 (2000) 29-36.
[77] M. Tobio, A. Sanchez, A. Vila, I.I. Soriano, C. Evora, J.L. Vila-Jato, M.J. Alonso, The role of PEG on the stability in digestive fluids and in vivo fate of PEG-PLA nanoparticles following oral administration, Colloids and Surfaces, 18 (2000) 315-323.
[78] J.M. Barichello, M. Morishita, K. Takayama, T. Nagai, Encapsulation of hydrophilic and lipophilic drugs in PLGA nanoparticles by the nanoprecipitation method, Drug Development and Industrial Pharmacy, 25 (1999) 471-476.
[79] P. Arbos, M.A. Campanero, M.A. Arangoa, M.J. Renedo, J.M. Irache, Influence of the surface characteristics of PVM/MA nanoparticles on their bioadhesive properties, Journal of Controlled Release, 89 (2003) 19-30.
[80] P. Arbos, M.A. Campanero, M.A. Arangoa, J.M. Irache, Nanoparticles with specific bioadhesive properties to circumvent the pre-systemic degradation of fluorinated pyrimidines, Journal of Controlled Release, 96 (2004) 55-65.
[81] P. Jani, G.W. Halbert, J. Langridge, A.T. Florence, Nanoparticle uptake by the rat gastrointestinal mucosa: quantitation and particle size dependency, The Journal of Pharmacy and Pharmacology, 42 (1990) 821-826.

[82] S.F. Chang, H.Y. Chang, Y.C. Tong, S.H. Chen, F.C. Hsaio, S.C. Lu, J. Liaw, Nonionic polymeric micelles for oral gene delivery in vivo, Human Gene Therapy, 15 (2004) 481-493.
[83] T. Jung, W. Kamm, A. Breitenbach, E. Kaiserling, J.X. Xiao, T. Kissel, Biodegradable nanoparticles for oral delivery of peptides: is there a role for polymers to affect mucosal uptake?, European Journal of Pharmaceutics and Biopharmaceutics, 50 (2000) 147-160.
[84] S. Pamujula, R.A. Graves, T. Freeman, V. Srinivasan, L.A. Bostanian, V. Kishore, T.K. Mandal, Oral delivery of spray dried PLGA/amifostine nanoparticles, The Journal of Pharmacy and Pharmacology, 56 (2004) 1119-1125.
[85] S.Y. Kim, H.J. Doh, M.H. Jang, Y.J. Ha, S.I. Chung, H.J. Park, Oral immunization with Helicobacter pylori-loaded poly(D, L-lactide-co-glycolide) nanoparticles, Helicobacter, 4 (1999) 33-39.
[86] J. Chen, W.L. Yang, G. Li, J. Qian, J.L. Xue, S.K. Fu, D.R. Lu, Transfection of mEpo gene to intestinal epithelium in vivo mediated by oral delivery of chitosan-DNA nanoparticles, World Journal of Gastroenterology, 10 (2004) 112-116.
[87] A. Sharma, S. Sharma, G.K. Khuller, Lectin-functionalized poly (lactide-co-glycolide) nanoparticles as oral/aerosolized antitubercular drug carriers for treatment of tuberculosis, The Journal of Antimicrobial Chemotherapy, 54 (2004) 761-766.
[88] S. Sakuma, M. Hayashi, M. Akashi, Design of nanoparticles composed of graft copolymers for oral peptide delivery, Advanced Drug Delivery Reviews, 47 (2001) 21-37.
[89] S. Sakuma, R. Sudo, N. Suzuki, H. Kikuchi, M. Akashi, Y. Ishida, M. Hayashi, Behavior of mucoadhesive nanoparticles having hydrophilic polymeric chains in the intestine, Journal of Controlled Release, 81 (2002) 281-290.
[90] S. Sakuma, N. Suzuki, R. Sudo, K. Hiwatari, A. Kishida, M. Akashi, Optimized chemical structure of nanoparticles as carriers for oral delivery of salmon calcitonin, International Journal of Pharmaceutics, 239 (2002) 185-195.
[91] H. Sang Yoo, T. Gwan Park, Biodegradable nanoparticles containing protein-fatty acid complexes for oral delivery of salmon calcitonin, Journal of Pharmaceutical Sciences, 93 (2004) 488-495.
[92] Y. Jiao, N. Ubrich, M. Marchand-Arvier, C. Vigneron, M. Hoffman, T. Lecompte, P. Maincent, In vitro and in vivo evaluation of oral heparin-loaded polymeric nanoparticles in rabbits, Circulation, 105 (2002) 230-235.
[93] J. Dai, T. Nagai, X. Wang, T. Zhang, M. Meng, Q. Zhang, pH-sensitive nanoparticles for improving the oral bioavailability of cyclosporine A, International Journal of Pharmaceutics, 280 (2004) 229-240.
[94] M.H. El-Shabouri, Positively charged nanoparticles for improving the oral bioavailability of cyclosporin-A, International Journal of Pharmaceutics, 249 (2002) 101-108.
[95] J. Molpeceres, M.R. Aberturas, M. Guzman, Biodegradable nanoparticles as a delivery system for cyclosporine: preparation and characterization, Journal of Microencapsulation, 17 (2000) 599-614.
[96] N. Ubrich, C. Schmidt, R. Bodmeier, M. Hoffman, P. Maincent, Oral evaluation in rabbits of cyclosporin-loaded Eudragit RS or RL nanoparticles, International Journal of Pharmaceutics, 288 (2005) 169-175.
[97] A. Lamprecht, N. Ubrich, H. Yamamoto, U. Schafer, H. Takeuchi, P. Maincent, Y. Kawashima, C.M. Lehr, Biodegradable nanoparticles for targeted drug delivery in treatment of inflammatory bowel disease, The Journal of Pharmacology and Experimental Therapeutics, 299 (2001) 775-781.
[98] A. Lamprecht, U. Schafer, C.M. Lehr, Size-dependent bioadhesion of micro- and nanoparticulate carriers to the inflamed colonic mucosa, Pharmaceutical Research, 18 (2001) 788-793.
[99] W.K. Lee, J.Y. Park, E.H. Yang, H. Suh, S.H. Kim, D.S. Chung, K. Choi, C.W. Yang, J.S. Park, Investigation of the factors influencing the release rates of cyclosporin A-loaded micro- and nanoparticles prepared by high-pressure homogenizer, Journal of Controlled Release, 84 (2002) 115-123.
[100] L. Eriksson, E. Johansson, N. Kettaneh-Wold, C. WikstrÄom, S. Wold, Design of Experiments: Principles and Applications, Umetrics Academy, 2000.
[101] D.C. Montgomery, Design and Analysis of Experiments, 3 ed., John Wiley & Sons, INC.,, USA, 1991.

[102] C.F.J. Wu, M. Hamada, Design of Experiments: Planing, Analysis and Parameter Design Optimization, John Wiley & Sons, INC., USA, 2000.
[103] NIST, SEMATECH e-Handbook of Statistical Methods, http://www.itl.nist.gov/div898/handbook/, in, 2012.
[104] B. Penth, Kontinuierliche fällung von nanoskaligen produkten in mikroreaktoren, in, Penth, B., Germany, 2006.
[105] D. Hörter, J.B. Dressman, Influence of physicochemical properties on dissolution of drugs in the gastrointestinal tract, Advanced Drug Delivery Reviews, 46 (2001) 75-87.
[106] J. Hu, K.P. Johnston, R.O. Williams Iii, Rapid dissolving high potency danazol powders produced by spray freezing into liquid process, International Journal of Pharmaceutics, 271 (2004) 145-154.
[107] N. Seedher, M. Kanojia, Reversible Binding of Antidiabetic Drugs, Repaglinide and Gliclazide, with Human Serum Albumin, Chemical Biology & Drug Design, 72 (2008) 290-296.
[108] K.A. Alkhamis, H. Allaboun, W.a.Y. Al-Momani, Study of the solubilization of gliclazide by aqueous micellar solutions, Journal of Pharmaceutical Sciences, 92 (2003) 839-846.
[109] S.S. Hong, S.H. Lee, Y.J. Lee, S.J. Chung, M.H. Lee, C.K. Shim, Accelerated oral absorption of gliclazide in human subjects from a soft gelatin capsule containing a PEG 400 suspension of gliclazide, Journal of Controlled Release, 51 (1998) 185-192.
[110] M. Vialpando, F. Backhuijs, J.A. Martens, G. Van den Mooter, Risk assessment of premature drug release during wet granulation of ordered mesoporous silica loaded with poorly soluble compounds itraconazole, fenofibrate, naproxen, and ibuprofen, European Journal of Pharmaceutics and Biopharmaceutics, 81 (2012) 190-198.
[111] G.E. Granero, C. Ramachandran, G.L. Amidon, Dissolution and Solubility Behavior of Fenofibrate in Sodium Lauryl Sulfate Solutions, Drug Development and Industrial Pharmacy, 31 (2005) 917-922.
[112] R.C. Rowe, P.J. Sheskey, P.J. Weller, Handbook of Pharmaceutical Excipients, in, Pharmaceutical Press, 2003.
[113] K. Yoncheva, J. Vandervoort, A. Ludwig, Development of mucoadhesive poly(lactide-co-glycolide) nanoparticles for ocular application, Pharmaceutical Development and Technology, 16 (2009) 29-35.
[114] H. Takeuchi, J. Thongborisute, Y. Matsui, H. Sugihara, H. Yamamoto, Y. Kawashima, Novel mucoadhesion tests for polymers and polymer-coated particles to design optimal mucoadhesive drug delivery systems, Advanced Drug Delivery Reviews, 57 (2005) 1583-1594.
[115] J.Y. Zhang, Z.G. Shen, J. Zhong, T.T. Hu, J.F. Chen, Z.Q. Ma, J. Yun, Preparation of amorphous cefuroxime axetil nanoparticles by controlled nanoprecipitation method without surfactants, International Journal of Pharmaceutics, 323 (2006) 153-160.
[116] M. Charoenchaitrakool, C. Polchiangdee, P. Srinophakun, Production of theophylline and polyethylene glycol 4000 composites using gas anti solvent process, Materials Letters, (2009).
[117] U. Bilati, E. Allemann, E. Doelker, Development of a nanoprecipitation method intended for the entrapment of hydrophilic drugs into nanopartilces, European Journal of Pharmaceutical Sciences, 24 (2005).
[118] A.F.M. Barton, Handbook of Solubility Parameters and Other Cohesion Parameters, CRC Press, 1983.

Poster/Oral presentations

- TÜRELI A. E.; Baumstümmler, E. M.Prinz. Sicherung der Qualitat durch das MJR- Verfahren and MJR Technologie zur Herstellung & Entwicklung von Nano & Mikropartikel, Nano-Additive Aktuelle und zukünftige Anwendungen, Berlin (2012)
- TÜRELI A. E.; B. BAUMSTUEMMLER; LANGGUTH P., Characterization of Fenofibrate nanoparticles for oral drug delivery. International Symposium on drug research and development, Antalya (2011)
- TÜRELI A. E.; B. BAUMSTUEMMLER; LANGGUTH P. Enteric coated mucoadhesive nanoparticles for oral drug delivery, 3rd PharmSciFair (2011)
- TÜRELI A. E.; TAUSCH L.; LANGGUTH P.; Polymeric Fenofibrate nanoparticles for oral drug delivery. *8th International congress and workshop biological barriers, Saarbrücken*, (2010)
- TÜRELI A. E.; KRÄMER J.; LANGGUTH P.; Self-assembly of chitosan/HPMCP HP50 nanoparticles for oral applications*. 7th PBP World meeting Malta*, (2010)
- TÜRELI A. E.; KRÄMER J.; LANGGUTH P.; Preparation of drug nanoparticles using microjet reactor technology. *2nd PharmaSciFair Congress, Nice,* (2009)
- TÜRELI A. E.; KRÄMER J.; LANGGUTH P.; A feasibility study: Controlled Nanoprecipitation with Microjet reactor. *69th international congress of FIP, Istanbul*, (2009)

Patent applications

- EP1165224 Verfahren und vorrichtung zur Durchführung chermischer und physikalischer Reaktionen
- WO2010091683 Device and method for producing pharmaceutically highly refined particles and for coating said particles in microjet reactors.
- PCT/DE2011/075044 Method and apparatus for the production of size controlled Micro- and Nanoparticles of water soluble and water insoluble substances through controlled precipitation, co-precipitation and self-organisation processes in microreactors

9. Appendix

Tab. 9-1: HPLC method validation results for Gliclazide

Parameter	Detail	Limits	Result	Compliance
SST	6 injections of standard solution	Area: RSD ≤ 2% Retention time: RSD ≤ 2%	1.94 % 0.78 %	yes
Selectivity	Visual comparison of chromatograms of the test compound in eluent	No interferences with eluent mixture	No interferences with eluent mixture	yes
Linearity	1st Order regression model r^2 min. 5 calibration levels	≥ 0.99	0.9998	yes
	Linear range	-	0.6144 - 61.440 µg mL^{-1}	yes
Accuracy	3 concentration levels (CON1 – CON3) n = 3 (deviation mean value/ true value)·100 %	deviation: 100 ± 2%	Deviation: CON1: 99.62 CON2: 99.73 CON3: 99.49	yes
Precision	3 concentration levels (CON1 – CON3) n = 3, RSD	RSD (n = 3): ± 2%	Deviation: CON1: 0.012 CON2: 0.210 CON3: 0.513	yes
Stability	Area %	2%	-7°C: 0.02	yes

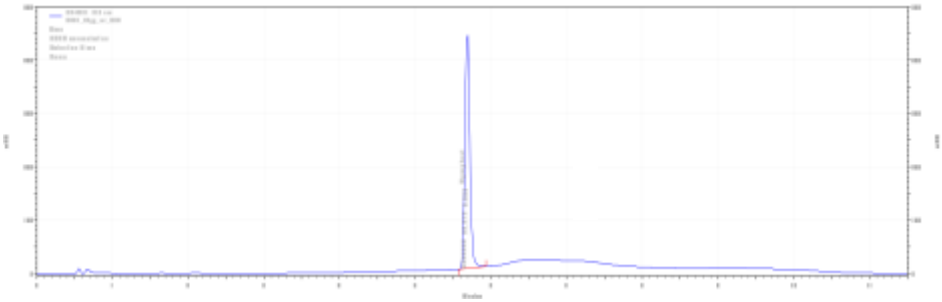

Fig. 9-1: Example chromatogram of Gliclazide assay method

Tab. 9-2: HPLC method validation results for Danazol

Parameter	Detail	Limits	Result	Compliance
SST	6 injections of standard solution	Area: RSD % ≤ 2 % Retention time: RSD% ≤ 2 %	0.58 % 0.19 %	yes
Selectivity	Visual comparison of chromatograms of the test compound in eluent	No interferences with eluent mixture	No interferences with eluent mixture	yes
Linearity	1st Order regression model r^2 min. 5 calibration levels	≥ 0.999	0.99989	yes
	Linear range	-	0.101 – 11.1 µg mL^{-1}	yes
Accuracy	3 concentration levels (CON 1 – CON 3), n = 3; (deviation mean value/ true value)·100 %	deviation: 100 ± 10 %	Deviation: CON 1: 105.9 % CON 2: 98.8 % CON 3: 101.7 %	yes
Precision	3 concentration levels (CON 1 – CON 3), n = 3, RSD %	RSD % (n = 3): ≤ 2 %	Deviation: CON 1: 0.9 % CON 2: 1.8 % CON 3: 1.0 %	yes

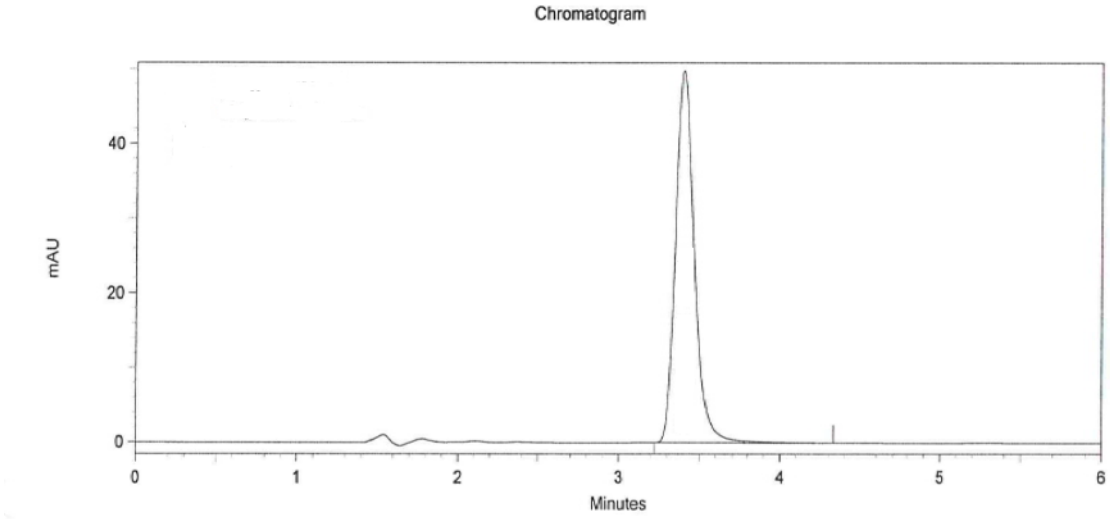

Fig. 9-2: Example chromatogram of Danazol assay method

Tab. 9-3: HPLC method validation results for Fenofibrate

Parameter	Detail	Limits	Result	Compliance
SST	6 injections of standard solution	Area: RSD ≤ 2% Retention time: RSD ≤ 2%	0.20 % 0.19 %	yes
Selectivity	Visual comparison of chromatograms of the test compound in eluent	No interferences with eluent mixture	No interferences with eluent mixture	yes
Linearity	1st Order regression model r^2 min. 5 calibration levels	≥ 0.999	0.999233	yes
	Linear range	-	5.06 – 60.72 µg·mL^{-1}	yes
Accuracy	3 concentration levels (CON1 – CON3), n = 3; (deviation mean value/ true value)·100 %	deviation: 100 ± 5 %	Deviation: CON1: 102.12 % CON2: 97.28 % CON3: 102.22 %	yes
Precision	3 concentration levels (CON1 – CON3), n = 3, RSD %	RSD % (n = 3): ≤ 2 %	Deviation: CON1: 0.3 % CON2: 0.05 % CON3: 0.04 %	yes
Stability	Concentration %	Deviation ≤ 2 %	24h at 7°C: 0.22%	yes

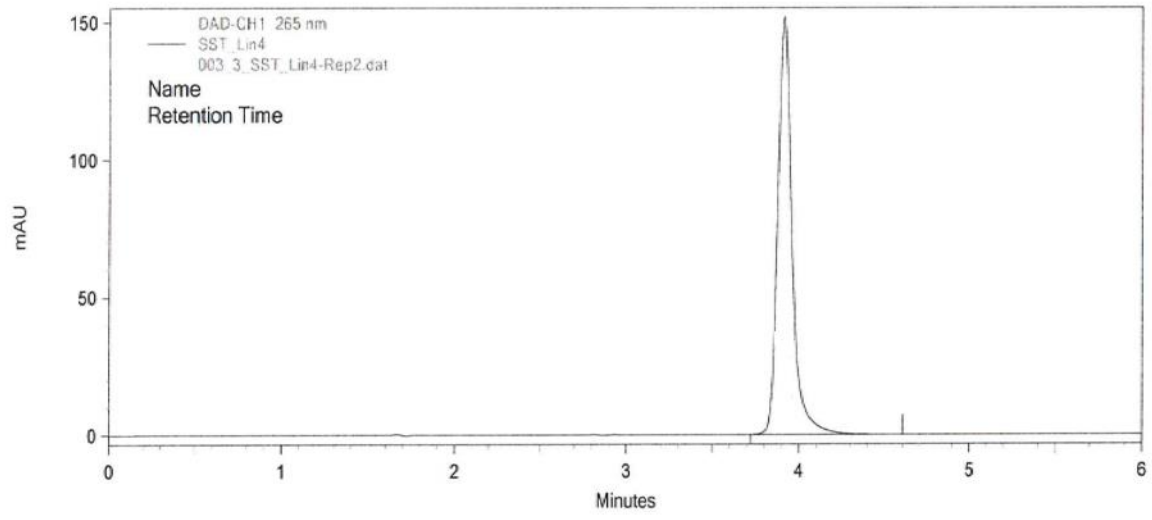

Fig. 9-3: Example chromatogram of Fenofibrate assay method